DESIGN AND DEVELOPMENT OF AN ADDITIVE MANUFACTURING TECHNOLOGY PLATFORM FOR MELT ELECTROSPINNING WRITING – A SYSTEMS ENGINEERING APPROACH

Felix Maximilian Wunner

M.Sc. Mechanical Engineering (TUM)

Submitted in fulfilment of the requirements for the degree of
Doctor of Philosophy

Short title: engineering the melt electrospinning writing technology

Principal Supervisor: Prof Dietmar W. Hutmacher

Associate Supervisors: Dr Elena M. De-Juan-Pardo and Prof. Dr. Axel Haase

Chemistry, Physics and Mechanical Engineering School
Science and Engineering Faculty
Queensland University of Technology

12/2017

Keywords

medical product development, 3D printing, additive biomanufacturing, systems engineering, tissue engineering and regenerative medicine, automation, process control, biomimetic, scaffold, product design

Abstract

The introduction of 3D printing principles to traditional fibre fabrication processes in 2011 is in a pioneering role at the vanguard of medical innovations and its effectiveness is increasingly evidenced for applications in the fields of additive biomanufacturing. Referred to as Melt Electrospinning Writing (MEW), this technological symbiosis is built on the functional benefits from both of its predecessors, namely additive manufacturing and electrospinning: high accuracy in material deposition and the capability of printing dimensions in the lower micron scale. The resulting highly porous architectures, predominantly made from biocompatible polymers, are implemented to effectively promote cell infiltration, proliferation, and attachment in the field of tissue engineering or a cell culture lattices for T-cells. The scaffolds are manufactured via precisely placing electrostatically driven viscous polymer jets onto a relatively moving collector in a layer-by-layer manner. Within the last years, the exponential growths of published work and patent applications evidenced the enormous potential of MEW to become a standardised technology in the medical fields; yet additionally offers high potential for applications in the filtration, energy or textile industries.

The research area for MEW, however is still in its infancy and the major focus consisted in exploring the benefits of the resulting scaffolds/lattices, while bypassing the essentials of developing highly functional devices to gain reproducible results. Hence, there is a lack of consensus in establishing a universal machine concept, which would be capable of fabricating scaffolds with homogeneous and constant morphologies. In general, the electrospinning of a fibre is known to be a delicate and highly complex process, and the quality of the outcome strongly depends on a well-balanced configuration of the parameters (e.g., extrusion rate, temperature, high voltage and translational collector speed). Although various studies provided basic insights into the technology and generated universal knowledge on the influences of these parameters, holistic process understanding could not be achieved, yet necessary for consistent and stabile manufacturing conditions. We identified an urgent need in developing a large data collection infrastructure to more precisely investigate the interplays between these parameters and their direct influence on the resulting scaffolds. From an engineering perspective, it became an inevitable milestone to reach

a stable process with a high degree of control. Beyond that, this constitutes the most important prerequisite for transferring the process to industrial levels.

Therefore, this Ph.D. project hypothesises that the application of systematic engineering methodologies assists in designing a technology platform to foster process control, reproducibility, and up-scale. The implementation of an automated monitoring and parameter control system is used to generate large data volumes which enable the identification of the optimum parameter settings for any given design. In particular, we draw a conclusion between the geometry of a fibre flight path and the quality of the final scaffold, which helps to assess from a manufacturing point of view the robustness and reproducibility of a process. Additionally, the novel hardware facilitates to increase the achievable scaffold fabrication height of 2-3 mm to 7 mm and helped to identify the influence of gravity on the process. In the last phase of this Ph.D. project, the results and technologies are utilised to design and develop a large-scale high-throughput MEW printer, which meets the requirements for industrial applications.

List of Publications

Peer-reviewed journal articles and book chapters:

[1] ***F. M. Wunner***, S. Florczak, P. Mieszczanek, O. Bas, E. M. De-Juan-Pardo, and D. W. Hutmacher, "Electrospinning with polymer melts – State of the art and future perspectives"

(Published in *Comprehensive Biomaterials II*, Elsevier, 2017)

[2] ***F. M. Wunner***, O. Bas, N. Toosisaidy, E. M. De-Juan-Pardo, P. D. Dalton, D. W. Hutmacher, "Melt electrospinning writing of three-dimensional poly (ε-caprolactone) scaffolds with controllable morphologies for tissue engineering & Regenerative Medicine Applications"

(Published in *Journal of Visuaizedl Experiments*, 2017, IF: 1.325)

[3] ***F. M. Wunner***, Marie-Luise Wille, Onur Bas, Paul D. Dalton, Elena M. De-Juan-Pardo, Dietmar W. H**utm**acher, "Melt electrospinning writing of highly ordered, large volume, scaffold architectures"
(Published in *Advanced Materials*, WILEY, 2017, IF: 19.791)

[4] ***F. M. Wunner***, O. Bas, S. Eggert, P. Mieszczanek, E. M. De-Juan-Pardo, and D. W. Hutmacher. "An explorative investigation of the influence of the system parameters on the geometry of a melt electrospun jet via an automated device",

(Accepted by *Progress in Additive Manufacturing*, Springer, 2017)

[5] **F. *M. Wunner***, J. Maartens, O. Bas, K. Gotschalk, A. Borrachhi. De-Juan-Pardo, and D. W. Hutmacher. "Electrospinning writing with molten polymers from different directions – examining the effects of gravity"

(Published in *Materials Letters*, Elsevier, 2017, IF: 2.572)

[6] ***F. M. Wunner***, J. Maartens, S. Eggert, P. Mieszczanek, R. Kent, O. Bas, E. M. De-Juan-Pardo, and D. W. Hutmacher. "Design and Development of a High-Throughput Melt Electrospinning Writing device"

(Accepted by *3D Printing and Additive Manufacturing*, Lieberthub, 2017, IF: 3.389)

[7] O. Bas[#], E. M. De-Juan-Pardo[#], M. P. Chhaya, ***F. M. Wunner***, J. E. Jeon, T. J. Klein, and D. W. Hutmacher, "Enhancing structural integrity of hydrogels by using highly organised melt electrospun fibre constructs", [#]These authors contributed equally to this work

(Published in European Polymer Journal, Elsevier, 2015, IF: 3.242)

[8] Patrina S.P Poh,. Mohit Chhaya, P. , ***Felix M Wunner***, Elena M. De-Juan-Pardo, Ardnt F. Schilling, Jan-Thorsten Schantz, Martijn van Griensven, Dietmar W. Hutmacher, "Polylactides in additive biomanufacturing"
(Published in ADVANCED DRUG DELIVERY REVIEWS, Elsevier, 2016, IF: 15.606)

[9] Onur Bas, Davide D' Angella, Jeremy G. Baldwin, Nathan J. Castro, ***Felix M. Wunner***, Navid T. Saidy, Stefan Kollmannsberger, Alessandro Reali, Ernst Rank, Elena M. De-Juan-Pardo, Dietmar W. Hutmacher, "An integrated design, material and fabrication platform for engineering biomechanically and biologically functional soft tissues"

(Published in ACS applied materials and interfaces, 2017, IF: 10.76)

[10] Bahman Delalat,, Frances Harding, Batjargal Gundsambuu, Elena M. De-Juan-Pardo, ***Felix M. Wunner***, Marie-Luise Wille, Marek Jasieniak, Kristen A.L. Malatesta, Hans J. Griesser, Antonio Simula, Dietmar W. Hutmacher, Nicolas H. Voelcker, Simon C. Barry, "3D printed lattices as an activation and expansion platform for T cell therapy"

(Published in BIOMATERIALS, Elsevier, 2017, IF: 8.402)

[11] Laure C Martine, Boris M Holzapfel, Jacqui A McGovern, Ferdinand Wagner, Verena M Quent, Parisa Hesami, ***Felix M Wunner***, Cedryck Vaquette, Elena M De-Juan-Pardo, Toby D Brown, Bianca Nowlan, Dan Jing Wu, Cosmo Orlando Hutmacher, Davide Moi, Tatiana structural Oussenko, Elia Piccinini, Peter W Zandstra, Roberta Mazzieri, Jean-Pierre Lévesque, Paul D Dalton, Anna V Taubenberger, Dietmar W Hutmacher, "Engineering a humanized bone organ in mice to study bone metastases"

(Published in NATURE protocols, 2017, IF: 10.032)

[12] Ferdinand Wagner, Boris M. Holzapfel, Jacqui A. McGovern, Abbas Shafiee, Jeremy G. Baldwin, Laure C. Martine, Christoph A. Lahr, **Felix M. Wunner**, Thor Friis, Onur Bas, Melanie Straub, Peter Prodinger, Ali Shokoohmand, Davide Moi, Roberta Mazzieri, Daniela Loessner , Dietmar W. Hutmacher "Humanization of bone and bone marrow in an orthotopic site reveals new potential therapeutic targets in osteosarcoma"
(Published in Biomaterials, 2018, IF: 8.402)

[13] J. Maartens***, FM Wunner***, E.DJP Pardo, A. Simula, N. Voelcker, S. Barry, DW Hutmacher " Challenges and opportunities in the manufacture and expansion of cells for therapy"

(Published in EXPERT OPINION ON BIOLOGICAL TECHNOLOGY, 2017, IF: 3.684)

[14] Onur Bas, Sara Lucarotti, Davide D'Angella, Nathan J Castro, Dr, Christoph Meinert, ***Felix M Wunner***, Ernst Rank, Giovanni Vozzi, Travis J Klein, Isabelle Catelas, Elena M De-Juan-Pardo, Dietmar W Hutmacher "Rational design and fabrication of multiphasic soft network composites for tissue engineering articular cartilage: a numerical model based approach"
(Published in The Chemical Engineering Science, 2018, IF: 6.126)

Project-related patents:

[1] Simon Barry, Bahman DELALAT, Batjargal GUNDSAMBUU, Frances Jane HARDING, Dietmar Hutmacher, Maria Elena Juan PARDO, Nicolas Hans VOELCKER, ***Felix M. WUNNER*** "Products and methods for activating and/or expanding t cells",
(Published: PCT/AU2016/050800, 2017)

Project-related presentations:

[1] ***F.M. Wunner***, O. Bas, E. M. De-Juan-Pardo, D. W. Hutmacher, "Electrospinning of well-ordered poly (ε-caprolactone) scaffolds exceeding 10mm in height by implementing a dynamic control over the electrostatic forces"

(Presented at Australasian Society for Biomaterials and Tissue Engineering (ASBTE), Canberra, Australia, April 18 - 20 2017, Poster)

[2] ***F.M. Wunner***, J. Maartens, E. M. De-Juan-Pardo, D. W. Hutmacher " Design and Development of a Technology Platform for Melt Electrospinning Writing"

(Presented at the CRC Impact Day, Adelaide, 2017, Poster)

[3] ***F.M. Wunner***, E. M. De-Juan-Pardo, D. W. Hutmacher, "Optimisation through in-process monitoring at Electrospinning Writing with polymer melts",

(Presented at the Graduate School of Bioengineering, Technical University of Munich, 2016, Oral)

[4] O. Bas, J. G. Baldwin, ***F.M Wunner***, N. T. Saidy, E. M. De-Juan-Pardo, D. W. Hutmacher, Biomimetic fibre-reinforced hydrogels for soft tissue engineering applications:

(Presented at Australasian Society for Biomaterials and Tissue Engineering (ASBTE), Canberra, Australia, April 18 - 20 2017, Oral)

[5] O. Bas, S. Lucarotti, ***F.M. Wunner***, E. M. De-Juan-Pardo, D. W. Hutmacher, Mechanically and functionally graded multiphasic constructs for osteochondral tissue repair:

(Presented at Australasian Society for Biomaterials and Tissue Engineering (ASBTE), Canberra, Australia, April 18 - 20 2017, Poster)

Non-project related art project in collaboration with QUT Creative industries and the University of Tasmania:

Svenja Kratz, Michelle Xen, Richard Candy, ***Felix Wunner***, Dietmar Hutmacher,

Biosynthetic Systems exhibition project, exhibited at QUT (Mar. 2017) and Tasmania (Aug. 2017)

Note: Based on the formatting requirements issued by QUT, this thesis has minor changes in the following:

- US English to British English
- Consistency in Numbering of Tables, Figures and Equations
- Combined reference list
- Consistency in Abbreviations (spelled out in each chapter)
- The term “scaffold” is used in chapter 2 – 6, and changes into “lattice” in chapter 7
- Appendix combined at the end of this thesis

Table of Contents

List of Figures

List of Tables

List of Abbreviations

AM	Additive Manufacturing
ABM	Additive Biomanufacturing
TE	Tissue Engineering
MEWTP	Melt Electrospinning Writing Technology Platform
RM	Regenerative Medicine
TE&RM	Tissue Engineering and Regenerative Medicine
FF	Fibre Forming
ES	Electrospinning
SES	Solution Electrospinning
ME	Melt Electrospinning
MEW	Melt Electrospinning Writing
SEM	Scanning Electron Microscope
SE	Systems Engineering
MBSE	Model Based System Engineering
INCOSE	International Council on Systems Engineering
SysML	Systems Modelling Language
2D	Two-dimensional
3D	Three-dimensional
u	Direction (x,y,z)
pc	Capillary Pressure
cos	Cosinus
kV	Kilo Volt
µl	Microliter
µm	Micrometre
h	Hour
mm	Millimetre
Fp	Pressure Force
Fm	Mechanical Force
Fe	Electrical Force
AP	Applied Pressure

AV	Applied Voltage
WD	Working Distance
CD	Collection Distance
MT	Melting Temperature
CS	Collection Speed
H1	Heating Element one
H2	Heating Element two
CTS	Critical Translation Speed
ROI	Region Of Interest
Mij	Sum of Results (DoE)
DoE	Design of Experiments
EHD	Electro hydrodynamic
ECM	Extracellular matrix
sc	Stability Criteria
#	Number of Experiment
svr	Surface to Volume Ratio
Mtp	Material Throughput
PCL	Polycaprolactone
mPCL	Medicalgrade Polycaprolactone
PP	Polypropylene
PE	Polyethylene
T-REG	Regulatory T-Cell
HT	High Throughput
HT-MEW	High-Throughput melt Electrospinning Writing
OoI	Order of Importance
RoI	Region of Interest
P_1	Parameter Settings 1
P_2	Parameter Settings 2
P_3	Parameter Settings 3
CRC	Cooperative Research Centre
CTMCRC	Cell Therapy Manufacturing Cooperative research Centre
GSB	Graduate School of Bioengineering
TUM	Technical University of Munich

PCT	Porphyria Cutanea Tarda
WIPO	Word Intellectual property Organization

Statement of Original Authorship

The work contained in this thesis has not been previously submitted to meet requirements for an award at this or any other higher education institution. To the best of my knowledge and belief, the thesis contains no material previously published or written by another person except where due reference is made.

Signature: QUT Verified Signature

Date: Munich, 03.07.2018_____

Acknowledgements

Above all, I would like to thank Distinguished Professor Dietmar W. Hutmacher for great supervision at all times and express my sincere appreciation for providing me with the opportunity to conduct my research in a highly creative, solution-orientated and applied manner. Thank you for being a great mentor.

Further, I would like to thank my co-supervisor Dr. Elena M. De-Juan-Pardo. As a material scientist, you always complemented my mechanical engineering skills and assisted with experience in the biological field.

I would specifically like to thank Professor Paul Dalton for his constant intellectual input and support. It has been an honour to me to further develop what was created at IHBI.

I really appreciate the efforts of Professor Axel Haase, Technical University of Munich (TUM), for helping me to start my research in Munich and the possibility to maintain contact with my Alma Mater via the Graduate School of Bioengineering (GSB).

Additionally, I would like to appreciate the funding bodies of this research: the Cooperative Research Centre Cell Therapy Manufacturing (CRC CTM), the ARC Centre in Additive Biomanufacturing and the Institute for Advanced Studies, Technische Universitaet Muenchen. I also appreciated to join the entrepreneurial Ph.D. program as a CRC CTM student and to be a member of the Graduate School of Bioengineering (GSB) at TUM.

The interdisciplinary character of our group is defined by special people with incredible skills and most importantly, its combination. Thanks, Onur, Chris, Gary, Jeremy, Pawel, Jo, Sebastian, Boris, Nina, Konstantin, Mohit, Flavia, Patrina, Boris, Christoph, Nathan, Antonia, Ross and all the others for creating this thriving research community, always thinking about the future with passion and joy.

Further, I would thank the members of Regenerative Medicine group, Cedryck, Phong, Laure, Daniela, Asha and Christina. I would specifically thank Jo Richardson for always organising everything for us so that we can conduct research with peace of mind; and Jose for keeping the lab in an excellent state!

I also want to thank Dr. Svenja Kratz for providing me with the opportunity to contribute to art projects, which all successfully lead to increased creativity and joy.

Ferdi, special thanks, for the music, the surf and Pina Colada. Furthermore, outstanding individuals made Australia special. Thanks, Ian, Tobi, Rob, Isa, Luke, Shanti, Chris, Mike, Emma and many more.

Sincere thanks, goes to my mother, who always supported my passion and decisions and my father, a great fly fisher and role model in teaching how to make life worth living. Thanks, Lisa, Lukas and, Paula for making distances disappear.

Describing my gratitude and appreciation for what you gave me within the last years, Luise, will exceed the feasible limits of this thesis. I want to dedicate this work to you.

Chapter 1: Introduction, Research Gap, Hypothesis and Aims

1.1 MELT ELECTROSPINNING WRITING – A TECHNOLOGICAL SYMBIOSIS

The introduction of additive manufacturing (AM) principles to the tissue engineering and regenerative medicine (TE&RM) research community initiated one of the most promising developments for medical innovation of the 21st century [1-4]. AM (also referred to as 3D printing) facilitates the production of objects via precise material deposition from so-called print heads, or extruding units, which follow computer controlled motion sequences [5, 6]. The material is added layer–by-layer and subsequently builds up to 3D printed objects. In general, this can be conducted with a variety of AM sub-technologies, such as extrusion-based, photo-polymerisation, powder-bed, and inkjet systems [7]. The capability to accurately deposit materials facilitates the manufacture of highly complex objects, which could not be fabricated with conventional manufacturing techniques, such as injection moulding [8]. AM technologies become particularly interesting for the medical research, as customized 3D-printed implants can be manufactured using biocompatible materials which can be implemented to substitute or repair natural tissues or organs [1, 2, 9]. This holds a great promise in the field of TE&RM, and prompted the development of advanced 3D bioprinters dedicated to tissue engineering applications [10]. Moreover, the capability to accurately deposit material in consecutive layers facilitates the fabrication of highly porous objects [11-13]. The generated space between the extruded material allows cells to infiltrate, proliferate and form new tissues around the porous scaffold [14], while the biocompatible polymer degrades after given time frames[15-17]. The fabrication of such scaffolds was predominantly conducted with extrusion-based AM technologies, such as Fused Deposition Modelling (FDM), as the mechanical design of the print heads allows for the processing of biocompatible polymers and the extrusion of single fibres [11-13]. Despite significant achievements and promising

applications within the fields of TE&RM, the major challenge of these devices consist in reaching a suitable resolution in the lower micron scale to meet the requirements of cells to effectively grow tissue [9]. These machines are characterised by a minimum achievable diameter of 200 µm, yet it is scientifically evidenced that cells most productively proliferate and effectively attach within architectures in the lower micron scale [18, 19]. Therefore, porous objects with high surface to volume ratios (svr) reveal a great potential for TE&RM applications [20, 21], and the community has utilised a plethora of so called fibre forming (FF) techniques, such as Melt Blowing [22], Melt and Solution Spinning [23, 24] and Solution Electrospinning (SES) [25]. Among those, the latter was identified as most promising due to its capability to reach submicron, to nano-scaled dimension [26].

In SES, a polymer is dissolved in a solution and extruded through a charged spinneret, which implements mobile charge carriers into the viscous material. This forms the extruded polymers into fibrous jets which can accelerate towards an earthed or oppositely charged collector. During the flight phase, the majority of the solvent evaporates and causes, in combination with the strong electrical field the straight jet to deviate from the linear flight path. This random deposition behaviour of the fibres results in disordered mesh architectures which represent a major challenge in TE&RM applications as controlled porosity is critically important for cell migration and proliferation. A few studies describe fibre deposition strategies using collectors with distinct patterns, which attract fibres on defined spots [25, 27] to obtain well-ordered geometries to regulate pore-size, height and fibre diameter. However, the control over the architecture of the resulting constructs is considerably limited in comparison to AM technologies. Additionally, the risk of solvent residuals entrapped within the deposited fibre constitutes a challenge for subsequent applications.

Larrondo et al. were the first in 1981 to electrospin solvent free polypropylene melts [28]. The key benefit of using polymeric melts over polymeric solutions includes the lack of toxic residues from the solvents in the final products [18, 29] yet, the increased viscosity also inhibits enhanced fibre stretching and thus, results in comparably thicker fibre diameters [30]. Melt Electrospinning (ME) constituted a promising approach to fabricate micron-scaled fibres and more importantly manufacture biocompatible architectures for TE&RM applications, yet still lacking accuracy in the deposition.

In 2011, the Hutmacher and Dalton laboratories described for the first time the adoption of AM principles to the process of electorspinning molten polymers (Fig.1) and, from this time onwards defined the terminology “direct writing” [31].

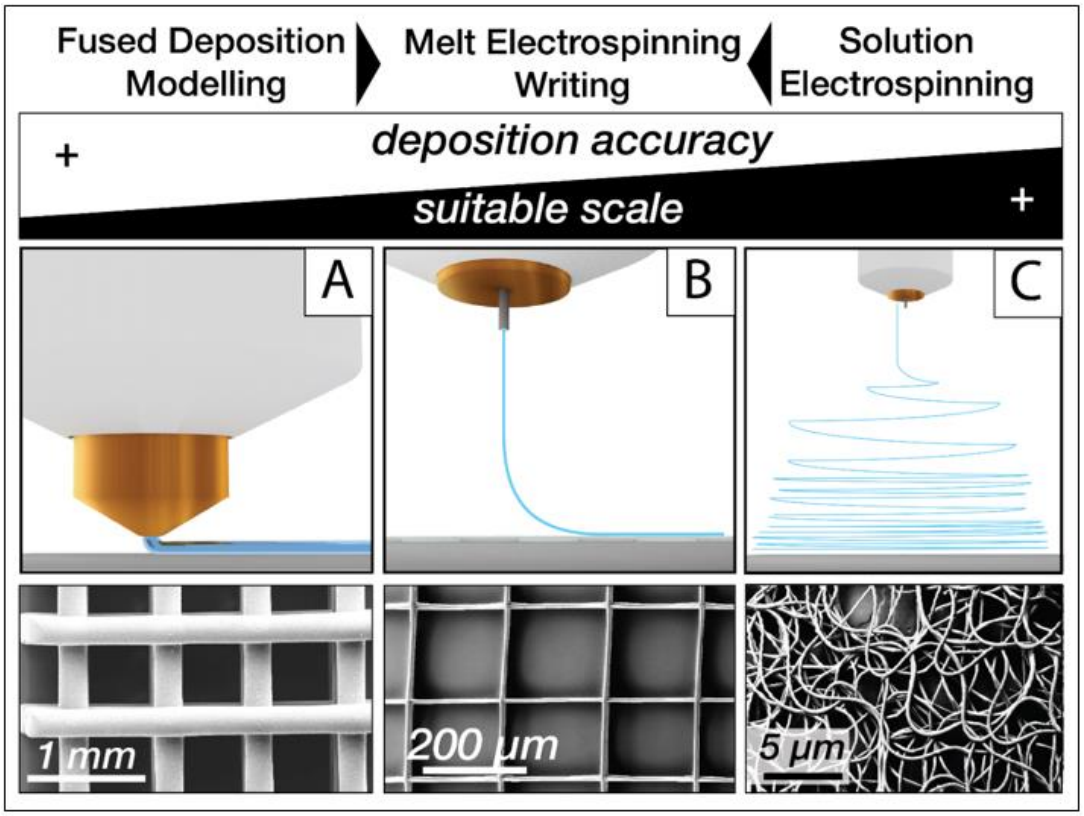

Figure 1: graphical representation of the convergence of FDM and SES to MEW, displaying the respective benefits, their schematics of working principles and resulting scaffolds with the respective resolutions

Similarly to the previously mentioned process of ME, the polymer is initially heated to reach a viscous state and subsequently mechanically extruded through the tip of a spinneret [32] (Fig.2). The application of an electrical filed triggers the implementation of mobile charge carriers into the polymer, which additionally urges the melt to eject from the tip [33]. Hence, the pressure initiated accumulation of molten polymer at the tip of the opening combined with the application of voltage evokes the formation of a Taylor cone [34], which ejects a micron-scaled fibre, which is accelerated along the vertical axis towards the collector [35, 36]. After emerging out of the Taylor cone, the jet is stable and the melt maintains directional control over the flight path without buckling, which allows for the collection of the fibres in a direct writing mode [31]. The fibres are deposited on a collecting platform which relatively moves between the tip of the needle and collector and fused with the previous layer [37] to build up the 3D printed objects.

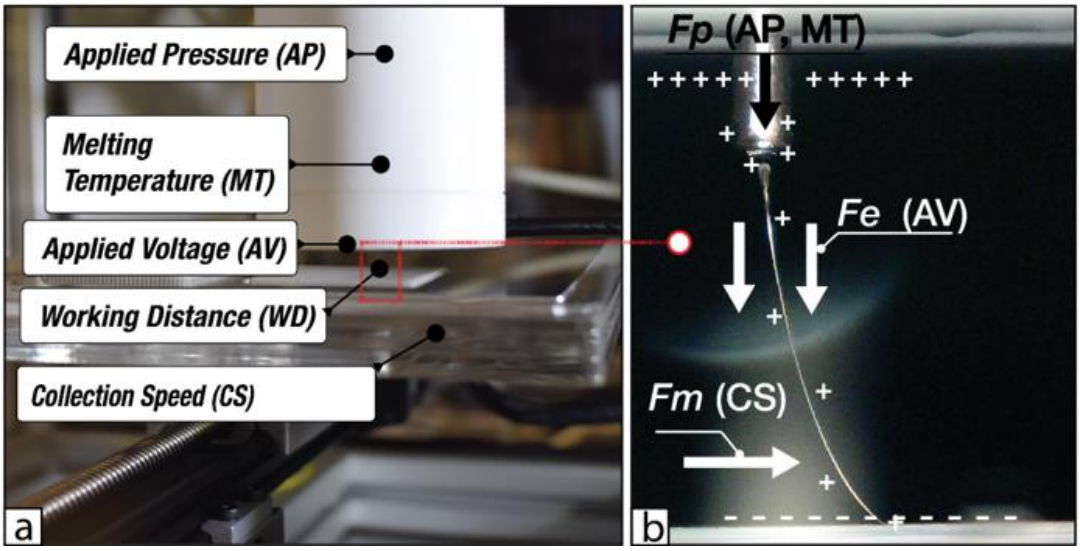

Figure 2: (a) MEW print head with the most prevailing system parameters Applied Pressure (AP), Melting Temperature (MT), Applied Voltage (AV), Working Distance (WD) and Collection Speed (CS). (b) shows an extruded fibre and the forces, which generate the fibre: Pressure force (Fp), Electrostatic force (Fe) and mechanical force (Fm), all induced via the respective system parameters.

1.2 RESEARCH GAP

Exponential growths of scientific work and patent applications on MEW scaffolds indicate a great potential for TE&RM applications [26, 38-40]. However, we identified in the current literature a trial and error approach instead of developing a universal understanding of the complex control of the most prevailing system parameters to achieve stable and reproducible printing conditions. Systems control and reproducibility are key factors to achieve high-quality standards and make subsequent biological studies more reproducible as well as to develop the potential to transfer the MEW technology to other industries.

1.2.1

Stability of the hardware

The majority of the devices found in the literature are in-house designed prototypes for benchtop applications. Additionally, these are customised to individual research environments and mostly built from different commercially accessible or self-made components [26], including the heaters, voltage supply or x,y,z stages. This calls for the need to engineer a holistic technology platform which can be utilised to perform as a basis to conduct more comparable research and to achieve more competitive scientific results.

1.2.2

Complexity of the process

MEW is governed by a high degree of complexity which is known to be the

"… stumbling block in the further development, optimization, and incorporation in the industrial scale applications…"[41].

As mentioned previously, multiple research activities targeted the identification and understanding of the most influencing parameter correlations, their interplay and the final effect on the fibre diameter [42]. These important findings which describe the reasons for varying fibre diameters induced by variations of the parameter settings certainly enriched the electrospinning community, yet unravelled the complexity only to a certain extend. To our knowledge, there is no study which can scientifically prove and explain the correlation of more than three parameters and their effect on the final fibre diameter at the same time.

We trace this lack back to the fact that the existing studies were conducted manually, or on a semi-automated level [43], which particularly decreases the achievable amount of collectable data. Dalton et al. electrospun onto glass plates, which were removed after printing to analyse the diameter of the fibres [44]. However, this technique is still associated with an interruption of the printing process itself and involves time and cost-effective characterisation efforts, conducted in a different environment, mostly under a microscopic. Eventually, this hinders the generation of large data volumes which could more precisely describe the process, its correlations and the effects on the final morphology. In this context, we also identified that the vast majority of characterisation is conducted on the deposited fibres, and respective conclusions on the stability of the process were drawn after production. Within this research project, we propose a more effective way of determining the stability of the process by analysing the shape of a fibre flight path during the MEW process. A few studies describe the use of cameras to monitor the fibre flight path to verify the bending behaviour in correlation to different collection speeds [45-47]. In the field of AM technologies, process monitoring and control is mainly found in the area of metal sintering aiming at maintaining accuracy during production [48, 49]. Hence, we identified the need to implement an automated process control with monitoring capabilities into the MEW process. This enables the collection of large data volumes as a basis to establish enhanced process understanding and to control the stability of the process.

Scale in production

Similar to conventional AM technologies, electrospinning with polymer melts is characterised by a considerably low output from a production point of view. Therefore, the technology was explored for scale-up to fulfil potential commercial applications.

1.2.3 A very limited number of machine concepts is published describing design solutions characterised by multiple extruding openings, examples are assemblies in a 2D plane [50], or alignments in a circular manner around a print head [51]. These concept demonstrate enhanced fibre extrusion throughput, yet fail in the capability of fibre depositing in a direct writing way to stack the fibres to accurate architectures and morphologies.

1.3 A NOTE ON THE METHODOLOGICAL FRAMEWORK – SYSTEMS ENGINEERING

Systems Engineering (SE) provides the methodological framework applied during this Ph.D. project. It assists in dissecting the interrelated challenges, managing the complexity of the interacting parameters and helps to integrate the findings into the MEW technology platform. In general, SE is a design methodology that facilitates the development of technical systems through structured guidelines and targeted decomposition of systems [52, 53]. Model Based Systems Engineering (MBSE) represents an advancement to perform all SE activities with computer controlled programs [52]. INCOSE, the International Council on Systems Engineering defines SE as

"… the formalized application of modelling to support system requirements, design, analysis, verification and validation activities beginning in the conceptual design phase and continuing throughout development and later life cycle phases… MBSE is expected to replace the document-centric approach that has been practiced by systems engineers in the past and to influence the future practice of systems engineering by being fully integrated into the definition of systems engineering processes …" [54].

Systems Modelling Language (SysML) is a graphical modelling language and allows for an effective execution of MBSE methodologies. It assists in visualising and communicating the most fundamental aspects of a product development process. Further, it assists in defining the design of a system, which includes the structure, correlation and behaviour of parameters and the overall requirements [55]. The SysML

tool Papyrus Eclipse IDE for Java Developers (Oxygen.1a Release (4.7.1a), USA) is applied as a tool for this Ph.D. project. Nevertheless, it is important to mention that SE was used as a methodology to facilitate the design and development of the MEW technology platform, yet we did not conduct research on the methodology itself. However, to our knowledge, there is no report on applications of such methodological engineering tools at the development of electrospinning devices for TE&RM applications.

We amended our design approach to the common principles of a SE process, which comprises the consecutive execution of the development steps (Fig.3).

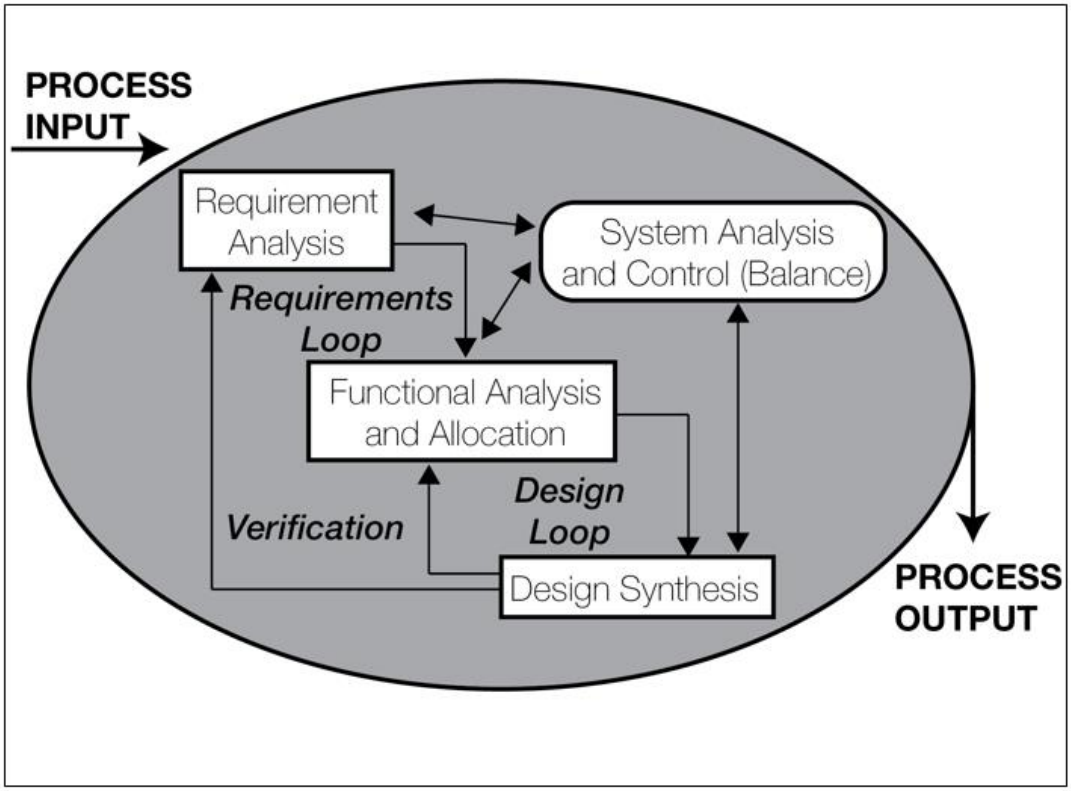

Figure 3: the Systems Engineering process (explained in the following), graphically modified from here [56] Potential inputs in the case of MEW can be material, energy or information, while a melt electrospun scaffold might describe a desired output.

Initially, the design and development process starts with *input*. The "input" defines the respective requirements on the targeted system, which, in the most optimal case represent an ideal system. The established framework of the identified needs leads to initial designs and developments, such as prototypes, which are tested against operational functionality and subsequently analysed regards the fulfilment of the technical requirements. Once confirmed, the further proceeding is conducted in the design synthesis phase, which defines the product on a physical basis while analysing the functionality. At last, the results are validated against the initially defined

requirements [52, 56]. In regards to the development activities within this research project, we amended the discussed process to the requirements and existing hardware and thus, established a dynamic product development concept. Within the framework of this Ph.D. thesis, the application of these steps and the respective iterations to optimise the experimental results and the hardware and software assisted in designing a comprehensive Melt Electrospinning Technology Platform (METP). The resulting structure of the system is displayed in the overview section.

1.4 HYPOTHESIS AND THESIS AIMS

Hypothesis:

Applying systems engineering design approaches to the development of a MEWTP with integrated monitoring and automation units assists in dissecting the impact of the process parameters which induce geometry variations of the electrostatically accelerated polymer jet and allow the identification of the most stable printing conditions.

Aim 1:

Engineering, building and verification of an integrated and automated MEW device concept

Aim 2:

Design of an in-process control system for determining process stability and identifying the correlations between the geometry of the jet and the diameter

Aim 3:

Engineering, building and verification of a high throughput METWP

1.5 THESIS OVERVIEW

This Ph.D. project aims at generating the knowledge as well as empirical data sets for a better understanding of the complex and multi-parametric MEW process. In order to develop highly functional MEW hard- and software we applied systems engineering principles, which assisted in providing an agenda for the development steps. The

technological achievements and scientific findings described and discussed in the individual chapters of the thesis build upon another and were performed in a logical manner.

Chapter 1 introduces the converging fields of AM, ES, and MEW and uncovers its potential for the TE&RM community. It further outlines the advantages of systematically engineering a platform technology, which resembles these converging fields and represents a methodological fundament for further research. Additionally, this chapter explains the rationale and the aims to answer the hypothesis.

The accomplishment of Aim 1 is reached with chapter 2 (published) and 3 (published)

In **Chapter 2,** a detailed review of the state of the art MEW devices is conducted to identify the most prevailing technological requirements from both, a polymer processing and 3D printer design point of view. A historical perspective of the electrohydrodynamic (EHD) phenomena, the creation of solution electrospun meshes and the recently discovered convergence of electrospinning and 3D printing principles emphasises the emergence of the technology. A bench marking with other 3D printing technologies highlights the uniqueness of MEW in fabricating ultra-porous (93%-98%) scaffolds with ordered architectures. The literature review serves as a basis to create the fundamental framework for the development of the MEWTP and the research conducted within this Ph.D. project.

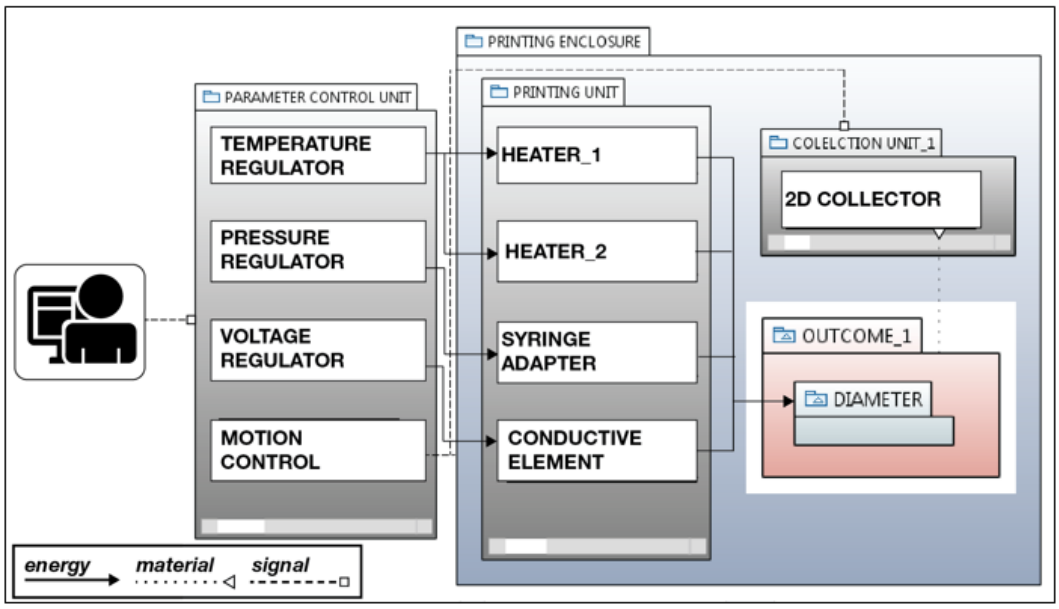

Figure 4: SysML block diagram of the MEW device, subdivided into parameter control units and the printing enclosure

This comprises the analysis of commonly applied fabrication steps, the subsequent definition of fundamental process functionalities and the identification of appropriate software and hardware. These findings are combined to form the requirements for deriving the most optimal configurations. Based on this MEW devices were build and tested in systematically applied Design of Experiments (DoE), which reveal compatible results.

The main purpose of **Chapter 3** comprises the verification of the functionality of the MEW devices; therefore, we formulate a protocol for users. Furthermore, qualitative observations of the effects of different system parameter settings on the geometry of a falling jet lead to initial findings on the stability behaviour of the process. Additionally, the chapter illustrates the feasibility of electrospinning different fibre diameters through experience-based adjustments of the parameter settings.

Aim 2 is enveloped in chapter 4 (publication in pre-submission format) and 5 (publication submitted)

Chapter 4 presents the systematic development and integration of an in-process control system to monitor the fibre flight path and the resulting fibre diameter under a large number of parameter settings. This set up did lead to generating large data volumes which were analysed to enhance the current understanding of the MEW process and the influence of the parameters. One fundamental deliverable of this chapter is the engineering of such a system, which includes the following:

(1) Manufacturing of a conductive conveyor belt to allow for continuous fibre generation and deposition
(2) Development of a two-camera monitoring system to record the fibre and diameter, respectively
(3) Coding of the software to automatically trigger parameter settings and recognise, process and store data of the resulting images in real time

The experiment results in a large data set format of approximately 15.000 entries, which did undergo an initial linear regression analysis. We found a significant correlation between the deviation of the angle and the diameter. This finding makes the process of monitoring the flight path of a jet an effective method in verifying the stability of the MEW process. Secondly, the application of a Generalised Estimation Equations (GEE) model is used to identify the effects of the four parameter settings: temperature, speed, voltage, and pressure. The results are visualised in heat maps and

allow for detailed investigations. The discoveries on the diameters support the majority of postulations described in the literature. Yet, an increase in diameter along higher process temperatures is a new finding. The discoveries regarding a fibre flight path which is defined by its characteristic angle, is original and has not been reported in the current literature. We discover, that the increases or decreases in angle implied due to forces from the collector or the electrostatics respectively, strongly depend on the amount of extruded polymer and its melt viscosity. The chapter concludes with the establishment of a design library, which displays the most stable system parameters to print targeted fibre diameters. Statistically, representative MEW experiments were performed to verify the design library. The elaborated understanding of creating stable printing conditions via adjusting the system parameters respectively is further developed by implementing a novel micro-controlled system to print multi-layered scaffolds. This is published in **Chapter 5** and describes the application of a mechatronic system, which adjusts the working distance via controlling the z-travel of the print head, while it increases the voltage at the same time. Latter is derived from simulations of the electrostatic forces and the concept is successfully applied at three different starting voltage profiles (7kV, 8kV, 9kV). For the first time in MEW, the concept allows for printing distortion free multi-layered scaffolds exceeding 7 mm in height.

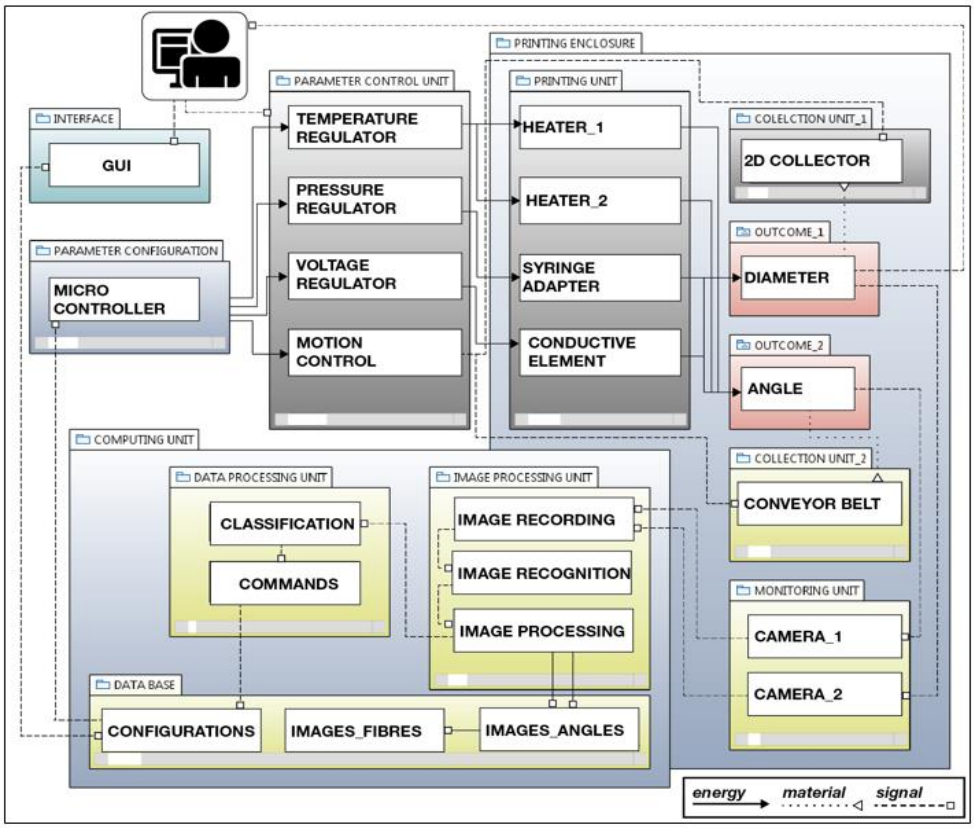

Figure 5: SysML Block Diagram of the developed MEW device and the novel attached collecting system (conveyor belt), which allows fibre detection (angle, diameter), analysis and storing in the Data base

The research performed in Aim 3 is summarised in chapter 6 (publication submitted) and 7 (publication in pre-submission format)

The effect of gravity on a MEW process is investigated in **Chapter 6** via comparing the results from electrospinning from the side, bottom up and top down. The analysis displays process parameter variations based on the printing directions and therefore, for the first time in MEW, this study demonstrates that gravity has an effect (within the parameter settings used in this experiment). Interestingly, the induced deviations do not affect the travelling fibre, but are observed to influence the geometry of the Taylor cone. This predominately occurs in process scenarios of high mass flow. The study identifies the most stable printing conditions for all printing directions.

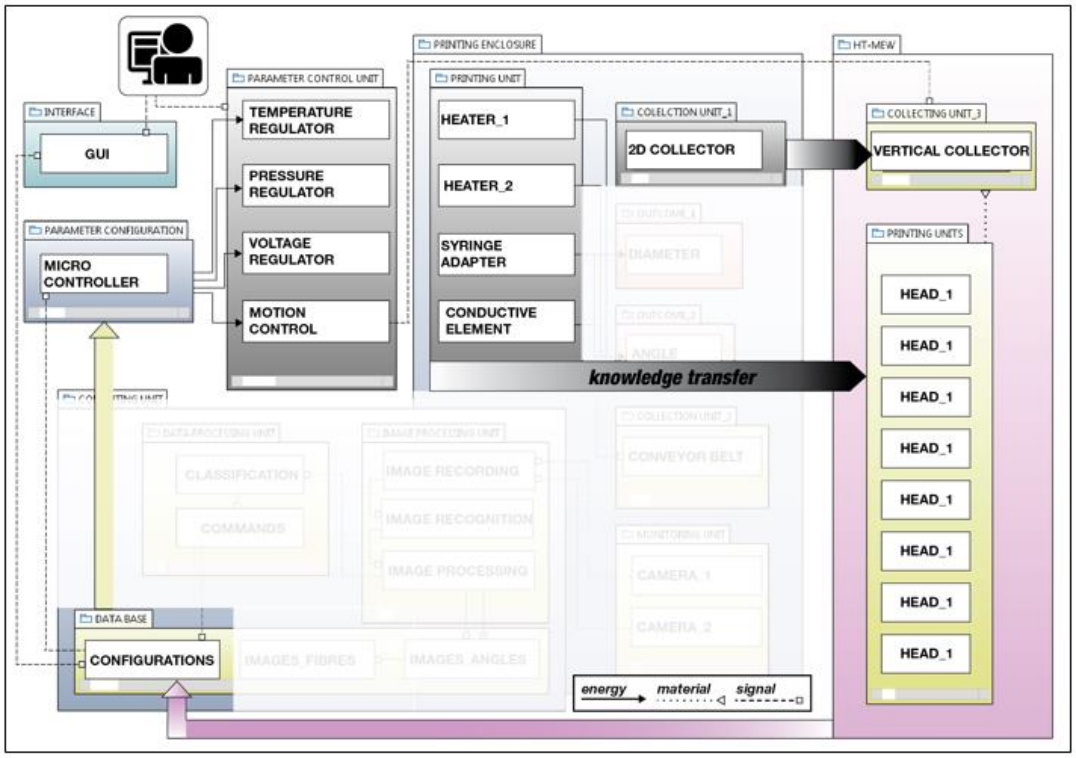

Figure 6: SysML diagram showing the achieved knowledge transfer of the elaborated to the HT-MEW device with eight print heads

The findings from Chapter 2 to 6 form the basis for designing the conceptual framework for a MEWTP which allows for high-throughput printing. This work is summarized in **Chapter 7**. The final design shows a vertically aligned collecting platform, which is subject to eight polymer extruding units, printing on both sides of a vertically aligned collector. The system parameter settings, analysed in the gravity study (chapter 6), are applied. The resulting lattices reveal homogeneous architecture and morphology with minor deviations across the dimensions of the collector (820x820 mm) which are in the framework of this proof-of-concept study. The high throughput capabilities are successfully confirmed by manufacturing scaffolds of 780 mm *780 mm and 1165 of 1,65 cm * 1,65 cm scaffolds within 48 hours. In a systems engineering approach, the data sets and results generated in chapters 2 to 7 were the foundation to demonstrate the feasibility of developing a MEWTP for industrial applications. Additionally, this conceptual work adds value to the discussion on how to achieve scale in additive manufacturing.

Due to the high interdisciplinary character of TE&RM and our group, this Ph.D. thesis was conducted in strong collaboration with biologists, electrical engineers, surgeons, chemists, data specialists and material engineers. Hence, this amplified the number of

publications, for which the findings of this work played a significant role. Therefore, the developed technology led to a translational research output and formed the basis for filing a patent which describes an invention in which the MEW lattices are used for high-throughput cell culture expansion of T-Cells *(WO2017035577 A1)*. In **Chapter 8,** a holistic discussion and future recommendations are finalising the Ph.D. thesis.

Chapter 2: Electrospinning with Polymer Melts – State of the Art and Future Perspectives

Felix M. Wunner[1], Sammy Florczak [1], Pawel Mieszczanek [1], Onur Bas [2], Elena M. De-Juan Pardo [1], Dietmar W. Hutmacher [1,2,3,4,a]

Published in Comprehensive Biomaterials II (2017)

Supporting information for the experimental section is provided in the appendix

[1] *Institute of Health and Biomedical Innovation (IHBI), Queensland University of Technology (QUT), 60 Musk Avenue, 4059, Kelvin Grove, Australia*
[2] *ARC ITTC in Additive Biomanufacturing, Institute of Health and Biomedical Innovation (IHBI), Queensland University of Technology (QUT), Kelvin Grove, Brisbane, QLD 4059, Australia*
[3] *Institute for Advanced Study, Technical University of Munich (TUM), Lichtenbergstraße 2a, 85748 Garching, Germany*
[4] *George W Woodruff School of Mechanical Engineering, Georgia Institute of Technology, 801 Ferst Drive Northwest, Atlanta, GA 30332*

[a,] Corresponding author at: Institute for Health and Biomedical Innovation, Queensland University of Technology, 60 Musk Avenue, Kelvin Grove 4059, Australia. E-mail addresses: dietmar.hutmacher@qut.edu.au (Dietmar W. Hutmacher).

Statement of Contribution of Co-Authors for

Thesis by Published Papers

The authors listed below have certified* that:

1. they meet the criteria for authorship in that they have participated in the conception, execution, or interpretation, of at least that part of the publication in their field of expertise;
2. they take public responsibility for their part of the publication, except for the responsible author who accepts overall responsibility for the publication;
3. there are no other authors of the publication according to these criteria;
4. potential conflicts of interest have been disclosed to (a) granting bodies, (b) the editor or publisher of journals or other publications, and (c) the head of the responsible academic unit, and
5. they agree to the use of the publication in the student's thesis and its publication on the QUT ePrints database consistent with any limitations set by publisher requirements.

Electrospinning with Polymer Melts – State of the Art and Future perspectives (published in Comprehensive Biomaterials II, 2017)

Contributor		**Statement of contribution**
Felix Wunner		Conducted the literature review, wrote the manuscript, designed the outline, prepared figures and tables. Conceived and conducted the experiments and the analysis
Signature	QUT Verified Signature	
Date	17/11/2017	
Sammy Florczak	QUT Verified Signatures	Co-wrote the manuscript
Pawel Mieszczanek		Aided experimental work
Onur Bas		Co-wrote the manuscript.
Elena M. De-Juan-Pardo		Co-wrote the manuscript and provided feedback.
Dietmar W. Hutmacher		Conceived and designed the experiments. Provided feedback on the manuscript. Supervised the entire work. Approved the final version of the manuscript.

Principal Supervisor Confirmation

I have sighted email or other correspondence from all Co-authors confirming their certifying authorship.

Dietmar W. Hutmacher QUT Verified Signature

Name Signature Date 17/11/2017

2.1 ABSTRACT

It is broadly valued by the biomaterials community that electrospinning from both the solution and melt is a technologically attractive method to process polymeric and composite materials; yet the number of publications reported in the current scientific literature regards the two methods has an estimated ratio of 1 to 400. Among the many reasons for the currently limited research output in melt electrospinning is that the fabrication of a well-designed melt-based electrospinning devices is technologically and scientifically more challenging than assembling a laboratory-scaled bench top solution electrospinning machine. Interestingly, the traditional polymer science-rooted melt electrospinning community has for the most part published studies using micron-diameter fibres; however, the biomaterials community prefers scaffold-processing technologies that allow the fabrication of sub-micron architectures. From a manufacturing point of view and compared to other fibre forming processes, less operational volatility is induced, as melt electrospinning is a solvent-free process. Additionally to this key aspect and from a users' safety perspective, no further concerns exist in regards to toxicity. If controlled appropriately, the charged polymer jet, which is formed during melt electrospinning can be accurately directed to the collector without instabilities. Through the application of melt electrospinning in a direct writing mode, i.e. the implementation of moving stages in two dimensions (X and Y), the resulting process can be considered as a new class of three-dimensional (3D) printing. This chapter reviews melt electrospinning research from a polymer processing and machine design point of view. It concludes postulating that the emergence of the progressive, innovative, and creative melt electrospinning technology will increasingly supersede the conventionally used solution electrospinning until it becomes successfully established within the biomaterials community.

2.2 ELECTROSPINNING – PAST AND PRESENT

The phenomenon of electric field induced changes in the geometry of liquid menisci was first observed in 1600 [57] and scientifically rediscovered around the turn of the 19th century, with literature describing the process of electrospinning with polymers dissolved in solutions, called Solution Electrospinning (SES) [58, 59]. At the beginning of the 20th century, a wave of interest in highly porous meshes arose among

the textile and filtration industries [60, 61] as well as the military sector [62]. Nevertheless, the majority of all research activities was concluded due to the typically low production rates for an industrial level. In the mid-1990s, electrospinning from polymer solutions was reinvestigated by the Reneker group [63], and ever since has remained in the limelight of scientific interest with an exponentially rising number of publications and patents [64]. However, several challenges exist for biomedical applications, most notably the randomised collection of fibres and the accumulation of residual toxic solvents within the fabricated non-woven meshes. In contrast, electrospinning with polymer melts, referred to as Melt Electrospinning (MES), avoids the use of solvents and therefore reveals significant advantages for the use in the biomedical field. In modern days MES faces an imminent paradigm shift, especially in the area of biomaterials and Tissue Engineering & Regenerative Medicine (TE&RM), owing to a rising number of researchers focusing on electrospinning with polymer melts rather than dissolving them in solvents [30]. Although initially investigated in 1936 [65], it was not until 1981, that Larrondo and St. John Manley provided a deeper understanding of electrospinning using polyethylene (PE) and polypropylene (PP) [28]. Around the turn of the 21st century, it was discovered that the molecular weight is of crucial significance to the process, notably due to temperature-induced degradation [66, 67]. Later, Reneker and Rangkupan investigated MES with PP under a vacuum. This environment increased the electric field strength and generated enlarged electrohydrodynamic forces acting on the jet, enabling further reductions in fibre diameter [68]. In 2006, Zhou et al. showed, that a heated zone between the spinneret and collector effectively influences the condition of a travelling fibre and considerably impacts its operational stability [47]. One year later, the Ogata group described a MES device operating under a laser system by solely melting the extruded part of a solid polymer rod, which was pushed through an orifice instead of being heated within the reservoir of a syringe. This concept aimed at circumventing the unfavourable process of polymer degradation, which appears in many thermopolymers under prolonged heating [69-71]. Joo and colleagues addressed the highly complex behaviour of travelling fibres and theoretically modelled different scenarios of the prevailing heat transfer mechanisms involved in the system [41, 72]. The still contentious necessity for enhanced throughput promoted concepts for enabling multiple jet extrusions simultaneously [50], for instance to manufacture filtration meshes [73]. In 2006, Dalton et al. proposed the design and fabrication of

biocompatible scaffolds from polymer melts for TE&RM applications [39], with great potential for both in vivo and in vitro studies. Since then, this has been extensively translated into practice by the Hutmacher group [16, 74, 75]. In parallel, the principles of Additive Manufacturing (AM), commonly known as 3D-printing, have entered multiple industry sectors, including growing interest for its application within the biomedical community [1, 11, 13] and recently defined as Additive Biomanufacturing (ABM). Commonly described as a layer-by-layer production of digitally designed components, it also embraces the adoption of these principles to electrospinning with polymer melts and was first performed by the Hutmacher group in 2011 [31]. An accurate deposition of micron-scaled fibres in a successive manner allowed for the formation of highly porous scaffolds with controlled morphological properties, such as pore size or number of layers (Fig.6).

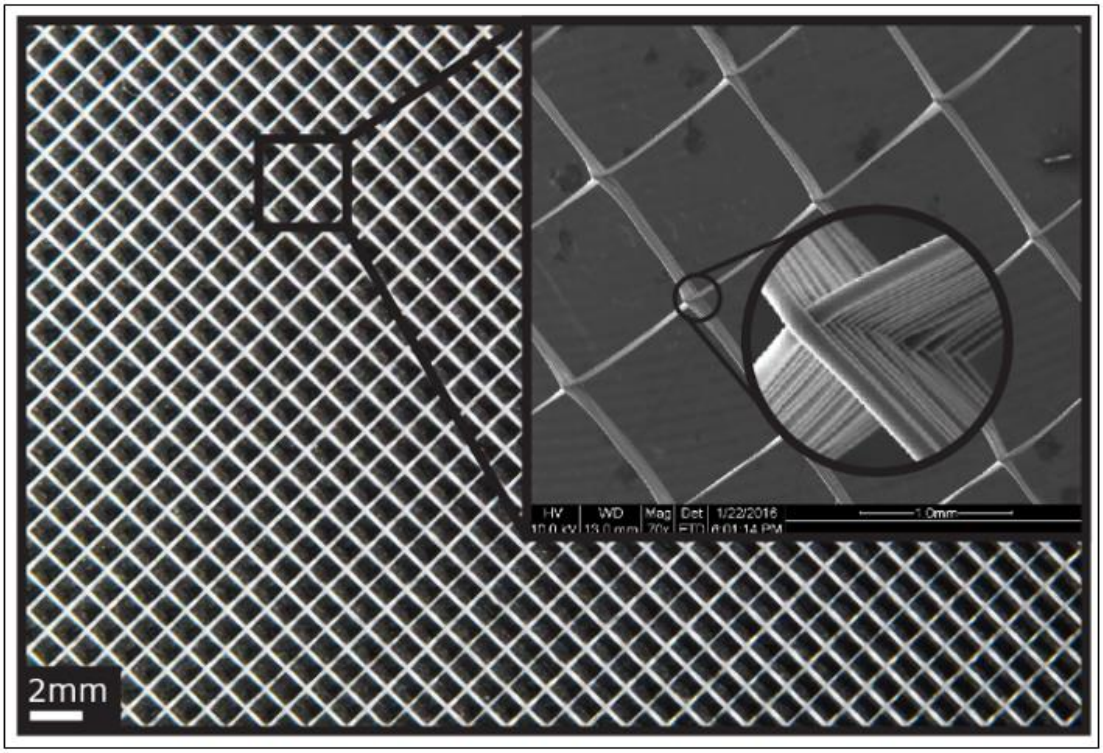

Figure 7: Scanning Electron Microscopy (SEM) images show a melt electrospun scaffold with highly ordered architecture and porosity fabricated by adopting a 0° - 90° pattern

This defined a new area in electrospinning research along with expanding the terminology of MES to Melt Electrospinning Writing (MEW) [44]. MEW refers to the method of fabricating scaffolds allowing a controlled deposition of fibres such that complex structures may be deposited directly onto a collector. It is undertaken by translating the collector in such a way that the plate moves relatively to the fixed spinneret, thus drawing out a pattern as defined by instructions sent from a computer [31]. Hence, three-dimensional (3D) constructs with ordered architectures can be

fabricated by MEW through simply overlaying multiple layers, hence allowing for the formation of thicker structures. Moreover, tubular structures may be fabricated by replacing the flat plate collector with a rotating mandrel while translating along its axis [76].

While the remainder of this chapter focuses on MEW applied in the biomedical sciences with a focus on TE&RM, there is also a constantly growing demand for electrospun membranes with high aspect ratios for use in the filtration technologies [77, 78], the textile industry [79] as well as in energy applications, including battery optimisation technology, [80, 81] piezo-electrics [82] or sensing [83, 84]. An exponentially rising number of publications within the past two decades shows continuously growing scientific interest in electrospinning with polymer melts (Fig. 7). A review reveals an estimated 190 publications by the end of August 2016 (source: SCOPUS), while the academic literature is expected to surpass 200 by the end of 2016 with an average of 100 publications per annum within the following decades [85].

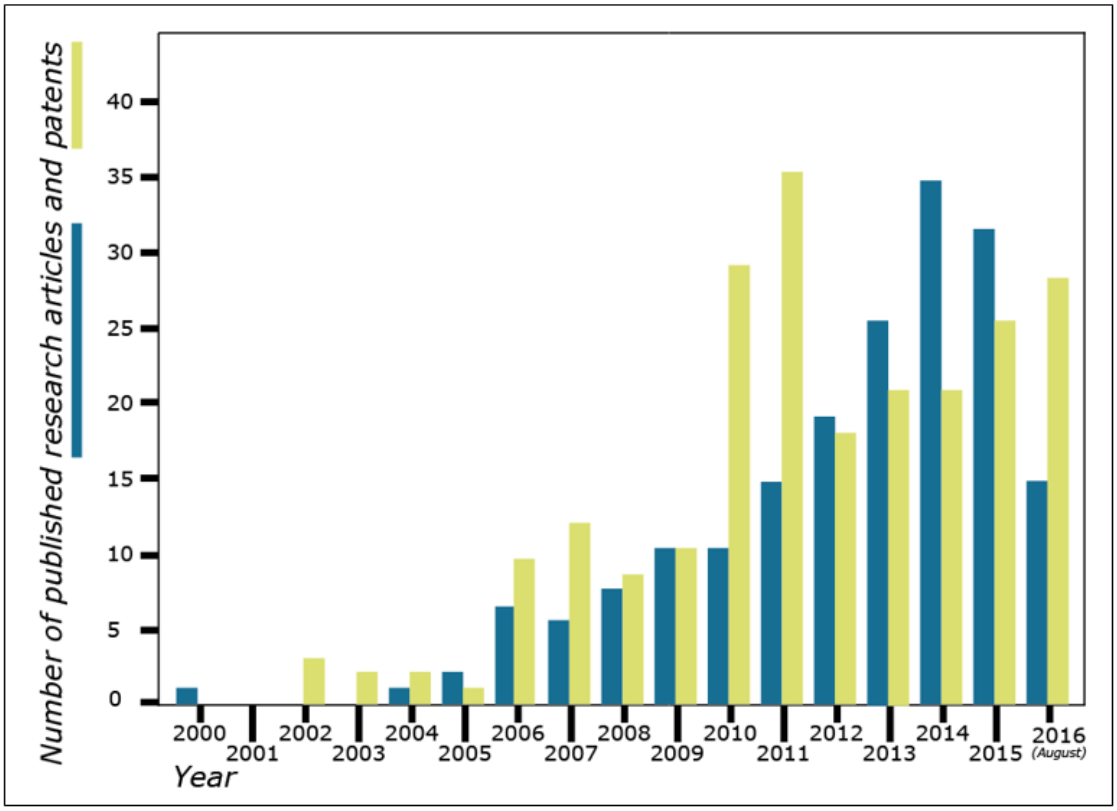

Figure 8: statistics of published research articles (source: SCOPUS) and patents (source: WIPO PATENTSCOPE) about melt electrospinning (keywords:"Melt Electrospinning", "Melt Electrowriting", "Melt Electro Spinning", "Melt Electro Writing", from 2001 to end of March 2016). One publication in 1981 on electrospinning with polymer melts [28] is not shown in this figure.

However, studies on MES still cover only a small proportion (less than 1%) of all publications related to electrospinning, which provide approximately 2000

publications per year [86]. Similarly, a survey of patents (source: WIPO Patentscope) provides an annual increase, showing a total of 227 filed applications by the end of August 2016. To our knowledge, SES machines exist at an industrial levels and as laboratory scaled versions, whereas the technology of electrospinning with polymer melts has not entered any market yet from both, a machine and end product point of view.

2.3 ELECTROSPINNING IN THE CONTEXT OF ADDITIVE BIOMANUFACTURING

Today, different ABM technologies facilitate the fabrication of products for applications in the TE&RM fields and can be categorised depending on their specific operating principles, that being [2]: Fused Deposition Modelling [12], Stereolithography [87], Selective Laser Sintering [88] and 3D-printing [89]. However, the production of biocompatible scaffolds with suitably high resolutions still faces prominent challenges and hampers the implementation of most 3D printing or AM technologies for use within the biomedical area [9]. Due to the considerable need for highly porous meshes in the micron to nano-scale [20, 21], the TE&RM community has embraced a plethora of fibre forming techniques, such as Melt Blowing [22], Melt and Solution Spinning [23, 24] and SES [25]. As discussed previously, SES represents one of the most widely used techniques to fabricate fibres with morphologies in the nanoscale. However, as toxic solvent residues may remain within the scaffold, major challenges exist for clinical implementation due to the resultant cytotoxicity [90, 91]. In addition, the presence of solvents provokes further complications, such as the need for solvent reclamation and recycling processes as well as additional investments for mandatory fume hoods [26]. Conversely, the solvent free fibre forming technologies mentioned above are commonly employed on industrial levels with a comparably high throughput and subsequently greater commercial value [92]. Major difficulties exist in maintaining homogeneous fibre diameters over long term production [93]. Melt electrospun fibres however, display minor deviations in diameter and are particularly suitable for applications in the TE&RM fields, where not only a high level of reproducibility but also biocompatibility plays an important role [30, 94]. Furthermore, MEW overcomes the drawbacks associated with randomly collected meshes, thus bridging a long-discussed gap in the Additive Manufacturing (AM) research community by introducing 3D printing principles to a fibre forming technique [9]. As

an example to illustrate the potential of MEW in producing a wide range of scaffolds with highly controlled morphologies and enhanced surface areas (Fig.8) shows the theoretical surface area of lattices of different fibre diameters and pore sizes.

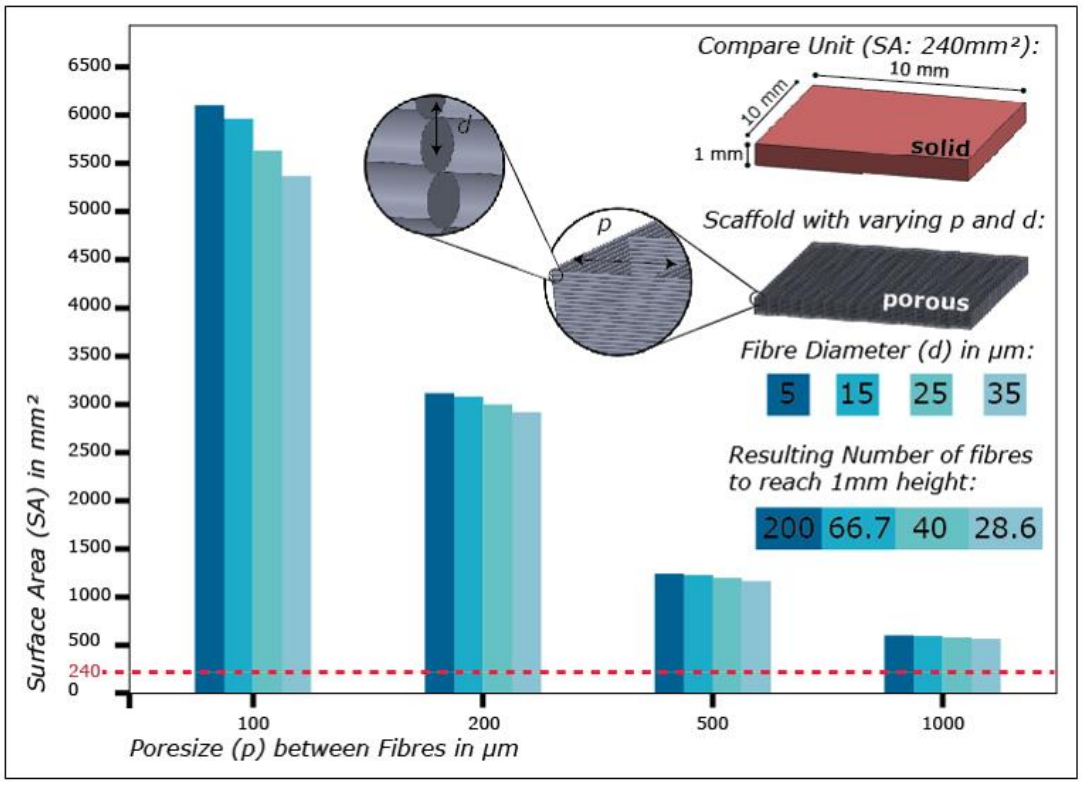

Figure 9: theoretical examination of surface areas of scaffolds comprising varying diameters and pore sizes that are specifically adapted to technically feasible dimensions printable with state-of-the-art MES devices. The computer modelling program Solidworks was utilised to design the scaffolds and calculate the theoretical surface area using an in-build function

2.4 DIRECT WRITING – CHALLENGES TO ADDRESS

Drawing polymer melts in an electrostatic field while attempting to achieve precise deposition of the fibres is a multi-parametric process. The outcome depends significantly on a synchronised interplay of multiple prevailing system parameters [41], including the flowrate , applied temperature ,voltage ,working distance and collecting speed. Therefore, numerous studies have provided the electrospinning community with intriguing insights on the influence of such parameters on the final fibre diameter [44, 94, 95]. Mathematical models have added further understanding to the ever-growing knowledge-pool of electrospinning with polymer melts [41, 72]. Although the abovementioned studies provide substantial insight into the process, most have focused only on the variation of one independent parameter at a time. The reason for this is seen in the number of possible parameter combinations, which exceed feasible limits on a conventional laboratory level. Consequently, it is imperative to

perform more holistic studies and gain a vital understanding of the process to eventually embrace the complex physical behaviour of the accelerated jets. It is noteworthy, that the performance of the electrospinning processes is strongly reflected by both the chosen system parameters settings as well as the employed mechanical design of the device [42]. The use of polymer melts in electrospinning presents inherent complications and risks when compared to SES devices. For instance, the necessity to integrate high-voltage power sources in close proximity to the heating elements as well as the shorter collector-spinneret distances for MEW applications significantly increase the risk of corona discharge [30]. One further challenge of electrospinning technologies is the fabrication of thick scaffolds designed with a large number of layers, based on an accumulation of charge and dielectric interference within the written scaffold, which subsequently forms inter-filament repulsion. This leads to an inaccurate deposition of the fibres as the number of layers increases beyond heights approximately of more than 1 mm [26]. Electrospinning with polymer melts is characterised by its low throughput and thus has not generated industrial interest to further invest into upscaling the process. The high degree of complexity contemporary hinders further steps to design machines for a broader industrial level [41].

2.5 A TECHNOLOGICAL REVIEW

In order to enhance understanding of the electrospinning process with polymer melts, an interpretation will follow dissecting the process into three discrete phases as suggested in the literature [31, 42]. These phases are as follows:

Phase 1: Polymer Preparation

The polymer preparation phase involves bringing the working polymer to a usable liquid state with the necessary mechanical, thermal and electrical influences to facilitate the formation of a Taylor cone at the orifice of the capillary. This signifies the threshold before the ejection of a fluid jet occurs under sufficient electro-hydrodynamic stress.

Phase 2: Jet Generation

Following the ejection of the jet from the Taylor cone, the second phase describes the period of time before the fibre makes contact with the collector. Within this period the environmental conditions significantly influence the thinning and solidification of the jet.

Phase 3: Fibre Collection

With the goal of fabricating well-ordered architectures, the manner of depositing fibres determines the degree of accuracy, while further aspects reveal the physical changes of the polymer in terms of solidification and accumulation of residual charge as well as dielectric interferences.

Figure 10: general phases of electrospinning with polymer melts to fabricate scaffolds

Chapter 4 will discuss the technology according to the perspectives of process hardware and system parameters, with each one being explained in relation to the aforementioned three phases. An experimental study will conclude this chapter and demonstrate the interdependencies of the most prevailing system parameters.

Process

2.5.1 The following chapter outlines the operational sequence required to transform the raw polymer melt into highly porous micron- or nano-fibre scaffolds. The focus is not only to inform about the processing steps, but also on the basic physical changes and mechanisms which occur during the process.

2.5.1.1 Taylor cone creation

Heating:

In comparison to SES, where a high solvent to polymer ratio achieves the processable viscosities, the method for printing with polymer melts is different. It requires an input of thermal energy to initiate a change of state of the material from solid to a viscous liquid facilitating flow through the capillary of the spinneret [30]. In the broadest case, heat transfer may be modelled numerically using the heat transfer equation, written in its general Cartesian form as the following partial differential equation [96]:

$$\frac{\delta u}{\delta t} - \alpha\left(\frac{\delta^2 u}{\delta x^2} + \frac{\delta^2 u}{\delta y^2} + \frac{\delta^2 u}{\delta z^2}\right) = 0 \qquad (1)$$

where u(x,y,z,t) is the temperature and α is the thermal diffusivity. The analytical solution is rarely attainable except for the simplest of models and therefore, finite-difference methods are commonly employed [97].

Pressure:

Homogeneous material flow is achieved by the generation of sufficient mechanical pressure within the polymer-containing reservoir, leading to the extrusion of the melt through the orifice of the capillary [36, 98]. Here, surface tension gives rise to a liquid droplet at the opening, which, under the subsequent application of high voltage, transitions from a paraboloid to a hyperbolical surface [34, 99, 100]. For the initial uncharged case, the capillary pressure (p_c) between two immiscible fluids may be expressed by the following equation [101]:

$$p_c = \frac{2\,\gamma\,cos(\theta)}{r} \tag{2}$$

where γ refers to interfacial tension, θ the wetting angle and r represents the radius of the interface.

Voltage:

The application of voltage to the conductive spinneret leads to the formation of a Taylor cone with a subsequent ejection of an electrohydrodynamic jet driven by electrostatic forces. It commences with the generation of a potential gradient from the spinneret to the grounded collector producing a resultant electric field between both electrodes [102, 103]. Literature has identified two key mechanisms responsible for charging of the polymer [33]: field emission (or field ionisation depending on the polarity) and field induced dissociation. These mechanisms are considered to be the primary mechanisms of charge injection for melt electrospinning due to the geometry of the electrode and intense electric fields typically employed. In MES, field emission (or the reverse case of field ion emission if positive polarity is applied to the spinneret) occurs when charges cross between potential energy barriers at the metal-liquid interface. This process occurs by means of quantum tunnelling in regions with a sufficiently intense electric field, which, in the case of electrospinning is located at the sharpest point of the capillary [104]. The intensity of these effects depends on the magnitude of applied voltage in combination with the geometry and work function of the capillary [105, 106]. The second mechanism, charging through disassociation occurs when molecules separate to form ionic pairs under significantly lower electric field regimes [79]. The Taylor cone geometry represents a state of equilibrium between the Maxwell stresses imparted into the molten fluid and surface tension maintaining the meniscus. The surface tension of the Taylor cone must be broken into order to

permit electro hydrodynamic flow. This is only achieved at a threshold voltage; a point whereby the electric field becomes strong enough such as to exert sufficient electrostatic forces on the charged liquid column towards the collector that the surface tension is overcome and the ejection of a fine fluid jet ensues [107, 108].

2.5.1.2 Jet thinning and solidification

Jet thinning

Jet thinning commences with a uniaxial viscoelastic elongation of the jet as driven by the electrostatic forces acting on the trapped charges within the liquid column leading from the apex of the Taylor cone to the collector. The uppermost region of the jet is typically unperturbed by instabilities, thus providing enhanced directional stability over the flight path providing a relatively thicker fibre. As the extensional elongation continues, the radius of the fibre is seen to asymptotically decrease as it approaches the collector [109]. During this stage, the fibre cools, reducing the viscosity of the jet and resulting in less elastic thinning than in the initial phase [41, 110]. The behaviour determining the elongation of the jet is primarily dictated by the extensional rheological and electrorheological properties of the fluid as well as parameters such as temperature, electrical conductivity and capillary gauge [111]. Jet thinning is a consequence of both, the conservation of mass and the Bernoulli principle with additional considerations for the presence of free charge. During operation, two main forms of hydrodynamic instabilities can typically be observed. Known as the Plateau–Rayleigh instability it arises from the tenancy of liquids with poor molecular cohesion to take about a minimal energy surface shape, that being, the decomposition of a low viscosity fluid thread into a string of fine droplets [112, 113].This is a consequence of varicose waves and minute perturbations on the liquid surface. Literature has shown that a charged liquid jet with a significant surface charge becomes dramatically more stable and can maintain a continuous jet over longer distances [114, 115], hence why electrospinning has been so successful at producing controlled microscale fibres. A more dominant form of instability is the bending instability. This is manifested as an oscillatory perturbation of the jet which is seen to increase in amplitude and propagate downstream as a function of jet length and jet velocity - usually proceeding a stable region. In solution electrospinning, bending instabilities are an especially prominent effect which displays a clear envelope of chaotic behaviour. As a consequence of lower conductivities and significantly higher viscosities typically observed in molten

thermo-polymers, melt electrospinning demonstrates many of these instabilities to a far lesser extent, eliminating the effects of Plateau–Rayleigh instabilities as well as reducing bending instabilities greatly.

Solidification:

Assuming the initial temperature of the polymer reservoir to be sufficiently high, the liquid jet should not undergo solidification before contacting the collector plate; heat transfer of the jet to the environment mid-flight however, is unavoidable and leads to a further increase in viscosity as the fibre approaches the collector. This implies that the elastic thinning ratio during the final flight phase is less than observed after the initial ejection of the jet [41]. This is further made true by a process called electrohydrodynamic quenching; a mechanism which has been observed to drastically accelerate the loss of heat seemingly in contradiction to predictions made by conventional heat transfer processes. Electrohydrodynamic quenching has been attributed to the generation of corona induced air currents which act to enhance thermal quenching of the jet and result in increased solidification [110].

2.5.1.3 Scaffold fabrication

Elongational stabilisation comes as the jet strikes the collector and undergoes cooling, leaving either solid fibres or a partially molten filament depending on the temperature, ambient conditions and the specific heat capacity of the material being spun. Intrinsic limitations are present within the melt electrospinning process and prevent the fabrication of completely unconstrained architectures. These are manifested by apparent bounds in the minimum attainable pore size and maximum height before significant compromises in structural coherence become apparent [116]. Furthermore, these electrostatic effects are likely to be a significant contributor to the deterioration in quality, especially when attempting to write multi-layered structures. This is due to surface charges as well as quasi-permanent trapped charges remaining within the material following its deposition [117, 118]. Thus, an accumulation of equally charged material can result in changes to the potential gradient between the spinneret and collector and cause deflections of the jet, while weakening the electrostatic forces acting draw it out. Literature [33] has revealed empirical observations of discharging during SES, and many of these mechanisms (not involving solvent evaporation) are likely to be applicable to melts. When the potential gradient between the polymer and

the grounded collector is of a sufficient magnitude (3.0 kV/mm in air), a dielectric breakdown of both the polymer itself and the surrounding air may occur within a localised region. This results in a visible 'spark', which jumps from the polymer to the collector [119]. Surface charge recombination is another mechanism of discharge and may occur either through direct contact with the collector, through condensation or via interaction with opposite polarity ions present in the surrounding atmosphere [120, 121]. As more material is laid onto the collector, the polarisation of the dielectric may become significant and thus produce bound surface charges that result from the presence of dipoles within the material. This might result from either the alignment of intrinsically charged molecular dipoles or through polarisation induced by a displacement of the atomic nuclei under the influence of an electric field (in either case described by the polarisability tensor for the material in question) [122]. Such effects can be problematic when attempting to write structures in which fibres are placed in close proximity parallel to each other (<50µm) as the dielectric polarisation will have an influence on the initial electric field. This occurs because under the influence of an electric field, the dielectric material (which in this case is the deposited polymer) produces its own dipolar electric field in response [123]. The net outcome is both a distortion and weakening of the initially applied external electric field, likely responsible for the observed 'jumping' of the jet towards fibres already laid down. With other considerations such as thermal degradation and mechanical robustness it is clear that a great number of variables must be tuned and accounted for in order to optimise the performance of the process and to achieve the desired level of control.

2.5.2

Hardware

The quality of electrospun scaffolds depends strongly on the implemented components as well as their particular interdependencies and mutual influences during operation. The following paragraph systematically describes the hardware found in literature and is explained accordingly to the three phases described in the previous section.

2.5.2.1 Polymer preparation unit

Generation of heat:

Most heating-components found in literature can be classified according to their main method of heat transfer: conduction, radiation and convection. Conductive heating describes the transfer of thermal energy through physical contact between components

and is applied via coil heaters [73, 116, 124], cartridge heaters [125-127], heating rings [128-130], band heaters [131-136], heating mantles [137-140] or resistive wires [141]. While these provide homogeneous heat distribution over the polymer, the HV source in most cases is placed in short distance to the heating element, thus presenting a risk of electrical discharge through dielectric breakdown of the surrounding material. Consequently, achieving sufficient electrical insulation represents one challenge in designing functional printers and is typically realised by incorporating sheathing with a high dielectric breakdown strength, such as ceramic sleeves [72]. Thermal radiation represents an alternative heating solution, describing the transfer of infrared thermal energy through open space. It is realised through the use of radiation heaters [68] or highly energetic lasers [69-71, 142, 143]. The absence of physical contact between components minimises the risk of short circuiting through dielectric breakdown and provides a safer alternative to conductive heating methods. The third method refers to convection, a process of transferring heat through moving fluids, such as water [17, 31, 43, 74-76, 95, 144], or oil [145-147], to the polymer container. Although capable of uniform heating, the use of moving liquids within the device enhances the design complexity and presents a danger of leakage and subsequent contamination of parts.

Application of pressure:

Compared to other fibre forming technologies, MES requires a steadily extruded polymer with a low flow rate. Conventional syringe pumps have efficiently proven to exert well-balanced pressure on the polymer container [17, 43, 47, 74, 76, 94, 95, 124, 131-133, 138, 139, 144, 146-153], while being capable of precisely adjusting the extruded volume to required ranges (2 – 20 µl/h) [43]. However, extended periods are needed to reach sufficiently stabilised extrusion rates [42] and the printing volume is limited to the size of a syringe. Hence, the implementation of screw-driven extruders in twin [66, 154-156] or single form [67, 157-159] allows for larger production volumes. However, these systems impose a lower limit on the mass flow, which results in larger diameters of the resulting fibres [160]. Pressurised gas such as air [73, 78, 116, 161] or nitrogen [162] have also been used to pneumatically drive the syringe plunger enabling more precise and stable printing. In devices that utilise laser heating, the mass flow is controlled by mechanically driving solid polymers into the melting zone [37, 69-71, 163-165]. Other concepts solely achieve extrusion via downwards gravitational force [68].

Establishment of an electrical field:

In order to establish an electrical field, the majority of MES machines described in literature implement the source of positive [17, 37, 41, 43, 69, 70, 74-76, 95, 110, 124, 126, 133, 142, 143, 151, 161, 164-168] or negative high voltage [39, 94] directly onto the polymer extruding component, while respectively grounding the collector on the opposite side. As explained previously, the increased likelihood of electrical discharge within the printing unit motivated several groups to earth the spinneret, while applying positive [51, 67, 128-130, 134, 146, 154, 158, 169-172] or negative high voltage to the collector [131, 132]. Attempts at alleviating the issue of accumulated residual charge within the deposited fibres were explored via the implementation of hybrid concepts. The application of altering positive and negative voltages has been reported on both collector and the spinneret side [144]

Polymer chamber and needle:

The selection of a suitable container for the melt should conform to the respective properties of the working polymer as the reservoir itself must withstand the respective impact of high temperatures and pressures. Conventional plastic syringes [31, 76, 95, 144] are commonly used for polymers with comparably low melting points, whereas glass syringes were employed [94, 124, 127, 146, 173] when printing with higher temperatures. In order to conduct extrusion under both high pressure and temperature, metal syringes or other metallic reservoirs [51, 128, 130-132, 142, 165, 169, 174] need to be used and are widely reported. A consistent polymer feed is achieved via commercially available flat-tipped needles of standardised gauge sizes [75, 76, 94, 124, 144, 148, 171, 173] or specially manufactured nozzles to fit in custom-made syringes or extruders [67, 69-71, 131-133, 143, 151, 169]. Alternative concepts for multiple jet extrusion will be explained in chapter 5, and experimental approaches describe square or star shaped orifices to maximise the surface area of the resulting fibres [175].

2.5.2.2 Flight environment

Distance:

The electrostatic drawing force responsible for the generation of the fibre is proportional to the potential energy gradient between the collector and spinneret and will therefore increase in magnitude as the distance decreases [133]. Furthermore, the

distance is highly associated with the fibre's time of travel. This, in turn, affects the degree of viscosity during the flight of the jet and thus, influences the stretching and solidification behaviour [176]. Increased deposition accuracy of the fibre with working distances of under 10 mm is reported [116]. Only a few devices were identified in literature have a controllable 3rd axis on the print head, commonly referred to as z-axis, to accommodate the height of the scaffold during production [160].

Ambient conditions

Controlling the ambient conditions within the printing enclosure effectively influences the viscosity and charge dissipation properties of a travelling fibre [177, 178]. This has motivated researchers to implement climate-controlled enclosures to maintain a constant temperature or humidity during the spinning process [47, 94, 148, 161, 164, 166, 179].Regulating and maintaining the level of humidity is commonly performed during SES, based on its strong impact on the amount of evaporating solvents [120]. In MES or MEW, to our knowledge, its effects on the morphology and behaviour of travelling fibres have not been proven to be significant yet [26]. Therefore, respective regulating devices are rarely reported [158, 180]. MES has also been conducted under vacuum [68, 181] and also under a pure Argon atmosphere [125].

2.5.2.3 Collection area

Material:

Electrospinning is only possible when a sufficient electric potential exists between the spinneret and collector. It is therefore a requirement that both components are conductive such that they may act as the electrodes between which the resultant electric field may be generated. Highly conductive metals are most commonly implemented. These include copper [41, 47, 51, 67, 78, 160], brass [127], stainless steel [182] and aluminium in form of a plate [68, 139, 161, 183], or foil [131, 133, 135, 149, 167, 184, 185]. Alternatively, conductive liquids were used as a collectors for the purposes of enhancing surface charge mitigation [39].

Collector dynamics:

To date, the majority of collectors found in the literature describe static printing environments leading to randomly collected fibres [44, 164]. However, the introduction of MEW principles requires a controlled relative movement between the printing and collecting unit to achieve the reproducible fabrication of ordered architectures [31]. Translating units were implemented to create targeted scaffold

morphologies by moving stages in a horizontal Cartesian plane [144, 173] or linearly moving rotating cylinders [76, 124].

System parameters

In order to further understand the effects of varying parameter combinations on the final morphology of the fibre, a differentiation between polymer-based and component-based parameters was introduced in literature [26, 42]. The following paragraph will consider this classification and describe the parameters including the most relevant interdependencies among one another.

2.5.3

2.5.3.1 Polymer induced parameters

To date, only a small number of polymers have been electrospun via MEW [26]. The application of highly viscous and non-conductive materials constitutes a prerequisite [30] to obtain both a stable operational behaviour as well as viable morphological and mechanical properties [16]. The molecular structure, in combination with the applied thermal energy strongly determines the degree of viscosity [41]. Polymers characterised by a high molecular weight counteract initial jet thinning and result in larger fibre diameters. However, materials of low molecular weight tend to generate thinner fibres accompanied with disruptive periods of inconsistent interruptions to the jet referred to as jet dripping [67]. Moreover, printing irregularities are also attributed to over-heating, which, owing to chemical decomposition, induces noteworthy deviations of the molecular weight [47]. The tacticity of the polymer has a significant impact on the process as, more isotactic structures are generally characterised by a higher degree of molecular order and thus result in reduced diameters compared to less structured atactic polymers [67, 134]. The conductivity of a polymer constitutes the amount of charge accumulation [186] and consequently influences the formation of a Taylor cone. Furthermore, it determines the stability of a jet regarding its tendency for electrostatically induced buckling behaviour close to the collector [132]. It is reported that polymers with greater conductivity are susceptible to breaking within an increased electrical field, whereas more insulating materials lack the capacity to initiate fibre formation [187]. Furthermore, a strong relation between the conductivity and temperature of the working material exists. The application of heat and subsequent change of state to a liquid may mobilise charge carriers and increase the conductivity of the polymer melt as temperatures increase. An increase in conductivity can also be

achieved through an incorporation of additives into the polymer, allowing for decreased fibre diameters through alternative means [131].

2.5.3.2 Component induced parameters

Applied pressure:

A vast majority of publications agree that the amount of extruded polymer significantly determines the final morphology of a fibre [43, 44, 95, 170], including reports of a direct proportionality between pressure and final diameter [42, 44, 95]. In general, increased pressure on molten polymers leads to greater material outflow and thus results in larger diameters [31, 95]. During operation, the electrically induced drag forces mainly act on the outside of a fibre, i.e. are widespread over the surface of the jet. In case of enhanced material flow, the surface significantly increases, while consequently, the electrical drag forces are reduced. Therefore, a concurrent increase of the applied voltage would represent a means of regaining small diameters [95]. Conversely, reduced material delivered through the orifice results in smaller diameters of the jet in a closer distance to the collector. This consequently increases the likelihood of electrically induced bending instabilities. As discussed previously, applied temperatures determine the viscosity of the polymer and thus, its specific flow characteristics. Higher temperatures induce lower viscosities, with generally greater tendencies to flow. In this case, a decreased application of pressure can be considered as sufficient to regain homogeneous material outflow [31, 95]. The amount of extruded polymer is caused by multiple system parameters [95] and has a great influence on the final diameter [162].

Melt temperature:

Due to the rheological properties of most thermopolymers, whose viscosities decrease with increasing temperature in the liquid state, most literature reveals intensified jet thinning with increasing temperatures [47, 128, 149]. In this case, decreased resistance acting against the electrical drag forces leads to enhanced flow characteristics with greater elastic properties. This is especially prominent in the first section of the fibre after the Taylor cone is formed, as solidification has not occurred yet. In order to maintain the mechanical properties of the resulting scaffold, great attention must be paid to sufficiently apply temperature and suppress premature solidification of the jet to allow adequate fusion of the resulting fibres layer by layers. This, in turn is strongly dependant on the working distance, which determines the timeframe over which the

fibre can lose heat. Although high temperatures provide more optimised viscosities, which enhance the thinning of a jet, operating under high temperatures over prolonged periods of times might lead to undesired degradation mechanism. For instance, overheating aliphatic polyesters such as PLA or PGA can result in cytotoxic degradation by-products which will compromise the quality of the final product [42].

Acceleration voltage:

The applied voltage significantly determines the extent of fibre stretching in its viscous state [31, 47, 128]. Most literature describes, enhanced thinning occurs due to enlarged electrical drag forces accelerating and consequently elongating the jet [44, 95, 157]. The effective strength of the generated electrical field is closely associated to the working distance and can be expressed as an inversely proportional relation to the distance [133]. In general, greater diameters can be collected when smaller voltages are applied [180], however, sufficient electrostatic force is still a prerequisite to transform a molten polymer into Taylor cone [43]. Conversely, randomly coiling fibres are observed at high voltages, based on the aforementioned electrostatically induced buckling behaviour (bending instabilities) close to the collector [44]. This, in turn, significantly deteriorates linear fibre deposition when direct writing but can be compensated to some extent by altering the collector speed [31]. Achieving homogeneous fibre production at higher flowrates requires a corresponding increase of applied voltage. The enlarged surface area of the fibre requires stronger electric fields to achieve similar drag forces, a phenomenon particularly observed within the range of higher temperatures as a result of enhanced flow characteristics [128, 160, 180].

Spinning distance:

The effective distance between needle and collector not only impacts the resulting morphology of the fibre by affecting the strength of the electrical field, as discussed above, but also determines the time-dependent degree of solidification [128, 180]. Short collecting distances do not elicit sufficient time to solidify a travelling fibre, which results in distorted shapes on the collector. Although, the accuracy of deposition is increased at smaller distances, potential voltage breakdown between charged and grounded element still poses a risk [31, 42]. Oppositely, large collection distances result in thicker fibres as a consequence of longer periods for fibre solidification, leading to higher induced viscosities and subsequently greater resistance to being elongated [164, 180]. However, different interpretations on these phenomena have

been proposed [37, 128]. In recent years, studies reveal MEW processes at working distances up to a millimetre. All remaining system parameters had to be adjusted accordingly to accommodate this to fabricate well-ordered scaffolds in the sub-micron range [116].

Collection Speed:

Compared to other fibre forming techniques, the motion and velocity of the spinneret relative to the collector (or vice versa) constitutes a major factor for direct writing applications. It greatly determines quality and reproducibility, however, is comparably under-investigated in the current literature. For both x-y translating collectors [31, 75] and rotating mandrels [124] , the linear or angular velocity must be controlled in order to avoid fibre buckling or over-accumulation of material onto the collectors. [44]. Here, relatively slow translational speeds result in coiled fibres and oppositely, over-speeded collection leads to inaccurate deposition [31]. Moreover, it is reported that high collecting speeds lead to a significant diameter reduction through enhanced mechanical stretching [76].

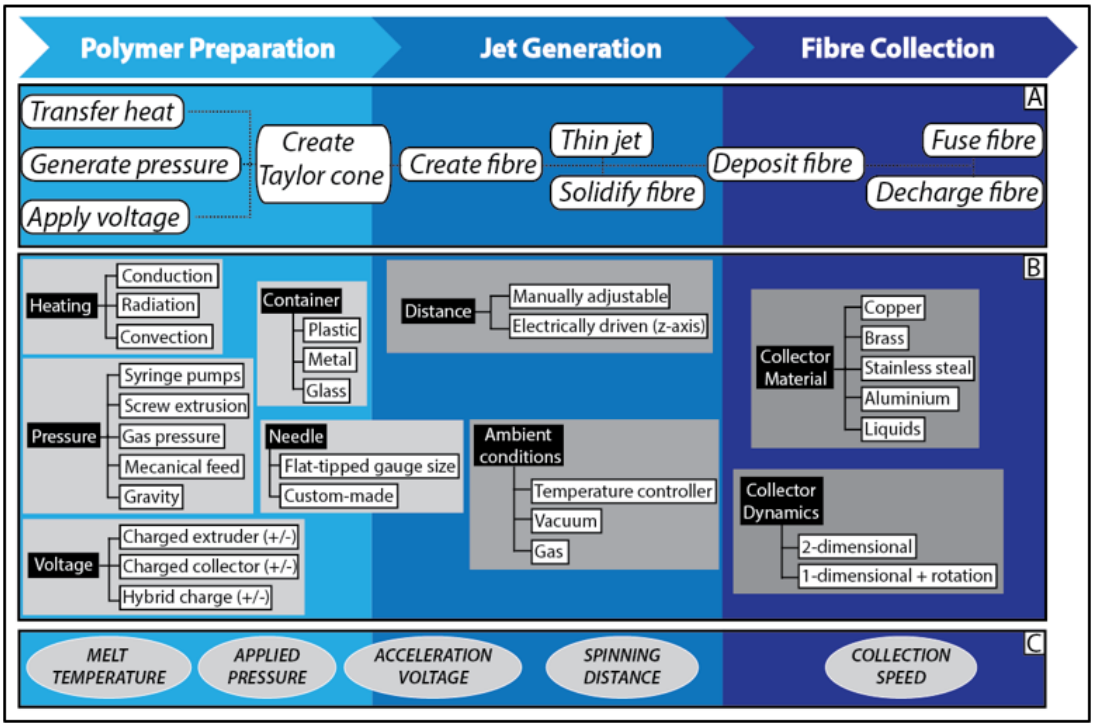

Figure 11: schematic description of (A) process, describing separate steps for the fabrication of scaffolds from polymer pellets or flakes, (B) existing hardware, whereas the components are subdivided into their tasks, and (C) classification of the most prevailing system parameters into the respective phases

2.6 EXPERIMENTAL

The following study aims at investigating the effects of the five main system parameters, explained in 4.3, on both, the fibre diameter and its deviation distributions. Based on experience from previously conducted work [31, 44], an orthogonal design study was designed and performed to investigate the spinning conditions using an in-house built MEW device. Such studies vary multiple parameters, which, in the framework of this study, include applied pressure (AP), acceleration voltage (AV), melt temperature (MT), collector distance (CD) collection speed (CS)), and their respective settings, referred to as levels. The experiments are conducted following defined courses of action, which significantly reduce the efforts of conducting multi-parametric experiments. Commonly used in science, an orthogonal design study solely focuses on the most significant parameter combinations to establish a hypothesis, which conclusively predicts the behaviour of such systems [129, 188].

An in-house built MEW device (Fig.11.a) comprises of an air pressure controlled polymer feeding system (Electro-pneumatic regulator, SMC Pneumatics Pty. Ltd, Australia), a high Voltage source (DX-250, EMCO, USA) and a two-zone heating system, consisting of a ring heating element (H1) (Ceramic-RH, Bach, Germany) around the needle and a ceramic tube heater (H2) (HtH-Rohrheizer, Rauschert, Germany) surrounding the polymer reservoir. A 23G hypodermic needle (#23GPOrange, Nordson, USA) was attached to a plastic syringe (EFD Barrel, Nordson, USA) and filled with medical-grade poly (ε-caprolactone) (Purasorb PC 12, Purac Biomaterials, The Netherlands) pellets. Fibres were deposited onto uncoated microscope glass-slides placed onto a 3 mm thick aluminium plate collector and controlled via a translational stage (XSlide, Velmex, New York, USA) and controlled with CNC Software (MACH 3, ARTSOFT, Newfangled Solutions LLC, USA).

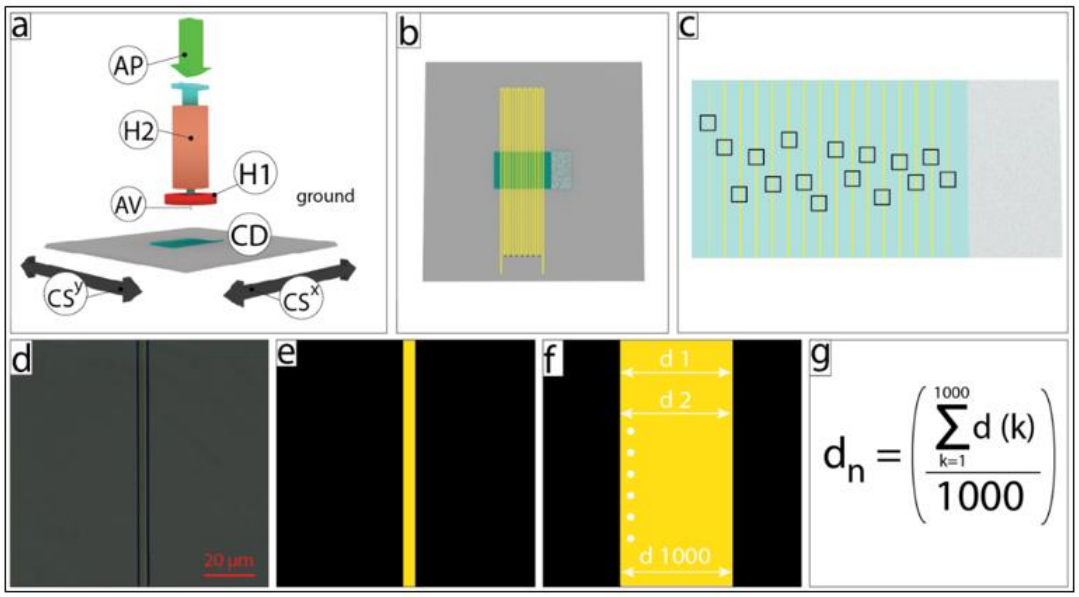

Figure 12: schematic representation of (a) MEW device, comprising applied pressure (AP), heating configuration (H1) and (H2), applied voltage (AV), spinning distance (SD) and collector speeds in x (CSx) and y (CSy) direction; (b) aluminium plate with glass- slide and spinning path of fibres; (c) glass-slide with fibres and random spots of imaging (black squares); (d) single image of fibre; (e) image after applied threshold calculation; (f) schematic description of operating principle of the Matlab code and formula for mean value (g).

The polymer was molten with H2 kept constant at 75°C and H1 varying respectively to the experiment. Similarly, AP, AV, CD and CS were adjusted in accordance to the systematics of the study, (Fig. 11.c). Linear structures (Fig. 11.b) were printed on the microscopic glass slides for all 27 variations (n=3) each followed by a stabilisation phase of 180 seconds after changing the parameters. An inverted bench-top light microscope (Eclipse Ts2R, Nikon, USA) was used to image the slides respectively, capturing each fibre under a constant illumination (Fig. 11.c). The resulting pictures were automatically analysed with an in-house programmed Matlab code. It initially defined a threshold to differentiate between polymer and background. Subsequently for each of the 1296 resulting images, 1000 vectors perpendicularly arranged to the fibres axis were generated to compute the mean diameters (Fig. 11.d. to .g).

Orthogonal design studies for electrospinning are known from the MES literature, however solely been focused on three [188] and four [170] system parameters. Based on targeted direct writing applications, the presented study additionally investigates CS, which represents one additional factor of the experiment alongside CD, AP, MT and AV. These, in turn, were individually subdivided into three levels as shown in (Fig. 12.b) Minitab Statistical Software (Minitab 17, United Kingdom, Free Trial) was used to generate an orthogonal design array to perform 27 different experiments (n=3), (Fig 12.c).

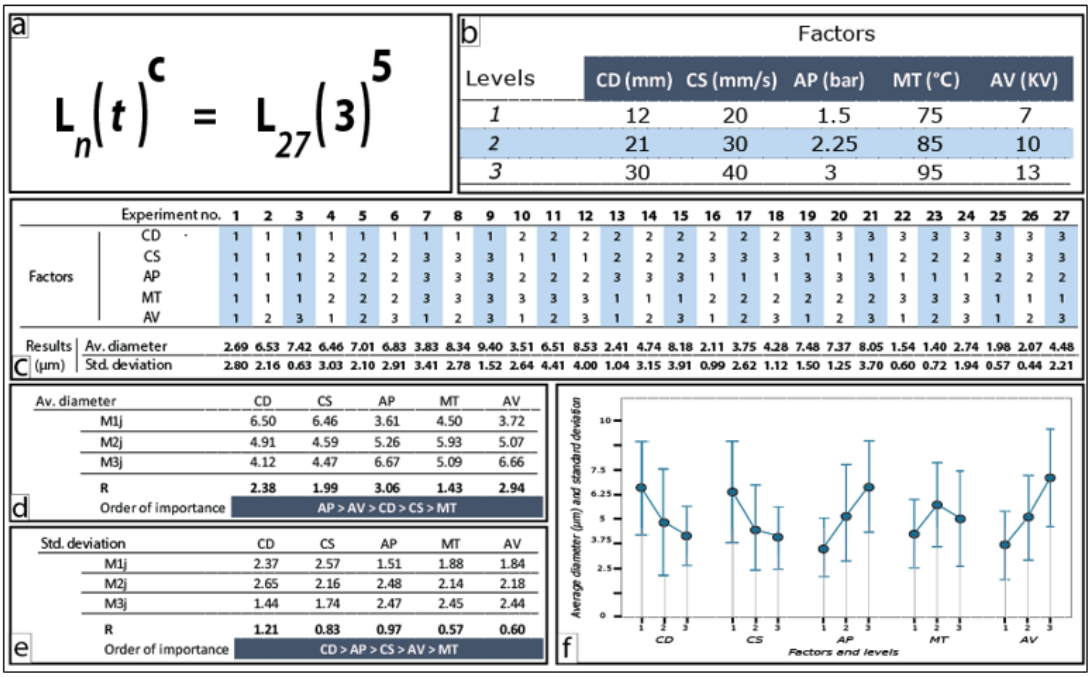

Figure 13: a) formula for generating the experimental design, b) with levels and respective factors for the five parameters and c) generated design table with resulting diameter and individual deviation. Figure d) and e) show the resulting R values hierarchically for diameter and deviation respectively and graphically illustrated in f)

Figure 12.d and 12.e summarise the results, where for instance, the value of M1j is composed of the sum of the results of the row "j" at level "1" and divided by the number of occurrence. M11 therefore, shows the value of 6.50, summarising all values of the row of CD, which are assigned to the first level. R refers to the difference between the maximum and the minimum values of the respective *Mij* row, for instance 2.38 at the average diameter of CD (6.50 (M11) – 4.12 (M13) = 2.38). In accordance to the orthogonal design the larger the R value, the more decisive a parameter influences the targeted outcome.

With regards to the average diameter (Fig. 12.d), the results revealed the appearing hierarchy: AP (3.06) is the most influencing parameter within the investigated ranges, while AV (2.94), CD (2.38), CS (1.99) and MT (1.43) follow in order of importance. The similar procedure was conducted for the standard deviation (Fig. 12.e) and demonstrates that CD (1.21) is the most influential parameter, followed by AP (0.97) and CS (0.83); while AV (0.60) and MT (0.57) differ marginally. The effect of the applied temperature appears to have the lowest influence on the average fibre diameter and can be explained via its strong influence on the current state of viscosity. Generally, temperatures above the polymer's specific melting point successively induce enhanced flow. In comparison to a solidified state, this behaviour is based on

decreased viscosity arising from a greater amount of freely floating molecular chains [170]. Since low viscosities represent a prerequisite for MEW applications in parallel to considering PCLs melting point of 60°C, the lowest temperature applied, (level 1 = 75 °C), already generates a respectively low viscosity, with minor potential changes appearing at elevated temperatures for the second (85°C) and third level (95 °C). This might indicate, that the applied temperature at all three levels shows the least influence on the final average diameters, including similar results to be observed for the standard deviation. Hereinafter, (Fig. 12.f) reveals decreasing average diameters at altering CS alongside with a falling standard deviation. As discussed in chapter 4.3., moving collectors induce increased fibre stretching. This is particularly evident at lower viscosities, which appear in the section closer to the Taylor cone and thus, are more prominent at a smaller CD. Conversely, the average diameter significantly decreases at greater CD, potentially provoked through extended travelling times, which lead to increased stretching. Against expectations, the average diameter increases with the AV increments (M1j = 3.72, M2j=5.02, M3j=6.66), however, can be explained as follows: the inversely proportional relationship between CD and AV determines the electrical field strengths, and, within this study, CD was set to 12mm at factor level one and altered up to 30 mm at level three, which corresponds to a 250% increase. This, in turn, effectively lessens the electrical field strengths, resulting in a corresponding decrease of fibre acceleration forces, thus leading to thicker diameters despite altering voltage. The AP appeared as expected and complies with predictions from literature, as increases are seen to result in larger diameters.

For most biomedical applications, it is beneficial to fabricate thin fibres, based on their particular advantages, such as significant increases in surface to volume ratios, as discussed in chapter 1.2. Therefore, the minimum R value (Fig. 12.f) represents optimal spinning conditions. In order to reach small fibre diameters, greater working distances in addition to higher speeds result in maximum stretching of the collected fibres. However, a loss of accuracy in aligning fibres to well-ordered architectures at high speeds and great distances must be considered by the user. Additionally, AP at its lowest value produced the thinnest fibres, based on less polymer delivered to the Taylor cone, described in chapter 4.3.

Following the order of an orthogonal design study, the effects of five system parameters for MEW applications and its systematic variations were individually examined. The final images were subjected to automated diameter recognition

programs, which indicate deviations of the results for AP, CD and CS. However, MT showed least influence on the morphology, which potentially might be attributed to the minimal effect of the small temperature increase steps (10 C) to dramatically change the viscosity of the polymer. In-homogeneities between single batches lead to the suggestion to increase the monitoring times in the framework of more in-depth studies. In the future, additional process understanding can be obtained by considering pair-wise interactions between the three factors.

2.7 FUTURE PERSPECTIVES – STEPS FROM BENCH TO BEDSIDE

Based on a rising number of publications, we foresee continuing innovations within the fields of MEW and the biomaterials and biomedical engineering community. To this date, however, the technology still remains in its infancy with currently no translation to a broader industrial level [26]. One major roadblock hampering this transition from bench to bedside is the high level of technological complexity of electrospinning with polymer melts. This, in turn, acts as a barrier for fundamental process optimisation to underpin the necessary technological foundation for successfully transferring the know-how from the laboratory scale and in-house designed and built equipment to machines which also can operate on commercial scale [41]. From a technological perspective, the lack of standardised hardware and techniques leads to a poorer general understanding of the process. In fact, only half-a-dozen of groups actively conduct research on in-house designed electrospinning devices, which all implement different hardware components and make use of only a small number of polymers. Consequently, a plethora of scientific findings are published which all differ to a smaller and greater extent and are therefore challenging to compare. This strongly impedes the adaption of standards for the hardware, software and biomaterials used in MEW [26]. As a greater degree of standardisation becomes more commonplace amongst MEW devices, it is expected that these changes will trigger further advancements in regards to in-process control. This will form a basis for future developments, in line with currents trends in ABM. Furthermore, improvements in process control will facilitate the development of high throughput machines for applications on a broader industrial level.

Multiphasic scaffolds

A recent development in scaffold design for TE&RM has been the fabrication of multiphasic scaffolds [189, 190]. A multiphasic scaffold can be defined as a construct that incorporates variations in architectural organisation (porosity, pore morphology and interconnectivity, etc.) and/or chemical composition, which aims to recapitulate the structural organisation of the target tissue to an extent that the tissue formation is biomimetically guided. It can be predicted that in future work novel machine designs, which will incorporate MEW with other ABM principles, will facilitate the design and fabrication of multiphasic scaffolds. The fabrication of multiphasic scaffolds will be realised via combining conventional AM technologies with melt electrospinning to obtain an optimal trade-off between mechanical-structural requirements under an appropriate level of porosity. In 2008, three different groups individually conducted studies on fabricating bimodal scaffolds, consisting of FDM fibres combined with electrospun meshes [191, 192]. Recently, Yang et al. described the fabrication of so-called hybrid scaffolds, where FDM printed patterns meet the required mechanical properties, while electropsun lattices generate high surface areas to promote a micro-environment for enhanced cellular activities [193]. Similarly, Kang et al. combine randomly aligned melt blown fibres to provide sufficient mechanical strengths with electrospun polymers and obtain a porous mesh to create a barrier for bacterial invasion [194]. These examples illustrate the capabilities and potential of combining ABM technologies. Recent approaches in biomedical research also demonstrated that melt electrospun lattices are implemented to act as the mechanical-structural reinforcement, often used for soft tissue applications. Kim et al. combined electrospinning polymer melts with solutions, where former determined the structural properties and were supported by a solution electrospun non-woven mesh [147]. Similar approaches were conducted by Li et al. [78], aiming at enhanced efficiency for filtration products, where the supporting part was fabricated through melt electrospinning with a multi-needle MES device. Bock et al. functionalised biodegradable micro-fibre meshes by coating melt electrospun fibres with micro particles for enhancing the control of carrying and releasing proteins [17]. Recent publications reveal the use of well-ordered PCL scaffolds fabricated by means of MEW as the supporting structures for hydrogels [173, 195]. The implementation of MEW fibre reinforcement into mechanically less rigid hydro-gels leads to a 35-fold-increase in the compressive Young's moduli. Based on a strong demand to closer

2.7.1

mimic natural tissues, these approaches exemplify future directions in the biomaterials and TE&RM field and are supported by the capabilities to fabricate smart and functional hierarchical polymer structures [4].

However, all aforementioned techniques are additive processes, which can solely be performed through composing the products as results from different fabrication techniques and mostly imply the transfer of the products between different devices. Thus, major drawbacks not only exist in the time- and cost-intense nature of the process, but also in a decrease in quality. Further, loss of accuracy and sterility evolve due to exposing the fabric to environmental conditions. One imminent direction to circumvent these drawbacks while fully benefitting from the potential of other existing technologies, will be a combination of the MEW with other manufacturing techniques into one integrated multi-operational printing unit. Further, we assume great potential in functionalising the extruded material itself. Prior to extrusion, selected sub-micron sized particles, added to the polymer will increase the operational performance during printing. For instance, it was shown, that the addition of antioxidants to PLA significantly improve thermally induced polymer degradation behaviour [130] or enhanced stretching can be achieved via viscosity lowering PEG and PDMS particles integrated into PP [132]. Moreover, adding micro particles to electrospinning with polymer melts allows the achievement of particular functional behaviour of the polymer after printing. Here, for example, distinct additives such as inorganic strontium-substituted bio-active glass (SrBG) blended with PCL deliver effectively lasting nutrients to osteoclasts at subsequent in vitro applications [196]. Based on its prominent demand in the TE&RM field, the processing of natural polymers, such as collagen moves into the focus of electrospinning research [26]. Electrospinning with polymer melts also bears great potential of varying the current fibre diameter through in-process parameter variations. For example, it is conceivable, that the next generation of scaffolds provides altering wall thicknesses facilitated via gradually descending diameters. Varying technical requirements on the printing-unit exist, such as maximum applicable temperatures for organic materials or the necessity to reach relatively high temperatures for polymers like PP. Therefore, the design of a precisely adaptable and mechanically stable MEW print head is crucial. In view of all of these considerations, it is noteworthy that a successful realisation of multiphasic TE constructs is only feasible in parallel to the development of software packages. This must not only comprise advanced motion control, but also an in-process control of the

prevailing system parameters. This will facilitate the fabrication of scaffolds to find an adequate balance between mechanical properties and space for effective cell growth [197].

Upscaling MEW

2.7.2 Compared to commercially exploited fibre forming techniques, electrospinning demonstrates a low production rate [198], which represents one major bottleneck in a breakthrough for broader industrial use [51]. Interestingly, the effective material throughput of electrospinning melts is significantly higher than with solutions, since here 90%-99% of the solvent, incorporated in the material, evaporates during the flight phase, compared to a 100% arriving at the collector with melts [95]. However, production rates of electrospinning are still limited in contrast to industrially used fibre spinning technologies such as Melt Blowing, Bio Component Spinning, Force Spinning or Flash Spinning [199]. Based on the need of additional heating elements, machines for electrospinning with melts slightly exceed the acquisition costs of devices for solution electrospinning, however, by far are not as cost-intensive as required to setup other fibre forming technologies [125]. In electrospinning research, the majority of multiple needle designs is seen at SES [200, 201], whereas in MES it is less commonly utilised: Li et al. demonstrate a novel electrospinning design approach comprising a round umbrella-shaped print head [51]. Despite the establishment of various Taylor cones at the same time along the outer ring of the print head with significantly enhanced material output, the circular fibre deposition is not suitable for direct writing applications. In 2012, Fang et al. show a melt electrospinning setup consisting of a conductive rotating disc, which dips into a polymer reservoir on the lower portion and releases a fibre to an electrically charged collecting platform on the opposite side. This concept bears great potential towards upscaling by assembling multiple discs in line [125]. Hacker et al. significantly increase the mass throughput with a novel print head design for the textile industry, comprising of 64 individually arranged nozzles in a square platform [50]. A line-like laser operated printing unit for elelctrospinning applications was introduced by Shimada et al., which demonstrates multiple Taylor cones in line, generated of a polymer sheet, which is fed to the orifice [163]. This approach is a further evolution of print heads utilising laser heating techniques. Similarly, Komarek et al. also reveal a linear print head geometry, referring to a “cleft”-like design, which aligns multiple Taylor cones in a row [126]. In general,

several approaches exist aiming at tackling one of the most contemporary drawbacks of electrospinning with polymer melts, namely to increase the throughput and production rate. To our knowledge, however, these did not transfer to industrial applications yet. Furthermore, , these concept do not comply with the requirements for direct writing applications, despite significantly increasing the output, based on their physical working principles as well as geometrical setups. In order to tackle this challenge, we foresee multiple Taylor cones in a row, which are extruded under controlled conditions to facilitate the fabrication of well-ordered lattices over large batch sizes. Within this purpose, several challenges must be considered: particular attention is required in finding a threshold regarding the inter-needle distance in correlation to the applied voltage. The closer the extrusion units are assembled, the higher the actual number of the fibres, and thus higher throughput could be expected. On the other side, the effects of the electrical field perpendicularly to the axis of the fibre are seen as a challenge, as too closely arranged needles induce parallel voltage peaks and introduce forces of mutual attraction, which deflect neighboured fibres and hence, disrupt the generation of a straight flight paths [198, 202]. Furthermore, industrial applications involve unlimited production, which in electrospinning research it was mainly realised via screw-driven extrusion (see chapter 4.2.1). One promising approach for MEW is shown by Mota et al., presenting a screw-extruder-based additive manufacturing system to fabricate ordered layer-b-layer constructs [160]. As described in chapter 4.1.1, equally applied pressure on all polymer chambers within one system represents a key factor in obtaining consistent fibre diameter distributions without major deviations [50]. The existing difficulties in MEW for single print head applications, described previously, must similarly be tackled for multi-needle designs to reach stable and homogeneous extrusion. Stimulating higher commercial acceptance of melt electrospun structures will only become reality if an increase in the production rate can be realised.

2.8 CONCLUSION

There exists an increasing interest for biocompatible polymeric scaffolds with highly precise architectures - and inevitably - the establishment of a universal market for MEW devices is expected. Tackling technical complexity through optimised hardware and the establishment of in-process control is one key factor for further success. The technology also presents an exciting prospect for further development at an industrial

level, where enhanced throughput will not only generate great value for use in the fields of biomaterials and TE&RM, but also further contribute to applications in filtration, energy, textiles and environment.

2.9 DISCLOSURE

The authors have nothing to disclose.

Acknowledgments

2.9.1 This work has been financially assisted by the Cooperative Research Centre Cell Therapy Manufacturing, ARC Centre in Additive Biomanufacturing and supported by Institute for Advanced Study, Technische Universitaet Muenchen. Further, the authors gratefully acknowledge Dr. Daniela Loessner for support in designing figures and assistance with formatting of references

Chapter 3: Melt Electrospinning Writing of Three-dimensional Poly (ε-caprolactone) Scaffolds with Controllable Morphologies for Tissue Engineering & Regenerative Medicine Applications

Felix M. Wunner[1], Onur Bas [1,2], Navid Toosisaidy [1], , Paul D. Dalton [3], Elena M. De-Juan-Pardo [1], Dietmar W. Hutmacher[1,2,4,5,a]

Published in Journal of Visualized Experiments (2017)

[1] *Institute of Health and Biomedical Innovation (IHBI), Queensland University of Technology (QUT), 60 Musk Avenue, 4059, Kelvin Grove, Australia*
[2] *ARC ITTC in Additive Biomanufacturing, Institute of Health and Biomedical Innovation (IHBI), Queensland University of Technology (QUT), Kelvin Grove, Brisbane, QLD 4059, Australia*
[3] *Department for Functional Materials in Medicine and Dentistry, University of Würzburg, Pleicherwall 2, 97070 Würzburg, Germany*
[4] *Institute for Advanced Study, Technical University of Munich (TUM), Lichtenbergstraße 2a, 85748 Garching, Germany*
[5] *George W Woodruff School of Mechanical Engineering, Georgia Institute of Technology, 801 Ferst Drive Northwest, Atlanta, GA 30332*

[a,] Corresponding author at: Institute for Health and Biomedical Innovation, Queensland University of Technology, 60 Musk Avenue, Kelvin Grove 4059, Australia. E-mail addresses: dietmar.hutmacher@qut.edu.au (Dietmar W. Hutmacher).

.

Statement of Contribution of Co-Authors for

Thesis by Published Papers

The authors listed below have certified* that:

1. they meet the criteria for authorship in that they have participated in the conception, execution, or interpretation, of at least that part of the publication in their field of expertise;
2. they take public responsibility for their part of the publication, except for the responsible author who accepts overall responsibility for the publication;
3. there are no other authors of the publication according to these criteria;
4. potential conflicts of interest have been disclosed to (a) granting bodies, (b) the editor or publisher of journals or other publications, and (c) the head of the responsible academic unit, and
5. they agree to the use of the publication in the student's thesis and its publication on the QUT ePrints database consistent with any limitations set by publisher requirements.

Melt Electrospinning Writing of Three-dimensional Poly (ε-caprolactone) Scaffolds with Controllable Morphologies for Tissue Engineering & Regenerative Medicine Applications (published in Journal of Visual Experiments, 2017)

Contributor	Statement of contribution
Felix Wunner QUT Verified Signature **Signature** **Date** 17/11/2017	Conceived and designed the experiments. Aided experimental work. Co-wrote the manuscript.
Onur Bas QUT Verified Signatures	Conceived and designed the experiments. Aided experimental work. Co-wrote the manuscript.
Navid Toosisaidy	Co-wrote the manuscript. Aided experimental work
Paul D. Dalton	Co-wrote the manuscript and provided feedback.
Elena M. De-Juan-Pardo	Co-wrote the manuscript and provided feedback.
Dietmar W. Hutmacher	Conceived and designed the experiments. Provided feedback on the manuscript. Supervised the entire work. Approved the final version of the manuscript.

Principal Supervisor Confirmation

I have sighted email or other correspondence from all Co-authors confirming their certifying authorship.

Dietmar W. Hutmacher QUT Verified Signature

Name Signature Date 17/11/2017

3.1 SHORT ABSTRACT

This protocol serves as a comprehensive guideline to fabricate scaffolds via electrospinning with polymer melts in a direct writing mode. We systematically outline the process and define the appropriate parameter settings for achieving targeted scaffold architectures.

3.2 ABSTRACT

This tutorial reflects on the fundamental principles and guidelines for electrospinning writing with polymer melts, an additive manufacturing technology for biomedical applications. The technique facilitates the direct deposition of biocompatible polymer fibres to fabricate well-ordered scaffolds in the micron- to nano-scale range. The establishment of an electrical field around a viscous polymeric bubble provokes the ejection of a jet which is accelerated towards a grounded collector and deposited as a continuous fibre according to its relative movement. One major benefit of the resulting porous scaffolds is a typically high surface to volume ratio which provides increased effective adhesion sites for cell attachment and growth. Controlling the printing process by fine-tuning the system parameters enables high reproducibility in the quality of the printed scaffolds. It also provides a flexible manufacturing platform for users to tailor the morphological structures of the scaffolds to their specific requirements. For this purpose, we demonstrate a protocol to obtain different fibre diameters via melt electrospinning writing through a guided amendment of the parameters, such as flowrate, voltage and collection speed. Further, we demonstrate pathways to optimise the jet, discuss often experienced technical challenges, explain troubleshooting techniques and showcase the wide range of printable scaffolds architectures.

3.3 INTRODUCTION

The manufacture of three-dimensional (3D) biocompatible structures for cells is one of the key contributions of additive biomanufacturing to tissue engineering (TE), aiming to restore tissues by applying customised biomaterials, cells, biochemical factors, or a combination of them. Therefore, the main requirements of scaffolds for TE applications include: manufacturability from biocompatible materials, controllable

morphological properties for targeted cell invasion and optimised surface properties for enhanced cell interaction [42].

MEW is a solvent-free manufacturing technique that combines the principles of additive manufacturing (often called 3D printing) and electrospinning for the production of polymeric meshes with highly ordered ultrathin fibre morphologies [26]. It is a direct writing approach and accurately deposits fibres according to preprogramed codes [31], referred to as G-Codes. Melt electrospun constructs are currently prepared using a flat [75, 203] or a mandrel [76, 124] collector to fabricate porous flat and tubular scaffolds, respectively.

This technique offers significant benefits to the TE and regenerative medicine (RM) community due to the possibility to directly print medical-grade polymers, such as poly(ε-caprolactone) (PCL), which presents excellent biocompatibility [16]. Other advantages are the possibility to customise the size and distribution of the porosity, by depositing the fibres in a highly-organised manner to fabricate scaffolds of high surface-to-volume ratios. Before MEW can be performed, the polymer first requires the application of heat [30]. Once in a fluid state, an applied air pressure forces it to flow out through a metallic spinneret that is connected to a high voltage source. The force balance between the surface tension and the attraction of the electrostatically charged droplet to the grounded collector leads to the formation of a Taylor cone followed by the ejection of a jet [99].

Images and a schematic drawing of the in-house build MEW device used for this protocol are shown in Figure 13. It additionally demonstrates the principles of using insulating tape to avoid electrical discharge between the heating elements and the electrically charged brass part surrounding the spinneret. Insufficient insulation would lead to internal damage of the implemented hardware.

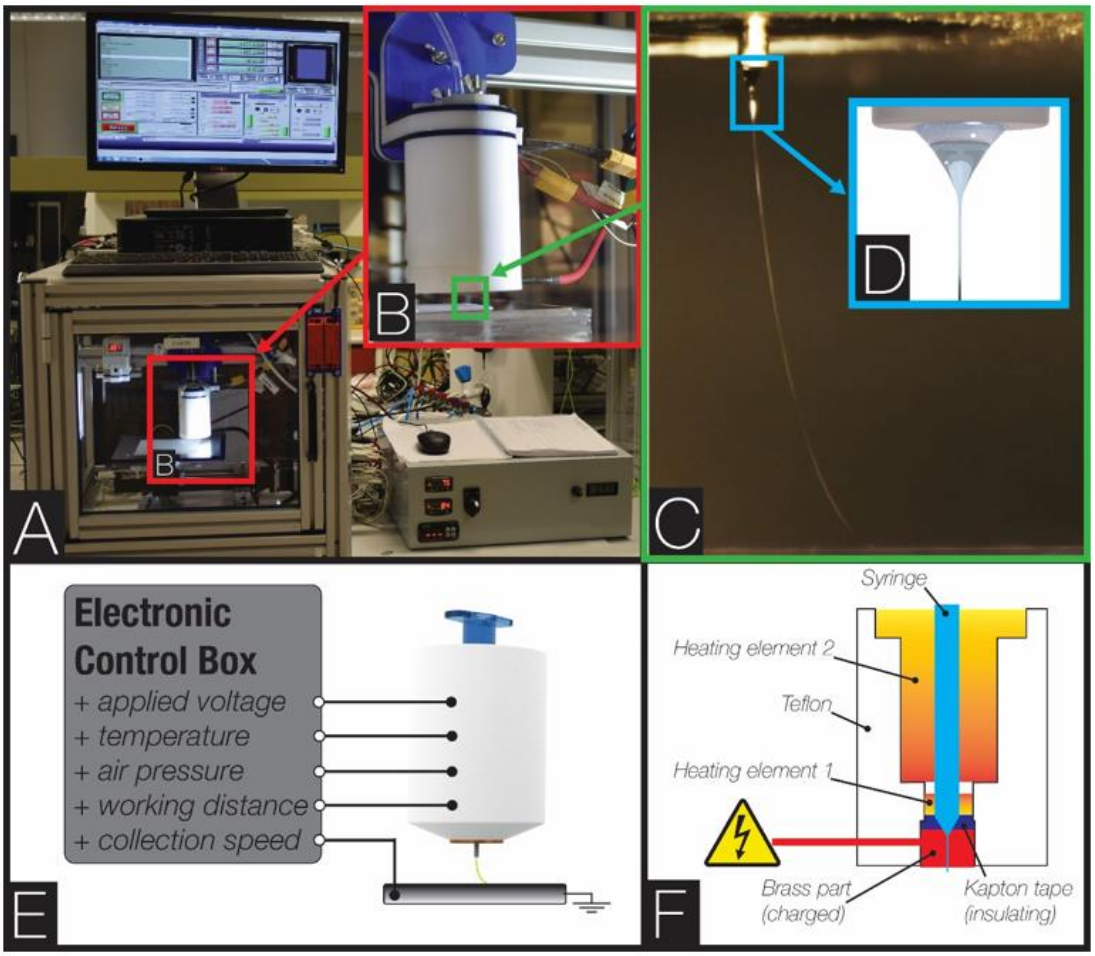

Figure 14: MEW setup (A) including a PC, the printing unit and the electrical control box, (B) the head and the collector, (C) the fibre in a perfectly balanced flight phase and (D) a schematic illustration of a Taylor cone. (E) shows a schematic of a printer and lists the five most prevailing system parameters, including "applied voltage" (High Voltage Generator, EMCO High Voltage Co., DX250R, USA), "temperature" (Temperature Controller, WATLOW, PM9R1FJ, USA), "air pressure" (Pressure Regulator, SMC Pneumatics Pty Ltd., ITV1050-31N2L, USA), "working distance" (adjustment via in-house designed movable z-axis) and "collection speed" (X and Y positioning slides, VELMEX Inc, XN-10-0020-M011, USA). (F) demonstrates the design of the insulation system within the print head via a "KAPTON tape"(Heat Resistant Polyamide Tape, 3 layers, DuPont, KAPTON MT, USA). This prevents arcing between the "heating element 1" and the charged "Brass part".

Depending on the adjustment of the three system parameters temperature, collection speed and air pressure, MEW enables the fabrication of fibres with different diameters, explained in the discussion section.

In most cases, however, fine-tuning and optimisation of the jet will be required before a stable jet will be ejected. The visualisation of the electrified travelling jet is an effective way to verify the consistency and homogeneity of the process. In an ideal case, the flight path resembles a catenary curve acquired as a result of a force balance controlled by the system parameters[204]. Further, the micro- and macro-structure of the scaffolds is dependent on the flight path of the polymer jet [205]. A detailed table

of different deflection behaviours and measures for optimisation is given in the discussion section.

In the present study, we present a protocol that describes the fabrication steps for the manufacture of highly controlled fibrous scaffolds using MEW technology. In this work, medical grade PCL (Corbion Purac, PURASORB® PC12, molecular weight 95-140kg/mol) was used, as this medical grade PCL has improved purity over technical grade, and its mechanical and processing properties are excellent for MEW. Broad melt processing range of PCL originates from its low melting point (60°C) and high thermal stability. Moreover, PCL is a slow-rate biodegradable polymer, which makes it an excellent material for many tissue engineering applications [206].

For this study, the temperature and collector distance will be kept constant (65°C and 82°C for the syringe and spinneret temperatures (respectively) and 12 mm for the collector distance); applied voltage, collector speed and air pressure, however, will be varied to fabricate fibres with targeted diameters. A detailed list of published studies using MEW scaffolds is provided in the results section and reveals different applications for the fields of TE and RM (Table 1).

3.4 PROTOCOL

3.4.1

Material preparation

I. Fill 2 g of PCL in a 3 mL plastic syringe with a funnel and insert a piston into the open end.

II. Place the syringe in a preheated oven at 65°C for 8 hours. Note: point the tip upwards to allow the air bubbles to aggregate close to the opening.

III. Push the piston with a thin object to release the trapped air within the molten material.

IV. Let it cool down to room temperature, which is achieved when the polymer is not transparent anymore after 10 minutes.

3.4.2

V. Store the PCL pre-loaded syringe at room temperature in a dry and dark environments until it is used

Hardware and software setup

VI. Attach a 23G flat tipped needle (spinneret) to the syringe and a barrel adapter at the other end to connect the syringe to the air pressure system.

VII. Place the syringe in the print head and press it down until the spinneret tip stands out 1 mm from the brass part on the bottom side of the head.

VIII. Mount a collector on the stage and clean the surface as well as the print head with 70% (vol/vol) ethanol to remove dust or residual polymer.

IX. Set the working distance by positioning a 12 mm high object between the spinneret and the collector and lower the print head until the spinneret tip just touches it.

X. Adjust the temperature regulators at the electrical box to 82°C and 65°C for the spinneret region and the syringe, respectively and power them on to melt the PCL.

XI. Wait for at least 10 minutes until the polymer is molten and initiate the air pressure by setting the regulator to 1.8 bar.

XII. Prepare the G-Code to define the size and shape, inter-filament distance and the number of layers of the scaffold and the collection speed of the process. Note: a detailed template for fabricating flat and tubular scaffolds is provided in the discussion chapter (Table 2).

XIII. Double-check manually that all ground cables are connected securely to the enclosure and the wall plug.

XIV. Start the software MACH 3 on the computer and upload the prepared G-code.

Scaffold fabrication

3.4.3

I. Close the front door of the enclosure, which connects the safety interlock and triggers the high voltage supply to the spinneret. Note: once the door is opened, for example when a print is finished or in case of an emergency, the high voltage drops and the scaffold can be removed safely.

II. Increase the high voltage gradually in 0.2 kV steps until a Taylor cone is formed and a fibre is ejected towards the collector (see exemplary Taylor cone in Figure 13.d).

III. Allow the polymer melt to be extruded on the still collector plate to stabilise the jet without movement for 5 minutes. Note: remove the pile of material before commencing a new print.

IV. Use the cursors on the keyboard to move the print head above the point where the G-codes will start.

V. Start the G-Code in the Mach 3 software on the computer

3.4.4

Fibre diameter adjustment

I. Keep the working distance (12 mm) and the temperature regulators (82°C and 65°C for the spinneret region and the syringe, respectively) on a constant level, as described before in steps 1.2.4 and 1.2.5. Note: a summary of adjusting different diameters is given in Table 3.

II. Print fibres with small sized diameters (3-10 µm): reduce the air pressure level to 0.8 bar, adjust the applied voltage to 8 kV and set the collector speed to 1700 mm/min.

III. Print fibres with medium sized diameters (10-20 µm): adjust the air pressure level to 1.5 bar, set voltage to 11 kV and lower the collection speed to 1200 mm/min.

IV. Print fibres with large diameters (20-30 µm): increase the air pressure level to 2.6 bar, alter the applied voltage to 12 kV and decrease the collection speed to 700 mm/min.

Jet optimisation

I. Illuminate the jet with a strong LED light from outside the enclosure for improved visibility.

II. Observe the behaviour of the fibre for 1 minute and adjust the system parameters to optimise the process in small steps, i.e. 0,1 kV for applied voltage, 100 mm/min for collection speed and 0,1 bar for air pressure. Note: a summary is given in Table 4.

3.4.5

III. Stabilise periodically deflecting behaviour by decreasing the air-pressure, increasing the speed and minimising the voltage until the flight path of the fibre resembles a stable catenary curve for more than 3 minutes.

IV. Correct the flight path of a lagging behind jet by increasing the voltage, reducing the air pressure and reducing the speed of the collector. Apply those measures until the flight path of the fibre moves back to a catenary curve shape.

V. Avoid fibres travelling vertically towards the collector by decreasing the applied voltage, increasing the speed of the collector and increasing the air pressure until the flight path of the jet retains the shape of a catenary curve again.

Scaffold collection

3.4.6

I. Open the door when the print is finished and use the cursor to move the collector plate towards the door for better accessibility.

II. Spray the scaffold with ethanol 70% (vol/vol) mix and wait 10 seconds until it visibly detaches from the collector.

III. Collect the finished scaffold by grabbing one edge with tweezers and lifting it out of the enclosure.

3.4.7

Troubleshooting

I. Decrease the applied voltage or open the door immediately if there is a spark between the spinneret visible or a cracking noise audible.

II. Remove all hazardous materials and liquids such as ethanol 70% (vol/vol) from the inside of the enclosure as a fire might ignite in case of potential sparking.

III. Program the G-Code accordingly that the spinneret moves away from the area where the scaffold is printed after all layers are done. Note: this avoids material accumulation above the point where the spinneret finally stops.

IV. Check the spinneret under a magnifier and verify that there is no damage to the spinneret as this will significantly influence the homogeneity of the Taylor cone

3.5 REPRESENTATIVE RESULTS

Two different methods of collection are commonly used in MEW, which are flat collection and mandrel collection. The resulting architectures depend on the programming of the G-Code (Table 2), which is executed by the Mach 3 software.

Flat collection: Applying flat collectors refers to the most common method and facilitates the direct deposition of material referring to the pre-programmed G-code. 0/90 and 0/60 structures of different sizes are widely reported in literature.

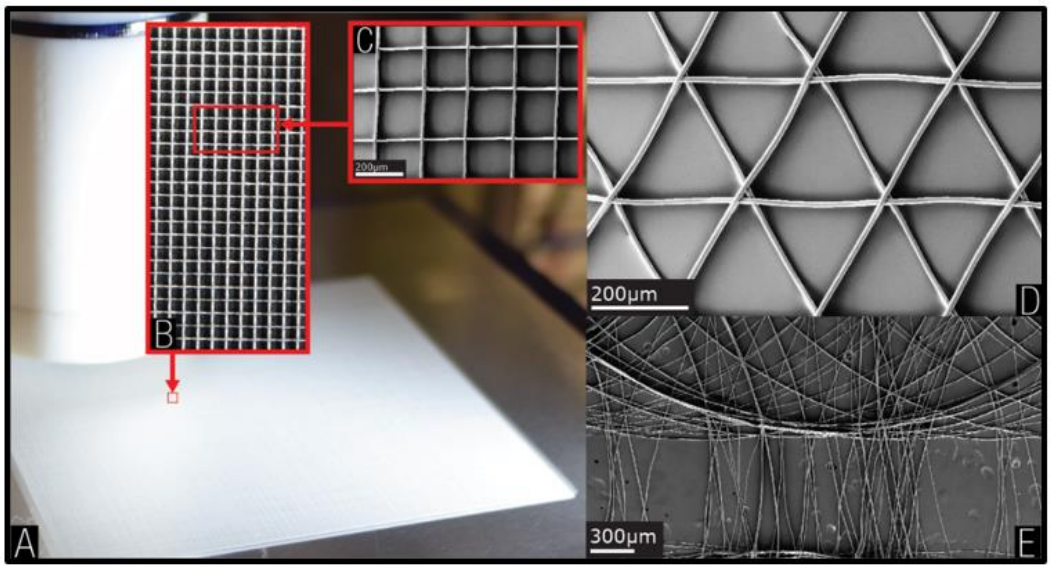

Figure 15: different scaffolds fabricated with a flat collector (A), 0/90 lattice (B) and the same lattice in greater resolution (C). (D) demonstrates a 0/60 structure and (E) a randomly controlled structure.

Furthermore, the capability of directly depositing molten fibres on the collector also facilitates the production of randomly yet organised structures when a patterned flat collector is used instead of a smooth one [25].

Tubular: There is a great demand for the manufacture of scaffolds with tubular architectures for TE applications. MEW is an effective method to achieve tubular scaffolds with customised porosity by utilising cylindrical collectors. These rotate along their own axis, while translating along the axis of the mandrel. Through fine tuning of the G-Code, the rotational as well as the translational speed is determined and the orientation of the fibres can be customised. Higher rotational speeds than translational speeds lead to radially orientated pores and vice versa. The total number of layers, distribution and morphology of the porosity will configure the mechanical properties of the scaffold. The inner diameter of the tubular scaffold will be determined by the external diameter of the implemented mandrel.

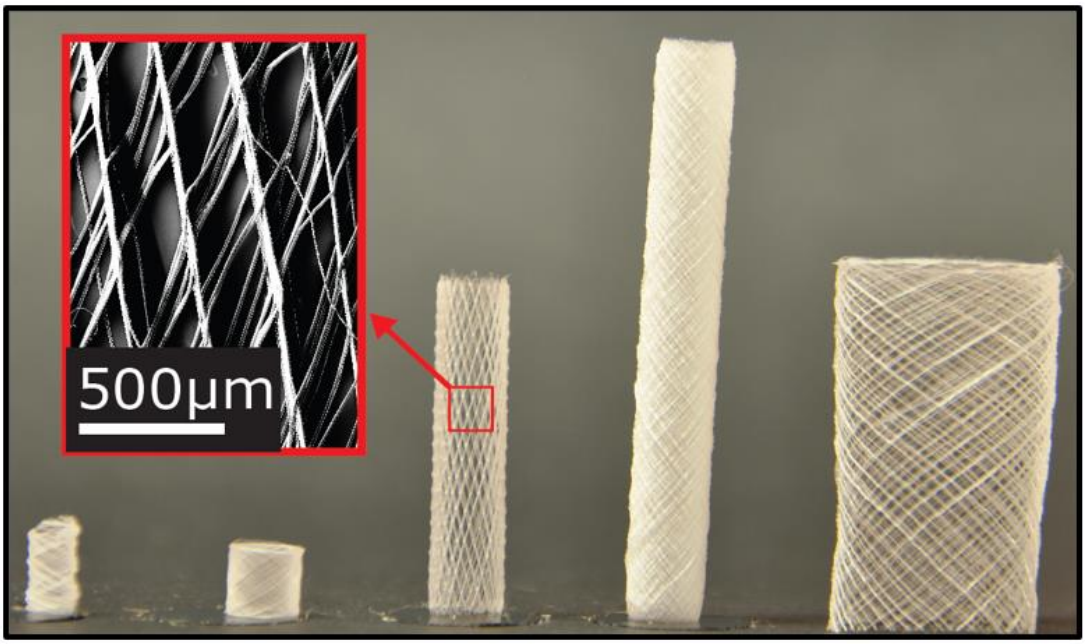

Figure 16: showcasing of different tubular scaffolds and one respective representative image from scanning electron microscopy (SEM).

The following table references to a list of studies, in which MEW scaffolds were fabricated and used for biological applications. The list provides results of implemented flat as well as tubular scaffolds.

Dermal fibroblast infiltration of poly(ε-caprolactone) scaffolds fabricated by melt electrospinning in a direct writing mode *(Farrugia et al., 2013)[75]* || *FLAT*
Dermal fibroblast seeded PCL MEW scaffolds are evaluated for cell infiltration.
A tissue-engineered humanized xenograft model of human breast cancer metastasis to bone *(Thibaudeau et al., 2014)[74]* || *TUBULAR*
Tubular MEW scaffolds are used to create a viable ectopic 'organ' bone in a mouse model to study human breast cancer metastasis to bone.
Species-specific homing mechanisms of human prostate cancer metastasis in tissue engineered bone *(Holzapfel et al., 2014)[207]* || TUBULAR
MEW scaffolds are used to create a tissue engineered bone for prostate cancer research.
Enhancing structural integrity of hydrogels by using highly organised melt electrospun fibre constructs *(Bas et al., 2015)[173]* || *FLAT*
MEW scaffolds with different lay-down patterns and poresizes are used to enhance the mechanical functionality of soft hydrogels.
Reinforcement of hydrogels using three-dimensionally printed microfibres *(Visser et al., 2015)[195]* || *FLAT*
Soft gelatin-based hydrogels are reinforced with MEW PCL scaffolds.
Melt electrospinning onto cylinders: effects of rotational velocity and collector diameter on morphology of tubular structures *(Jungst et al., 2015)[124]* || *TUBULAR*
The influence of the translational and rotational speeds on the final morphology of tubular MEW scaffolds are systematically investigated.
Hierarchically structured porous poly(2-oxazoline) hydrogels *(Haigh et al., 2016)[208]* || *FLAT*
MEW scaffolds are used as a sacrificial template to create a hierarchical 3D porosity network within a hydrogel.
A validated preclinical animal model for primary bone tumor research *(Wagner et al., 2016)[209]* || *TUBULAR*

MEW scaffolds are used to create humanized tissue engineered constructs for preclinical research on primary bone tumors.
Periosteum tissue engineering in an orthotopic in vivo platform *(Baldwin et al., 2017) [210] || TUBULAR*
A multiphasic scaffold consisting of a MEW mesh and a hydrogel is developed for periosteum tissue regeneration applications.
Dimensional metrology of cell-matrix interactions in 3D microscale fibrous substrates *(Tourlomousis and Chang. 2017)[211] || FLAT*
Cell-matrix interactions are investigated on MEW scaffolds with different architectures.
Endosteal-like extracellular matrix expression on melt electrospun written scaffold *(Muerza-Cascante et al., 2017)[212] || FLAT*
MEW PCL scaffolds are used to develop an endosteal bone-like tissue that promotes the growth of primary human haematopoietic stem cells.
3D printed lattices as an activation and expansion platform for T cell therapy (*Delalat et al., 2017)[19] || FLAT*
Scaffolds with different fibre spacing (200 µm, 500 µm and 1000 µm) are surface functionalised and seeded with T cells for expansion.
Biofabricated soft network composites for cartilage tissue engineering *(Bas et al., 2017)[213] || FLAT*
Biomimetic soft network composites consisting of a hydrogel matrix and reinforcing MEW meshes designed for articular cartilage repair are reported.
Via precise interface engineering towards bioinspired composites with improved 3D printing processability and mechanical properties *(Hansske et al., 2017)[214] || FLAT*
Magnesium fluoride nanoparticle reinforced PCL scaffolds fabricated by means of MEW are designed and developed for bone tissue engineering applications.

Table 1: list of publications using MEW scaffolds in either flat or tubular form.

3.6 DISCUSSION

Integrating AM in order to find innovative solutions for the challenges in the medical field presents a new paradigm for the 21st century. The so-called field of "Bio-fabrication" is on the rise and innovations in fabrication technologies enable the production of highly sophisticated architectures for TE applications. We believe that the electrospinning of polymer melts in a direct writing mode (here MEW) is seen as one of the most promising manufacturing candidates to comply with the needs of the TE community, where ordered structures of biocompatible materials in the micron to nanoscale are required [1].

This tutorial aims at generating fundamental knowledge of the operations of MEW by explaining the physical principles and demonstrating action steps in order to manufacture reproducible scaffolds using this technology.

Since the general principles of MEW are comparable to those of conventional additive manufacturing technologies, i.e. a targeted deposition of extruded material in a layer by layer manner, it is crucial to control the relative movement between the head and the collector. From our experience, we recommend to work with MEW devices that

keep a fixed head, while the respective movement of the collector is undertaken by the stages (X and Y). A fixated head remains in a stable position and does not generate kinematic forces, which would act on the Taylor cone and potentially lead to disturbances during its creation. In addition, the wiring associated with high voltage and heaters is not subject to sustained repetitive movement. The collector movement is defined by the G-Code, which needs to be uploaded in the Mach 3 software. This code, also known as RS-274, is widely used in the computer-aided manufacturing field to control the pathway of tools. For MEW applications with flat collectors, the G-Code file determines the movement and speed in X and Y direction; for cylindrical collectors or mandrel applications, the G-Code file defines both the translational (X direction) and rotational speeds. The following table explains the programming of a G-code in more detail.

CODE	EXPLANATION	ILLUSTRATION
G17 G21 G40 G49 G54 G80 G94	START OF PROGRAM	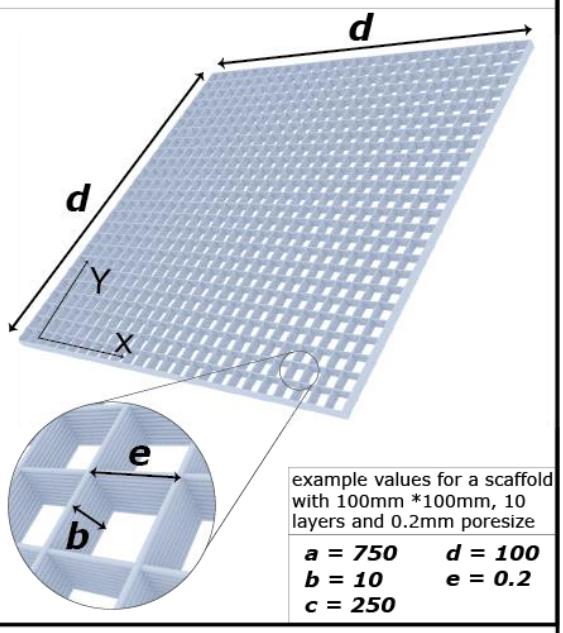
F***a*** G91	***a*** = speed of movement [mm/min]	
M98 p1236 l***b*** M30	***b*** = number of layers	
O1236 M98 p1237 l***c*** G1 x***d*** G1 y-***d*** M98 p1238 l***c***	***c*** = ***[d/2*e];*** number of repetitions	
O1237 G1 x***d*** G1 y***e*** G1 x-***d*** G1 y***e*** M99 O1238 G1 y-***e*** G1 x***d*** G1 y-***e*** G1 x-***d*** M99	***d*** = scaffold dimensions in X and Y [mm] ***e*** = interfilament space [mm]	
M2	END OF PROGRAM	

CODE	EXPLANATION	ILLUSTRATION
G17 G21 G40 G49 G54 G80 G94	START OF PROGRAM	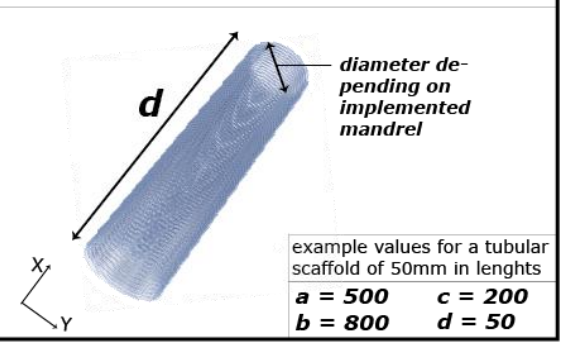
F***a*** G91	***a*** = speed of movement [mm/min]	
R***b*** G98	***b*** = rotational speed [rad/min]	
M98 p1236 l***c*** M30	***c*** = number of reptitions in X [mm]	
O1236 G1 x***d*** G1 x-***d*** M99	***d*** = scaffold dimensions in X [mm]	
M2	END OF PROGRAM	

Table 2: explanation of programming a G-Code for flat and tubular scaffolds, using a text file (.txt) to be uploaded in the Mach 3 software.

Compared to other additive manufacturing technologies, MEW enables the fabrication of fibres with various diameters by the adjustment of the system parameters temperature, collection speed and applied voltage, as described in the protocol.
In order to achieve small fibres (3-10 µm), it is advised to use low pressures, moderate voltages and high collection speeds. Generally, reduced pressure leads to less extruded mass. This is accompanied by a corresponding decrease in the surface area of the jet. Hence, smaller electrostatic forces are required to accelerate the mass of the fibre towards the collector, i.e. lower voltage needs to be applied. Additionally, comparable higher collection speeds lead to enhanced stretching of the fibre, causing an additional reduction of the final fibre diameter.

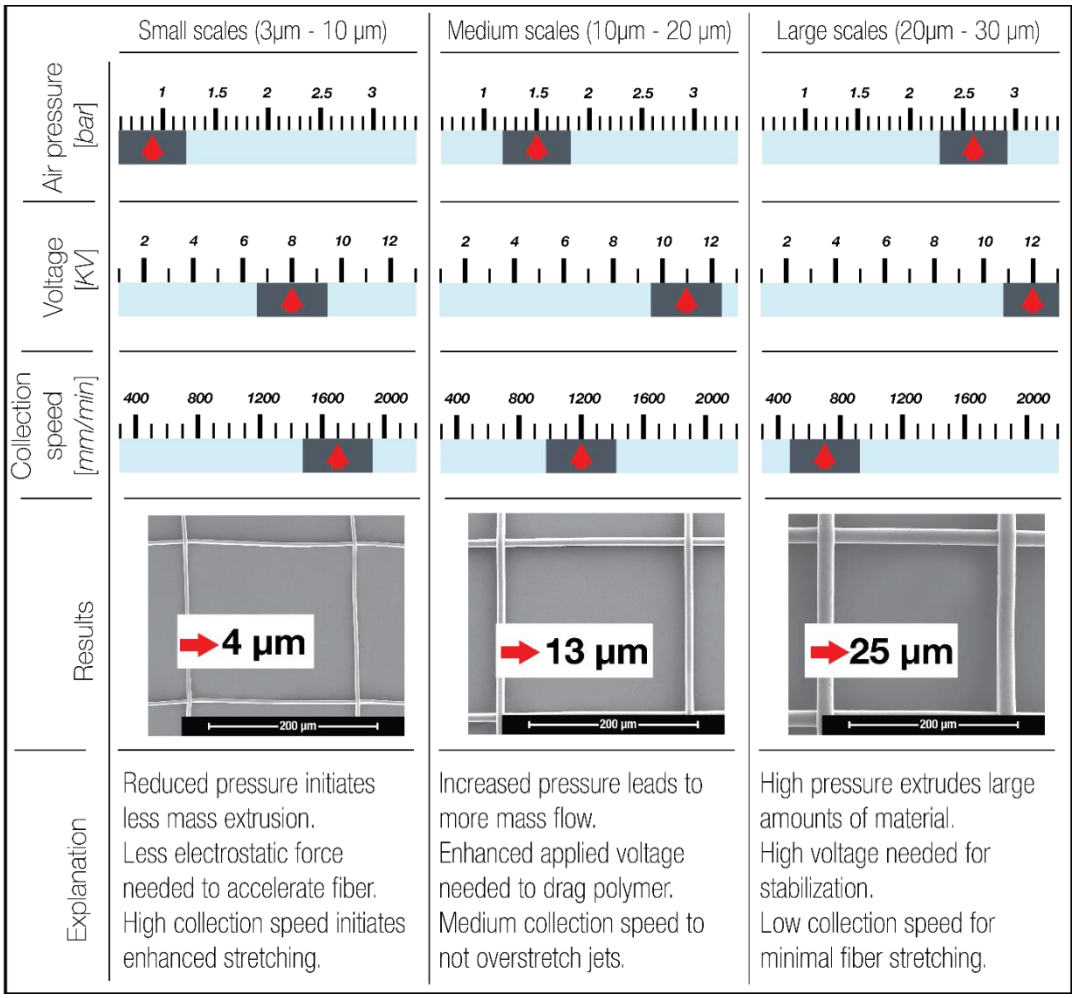

Table 3: representative values of the parameters air pressure, voltage and collection speed (temperature and collection distance constant) to reach three different diameter ranges (small, medium and large). The red arrows propose exact values within the respective categories to reach the fibre diameters.

Increasing the pressure induces more flow of molten polymer and thus, leads to larger fibre diameters (10-20 µm). In this case, greater electrostatic force is required to

compensate for the enlarged polymer surface (thicker fibres). In order to obtain a stable polymer jet stream, voltage must be altered and the collection speed should be reduced. Large fibre diameters (20-30 µm) require enhanced polymer extrusion, i.e. higher air pressure. This provokes relatively thicker fibres and is suggested to be applied in combination with higher voltage to supply sufficient electrostatic force on the fibre. Additionally, reduced collecting speeds induce less fibre stretching.

All three cases mentioned above, however, still require fine-tuning and optimisation to maintain a stable catenary curve shaped fibre over time, explained in the protocol. In MEW, only a perfectly balanced equilibrium between the forces determining the flow of the polymer mass and the forces attracting the jet towards the collector will eventually lead to reaching consistent scaffold morphologies [205, 215]. Hence, divergences of the pathway of the jet reflect strong deviations of the fibre diameter or inaccurate deposition. From our experience, three different variations in behaviour can be obtained.

First, a fibre can pulse, a phenomena, initially reported by the Dalton group [205]. An unbalanced distribution between delivered mass and respective drag-forces on the fibres result in a constantly overfed Taylor cone, which periodically releases accumulated polymer. This causes significant variability in the angles of the pathway and results in differing diameters.

Second, a lagging electrified jet occurs when the speed of the collector is higher than the extrusion speed of the jet. The final deposition of the jet happens far away from the vertical direction of the spinneret, causing a lagging jet stream. The flight path resembles an overemphasised curvature, which also minimises the dimensions of a printed scaffold.

Third, a buckling electrified jet is caused by the perpendicular impact of the jet onto the collector and manifests, when the collector speed is set slower than the speed at which the jet is flowing out of the spinneret. Applying high voltages can also cause buckling, by producing an excessive acceleration towards the collector and a straight flight path of the fibre. Undesired deposition of loops is observed in this case.

Means to re-stabilise the process are provided in the protocol and shown in the following table.

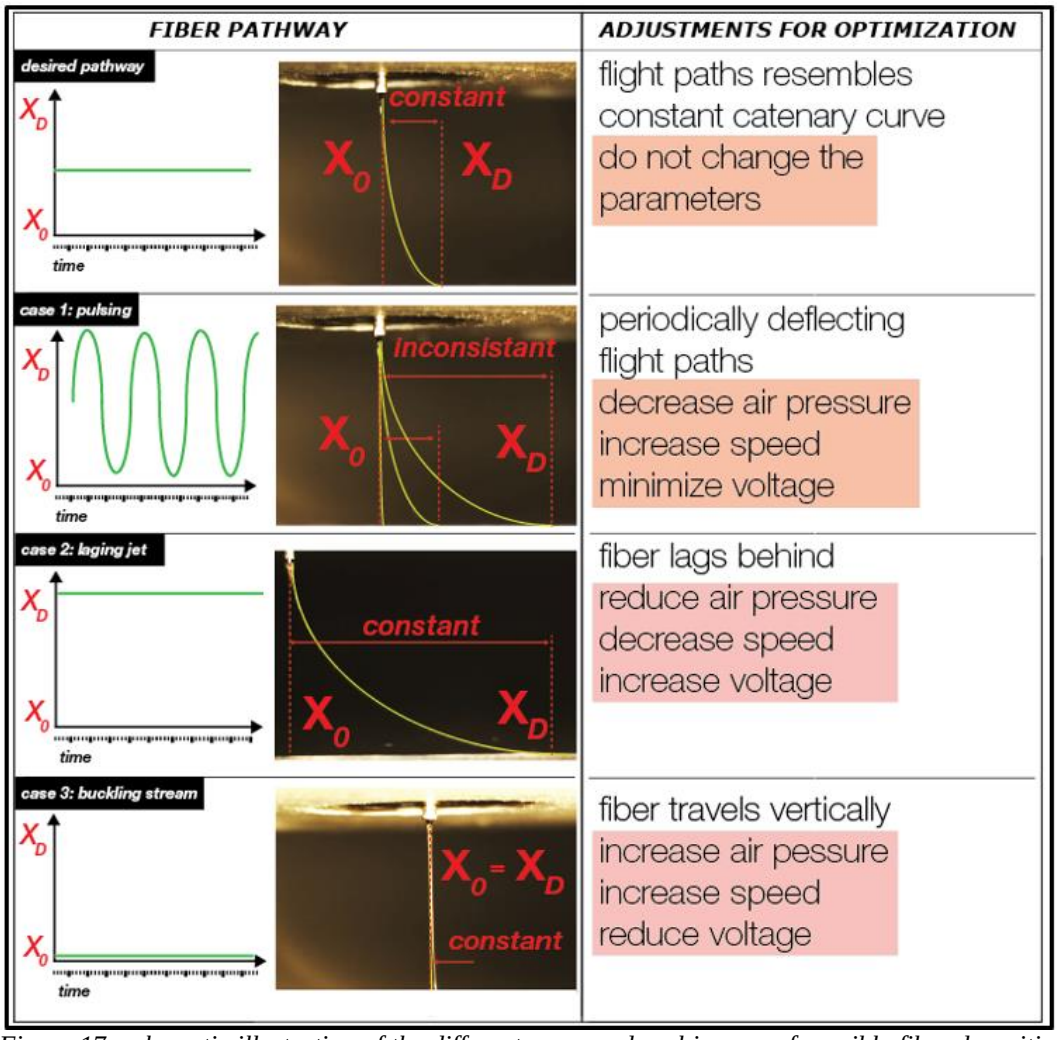

Figure 17: schematic illustration of the different cases and real images of possible fibre deposition at MEW as well as means to optimise.

From the perspective of scaffold implementation, multiple benefits exist when using PCL and MEW, such as biocompatibility, reproducibility through direct writing, or predesigned customisation of the resulting architectures. MEW can be conducted on any conventional laboratory bench, since it uses solvent-free polymer melts, therefore it does not require expensive fume hoods or exhaustive recycling of residual materials [64]. There is no odour when entering a room containing MEW devices.

Additionally, an achievable high surface to volume ratio within a porous scaffold is of great advantage and makes MEW scaffolds well suited for biological applications [38]. In comparison to well-known 3D printing technologies, such as Fused Deposition Modelling [216], MEW has limitations in printable heights of ordered structures. The reason is seen in the inherent process of applying electrostatic forces, which traps mobile charge carriers within the deposited fibres. Once the height of scaffolds exceeds approximately four mm, it is reported that the sum of the excess charge

accumulated within the scaffold acts repelling for upcoming fibres [217]. Subsequently, in most cases, the resulting top layers are significantly distorted.

Another difference to conventional 3D printing technologies lies in the fact that the deposition of material during the process cannot be interrupted and solely stopping all system parameters eventually holds material extrusion. This represents a design limitation and must be regarded when programming the G-Code. While the jet initiation can be performed mechanically [218], G-Code programming needs to consider a continuous direct-writing approach.

Increasing the throughput and process efficiency of MEW also remains a challenge and represents the main reason in our view and others', why this technology has not been up-scaled to industrial level yet [50]. First, the MEW process is inherently low in throughput due to the low flow rates and limited collection speeds. Both aspects, however, are essential to ensure the controlled deposition of the jet and reproducibility in the printing. Indeed, the maximum collection speed during the printing process is restricted to the physical boundaries of the material used, i.e. too high speeds would cause breakage of the jet when the drag forces exceed feasible limits. Another strategy to upscale relies on using multi-extruding MEW devices, i.e. machines with multiple printing heads in close distance to each other; however, these multi-heads would cause interferences between the electrical field of each head, and subsequently distort the final fibre deposition [198]. Needleless melt electrospinning heads have generated a significant number of electrified jets[51], although controlling the exact placement of the direct-written fibres could be difficult to achieve. Future developments towards increasing the efficiency of MEW, however, would not only benefit the biomedical community, but also the industries of filtration, textile, or applications for energy [26].

Although this tutorial provides guidelines to fabricate customized scaffolds under the proposed parameter settings, it must be noted that minor dependencies on environmental conditions, such as room temperature or humidity exist and might lead to unintended deviations [219]. The results presented in this tutorial are based on know-how accumulated at the Hutmacher group, conducted in stable environmental conditions within controlled laboratory spaces.

PCL is the most prominent candidate for MEW. From an engineering perspective, its low melting point (60°C) is beneficial as this does not require the challenging implementation of high temperature heaters (>>100°C) in close distance to high voltage sources. On a material engineering level, PCL is semi-conductive and provides

strong macromolecular cohesion both as a fluid and as a solid. Despite strong mechanical stretching, the viscous material bonds to a certain degree, which results in prominent fibre thinning when increasing collector speed or applied voltage. Conventional melt electrospinning without moving collectors has been reported with different polymers, such as Polypropylene, Polyethylene or Nylon [30]. The application of direct writing principles however, has predominantly been reported with PCL and some PCL blends with additives to further lower its viscosity [95], although there are exceptions [162, 220]. In the future, however, we foresee a wider range of materials processed by MEW. This, in turn, will imply the upgrade of hardware components for this technology, as for example processing polypropylene (melting point at 160°C) alters the current technical requirements of the hardware of MEW devices.

An increasing interest in biocompatible polymeric scaffolds with highly precise and controllable architectures exists MEW, to this date, represents the only technology, which, in comparison to other biomanufacturing techniques, is capable of fabricating ordered architectures in the lower micron range (with exceptions in the sub-micron range [116]). Within the last years this lead to an exponentially growing amount of patents and publications [38]. Therefore, tackling technical complexity through implementation of optimised hardware and the establishment of in-process control of MEW is of great importance. This will facilitate the production of scaffolds with tailored architectures for a wide range of applications in the future.

3.7 DISCLOSURE

The authors have nothing to disclose

3.8 ACKNOWLEDGMENTS

This work has been financially supported by the Cooperative Research Centre CRC for Cell Therapy Manufacturing, the Australian Research Council ARC Centre in Additive Biomanufacturing and the Institute for Advanced Study of the Technical University of Munich. Further, the authors gratefully acknowledge Maria Flandes Iparraguirre for support in filming, Philip Hubbard for the voice over and Luise Grossmann for filming and editing.

Chapter 4: An advanced in-process controlled melt electrospinning writing device for large data generation and optimisation

Felix M. Wunner [1], Onur Bas[1], Sebastian Eggert[1,] Pawel Miescwkick[1], Elena M. De-Juan-Pardo [1], Dietmar W. Hutmacher [1, 3, 4, a]

Accepted by *Progress in Additive Manufacturing* (2017)

[1] *Institute of Health and Biomedical Innovation (IHBI), Queensland University of Technology (QUT), 60 Musk Avenue, 4059, Kelvin Grove, Australia*
[2] *Institute of Biomaterials, Department of Materials Science and Engineering, University of Erlangen-Nuremberg, 91058 Erlangen, Germany*
[3] *Institute for Advanced Study, Technical University of Munich (TUM), Lichtenbergstraße 2a, 85748 Garching, Germany*
[4] *George W Woodruff School of Mechanical Engineering, Georgia Institute of Technology, 801 Ferst Drive Northwest, Atlanta, GA 30332*
A, Corresponding author at: Institute for Health and Biomedical Innovation, Queensland University of Technology, 60 Musk Avenue, Kelvin Grove 4059, Australia. E-mail addresses: dietmar.hutmacher@qut.edu.au (Dietmar W. Hutmacher).

Statement of Contribution of Co-Authors for

Thesis by Published Papers

The authors listed below have certified* that:

1. they meet the criteria for authorship in that they have participated in the conception, execution, or interpretation, of at least that part of the publication in their field of expertise;
2. they take public responsibility for their part of the publication, except for the responsible author who accepts overall responsibility for the publication;
3. there are no other authors of the publication according to these criteria;
4. potential conflicts of interest have been disclosed to (a) granting bodies, (b) the editor or publisher of journals or other publications, and (c) the head of the responsible academic unit, and
5. they agree to the use of the publication in the student's thesis and its publication on the QUT ePrints database consistent with any limitations set by publisher requirements.

An advanced in-process controlled melt electrospinning writing device for large data generation and optimisation (accepted by Progress in Additive Manufacturing, 2017)

Contributor	Statement of contribution
Felix Wunner QUT Verified Signature **Signature** **Date** 17/11/2017	Conceived and designed the experiments. Aided experimental work. Co-wrote the manuscript.
Onur Bas QUT Verified Signatures	Conceived and designed the experiments. Aided experimental work. Co-wrote the manuscript.
Sebastian Eggert	Conceived and designed the experiments. Aided experimental work. Co-wrote the manuscript.
Pawel Mieszczanek	Conducted experimental work
Elena M. De-Juan-Pardo	Conceived and designed the experiments. Aided experimental work. Co-wrote the manuscript.
Dietmar W. Hutmacher	Conceived and designed the experiments. Provided feedback on the manuscript. Supervised the entire work. Approved the final version of the manuscript.

Principal Supervisor Confirmation

I have sighted email or other correspondence from all Co-authors confirming their certifying authorship. QUT Verified Signature

Dietmar W. Hutmacher

Name Signature Date 17/11/2017

4.1 ABSTRACT

Melt Electrospinning Writing combines the fundamental principles of fibre forming technologies with 3D printing principles and therefore enables the fabrication of highly structured micron scaled architectures from biocompatible polymers. The manufacturing however, is highly complex and the quality of the results strongly depends on the interplay of the most prevailing input parameters. These are melting temperature, applied voltage, collection speed and applied pressure. In combination, they determine the most relevant forces on the jet, which are pushing the viscous polymer out of the needle and mechanically and electrostatically dragging it for deposition. Within the last years, important studies added great value to better explain the underlying mechanism of electrospinning with polymer melts in a direct writing mode. However, contemporary devices, used in laboratory environments lack the capability to collect large data and further embrace the complexity of the process. Therefore, we systematically engineered an advanced automated MEW system with monitoring capabilities to generate large data volumes, which facilitate enhanced process understanding. Additionally, the novel monitoring design helps to identify the main effects of the system parameters on the geometry of the fibre flight path. This facilitates to draw for the first time a correlation between the input parameters and new discoveries regards the geometry of a jet. This helps to verify the most stable conditions for reaching homogeneous scaffold morphologies, which establish the first ever MEW library.

4.2 INTRODUCTION

The introduction of additive manufacturing (AM) technologies to the fields of tissue engineering and regenerative medicine (TE&RM) bears great potential in discovering and defining future pathways for next generation medical devices [10, 221]. Above all, the application of layer-by-layer fabrication principles allows for the precise manufacturing of architectures, tailored to patient specific needs [11-13]. Within this field of innovations, Melt electrospinning writing (MEW) is a promising candidate to print controlled micron scaled architectures from biocompatible polymers [9, 32, 38, 222]. In MEW, the extrusion of viscous polymer and its electrostatic acceleration generates a polymer jet, which travels linearly towards a grounded or differently charged collector. The deposition can be controlled via the preprogramed movement

of the collector [42]. This makes MEW capable of fabricating highly porous objects, which for instance are used to provide an effective environment for cells expansion [40, 173, 223].

However, MEW is a highly complex 3D printing technique. Numerous correlations between the input parameters exists and significantly determine the quality of the outcome (diameters). This was frequently recognised in literature as one major to reach scale, demanded by industry [64]. Therefore, it now becomes necessary to further investigate this multi parametric environment and foster the stability of the process to ease the translation into the commercial fields.

The interaction of the most prevailing system parameters leads to the creation of a micron to submicron scaled polymer jet, which undergoes thinning and deposition due to the forces, explained hereafter. The viscosity and amount of material flowing into the cone is defined by the applied pressure and temperature, in combination defined as "polymer pushing force" (Fp). All findings in literature agree on a significant growths in diameter among increasing pressure due to increased delivery of mass [43, 44, 95, 170]. Higher temperatures are reported to decrease the diameters [47, 128, 149], because polymers of lower viscosity provide less physical resistance against being stretched [224]. The implementation of mobile charge carriers via the application of voltage into the molten polymer around the charged needle initiate the formation of a Taylor cone [43]. It describes a funnel shaped polymer droplet at the tip and ejects a molten jet [225]. This triggers physical electrostatic acceleration of the viscous melt and transports it towards the grounded element, the collector. Within the framework of this study, we assign this force as the electrostatic acceleration force (Fe), which is reported to have a small thinning effect on the fibre [128, 153, 160, 180]. While the electrostatic acceleration forces drag the charged polymer along the electrostatic field lines, a moving collector transforms the ejected jet into a catenary shaped curve, which creates a lag in deposition [31, 226]. This collector speed initiates mechanical drag forces (Fm) on the jet and leads to enhanced stretching and significant thinning of the final diameter [76].

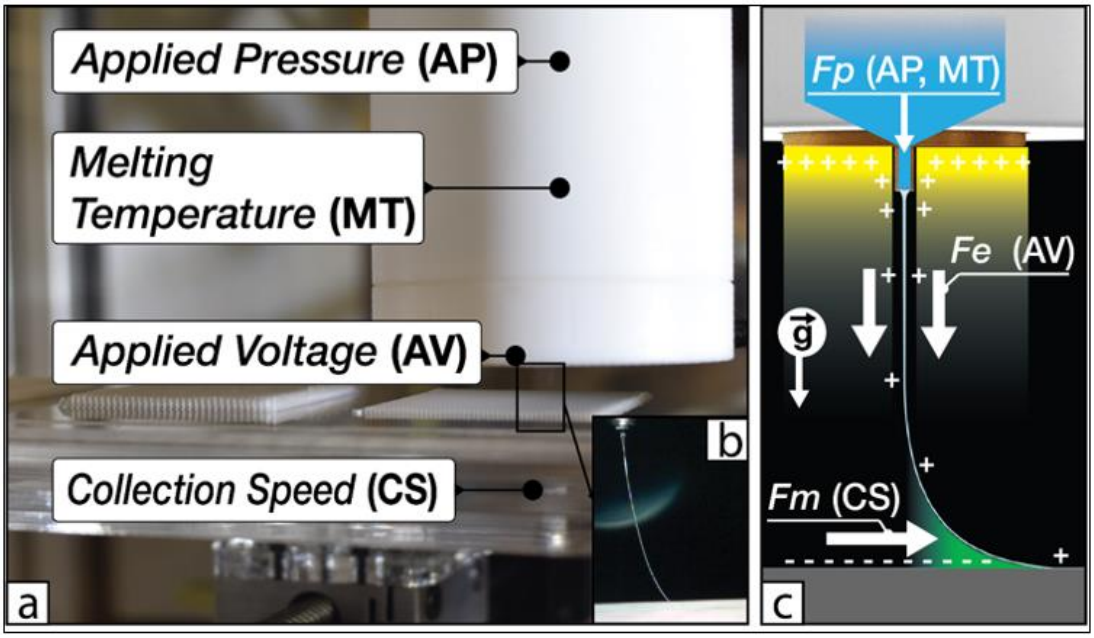

Figure 18: (a) shows a print head with the most prevailing system parameters in MEW and used during this experiment. (b) shows an enlargement of a fibre and (c) demonstrates schematically the extruded fibre due to pressure forces (Fp, Applied Pressure (AP), Melting Temperature (MT),) under the influence of electrostatic acceleration forces (Fe, Applied Voltage (AV)) and mechanical drag forces (Fm, Collection Speed (CS))

Hence, MEW is a multi-parametric process and the achievement of high quality scaffold architectures strongly depends on a well-balanced interplay of all process parameters [42].

MEW is also a relatively young technology, yet experiencing an exponential rise in scientific work within the next years [38]. Nevertheless, the prototyping nature of conventionally used devices in laboratory environments does not allow for generating large data volumes. These however, are required to further investigate this multi-parametric environment and to more precisely identify the effects of the parameters on the scaffolds. In fact, various studies provide the MEW community with important findings [69, 95, 143, 158, 203]. These, were typically conducted via analysing the results with microscopes in separate facilities and describes a time consuming and inefficient process. Additionally, this manual method is not feasible in embracing the influence of variations of multiple system parameters at the same time. To our knowledge, there is no report, which investigates overall changes of four parameter settings simultaneously. Hence, we identify this urgent need for large data acquisition, which will help to gain advanced process understanding and unravel undiscovered correlations between input and output of MEW.

Deposited scaffolds, however are challenging to characterise, as the micron-scaled structures required the application of microscopic equipment. This study presents an effective alternative to verify the stability of MEW via analysing and characterising the geometry of a falling jet and draw correlations to the final morphology of the scaffold.

Therefore, we first designed and developed an automated in-process monitoring device, which uses two cameras to detect the fibre and the diameters in real time to generate large data volumes. The results reveal a significant correlation between deviations in fibre diameter and angle. Additionally, an explorative analysis of the geometry of the jet supports to derive the stability of a process. Finally, we apply the most stable settings and verify the experiment via application on conventionally used machines. We foresee fibre detection as one promising alternative for future means to control the quality of the process.

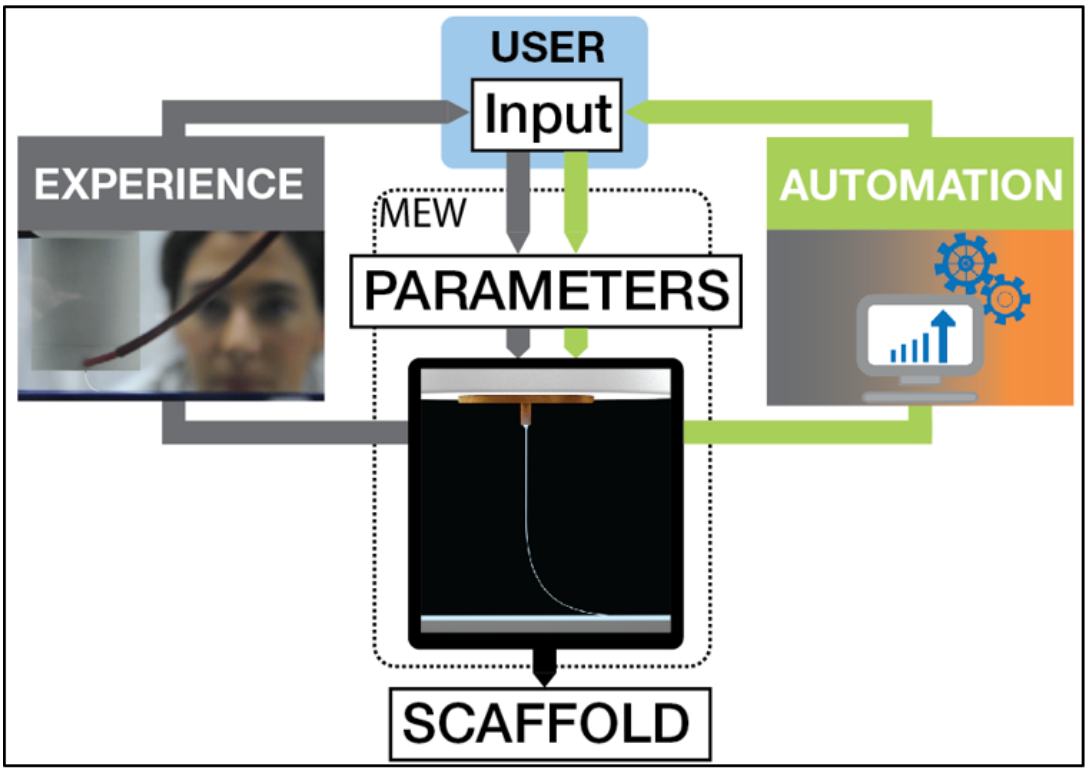

Figure 19: schematic illustration of the approach of this study to automise data collection

4.3 MATERIALS AND METHODS

In process controlled MEW machine design

An in-house designed MEW device [38, 222] was complemented by the integration of an in-process control system, (Fig.19). The novel setup consist of a computing platform, a parameter configuration unit and the printing environment. The latter

implies an existing MEW print head, a fibre collection system and the monitoring unit. The system was systematically engineered and compiled using Papyrus Eclipse IDE for Java Developers (Oxygen.1a Release (4.7.1a), USA).

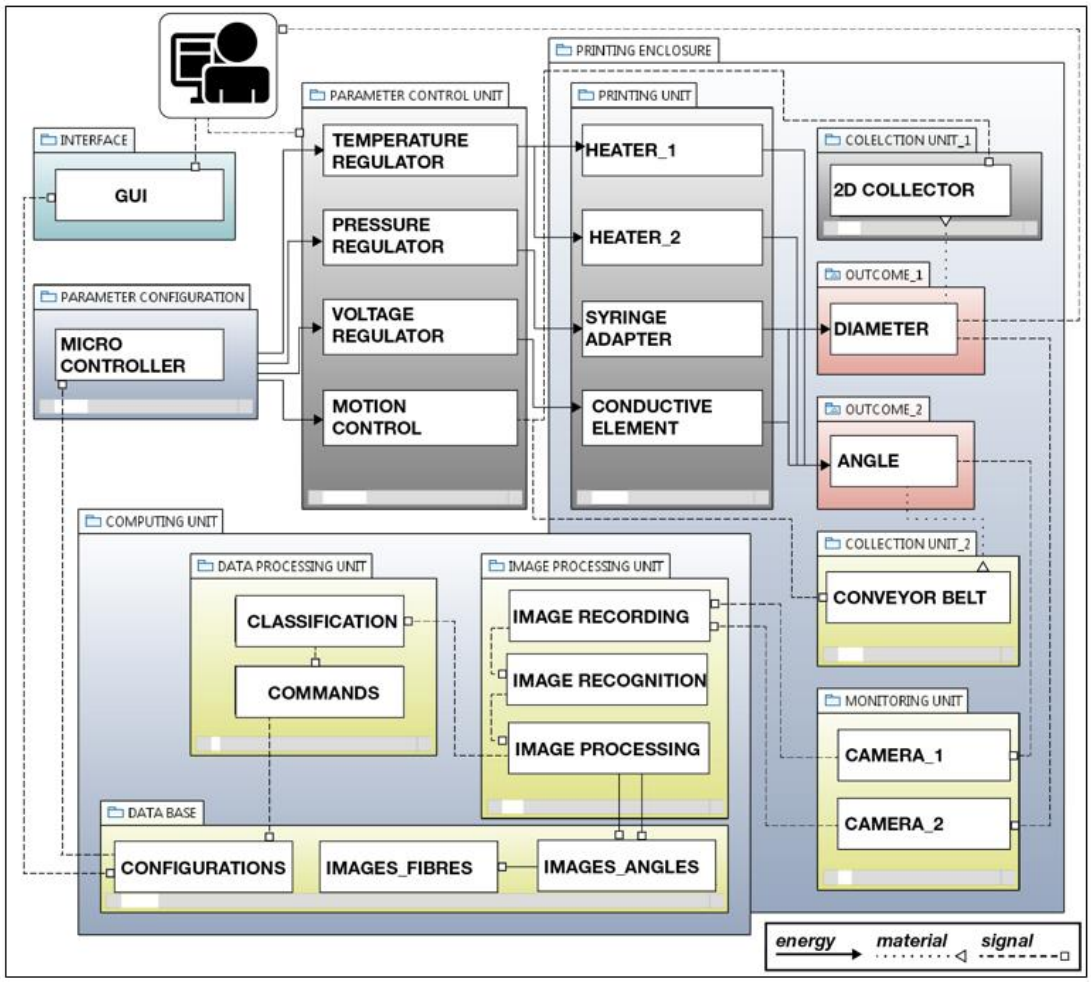

Figure 20: shows a systematic machine design system generated in the programming language SYSML. The Units shown in grey represent existing state of the art hardware, while the blue units and the GUI (Graphical User Interface) indicate the novelties of this concept. Individual exchange between units is divided in energy, material and signal and supports the understanding of the work flow and the control loop principles

Parameter control unit

Similar to existing processes [19, 38, 222], the system parameters Melting Temperature, Applied Pressure, Collection Speed and Applied Voltage were triggered via the parameter control unit. Parameter adjustment automation was realised via the electronic prototyping platform ARDUINO (MEGA 2560, ARDUINO, USA).

Printing enclosure

An existing MEW head [38, 222] was used to print fibres on a conductive conveyor belt (collection unit_2), (IG X). The high degree of flexibility of the metal band facilitates frictionless rotation without fatigue fractures. The rotational movement was

established via a brush motor (CNC-004, 175oz-in High Speed CNC, Ocean Controls, Australia).

Monitoring unit

The monitoring unit consists of two cameras to capture the flight path of the fibre and the diameter respectively. Camera_1 (AM413ZT, Dino Lite, USA) was mounted horizontally in a distance of 100 mm to focus on a region of interest (ROI) of 15 mm *15 mm. Within this ROI, the fibre appears as a dark line in front of an in illuminated background. A microscopic setup was modified with 3D printed components to fit a microscopic camera (TP-305000A, Eyepiece, USA) on the top end and a 10 x magnification lens on the bottom to focus on a ROI of 200 µm * 200 µm.

Computing unit

The software environment, integrated in a high performance personal desktop computer (WINDOWS 64bit, USA) was designed in MATLAB (MATLAB R2015b, MATHWORKS, USA) to allow communication with the control unit and access the data base. In parallel the computing unit received the images from the monitoring unit to transform them into integer values.

Applied system parameters

	Applied Voltage	*Collection Speed*	*Melting Temperature*	*Air Pressure*
[unit]	[kv]	[mm/min]	[°]	[bar]
0	8	1000	70	0.8
1	10	2000	82.5	1.4
2	12	3000	95	2.2

Table 4: system parameters, values and their levels in the experiment

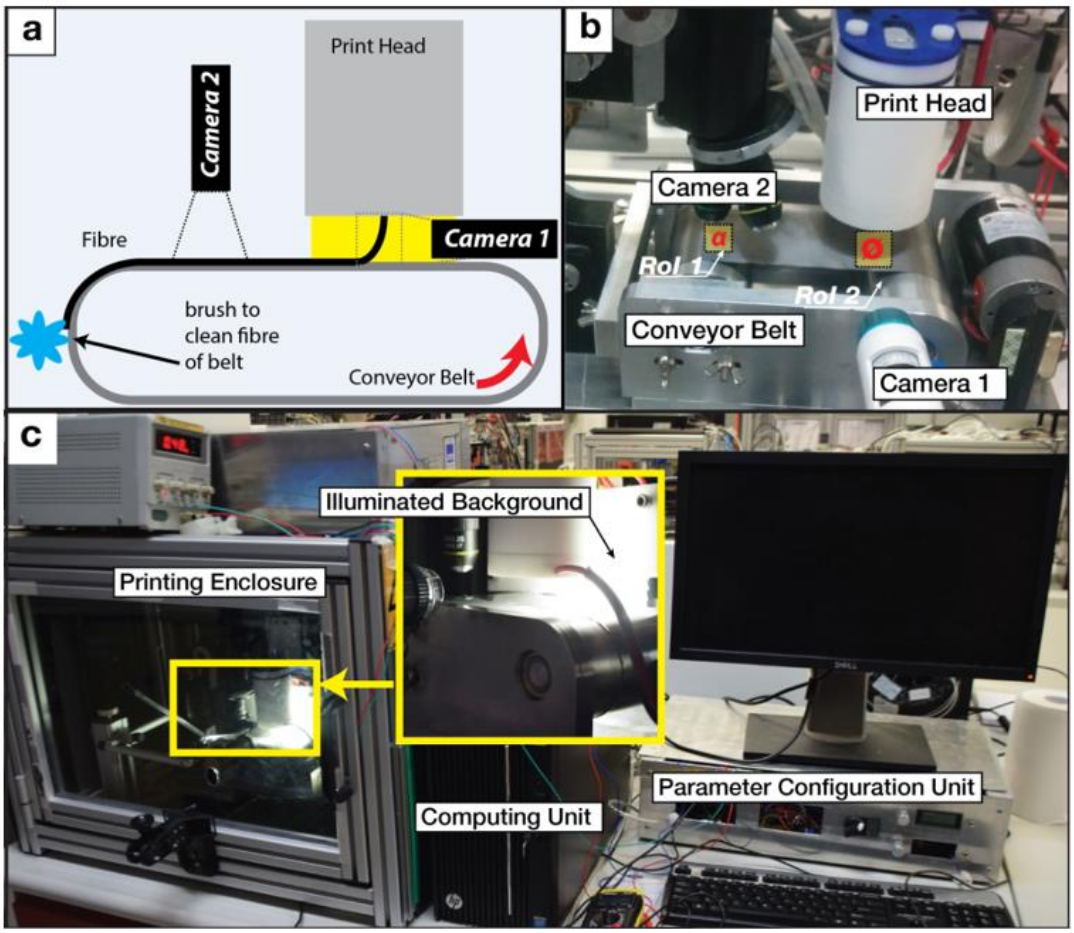

Figure 21: (a) demonstrates a schematic setup of the conveyor – camera system with the hardware in (b). (C0 shows the process control setup and gives an insight into the illuminated region around the conveyor belt

Design of experiment

An orthogonal array [227], designed in Minitab Statistical Software (Minitab 17, United Kingdom, Free Trial) prescribed the structure of the experiment to print every possible correlation.

$$(No.levels)^{(No.parameters)} = 3^{(4)} = 81 \quad (3)$$

The resulting 81 different printing scenarios, (Fig. 20.a), were conducted in an ordered manner (n=3) while recording of 30 images (diameter, angle) within 90 seconds.

Characterisation

The software was coded in MATLAB (R2015b, MathWorks, USA) to determine the diameter and the angle in real time (Fig.20.b). A threshold is applied to both images to convert them in black-and-white, which enhances the accuracy of the measurements. The diameters were detected via 160 measurements along the y-axis (every 10 pixels) to calculate the means (Fig.20.b). Calibration via a gauged ruler converted pixels into

microns. The angles were determined by similarly segmenting the image to a greyscale to define the fibre (fi.X). The subsequent application of curve fitting and extrapolation models verifies the point of deposition. This determines the angle between Tc and deposition point. Diameter and angle values were calculated within three seconds (+/- 0.5 seconds) and send to the library, which resulted in a total of 14580 integers.

Statistical model

Linear regression modelling was applied to investigate the dependencies between the deviations of angle and diameter, conducted in a statistic software (PRISM 7, GraphPad Prism 7 Software, USA).

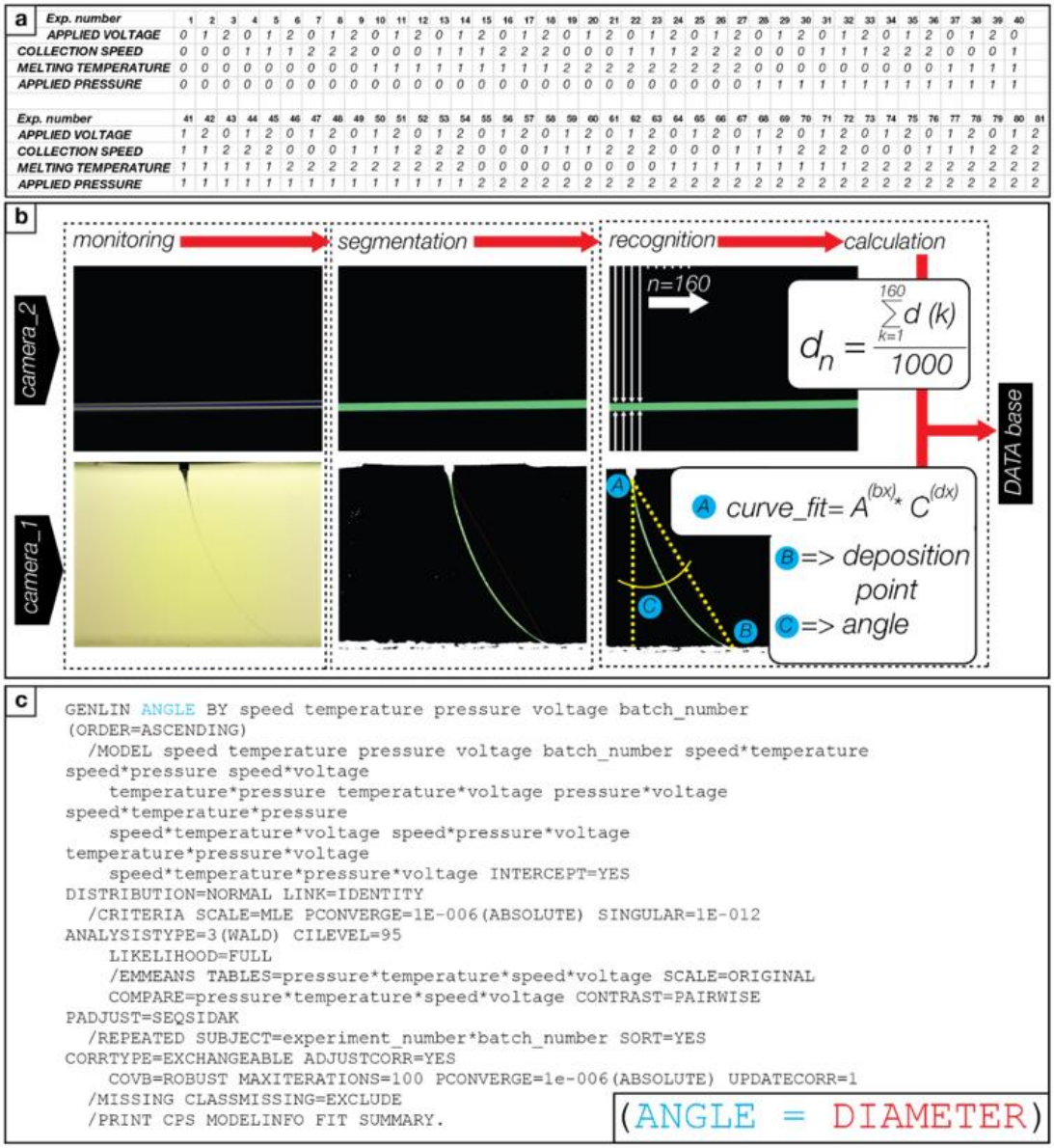

Figure 22: (a) shows the array of 81 different settings of the permutated experiment under the application of the different levels. (0) is the lowest, (1) the medium and (2) the highest level of the parameters. (b) demonstrates the working principles of both image recognition codes. (c) shows the code we applied to the Data set in SPSS for both, the angle and the diameter.

Due to the large data volume (14580 values), strong correlation of the four parameters and repetitive character of the experiment (n=3), the statistical software SPSS (SPSS STATISTICS 23, IBM, USA) was used to apply a linear model using Generalised Estimated Equations (GEE). The model accounts for repeated measurements at individual experiments (Fig.20.c). The input, a linear array of the 14580 experiments was prepared in MATLAB and the results were visualised via heat maps.

4.4 RESULTS AND DISCUSSION

The linear regression model were applied to investigate the correlations between deviations of angle and diameter. They revealed that the majority of all 81 relationships is significant (exemptions of 7.41 % in batch one, 4.9 % in batch two and 9.9 % in batch three). Individual insignificance cases do not appear in a logical order and hence might occur due to the prototyping nature of the setup. Yet, this result allow for the following interpretation: fluctuations in angle also leads to deviations in diameters. In future applications, this finding can be used as an effective indicator to early detect process instabilities.

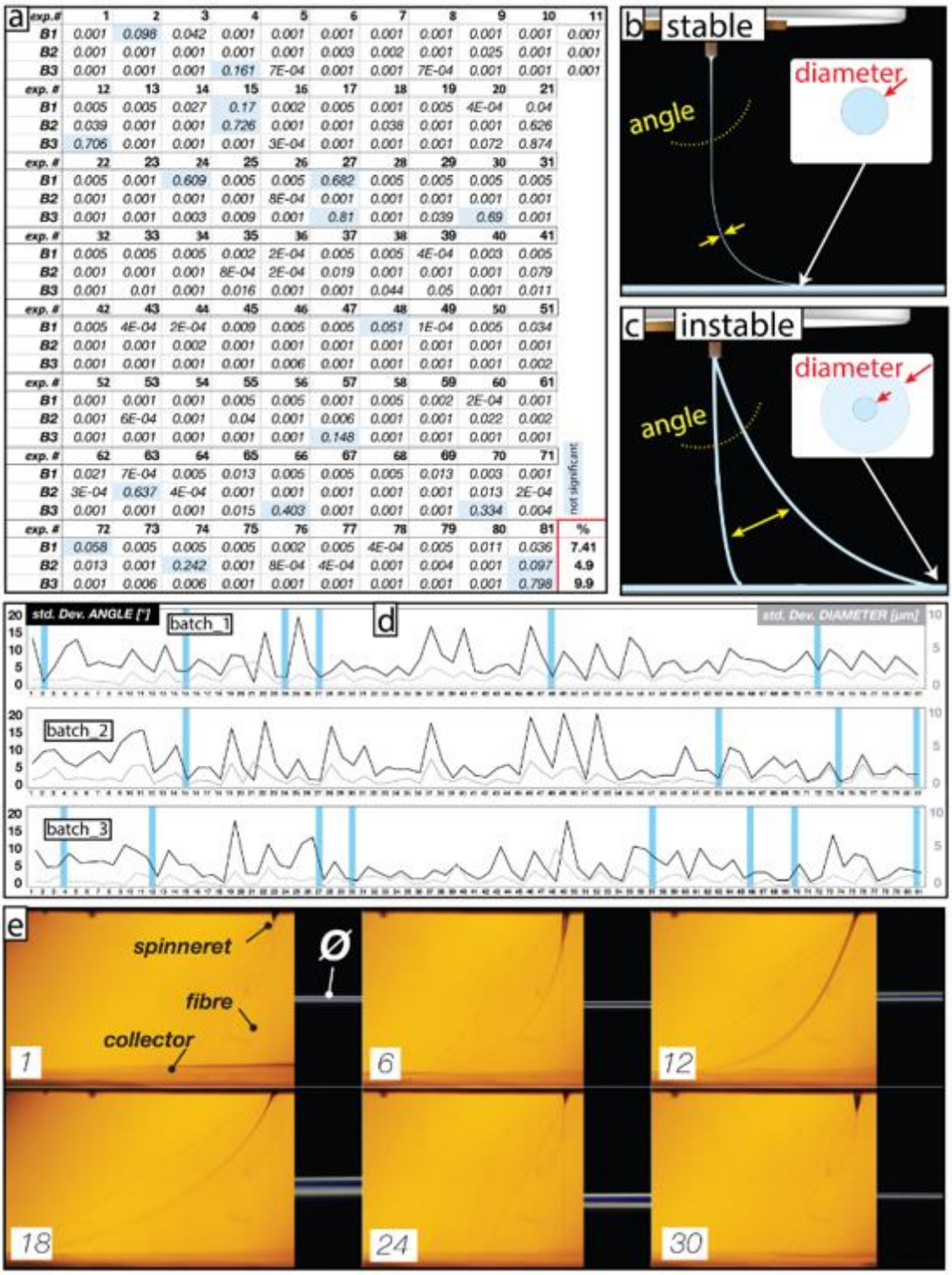

exp.#	1	2	3	4	5	6	7	8	9	10	11
B1	0.001	0.098	0.042	0.001	0.001	0.001	0.001	0.001	0.001	0.001	0.001
B2	0.001	0.001	0.001	0.001	0.001	0.003	0.002	0.001	0.025	0.001	0.001
B3	0.001	0.001	0.001	0.161	7E-04	0.001	0.001	7E-04	0.001	0.001	0.001
exp. #	12	13	14	15	16	17	18	19	20	21	
B1	0.005	0.005	0.027	0.17	0.002	0.005	0.001	0.005	4E-04	0.04	
B2	0.039	0.001	0.001	0.726	0.001	0.001	0.038	0.001	0.001	0.626	
B3	0.706	0.001	0.001	0.001	3E-04	0.001	0.001	0.001	0.072	0.874	
exp. #	22	23	24	25	26	27	28	29	30	31	
B1	0.005	0.001	0.609	0.005	0.005	0.682	0.005	0.005	0.005	0.005	
B2	0.001	0.001	0.001	0.001	8E-04	0.001	0.001	0.001	0.001	0.001	
B3	0.001	0.001	0.003	0.009	0.001	0.81	0.001	0.039	0.69	0.001	
exp. #	32	33	34	35	36	37	38	39	40	41	
B1	0.005	0.005	0.005	0.002	2E-04	0.005	0.005	4E-04	0.003	0.005	
B2	0.001	0.001	0.001	8E-04	2E-04	0.019	0.001	0.001	0.001	0.079	
B3	0.001	0.01	0.001	0.016	0.001	0.001	0.044	0.05	0.001	0.011	
exp. #	42	43	44	45	46	47	48	49	50	51	
B1	0.005	4E-04	2E-04	0.009	0.005	0.005	0.051	1E-04	0.005	0.034	
B2	0.001	0.001	0.002	0.001	0.001	0.001	0.001	0.001	0.001	0.001	
B3	0.001	0.001	0.001	0.001	0.006	0.001	0.001	0.001	0.001	0.002	
exp. #	52	53	54	55	56	57	58	59	60	61	
B1	0.001	0.001	0.001	0.005	0.005	0.001	0.005	0.002	2E-04	0.001	
B2	0.001	6E-04	0.001	0.04	0.001	0.006	0.001	0.001	0.022	0.002	
B3	0.001	0.001	0.001	0.001	0.001	0.148	0.001	0.001	0.001	0.001	
exp. #	62	63	64	65	66	67	68	69	70	71	
B1	0.021	7E-04	0.005	0.013	0.005	0.005	0.005	0.013	0.003	0.001	
B2	3E-04	0.637	4E-04	0.001	0.001	0.001	0.001	0.001	0.013	2E-04	
B3	0.001	0.001	0.001	0.015	0.403	0.001	0.001	0.001	0.334	0.004	
exp. #	72	73	74	75	76	77	78	79	80	81	%
B1	0.058	0.005	0.005	0.005	0.002	0.005	4E-04	0.005	0.011	0.036	7.41
B2	0.013	0.001	0.242	0.001	8E-04	4E-04	0.001	0.004	0.001	0.097	4.9
B3	0.001	0.006	0.006	0.001	0.001	0.001	0.001	0.001	0.001	0.798	9.9

not significant

Figure 23: (a) lists the individual results of the linear regression models and indicates the non-significant cases (blue). (b) shows schematically a fibre in its stable state and therefore minor diameter deviations and in (c) an instable case including deviations. (d) shows the plots of the deviations of the angles and the diameters and shows the cases of insignificant correlation (verified in (a)). (e) exemplary demonstrates a pulsing fibre (instable) and shows the relation to the diameter, when the angle increases. The images show the fibre and the diameter on the right from six out of the 30 images.

Next, the application of the GEE helped to further investigate the inter-correlation of the four system parameters and revealed a four-way interaction for both (angle, diameter). This means, that every individual modification of a single system parameter leads to statistically incomparable and different outcomes. Therefore, all 81 cases would require individual explanation, yet exceeding the limitations of this work, but introducing the opportunity for advanced analytical analysis in future studies. The results of the GEE were visualised in 2D heat map diagrams (angles (Fig. 22), diameters (Fig. 23)). Each diagram consists of nine fields, which individually represent the applied voltage over the collection speed. The first row of the nine fields (l-lll) refers to the lowest applied pressure (AP=0) with increasing melting temperature levels from left to right. For all cases, the standard errors of the GEE are additionally noted in the heat maps. An explorative interpretation regards the three major influences on the angle and the diameter is provided in the following.

Angle

4.4.1 *Electrical acceleration forces on the fibre (Applied Voltage)*

Increasing electrostatic forces tend to decrease the angle at all cases. Here, higher voltages result in larger electrostatic forces, which are increasingly taking effect on the extruded melt and accelerate it towards the grounded element [34]. The establishment of these forces origins from the mobile electrical charge carriers, which reside in the molten jet and on its surface [104, 228]. As a result, the molten fibre is physically attracted towards the collector and is forced to travel in parallel along the electrostatic field lines, which minimises the angle [39]. Due to the minimum applied collection speeds of 1000 mm/min within this experiment, the resulting angles reveal values greater than zero at all times. Moreover, it can be observed, that this electrostatically induced mechanism is more apparent at small and medium mass flow (AP=1,2) and at lower viscosities (MT=3). This hints that the degree of electrostatic material acceleration is correlated to the respective charge density within the melt and its characteristic flow properties.

Mechanically induced drag forces (Collector Speed)

At all fields, the Applied Voltage, the heat map also reveals repeating patterns for variations in collection speeds, ranging from 1000 mm/min (CS=0) to 3000 mm /min (CS=2). In fact, the horizontally acting mechanical forces (Fm) increase the angle at higher collection speeds. The forces initiated from the relatively moving collecting are

described in the literature [205, 229] and facilitate direct writing applications at MEW [31]. The movement initiates the formation of a catenary curve of fibre [204] and leads to a lag in the point of deposition on the collector. Similar to the influence and effects of the Applied Voltage, we observe an increasing correlation between the mechanical induced drag forces and the outcome (angle) in relation to the viscoelastic properties, the amount of the extruded material. Putting the mechanically and electrostatically induced forces in context, the former appear to be more dominant in determining the angle. In general, changes in angle due to the effect of collection speed are most prevailing in the cases of lowest pressure (AP=0). An average increase can be observed from 14,9° at lowest collections speeds to 43,8°at highest collection speed. This represents an approximate increase of 188 %. In cases of high mass flow (AP=2), the respective average angles ranges from 32° to 51,3°, and represents a rise of approximately 59 %. In this case, a relatively large initial angel initially exists (32°). This can be traced back to the larger amount of extruded mass, which is likely to be drawn straight to the collector by the electrostatic forces. The electrostatic forces appear only influence the angle at lower collection speeds (CS=0). In these cases the percentage in decline of angle is approximately 38% at (AP=0), 46.1% at (AP=1) and 32% at (AP=2). The decrease at highest speeds is significantly less impactful and the values are comparably small of approximately 2.1% at (AP=0), 5.9% at (AP=1) and 4.0 % at (AP=2). In the framework of this experiment and based on this explorative analysis, we perceived, that first, the forces induced by collector movement prevail as the most dominant; second, the electrostatic effect is mainly present at the lowest collection speeds (CS=0), and third, the most significant changes in angle occur in cases of the lowest viscosities. Last underlines the strong dependencies on the material resistance forces of the fluid [31, 230], explained in the following section.

Influence of mass flow and the dependency on viscosity (Applied Pressure, Melting Temperature)

In general, higher angles occur due to increases in pressure and rising temperatures decrease the angles, yet only at lower and medium pressure levels.

First, the increasing angles along higher mass flow can be explained by the relation between the amounts of implemented charge carriers into the volume of the extruded material. This ratio defines the specific charge density and significantly influences the

tendency of the viscous polymer to be physically attracted towards the grounded element [63, 231]. Charge effect and migration mechanisms are relatively under investigated in the fields of MEW, however, amplified voltages do increase the ratio of charge carriers per volume unit [33]. This overcomes the fluid's resistance against being physically stretched [42]. For instance, and seen at all cases of low to medium pressure, a smaller amount of extruded material is specifically more affected by the greater electrostatic forces, i.e. generate smaller angles at higher Applied Voltages. Oppositely, the influence of the mechanical drag by the collector speed becomes more influential at higher mass flow.

Further, the variations in the heat map also indicate a dependency of the angle on the state of viscosity of the polymer. Higher temperatures generate lower viscosities and therefore enhance the flow properties of the melt [16]. This generates less resistance of the fibres to be electrostatically accelerated [124] and leads to smaller angles. However, we observe this temperature induced influence mainly appears dominant at small melt extrusion rates (AP=0). At lower temperatures, the angles are generally higher and vice versa and there is no significant viscosity based difference in the cases of high mass flow (AP=2). We assume, that the larger volumes of polymer are more likely to form stronger macromolecular cohesions than thin fibres. Therefore, the temperatures can be assumed as less influential at large mass flows.

The influence and interaction of mass and viscosity determine the angle can best be explained by comparing fields three and seven. Under the same electrostatic forces and collection speeds, the former provides low viscosities and small mass flow, while seven reveals large mass flow and highest viscosities. The angles differ by approximately the double and decrease at low collection speeds (CS=0) from 19 degree to 4 degree in field one and, in comparison from 37 degree to 28 degrees in field seven. This is an approximate decrease of 80% for the first and 25% for the second. This difference indicates that the pressure strongly influences the angle of the fibre, and the applied temperature, defining the fluidity of the molten majorly acts in cases of small extrusion rates.

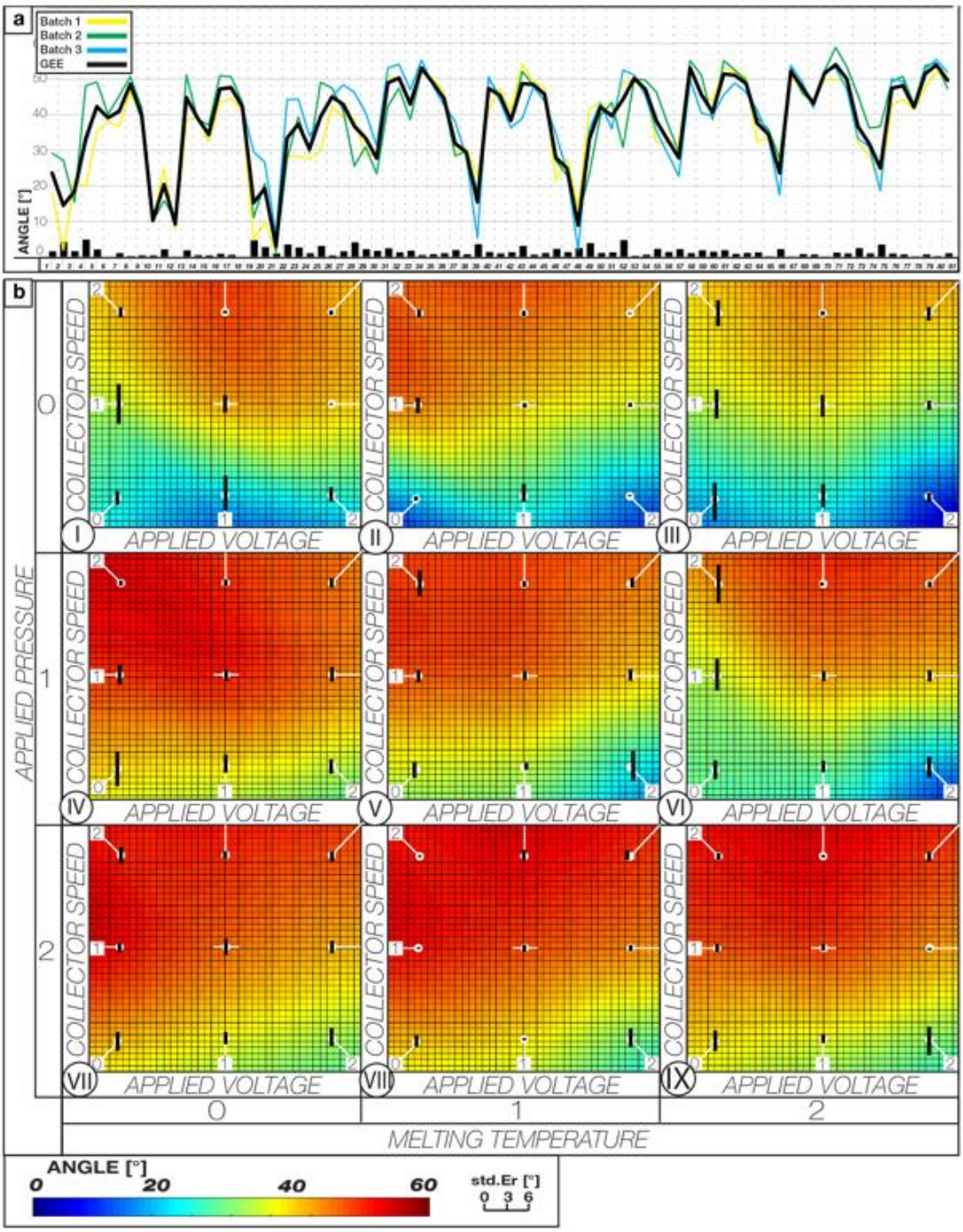

4.4.2

Figure 24: (a) resulting plots for the individual courses of the angles of the three batches and the fitting graph of the GEE model. (b) Heat map of the parameter induced variations subdivided in the nine fields including their standard errors

Diameter

Electrical acceleration forces on the fibre (Applied Voltage)

As known from literature, the generated electrostatic forces accelerate the melt towards the collector and the majority of published work describes intense thinning behaviour of the jet [128, 142, 157], however, there are exemptions [37, 125]. We trace these back to the great diversity of mechanical design of the print heads [26], which make it

challenging to define a consensus on the electrostatic effect on the diameter. Moreover, this experiment is conducted under a relatively short working distance (12 mm). This introduces a lack of excessive electrostatically induced thinning, which can be observed in cases one to seven. Significant diameter growths occurred along increased voltages in the cases six, eight and nine. Interestingly, they all reveal high mass flow and/or low viscosities. We assume, that the large amount of implemented charge carriers at the creation of a Taylor cone amplifies the material extrusion from the spinneret. In fact, the increase in voltage leads to more electrostatically driven polymer flow into the cone, as the increased number of charge carriers impart more kinetic energy into the liquid [33, 232]. This leads to greater extrusion rates and hence, enlarges the average diameters.

Mechanically induced drag forces (Collector Speed)

At all experiments, increasing collector speeds are observed to initiate smaller diameters. This confirms the findings from literature [76, 222] describing effectively decreasing diameters along increasing collection speeds. This is initiated by the mechanically induced stretching of the melt during its flight phase. This effect can be observed within the framework of this experiment and occurs as a repetitive pattern.

Similar to the angle, a compare between the electrostatically and mechanically induced forces reveals that the mechanically dragging forces are dominant.

Influence of mass flow and the dependency on viscosity (Applied Pressure, Melting Temperature)

The applied pressure defines the amount of extruded material, which is known as one major influence in determining the size of the final diameter [38, 43, 95, 170, 203]. This can be confirmed by the results of this experiment. Further, the extruded mass is in strong correlation with the temperature induced viscosity of the material, and we observe significant diameter increases along altering temperatures. This is different to most findings from literature [47, 128, 149], however can again be traced back to the small working distance, which potentially prevents enhanced thinning of the elastic fibre in its flight phase. Additionally, we assume that this diameter growths along temperatures arises due to the enhanced flow properties of the material. This leads to significantly increased outflow out of the needle into the cone.

Deviating diameters are known from literature [205] and expressed in the heat map in form of black error bars. Minimum deviations are verified in the following chapter.

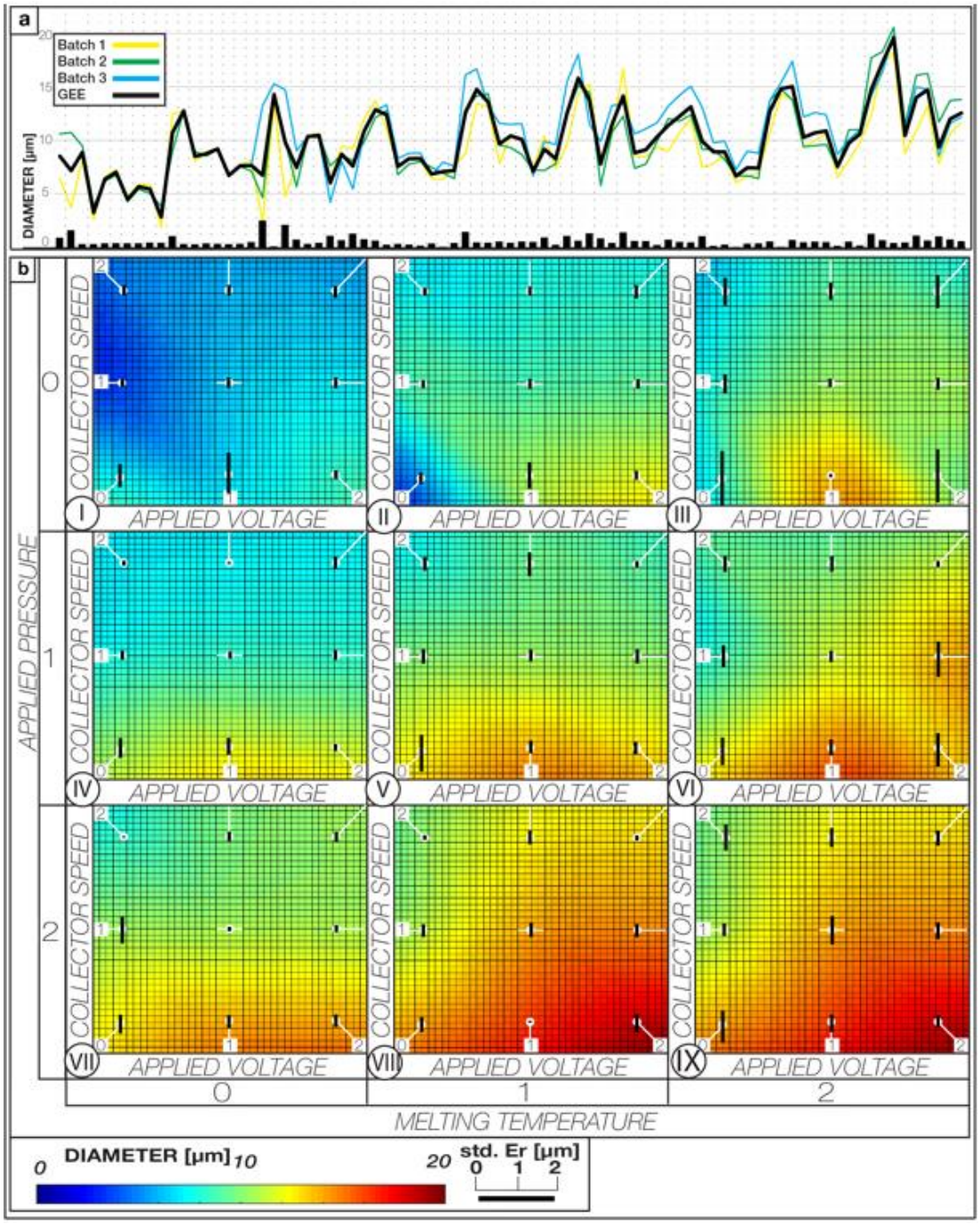

Figure 25: (a) similar to figure 22, the resulting plots for the individual courses of the diameters of the three batches and the fitting graph of the GEE model. (b) Heat map of the parameter induced variations subdivided in the nine fields for the diameters including their standard errors

Concluding both statistical analysis (linear regression and GEE), we can confirm the following: a strong correlation between the deviations in angle and the deviations in diameter exists, i.e. if the jet fluctuates, the diameter in the vast majority of all cases also varies. Nevertheless, it is not possible to determine the resulting thickness of a fibre only from its flight path. If the parameter settings are given and the angle is in a certain range, the diameter can be predicted.

4.5 VERIFICATION OF THE RESULTS

The results of the GEE were subject to a mathematical selection process to create a library, which contains the most stable printing conditions. First, the diameters were listed in an ascending sequence and experiments (#) with similar diameters were grouped to sections (Fig.24). In order to identify cases of maximum stability (diameter and angle), a mathematical normalisation of their standard errors was applied. Subsequently, the mean value of both normalised values was calculated, defined as the stability coefficients (sc).

$$N(dia, angle) = \frac{(\mathrm{Xi} - \mathrm{MIN(Xi, Xj)}}{(\mathrm{MAX(Xi, Xj)} - \mathrm{MIN(Xi, Xj)})} \; ; \; \sum_{i=1}^{j} X + i \qquad (5)$$

$$sc = MEAN\left(N(dia), N(angle)\right) \qquad (6)$$

where N describes the normalised value of the angle or diameter respectively, X the value of the angle or the diameter of the particular experiment (#1 – #81) and sc the mean value of both normalised values. Hence, the most stable printing conditions are defined by the lowest values of the sc and describe the least diameter and angle deviations at the same time. The physical verification was conducted by applying the settings to print 7 µm, 11 µm and 15 µm on conventionally used in-house designed bench-top MEW devices. The angles (n=30) were captured with the same USB camera, used for the conveyor belt experiment and the fibres were printed on a microscopic slide. An inverted light microscope (X) was used to capture the images of the diameters (n=30). Both results were measured manually using ImageJ (Version 1.51q, National Institutes of Health, USA). The result for all three parameter settings revealed that printing the targeted diameters is possible.

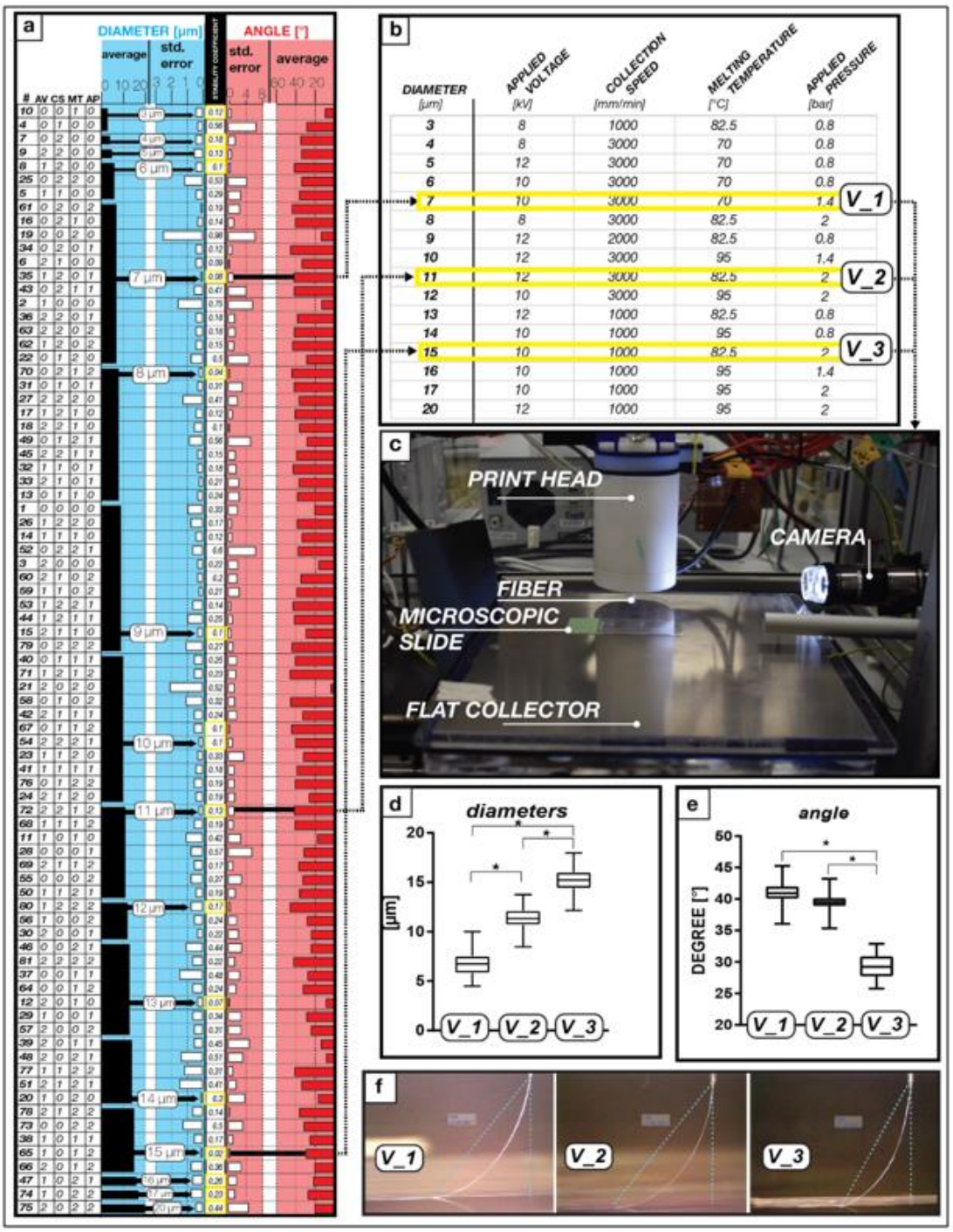

Figure 26: (a) represents the hierarchical order of the resulting diameters and the application of the formula to determine the smallest stability coefficient. (b) shows the final library, which consist of the most stable cases for each diameter. V1, V2 and V3 were chosen to test at a conventionally used printing setup (c). (d) and (e) show the resulting diameter and angle distributions (statistical verification via t-test: p,0.05) and (f) exemplary displays images of the respective fibre angles.*

The results show averages and standard deviations of 7,2 µm (±1.15 µm) for V_1, 11.6 µm (±1.06 µm) for V_2 and 15.3 µm (±1.35 µm) for V_3. The minor increases in diameter in V_2 and V_3 compared to the conveyor belt study can be traced back to the prototyping nature of the devices. The measurements of the angles for the three

cases revealed 41,1 ° (±1.7°), 39,5 ° (±1.45°) and 29,3° (±1.85°), respectively. Similarly to the diameters, the arising deviations from the target values are negligible and can be traced back to the different mechanical designs of the collecting units. The overall trends of the parameters within the library are well aligned with the derived results from both heat maps. Here, generally increasing voltages, collection speeds and air pressure levels lead to larger diameters and oppositely, higher collection speed initiates enhanced stretching.

4.6 CONCLUSION AND FUTURE DIRECTIONS

For the first time, a MEW device was equipped with an automated parameter control system including monitoring capabilities to facilitate the collection of large data volumes. The in-process control loop consist of software programs, which were coded to automatically adjust the parameters during the process. Additionally, the software is capable of digitalising the images of the resulting fibre angles and diameters in real time and store their characterising values to a database.

The innovative system enabled the generation of large data volumes in a short period of time. This, required the application of complex statistical modelling (GEE) to investigate the highly correlated outcomes. However, for the first time in MEW, the printing process could be analysed via considering all variations of the four most prevailing system parameter. The significant association between deviations in diameter and angle at the majority of all cases represent one major discovery. Further, the resulting heat map visualise the diameter variations and support the findings, already known from literature. Yet, differences in the assumed outcome of the applied temperature occur. For the first time, the analysis exposes the behaviour of a fibre flight path and identifies the major influences of the parameters, which is new to the electrospinning community. The generated large data forms a basis for further investigating the complex system on an advanced mathematical level. This will embrace dynamic mathematical correlations between the parameters and the diameter and angles. Finally, the data set helped to identify the most stable conditions for reproducing a wide range of conditions. This was successfully verified by transferring the results to a conventionally used bench top MEW device.

From an engineering perspective, the system was designed to form a prototyping basis for future in-process control opportunities. For instance, we foresee that MEW systems

potentially will provide users with the opportunity to automatically print desired scaffolds with changing morphologies, i.e. small and large diameters combined within one scaffold. Moreover, the novel system makes in-process control at large industrial applications more economic and effective. In future industrial machines, numerous fibre extrusion units will generate large electrospun lattices, yet require quality measures. For this purpose, our developed system evidences that the quality determination of the final scaffold is feasible via monitoring the travelling fibre, while considering the parameter settings. This way of identifying the geometry of the jet is by far less expensive then implementing cameras for detecting the morphologies of the micron scaled polymer lattices.

In conclusion, this study evidences the correlation between the parameter settings, the fibre and the final diameter. It calls for the need for integrating advanced manufacturing technologies (automations, monitoring) to generate large data volumes, which lead to a more holistic understanding of the process and will paves the way to enter industrial fields.

4.7 ACKNOWLEDGMENTS

The research was undertaken in the framework of the ARC Training Centre in Additive Biomanufacturing (IC160100026) and further assisted by the Institute for Advanced Study, Technische Universität München and by the Cooperative Research Centre for Cell Therapy Manufacturing.

4.8 DISCLOSURE

The authors have nothing to disclose

Chapter 5: Melt electrospinning writing of highly ordered, large volume, scaffold architectures

Felix M. Wunner [1], Marie-Luise Wille [1], Thomas Noonan [1], Onur Bas [2], Paul D. Dalton [3], M. De-Juan-Pardo [2], Dietmar W. Hutmacher [1,2,4,5,*]

Published in Advanced Materials (2018)

[1]*Centre in Regenerative Medicine, Institute of Health and Biomedical Innovation, Queensland University of Technology (QUT), Kelvin Grove, Brisbane, QLD 4059, Australia*
[2]*ARC ITTC in Additive Biomanufacturing, Institute of Health and Biomedical Innovation (IHBI), Queensland University of Technology (QUT), 60 Musk Avenue, 4059, Kelvin Grove, Australia.*
[3] *Department for Functional Materials in Medicine and Dentistry, University of Würzburg, Pleicherwall 2, 97070 Würzburg, Germany*
[4]*Institute for Advanced Study, Technical University of Munich (TUM), Lichtenbergstraße 2a, 85748 Garching, Germany.*
[5]*George W Woodruff School of Mechanical Engineering, Georgia Institute of Technology, 801 Ferst Drive Northwest, Atlanta, GA 30332, USA.*

[a]*Corresponding author at: Institute for Health and Biomedical Innovation, Queensland University of Technology, 60 Musk Avenue, Kelvin Grove 4059, Australia. E-mail addresses: dietmar.hutmacher@qut.edu.au (Dietmar W. Hutmacher).*

Statement of Contribution of Co-Authors for

Thesis by Published Papers

The authors listed below have certified* that:

1. they meet the criteria for authorship in that they have participated in the conception, execution, or interpretation, of at least that part of the publication in their field of expertise;
2. they take public responsibility for their part of the publication, except for the responsible author who accepts overall responsibility for the publication;
3. there are no other authors of the publication according to these criteria;
4. potential conflicts of interest have been disclosed to (a) granting bodies, (b) the editor or publisher of journals or other publications, and (c) the head of the responsible academic unit, and
5. they agree to the use of the publication in the student's thesis and its publication on the QUT ePrints database consistent with any limitations set by publisher requirements.

Melt Electrospinning Writing of highly ordered, large volume, scaffold architectures (published in Advanced Materials, 2018)

Contributor	Statement of contribution
Felix Wunner QUT Verified Signature **Signature** **Date** 17/11/2017	Conceived and designed the experiments. Aided experimental work. Co-wrote the manuscript.
Marie-Luise Wille	Aided experimental work
Thomas G. Noonan	Aided experimental work
Onur Bas	Conceived and designed the experiments
Paul D. Dalton	Co-wrote the manuscript and provided feedback.
Elena M. De-Juan-Pardo	Co-wrote the manuscript and provided feedback.
Dietmar W. Hutmacher	Conceived and designed the experiments. Provided feedback on the manuscript. Supervised the entire work. Approved the final version of the manuscript.

QUT Verified Signatures

Principal Supervisor Confirmation

I have sighted email or other correspondence from all Co-authors confirming their certifying authorship.

Dietmar W. Hutmacher QUT Verified Signature 17/11/2017

Name Signature Date

5.1 ABSTRACT

3D printing of highly ordered and micron-scaled scaffolds that converge additive manufacturing and melt electrospinning is on the forefront of tissue engineering & regenerative medicine applications. The printing of such scaffolds for the regeneration of larger tissue volumes, however, remains a major challenge, as the accumulation of excess charge in the deposited material leads to repelling forces and hence, significantly distorted scaffold architectures with build height. Here we study the underlying physical principles causing the constraints of melt electrospinning writing of 3D printed thick and large volume scaffolds and demonstrated in vitro that cells can migrate and proliferate throughout a 7 mm thick melt electrospun scaffold and in vivo that a functional vascular network can be formed. Through computational modelling, we establish numerical values for variable working distances that maintain a constant electrostatic force during printing. Based on the computational simulations, three different voltage profiles are tested and their effect on the maximum height of large volume scaffolds. To our knowledge this is the first report that combines a z-axis and increasing the voltage during MEW. This process results in the fabrication of high volume scaffolds that exceed 7 mm in height with uniform morphologies and constant fibre diameters.

5.2 INTRODUCTION

Polymer scaffolds manufactured via Melt Electrospinning Writing (MEW) exhibit highly defined designs with controllable three-dimensional (3D) architectures in the lower micron to submicron range [30]. Their high surface to volume ratio makes such scaffolds amenable to tissue engineering and regenerative medicine by promoting cell attachment and proliferation [173]. Traditionally in electrospinning, polymers are dissolved in a solvent, which combine with the induced electrostatic forces to produce fibres with sub-micron diameters. Solvents, however, increase the instability of the electrified jet during its flight phase. This so called “whipping” leads to an unpredictable deposition of the polymer and result in scaffolds with randomised structures [233]. Using a highly viscous melt instead of a polymer solution of lower viscosity significantly improves the directional stability of the fibre during its flight phase towards the grounded collector [28] in two aspects: first, the surface tension of the melt is higher due to an increased level of viscosity than typically seen with

polymer solutions. Secondly, a higher amount of charge is stored within the solvent and contributes to the electrically provoked whipping phenomena. Hence, the flight path of an electrified molten polymer jet is more stable [31], and allows for targeted material deposition by using additive manufacturing (AM) principles to fabricate 3D objects [9]. Compared to conventional AM techniques, however, to our knowledge maximum printable heights for MEW are not reported to exceed 2-3 mm before a decline in the quality of fibre placement and scaffold morphology occurs [217]. It is known that due to the semi conductive nature of the melt, a considerable amount of excess charge is trapped within the deposited polymer and subsequently counteracts accurate placement of successive fibres because of the electrical repulsion [26]. Therefore it is important to consider charge accumulation within deposited fibres is for exploiting the full range of technological capabilities of MEW. Hence, this study aims to provide an applied solution to mitigate the arising repellent forces and fabricate multi-layered scaffolds.

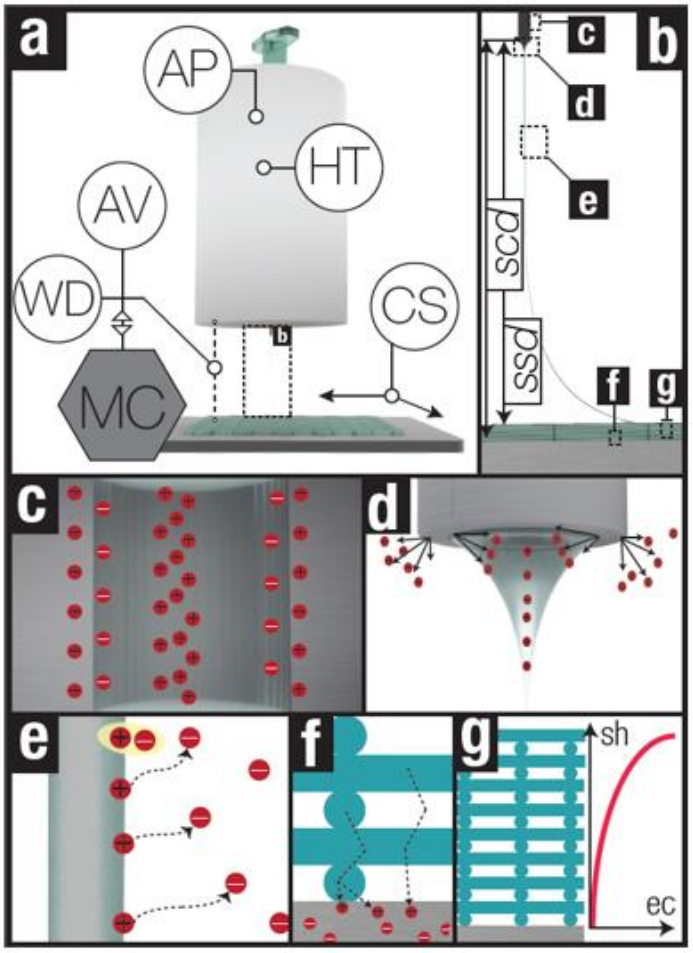

Figure 27: ((a) schematic of the print head, including a microcontroller (MC) controlling the Applied Voltage (AV) and Working Distance (WD). Further parameters are Heating Temperature (HT), Applied Pressure (AP) and Collection Speed (CS). (b), shows the spinneret to scaffold (ssd) and the spinneret

to collector distance (scd) and indicates areas of charge dissociation (c) and charge emission (d). (e) demonstrates the exchange of charge with the environment, such as humidity and (f) shows discharge mechanism of surface contact discharge (left) and inverse corona discharge (right). (g) illustrates the assumed theoretical increase in excess charge (ec) among the height (sh)

5.3 BACKGROUND

The application of pressure to a molten polymer within a syringe results in the extrusion through the spinneret (Fig. 25. a). The establishment of an electrical field between the spinneret and the oppositely charged or grounded collector transforms the extruded material into a Taylor cone [38]. Typically, it stabilises the molten fluid column, which travels from the spinneret towards the collector without undergoing Raleigh-Plateau instabilities [225]. The applied voltage sustains the electro-hydrodynamic mass flow of the molten jet to be directly written onto a substrate (Fig. 25.b). During a flight phase, the jet experiences significant thinning through the electrostatic acceleration of the induced charge carriers [109]. To print ordered structures, the speed of the collector must surpass the rate of the polymer mass flow, termed the Critical Translation Speed (CTS). Increasing the collector speed beyond the CTS enhances the stretching of the viscoelastic mPCL and shapes the jet to a more pronounced catenary profile [31]. Similar to conventional 3D-printing techniques, fabricating multi-layered scaffolds requires to move the print head in the z-direction. Although this is rarely implemented in the electrospinning field (an exemption can be found here [157]), it is essential to prevent the scaffold from building up too close to the heated and electrostatically charged region around the spinneret. Based on Coulomb's law, however, this increase in height leads to a decline in electrostatic forces [133]. Such insufficient electrostatic forces results in an enhanced material accumulation of molten polymer within the Taylor cone, which is periodically released in form of beads with diameters up to 1 mm [205]. The majority of literature describes the accumulation of volumetric and surface charge around deposited material during solution electrospinning [231] and is extensively reviewed by Collin et al. [33]. Generally, the utilisation of high voltage leads to two mechanisms of injecting charge into a viscous polymer [234]. The first describes that electrical field induced emission occurs at conductive materials close to strong electrical fields and triggers mobile charge carriers [235]. These are emitted into the surrounding media, and impart kinetic energy into the liquid [236]. The second of charge injection, called induced disassociation (Fig. 25.c) is described as a continuous separation and recombination of

already present ion pairs [104]. Both mechanisms lead to the introduction of mobile charge carriers into the molten polymer, which accelerate the jet towards the collector. During the flight phase charge dissipation occurs due to interactions with the environment (e.g. humidity [110, 237]) (Fig. 25.e). The deposited material solidifies and traps a significant amount of surface and volumetric charge. Discharging of the first deposited layers (Fig. 25.f) was described by Filatov et al. as spontaneous dielectric breakdowns occurring between the solidified fibres and the collector [119]. Although those phenomena are investigated by today only for solution electrospinning, the effects may hypothetically be related to MEW scaffolds.

We hypothesised that to print high volume; thick and micron fibre-sized scaffolds it is a condition sin qua non maintaining the distance between the top layer of the scaffold and the spinneret constant by adjusting the z-axis of the stage. This requires an increase of applied voltage during the fabrication process respectively to maintain the electrostatic force on a constant level and improve the fibre stacking quality at large build heights. First, we simulated the environment and in order to validate our in-silico findings experimentally, a microcontroller system (MC) was designed to mitigate the influence of the excess charge during fabrication. It facilitates incremental rises of the print head and a simultaneous increase of the AV, the values were established from the previously conducted simulations and essential to retain the electrostatic forces at a constant level. Five different MEW scaffolds were fabricated. The first two included a "control" scaffold (A) under constant AV and unchanged scd and scaffold (B) under constant AV, but increasing scd. The three scaffolds from series (C) were printed under a dynamic iteration of both (scd and AV), while each case was started under different values (7 kV, 8 kV and 9 kV) to investigate the effect of different starting AV on the final morphology.

5.4 RESULTS

Scaffold (A) exhibited considerably distorted structures including mismatched fibre bundles starting at an average height of approximately 2 mm (Fig. 26. b). The bundles randomly reached 4 mm high peaks of distorted fibres. Interestingly, at the high points, individual fibres were visibly detached and directed upwards with molten endpoints. Scaffold (B), showed poor fibre placement starting at heights of approximately 3.5 mm (Fig. 26.b). In contrast to scaffold (A), the distortion was initiated due to a high deviation in diameters, including randomly deposited 1 mm thick polymer beads. The

build heights of group (C) with an maximum at 7.1 mm (Fig. 3.c) were achieved with the lowest starting voltage of 7 kV. The higher starting voltages of 8 kV and 9 kV reached average build heights of 6.2 mm and 5.7 mm, respectively (Fig. 3.d). Although the scaffolds in group C showed substantial heights, distortion events similar to scaffold (A) were observed, including peaking fibre bundles and random fibres with molten ends.

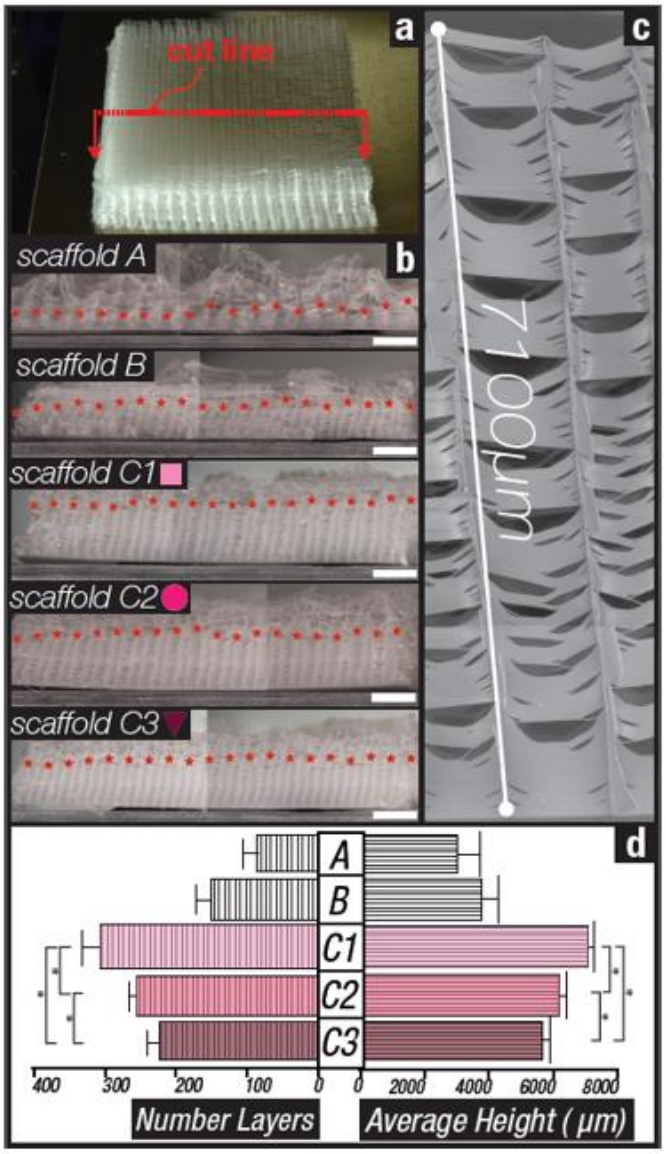

Figure 28: (a) shows scaffold (C1) on the collector with the line where the cut was applied. (b) shows all scaffolds including indications to maximum levels of undisturbed layers reached (scale bars are 5 mm). Image (c) is compiled via Adobe Photo Photoshop showing a section of a scaffold, which was printed after the experiments using the settings from (C1) and demonstrates the height of 7,1mm. (d) shows the average number of layers for all scaffolds (left) and the average heights of the individual scaffolds (right). GraphPad v6.05 (GraphPad Software, Inc., USA) was used to conduct a One-Way ANOVA and verify the statistical difference of the mean values ($p<0.05$).

5.5 DISCUSSION

From a reproducibility and manufacturing point of view does the inherent presence of the electrical field the precise placement of fibres of a high volume and thick scaffold design challenging. We determined both from simulations and experiments that a single defect triggers a snowball effect, as it initiates additional imperfections in the next built layers. This keeps propagating poor fibre placement and results in distorted scaffold architectures. Two major causes are known to be responsible for creating such defects. The first is the deflection of fibres from their vertical trajectory and was seen in all scaffolds. It arises from the accumulation of charge within the top layers of higher scaffolds, which prevents new upcoming fibres from linear stacking [203]. Additionally, it can be assumed that the travelling fibres are more electrostatically attracted to the collection areas between the fibres, because these areas are not covered by insulating polymer structures (Fig. 28.a). The second failure is initiated by the deposition of large polymer droplets, such as those seen in scaffold (B). Insufficient electrostatic forces due to an increasing WD lead to the discussed pulsing behaviour and the formation of large beads. Once released from the spinneret, they unpredictably buckle on the scaffold and significantly prevent further homogeneous deposition (Fig. 28.b). Interestingly, a third and not yet described failure mode was identified and most prominently detected in group (A), followed by (C3), (C2) and (C1). During fabrication, single deposited fibres were spontaneously ejected vertically towards the charged spinneret. After the print-head moved further, the lifted fibres collapsed and formed random material peaks, which, similarly to the aforementioned beads, prevented subsequent homogeneous fibre stacking (Fig. 28.c). Since this phenomenon most prominently appeared in group (A), where the top layers get the closest to the source of heat and electrostatic force, we hypothesise that the high temperature around the spinneret significantly lowers the viscosity of the top layers, which is known to mobilise trapped charge carriers within a polymer [232]. Subsequently, the presence of the strong electrical field, arising from the charged spinneret at a close distance, provokes the temporarily mobilised charge carriers to generate a dipole. More specifically, the mobilised excess charge of same polarity, which is predominant, might be repelled, while small residuals of oppositely charged ions might be attracted to the spinneret. Hence, the latter accumulate on the upper side of the scaffold until they impart sufficient kinetic energy into the molten polymer to be physically dragged

towards the spinneret. The existence of this mechanism can be underlined by the fact, that the highest structures were achieved with the lowest AV (i.e. group (C)). In vitro experiments demonstrated that thick MEW scaffolds with large pores and pore interconnections support cell attachment, migration, and proliferation and ECM formation throughout the entire scaffold architecture (Supplementary Information). Preliminary studies showed at thick MEW scaffolds allow the development of a functional vascular network in hard and soft tissue engineering applications.

5.6 CONCLUSION

Therefore, it may be concluded, that the smallest implementation of initial excess charge, as seen in scaffold (C1), will generate the most non-distorted layers. Furthermore, it was observed that the anticipated effect most prominently appeared at free hanging fibres, which are typical for scaffolds with 90° architectures, (fibre placement in X and Y direction) and cause enhanced material accumulation at fibre intersections. After multiple repetitions, sagged fibre structures between the junction points occurred and were spontaneously spanned by a single upcoming fibre. Since no fusion of the free hanging fibre to previous fibres existed between these crossover points these strands were observed to be subject to the most intensive attraction to the spinneret. A detailed documentation of spontaneously occurring and oppositely directed forces on the material allude to the need for further investigation on this newly identified phenomenon.

5.7 SUMMARY

In summary, a mechatronic system was designed and applied to MEW, which adjusts the WD to accommodate the build height of high volume scaffolds. In parallel, it triggers a simulation based increase of the AV to maintain the electrostatic forces at a constant level. The different scaffolds demonstrated that generally lesser amounts of initially induced charge (i.e. a low starting AV) result in a higher number of accurately deposited layers. Hence, this introduces an effective method to minimise the inherent, yet adverse side-effects of electrostatic forces in the MEW process to fabricate significant thicker scaffolds. The high volume and thick scaffolds showed promising in vitro and in vivo results.

5.8 EXPERIMENTAL SECTION

Simulation

5.8.1 The process was first modelled in silico using COMSOL Multiphysics® Simulation Software (Version 5.2, COMSOL Inc., USA). The geometries of the components of our in-house built MEW device were recreated and the electrical conductivities of the simulated objects were assigned according to properties of the physical components (stainless steel spinneret: 1.45×10^{6} [S/m]; air (at 20 °C): 5×10^{-15} [S/m]; aluminium collector: 3.774×10^{-7} [S/m]). The decline of the intensity of the electrostatic forces was simulated for 7 kV, 8 kV and 9 kV at all distances between 8 mm and 18 mm (Fig. 27.a and Fig. 27.b). Using 7 kV as the lowest starting AV is based on experience, as lower AV at a WD of 8 mm would not provide sufficient electrostatic force to generate homogeneous fibres. Along the increasing distance, the simulation further included a simultaneously growing scaffold (1000 µm pore size, 20 µm fibre width) with an assumed electrical conductivity of 10 x 10^{-10} [S/m], which is typical for molten polymers [41].

Next, the results established from the simulations (Fig. 27.b) were converted into increasing values for the AV to maintain the initial electrostatic force on a constant level for all remaining distances (C1,C2,C3 in Fig. 27.b and Figure 27.c)) in the physical experiment (Fig. 27.c).

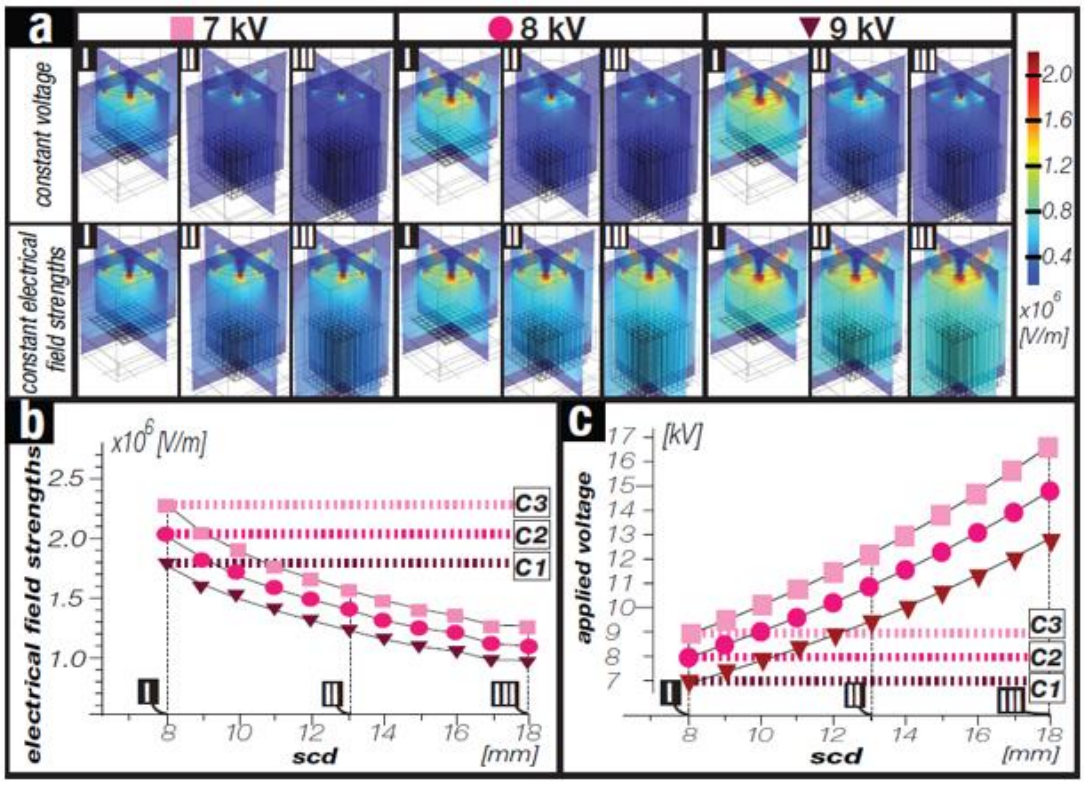

Figure 29: (a) shows the print head simulations in a 3D environment for a, b and c at three starting voltages, which were kept constant (top row) and altered (second row) to keep the electrostatic forces constant. (b) reveals the simulated values of the declining electrical field strengths and (c) the calculated respective voltage be applied for maintaining the electrostatic force (C1,C2,C3) on a constant level.

5.8.2

Scaffold fabrication

All scaffolds were fabricated using a constant MT and AP under ambient conditions. The overall diameter homogeneity (20 µm ± 1.5 µm) was achieved via adjusting the CS respectively to reach an identical catenary shaped flight path of the jet. Once printed, all scaffolds were dissected across the middle (Fig. 26.a).

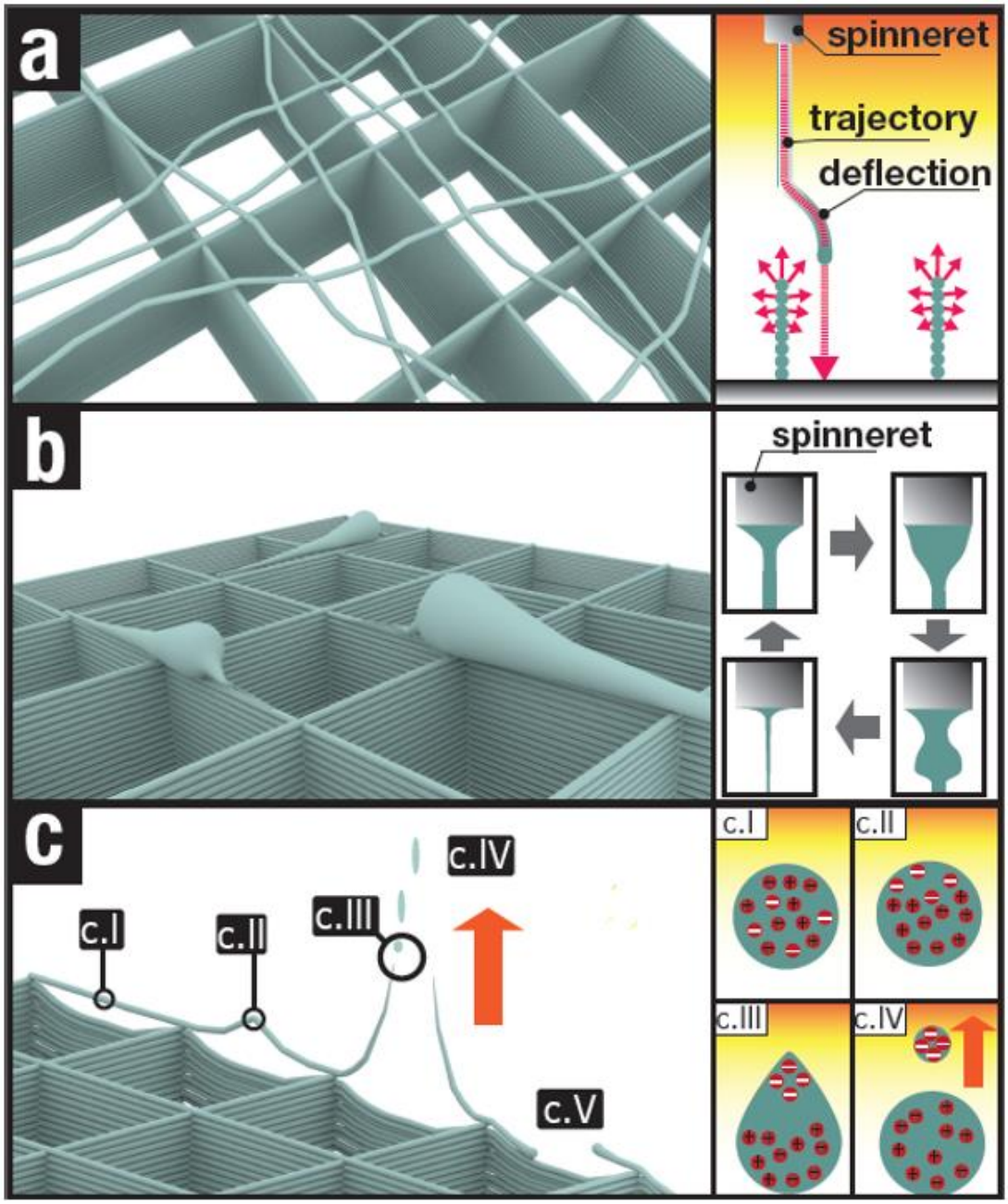

Figure 30: (a) shows distorted fibres due to the electrostatic repulsion of the build-up material and the attraction of the collector. (b) illustrates polymer beads and reveals their generation around the tip of a spinneret. (c) demonstrates the observed effect of fibre attraction: in (c.I) a bridged fibre is visible, which is lifted (c.II) and at a certain stage (c.III) vertically attracted including material ejection (c.VI) towards the spinneret. (c.V) shows solidified and collapsed fibres.

5.8.3

Characterisation

The morphologies were investigated using a LEICA M125 Stereo Microscope. The resulting images were tiled with Adobe Photoshop (Adobe, USA) and analysed with ImageJ (National Institutes of Health, USA) to measure the heights of uniformly deposited and non-distorted layers. In order to examine the number of layers, a Scanning Electron Microscope (TM3000, Hitachi, Japan) at an acceleration voltage of 15 kV was used.

Scaffolds of group D were seeded and cultured for up to 4 weeks with human periodontal ligament and mesenchymal precursor cells and then imaged via confocal laser microscopy.

Acknowledgements

This work has been financially supported by the Cooperative Research Centre CRC Cell Therapy Manufacturing, ARC Centre in Additive Biomanufacturing and assisted
5.8.4 by the Hans Fischer Senior Fellowship at the Institute for Advanced Study, Technische Universitaet München.

Chapter 6: Electrospinning Writing with molten poly (ε-caprolactone) from different directions – examining the effects of gravity

Felix M. Wunner[1], Joachim Maartens[1], Onur Bas[1,2], Konstantin Gottschalk[1], Elena M. De-Juan-Pardo[1], Dietmar W. Hutmacher[1,2,3, a]

Published in Materials Letters (2018)

[1]Centre in Regenerative Medicine, Institute of Health and Biomedical Innovation, Queensland University of Technology (QUT), Kelvin Grove, Brisbane, QLD 4059, Australia
[2]ARC ITTC in Additive Biomanufacturing, Institute of Health and Biomedical Innovation (IHBI), Queensland University of Technology (QUT), 60 Musk Avenue, 4059, Kelvin Grove, Australia
[3]Institute for Advanced Study, Technical University of Munich (TUM), Lichtenbergstraße 2a, 85748 Garching, Germany

a) Corresponding author at: Institute for Health and Biomedical Innovation, Queensland University of Technology, 60 Musk Avenue, Kelvin Grove 4059, Australia. E-mail addresses: dietmar.hutmacher@qut.edu.au (Dietmar W. Hutmacher).

Statement of Contribution of Co-Authors for

Thesis by Published Papers

The authors listed below have certified* that:

1. they meet the criteria for authorship in that they have participated in the conception, execution, or interpretation, of at least that part of the publication in their field of expertise;
2. they take public responsibility for their part of the publication, except for the responsible author who accepts overall responsibility for the publication;
3. there are no other authors of the publication according to these criteria;
4. potential conflicts of interest have been disclosed to (a) granting bodies, (b) the editor or publisher of journals or other publications, and (c) the head of the responsible academic unit, and
5. they agree to the use of the publication in the student's thesis and its publication on the QUT ePrints database consistent with any limitations set by publisher requirements.

Electrospinning writing with molten poly (ε-caprolactone) from different directions – discovering the effects of gravity | (published in Materials Letters, 2018)

Contributor		**Statement of contribution**
Felix Wunner	QUT Verified Signature	Conceived and designed the experiments. Aided experimental work. Wrote the manuscript.
Signature		
Date	17/11/2017	
Joachim Maartens	QUT Verified Signatures	Co-wrote the manuscript
Onur Bas		Co-wrote the manuscript.
Konstantin Gottschalk		Helped with experimental work.
Elena M. De-Juan-Pardo		Co-wrote the manuscript and provided feedback.
Dietmar W. Hutmacher		Conceived and designed the experiments. Provided feedback on the manuscript. Supervised the entire work. Approved the final version of the manuscript.

Principal Supervisor Confirmation

I have sighted email or other correspondence from all Co-authors confirming their certifying authorship.

Dietmar W. Hutmacher QUT Verified Signature

Name Signature Date 17/11/2017

6.1 ABSTRACT

This work investigates the effect of gravity during melt electrospinning writing (MEW) and explores the feasibility of developing melt electrospinning writing devices with lateral and upside down print head configurations. Average fibre diameters of printed constructs using different printing directions and their variability reveal particular differences. These give an inside of an effect of gravity, which was observed to affect the Taylor cone, yet interestingly not the fibre jet. Additionally, stable processing conditions were studied and show that with MEW it is possible to reproducibly print from all directions.

6.2 INTRODUCITON

Products with high surface-to-volume ratios have contributed to various applications across diverse industries [19, 64], most recently to the fields of tissue engineering and regenerative medicine (TE&RM). An electrohydrodynamic process - defined in the literature as electrospinning - can generate micron- to submicron-scale fibres from viscous polymers (dissolved in a solution or molten) when in close proximity to an electrical field. In both solution and melt electrospinning (SE and ME, respectively), the interaction of the prevailing system parameters (Fig. 29.a) leads to the establishment of a Taylor Cone on the tip of a spinneret (Fig. 29.b). Its conical shape resembles an equilibrium between pressure-induced mass flow into the Taylor cone and forces pulling material out of the cone arising from electrostatic, gravitational and mechanical drag forces (Fig.29.c) [238-240].

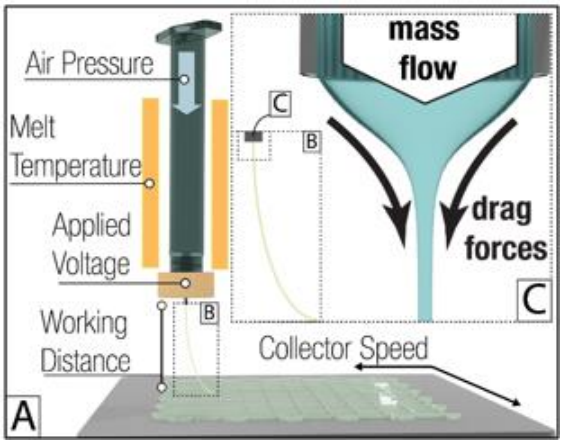

Figure 31: A) schematic of a typical setup for a MEW process including the parameters applied pressure (AP), melt temperature (MT), applied voltage (AV), working distance (WD) and collection speed (CS). B) Shows the fibre flight path and C) a sectional view of a Taylor cone with schematically represented mass flow and drag forces on the extruded polymer

The disparity in viscosity between molten polymers and polymers dissolved in solvents leads to significant differences in both mass flow and fibre diameters, with the former producing diameters typically two orders of magnitude larger due to the significantly larger mass flows. As the mass flow in the SE process is very small, the effect of gravity during is suggested to be negligible [241]. This fact enabled the design of SE machines for multidirectional printing, broadening industrial applications. Significantly larger mass flows occurs during ME, indicating that the influence of gravitational forces may have an effect on the process. However, there is a lack of research directed to address the effect of gravity, especially in ME Writing (MEW). To our knowledge, MEW is conducted exclusively from a top-down orientation and, although in rare cases gravity is included as a parameter in computational modelling of the process [72], its effect on the fibre itself, compared to the arising electrostatic forces, is routinely ignored [242]. One recent study describes a common unstable behaviour of the Taylor cone during MEW, termed fibre pulsing [205]. Viscoelastic forces hold the melt together but in the case of an imbalanced mass flow, material aggregates within the Taylor cone until a large material excess is released towards the collector in the shape of an extended bead. Fibre pulsing compromises the quality and thus MEW parameters need to be optimised to ensure balanced mass flow rates. Interestingly, the authors explained the drag forces acting on the Taylor cone exclusively in terms of a combination of mechanical and electrostatic forces, yet momentarily discount the impact of gravitational forces. Here we hypothesise that gravitational forces influence the MEW process and therefore investigate the effect of printing direction (top, side and upside down) on the quality and reproducibly of the process and product. Our final aim is to explore the possibility of developing MEW devices with a vertical configuration as an alternative to the standard horizontal printing to widen the potential of this technology.

6.3 MATERIALS AND METHODS

Medical grade poly(ε-caprolactone) (PCL Purasorb PC 12, Purac Biomaterials, Netherlands) was processed on a in-house built MEW device [222]. The influence, intensity and inter-correlation of the system parameters that control the printing process were analysed conducting a multifactorial orthogonal design study (Table 1.A) [170], a methodology well-known within the electrospinning community [38, 188]. It was applied to the five main system parameters that control MEW (Table 1.B), i.e.

collector distance (CD), collector speed (CS), applied pressure (AP), melting temperature (MT) and applied voltage (AV), and resulted in sixteen different parameter configurations, individually conducted at each print orientation. A schematic analysis helped to identify parameter hierarchies by calculating the R value (Table 1.C). Scanning Electron Microscope (Hitachi, TM3000, Japan) images were used to quantify the diameters (n=24/scaffold). The image-processing software (ImageJ; National Institute of Health, USA) was applied to measure average fibre diameters and their standard deviations using GraphPad (GraphPad v6.05, Software, Inc., USA).

6.4 RESULTS AND DISCUSSION

Table 1.A shows the results of the Design of Experiments and reveals similar trends between the three printing directions with varying system parameters (Table 1.B). An increase in AP leads to enhanced material flow and larger fibre diameters [238, 239]. The effect of higher temperatures (MT) on viscosity and concomitant increased material flow explain the resultant increase in fibre diameter. Due to the small working distances employed (6-12mm) the influence of the consistently high voltage (Coulomb's Law) across the suite of experiments is constant[133]. Also, increased collection speeds are known to stretch fibres and thereby reduce fibre diameters [238]. Within the range of the printing conditions applied in this experiment, mutual trends between the three printing directions are observed for all five parameters. However, the resulting hierarchy of each individual parameter (Table. 1.C) shows significant differences, as demonstrated by the distinctive R values.

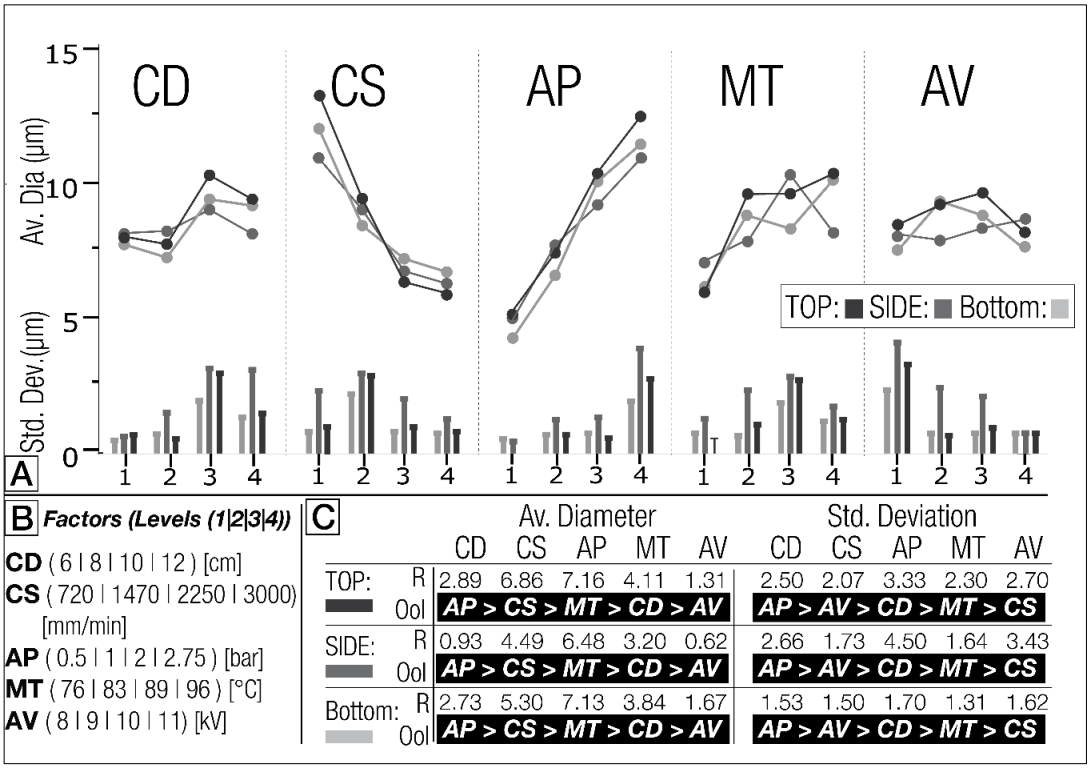

Table 5: A) results of the applied design of experiments showing the five parameters regarding diameter and standard deviation, B) their factors, levels and applied values and C) the results from the analysis which reveals the intensity of the influence (R) and its order of importance (OoI)

Next, we conducted a comparative analysis of the individual results and identified two distinct cases: (1) low mass flow and high drag forces on the fibre, which leads to homogeneous diameters, and (2) high mass flow with weak drag forces, which generates fibre pulsing and hence, gives rises to scaffolds with highly distorted morphologies. Case 1 was apparent at experiments with low pressure (<2 bar), combined with relatively high collection speeds and voltages. In experiments #1 and #2 (Table 2) the flow of molten polymer in and out of the Taylor cone appears balanced, with no significant differences in diameter dimensions. The consistently high electrostatic forces (CD, 6mm) ensure constant homogeneous polymer flow in and out of the cone and inhibits pulsing. Cases #6, #11 and #16 printed under similar low mass flow, high speeds and increased applied voltage, generate equally small fibre diameters. These cases reveal minor fibre diameter differences (<1.5 µm). Hence, this fact evidences that side and bottom printing is feasible under the given parameter settings and can result in similar scaffold quality regardless of the printing orientation.

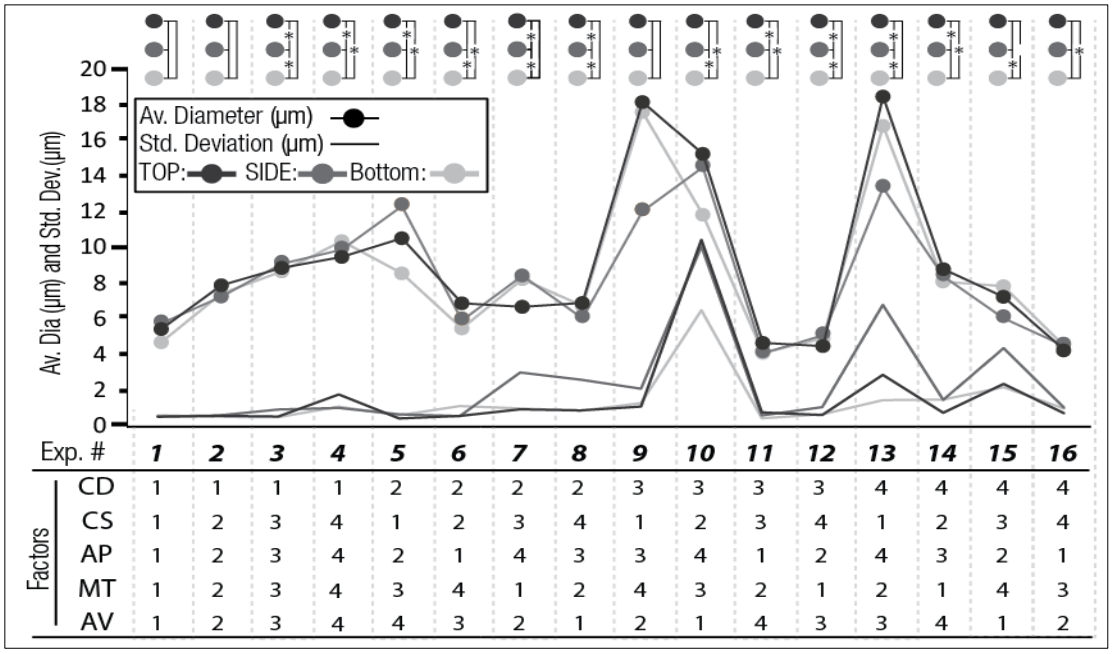

Exp. #	1	2	3	4	5	6	7	8	9	10	11	12	13	14	15	16
Factors CD	1	1	1	1	2	2	2	2	3	3	3	3	4	4	4	4
CS	1	2	3	4	1	2	3	4	1	2	3	4	1	2	3	4
AP	1	2	3	4	2	1	4	3	3	4	1	2	4	3	2	1
MT	1	2	3	4	3	4	1	2	4	3	2	1	2	1	4	3
AV	1	2	3	4	4	3	2	1	2	1	4	3	3	4	1	2

Table 6: individual results (average diameter and standard deviation, $p<0.05$) of the 16 experiments and a referencing table to the respective parameter settings (values can be found in Table 1)

In contrast, case 2, characterised by high polymer flow, was established when the level of pressure and temperature is 3 or 4 (2 or 2.75 bar for AP, and 89 or 96ºC for MT, respectively). This leads to over-filling of the Taylor cone, subsequent pulsing and highly distorted scaffold architectures as evidenced [205], and replicated in experiments #4, #7, #10 and #13 (Table 2). Interestingly, during all experiments in the horizontal direction gravity-induced bending of the fibres could be detected (Fig. 30.b-d). However, a higher mass flow and subsequent filling mechanism of the Taylor cone which consequently is more likely to be affected by gravity (Fig. 30.d) was observed. In all these cases, the Taylor cone did slide along the gravity vector perpendicular to the needle axis before depositing on the collector.

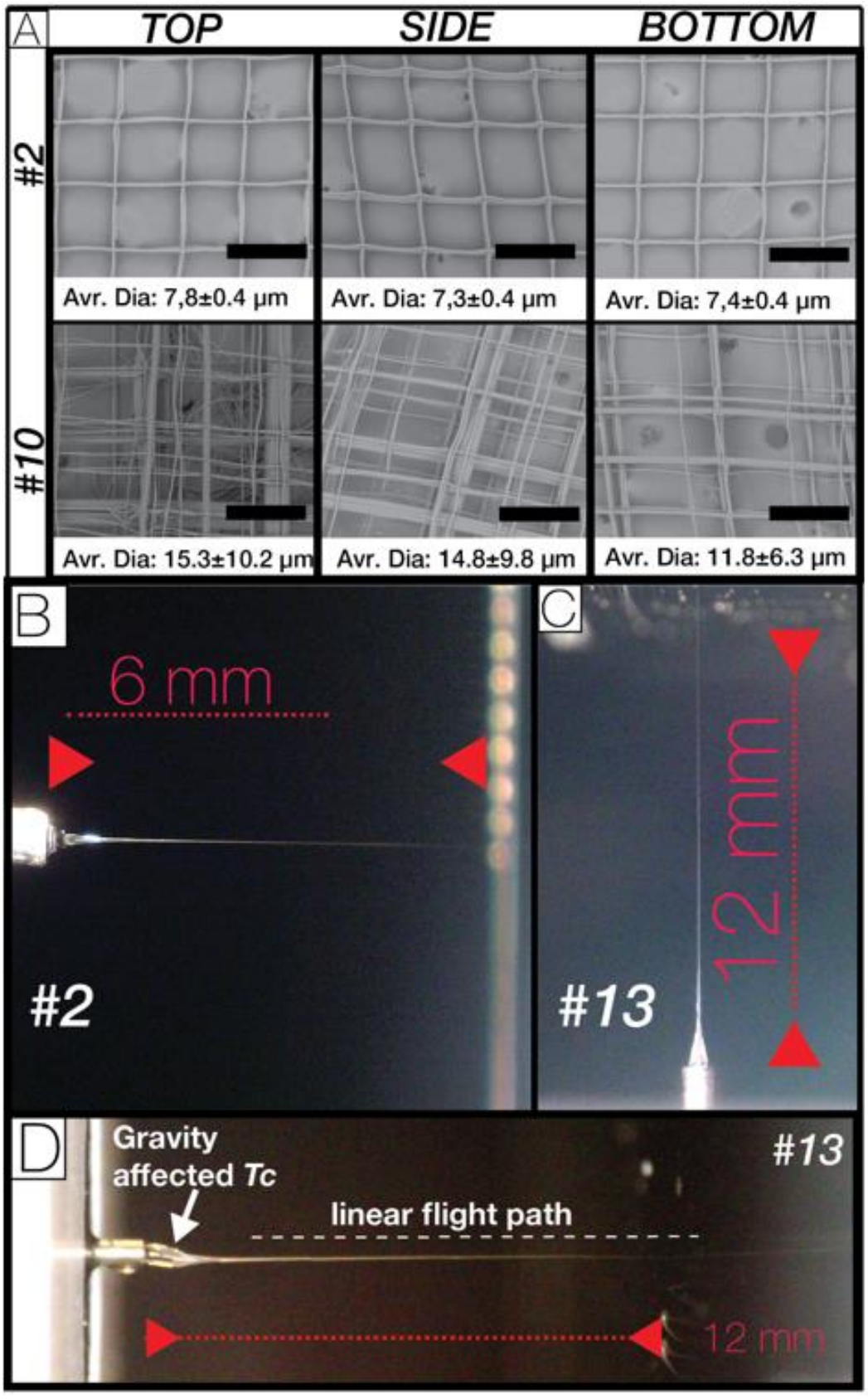

Figure 32: A) SEM of scaffolds from experiments #2 and #10 from all directions including average diameters and standard deviation. B) shows a fibre without distortion from side position (#2) and C) from a bottom position (#13). D) shows the gravity affected Taylor cone and linear flight path of the fibre (#13).

6.5 CONCLUSION

This study validates the feasibility of developing MEW devices with either top, side or upside down printing configurations. Although gravity does influence the MEW process, it is possible to control its effect by adjusting the system parameters accordingly, regardless of the printing orientation. In cases of increased mass flow, however, the results indicated that gravity affects the shape of the Taylor cone across the different printing orientations. Therefore, the findings open up new avenues for furthering design iterations for MEW devices.

6.6 ACKNOWLEDGMENTS

This research was funded by the ARC Training Centre in Additive Biomanufacturing (IC160100026), the Centre in Regenerative Medicine and the Cooperative Research Centre for Cell Therapy Manufacturing and the Institute for Advanced Study, Technische Universität München.

6.7 DISCLOSURE

The authors have nothing to disclose

Chapter 7: Design and Development of a High-Throughput Melt Electrospinning Writing Device

Felix M. Wunner[1], Sebastian Eggert[1], Joachim Maartens[1], Onur Bas[2], Elena M. De-Juan-Pardo[1], Dietmar W. Hutmacher[1,2,3,4,a]

Accepted by *3D printing and Additive Manufacturing* (2018)

[1]Centre in Regenerative Medicine, Institute of Health and Biomedical Innovation, Queensland University of Technology (QUT), Kelvin Grove, Brisbane, QLD 4059, Australia
[2]ARC ITTC in Additive Biomanufacturing, Institute of Health and Biomedical Innovation (IHBI), Queensland University of Technology (QUT), Kelvin Grove, Brisbane, QLD 4059, Australia
[3]Institute for Advanced Study, Technical University of Munich (TUM), Lichtenbergstraße 2a, 85748 Garching, Germany.
[4]George W Woodruff School of Mechanical Engineering, Georgia Institute of Technology, 801 Ferst Drive Northwest, Atlanta, GA 30332, USA.
[a]Corresponding author at: Institute for Health and Biomedical Innovation, Queensland University of Technology, 60 Musk Avenue, Kelvin Grove 4059, Australia. E-mail addresses: dietmar.hutmacher@qut.edu.au (Dietmar W. Hutmacher).

Statement of Contribution of Co-Authors for

Thesis by Published Papers

The authors listed below have certified* that:

1. they meet the criteria for authorship in that they have participated in the conception, execution, or interpretation, of at least that part of the publication in their field of expertise;
2. they take public responsibility for their part of the publication, except for the responsible author who accepts overall responsibility for the publication;
3. there are no other authors of the publication according to these criteria;
4. potential conflicts of interest have been disclosed to (a) granting bodies, (b) the editor or publisher of journals or other publications, and (c) the head of the responsible academic unit, and
5. they agree to the use of the publication in the student's thesis and its publication on the QUT ePrints database consistent with any limitations set by publisher requirements.

Design and development of a High-Throughput Melt Electrospinning Writing device
(Accepted by 3D Printing and Additive Manufacturing, 2018)

Contributor	Statement of contribution
Felix Wunner **Signature** QUT Verified Signature **Date** 17/11/2017	Conceived and designed the experiments. Aided experimental work. Wrote the manuscript.
Sebastian Eggert	Co-wrote the manuscript. Aided experimental work.
Joachim Maartens	Provided feedback on the manuscript
Onur Bas	Co-wrote the manuscript. Aided experimental work.
Elena M. De-Juan-Pardo	Co-wrote the manuscript and provided feedback.
Dietmar W. Hutmacher	Conceived and designed the experiments. Provided feedback on the manuscript. Supervised the entire work. Approved the final version of the manuscript.

QUT Verified Signatures

Principal Supervisor Confirmation

I have sighted email or other correspondence from all Co-authors confirming their certifying authorship.

Dietmar W. Hutmacher QUT Verified Signature 17/11/2017

Name Signature Date

7.1 ABSTRACT

Three-Dimensionally (3D) printed scaffolds and cell culture lattices with microscale features are increasingly used in tissue engineering and regenerative medicine (TERM). One additive manufacturing technology to design and fabricate such structures is Melt Electrospinning Writing (MEW), a process which needs to be scaled in production to effectively translate to industrial applications. Based on the basic MEW working principles, we designed and developed a printer with eight simultaneously extruding heads. Importantly, we could fabricate identical structures using parameters developed from a single head system, therefore establishing a MEW printer "ecosystem" that allows for the direct upscaling from laboratory research. The successful transfer to vertically mounted collectors produced homogeneous, reproducible, scaffolds with identical morphologies and fiber diameters. These proof-of-concept experiments also show that MEW is capable of large-scale fabrication, successfully demonstrated by manufacturing 78 cm x 78 cm sheets of scaffolds/lattices. This study demonstrates that upscaling MEW can be realized by multiplying the number of extruding heads, while a vertical mounting of the collector significantly reduces the MEW footprint. Additionally, economic aspects were considered during the development and costly components such as the x,y,z linear axis, were minimized. Herein, we demonstrate for the first time the development of a high throughput machine for MEW technology.

7.2 INTRODUCTION

The recent adoption of additive manufacturing (AM) technologies within the fields of tissue engineering and regenerative medicine (TERM) has greatly expanded the design potential and fabrication perspective of various medical products [243-246]. These include patient-specific implants and medical devices [247], on-chip technologies [248, 249], physical models [246] and three-dimensional (3D) scaffolds for cell culture [250], here termed "lattices" [19]. Such a diverse range of applications belies a thriving sector of additive biomanufacturing (ABM) technologies for the 21st century's medical industry [243, 251, 252]. In the classical TERM approach, cell seeding and reimplantation defined the design and fabrication of 3D structures – known as scaffolds [253-255]. Ideally, such ABM platforms should be capable of creating 3D architectures with a highly-porous interconnected network that guide tissue growth

and remodeling [250]. Since traditional fabrication techniques for scaffolds, such as solvent casting, freeze-drying, porogen leaching, fiber bonding, dual-phase separation, and gas foaming [256], only allow limited control over the final geometry and porosity, various research efforts have been applied to AM techniques. These are, for example, stereolithography, selective laser sintering and fused deposition modeling (FDM) approaches, that enable direct material deposition to further increase design freedom and control over scaffold architecture [243, 256, 257]. Dissolvable structures, termed fugitive inks, have expanded the volume of the construct made through improved nutrition to cells [258-260].

Separate to ABM, the TERM community also embraced electrospinning technologies [198] to generate structures from polymer fibers in the micron to submicron scale, to significantly increase the surface area available to cells [9, 261]. The generation of an electrical field around an extruded viscous fluid leads to the ejection of a charged jet, that is collected on a grounded or oppositely charged collector [262]. Most commonly, the sufficient viscosity for generating a continuous, charged jet can be achieved by dissolving the polymer in a solution [263]. During its flight phase the charge density along the jet increases[264], which significantly distorts the straight flight path of the traveling fiber, causing buckling of the jet [242] and results in scaffolds with highly randomized architectures [265]. On the one hand, electrospinning, compared to other polymer fabrication technologies, enables high mass flow and hence, greater material throughput; on the other hand, it is challenging to accurately place the fibers. It is worth noting that a considerable amount of solvent is lost in this process, typically 80-90%, but sometimes greater [256]. From an engineering perspective, the low manufacturing rates facilitated the design of scale-up electrospinning machines with multiple nozzles [266]. These can be aligned in close proximity, as the interference of the electrical field lines does not significantly affect the placement accuracy. Hence, this lack of ability to accurately deposit fibers significantly decreases the complexity of the machine design and permitted the technologies transfer to industrial applications for high throughput. From an industrial perspective, the simplicity and comparatively large production rates of solution electrospun scaffolds with non-woven structures paved the way towards commercialization [64].

The principles of electrostatically generating fibers from fluids can be similarly realized with molten polymers, referred to as melt electrospinning [267, 268].

Compared to solution electrospinning, the lack of solvents in melt electrospinning increases the viscosity of the polymer and reduced the charge component of the electrified jet, in turn stabilizing the flight path of the fiber for more precise deposition on a collector [31, 269]. The integration of a computer controlled translational collector for melt electrospinning results in a hybrid approach, termed melt electrospinning writing (MEW) which can 3D print micron-sized fibers in a controlled manner [9, 267, 268]. Using direct-writing principles, MEW produced highly-porous 3D scaffolds with fiber diameters in the lower micron [38] to submicron scale [116]. As an ABM technology, MEW has potential to manufacture highly porous and well-organized scaffolds using biocompatible, degradable polymers [19, 270-273]. Such ABM products can also be used temporarily for in vitro expansion, demonstrated by the application of MEW lattices as an alternative to beads for regulatory T (Treg) cell expansion, with potential for clinical translation [19]. However, while there has been work on scaling melt electrospinning [51, 268], there is no concept described in the current literature that outlines how MEW scaffolds and cell culture lattices can be scaled up. To successfully translate such promising applications for MEW within the TERM community [26], achieving the economics of scale is an essential next step for the technology.

Similar to other AM technologies, such as FDM, the physical properties of a molten polymer typically limit the extrusion speed of the material through the needle during MEW, however accurate deposition results. Conversely, material throughput (mtp) per time for solution electrospinning is comparably low, due to the specifically small extruded volumes; yet these scaffolds provide significantly increased surface areas [30]. As a manufacturing technology MEW retains more material through processing than SES [26] however, it requires significantly lower extrusion speed rates, compared to FDM [274]. Therefore, existing MEW printers are associated to lengthy fabrication times and fail to achieve 3D printed structures with high surface to volume rations (svr) per amount of extruded material (svr/mtp) in profitable time frames. This adversely affects the economics of scale in comparison to other conventional production technologies [275].

In order to reduce the manufacturing time for MEW printers, there are some general aspects to consider. High printing temperatures accelerate the degradation of the polymer and in turn generate more electrically charged degradation products [220].

Moreover, shear thinning polymers with rapid solidification are essential for extrusion-based printing [276]. Low viscosity polymers are difficult to fabricate with good shape fidelity and high resolution. A different strategy to reduce MEW printing times is to increase the collection speed, although this leads to inaccurate fiber placement. There are limits in higher voltage application due to Corona discharge, i.e. sparking at amplified voltages under respectively small distances [277]. Finally, different multi-nozzle systems have been proposed for MEW [50, 126, 130, 163] however, these concepts are not targeting accurate architecture, yet produce randomized structures (Fig.33). Existing alternatives comprise print heads extruding multiple fibers, either distributed in a 2D-plane assembly [50] or circularly aligned on one print head [51]. Nozzle-free melt electrospinning has demonstrated numerous jets without positional control, however over 60 individual linear jets can be generated with a single head [51]. Although manufacturing throughput is improved, these concepts have not improved resolution or fabricated well-ordered microscale architectures. Nonetheless, multi-head strategies appear to be an essential part of scale-up for MEW as a technology.

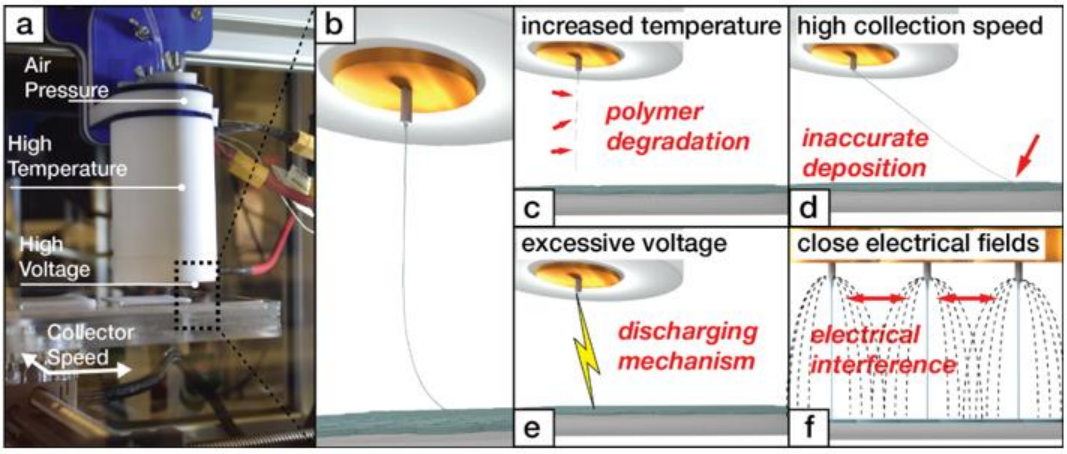

Figure 33: (a) explanation of the system parameters used to generate lattices with a single-head MEW printer. (b) Rendering of the fibre generation zone and visual demonstration of the reasons of limitations in scaling-up MEW. These are: (c) increased temperatures, which lead to polymer degradation, (d) high collection speeds, which decline deposition accuracy, (e) excess amount of voltage voltages, which cause arcing between needle and collector and (f) interference of the electrical fields in case of multi-nozzle designs.

Recently described high-throughput concepts for AM can be categorized in two classes: 1) multi-nozzles integrated into one print-head and 2) multiple individually moving print heads. Hansen et al. [278] demonstrated the capacity of multi-nozzles arrays – described as a hierarchical branching network – within one print head to fabricate multi-layered architectures, resulting in a highly flexible and scalable concept

for extrusion-based deposition. In contrast, 'Project Escher', introduced by Autodesk Inc. (Mill Valley, California, USA) and commercialized by Titan Robotics, Ltd. (Colorado Springs, Colorado, USA) validated a 3D printer with multiple, independently controllable heads designed to manufacture larger and more complex objects. Another approach to scale up assembly was based on combining parallel 3D printer heads with automatization of the part removal, demonstrated by the Form Cell printer (Formlab Inc., USA) or shown in a concept, called " Figure 4"(3D Systems, USA).

In this study, we demonstrate for the first time the successful design and development of a high-throughput HT-MEW printer (Fig.34), using medical-grade poly(ε-caprolactone) (PCL). The HT-MEW printer simultaneously deposits polymer fibers from eight single print heads which allows manufacturing either over thousands of small dimensioned or one large multilayered scaffold/lattices with homogeneous morphologies in the lower micron scale.

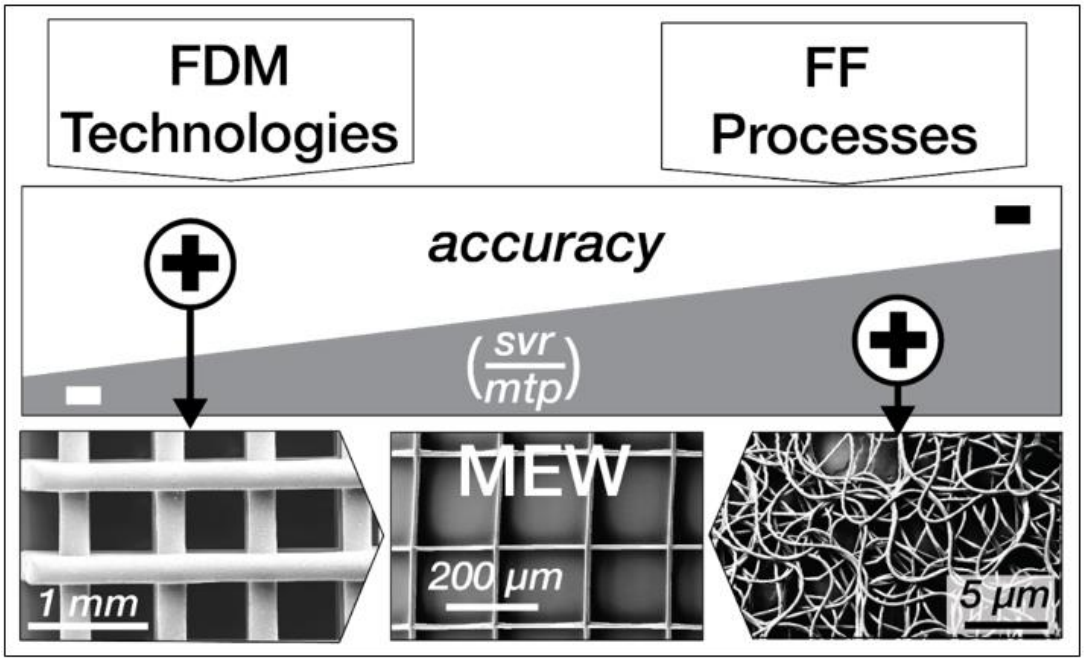

Figure 34: (Top) schematic comparison of MEW's technological predecessors (Fused Deposition Modelling, FDM and Fibre Forming). (Middle & Bottom) Illustration of the conceptual combination of accuracy and the desired high surface per volume ratio (svr) of the lattice per material throughput (mtp).

7.3 MATERIALS AND METHODS

HT MEW printer design

The printer consists of an enclosure, including the extrusion heads, a collecting platform, and the external parameter-controlling units, including a PC (high voltage controller, driver unit for the translational collector and temperate controller box). A
7.3.1 systematic design overview is shown in Fig.35 and explained in more detail in the following sections.

The parameter-controlling units

The in-house designed temperature controller box regulates the temperature of the
7.3.2 eight print heads, which individually are equipped with two heating elements; a detailed design can be found here [38]. All print heads are regulated by temperature controllers (N1030-PR-24V PID Temperature Controller, NOVUS, Australia) and switched by relays (SSR-120, Conch, USA) while power is provided by an 8kW power supply (RSP-750-12, Mean Well, Taiwan). Pressure is regulated by two commercially available regulators (Electro-pneumatic regulator, SMC Pneumatics Pty. Ltd, Australia) which receive as input air-pressure from a typical laboratory pressure line to distribute air equally to the individual heads.

The electrostatic field between the head and the collector is established via a high voltage power supply unit (D-ES40PN-5E/DC, Gamma, High Voltage Research, USA). In-house designed splitters consist of Perspex boxes, filled with highly insulating resin (EL171C/566 Polyurethane, Robnor, England), which distribute the voltage via appropriately insulating cables (HS 30 PTFE, GES GmbH, Germany). A computer is used to transfer motion signals to the in-house designed motion control box, which consist of a power supply (SP-320-48, Mean Well, Taiwan) and three drivers (ND556, Leadshine, USA) individually controlling each of the three axes via
7.3.3 communication through a parallel port interface (KTA-205, Ocean Controls, Australia). The previously mentioned hardware drives the instrument parameters, excluding the collector distance, which is adjusted manually.

The printing enclosure

The printing enclosure consists of two vertically-aligned stages mounted to a frame, a horizontally fixed stage, and the print heads, pointing towards a vertically mounted

collector. On each side of the collector, the four print heads are equidistantly mounted on a custom-made laser cut Perspex construction. Both head assemblies are connected to the vertically aligned linear stages (XN10-0030-E01-71, VELMEX, USA) and powered with a stepper motor (FL57STH51-2804A, Ocean Controls, Australia). The horizontal axis, a linear stage (MN10-0300-E02-21, VELMEX, USA) is driven by the same standard stepper motor as mentioned above and moves the in-house designed collecting platform (9). The latter consists of two aluminum plates of 3 mm, mounted on each side of the Perspex frame, which provides stability. Both plates are electrically grounded through a wire and additionally insulated with 2 layers of insulating tape (KPT-4 KAPTON, DuPont, USA), which is between the aluminum and the Perspex. This design solution aims at preventing electrical interference between two oppositely located charged heads and was verified by a simulation conducted with COMSOL Multiphysics® Simulation Software (Version 5.2, COMSOL Inc., USA). The results reveal no electrical interference between the individual heads at maximum voltage and closest applied distance (additional information is provided in the appendix). The upper end of the collecting platform is attached to two linear stages (TW-01-20, drylin® T linear guides, USA), facilitating stable and frictionless movement.

Both vertically aligned slides are fixed to a supporting frame, which is made from pre-cut extruded aluminum profiles (ITEM, Modular Component & Automation, Australia). In order to avoid potential vibration, the structure is bolted to two custom-made metal plates (Aluminum, Kilners Engineering, Australia), which are connected to a heavy-duty table (OZ Storage Solutions, Australia).

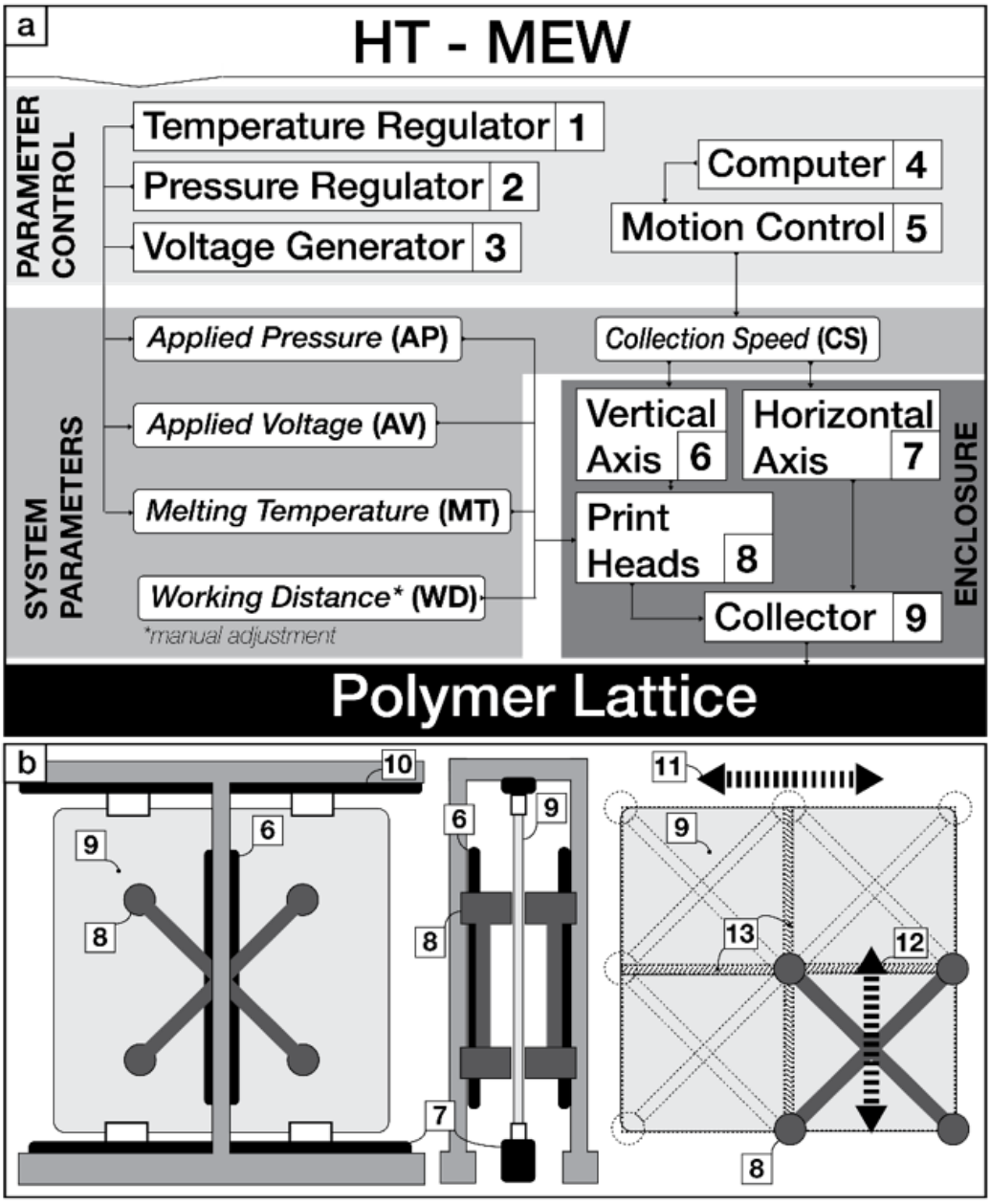

Figure 35: (a) schematic of the HT-MEW printer with three instrument parameters investigated; (1) temperature, (2) pressure and (3) voltage. A (4) computer regulates the (5) motion of the (6) vertical axis and the (7) horizontal axis. The (8) print heads are connected to the former and the (9) collector is fixed on the latter. (b) illustrates the conceptual drawings of the HT-MEW device and shows the components, mentioned before. Additionally, it demonstrates the (10) linear slide bearing on top, which allows for (11) horizontal collector movement. (12) shows the head in its starting position and possible movement, which is designed to overlap (13) and fabricate large-scale lattices.

The custom-made enclosure had three doors (ITEM, Modular Component & Automation, Australia) to provide access to the collector and the printing heads. Operational safety is guaranteed by separately configured magnetic interlocks (XCSDMP5902, Telemecanique Sensors, France), which interrupt the high voltage

supply to the heads when opening during operation. The HT-MEW printer is grounded through the common earth of the laboratory power socket.

7.4 INSTRUMENT PARAMETER CONTROL

The movement of all three stages is controlled by the software MACH3 (MACH 3, ARTSOFT, Newfangled Solutions LLC, USA), which accepts individually written G-Codes to fabricate the lattices. The distance between the heads was designed in accordance with the dimensions of the collector, which allows overlapping structures of the printable areas of each individual head. The syringes (EFD Barrel O.3 mL clear 50, Nordson Australia Pty. Ltd., USA) were filled with 3 mL of medical-grade PCL (Purasorb PC 12, Purac Biomaterials, The Netherlands) and inserted into the print head.

One innovative feature of this HT-MEW printer is its vertical collector configuration. Due to the small amount of extruded melt, the electrostatic force predominates gravity, which allows accurate MEW from the side. In turn, this vertical mounting allows both sides of the collector to be direct-written upon. To commence MEW, the heads are driven to the starting position, shown on the left side of Fig.35.b. After completion of the printing process, the scaffolds can be collected by detaching the collecting platform from the horizontal slide and removing it through the front door.

7.5 ASSESSMENT AND CHARACTERIZATION OF HIGH THROUGHPUT PRINT QUALITY

If the diameter and the fiber spacing of scaffolds printed with a “research-level”, single head MEW device, in a horizontal mode [38] can be replicated by a vertically-mounted multi-nozzle system, then a MEW printer “ecosystem” can be developed. Secondly, the reproducibility of the MEW lattices was characterized by analyzing 32 out of the 1152 scaffolds printed with eight different heads on both sides of the collector. Finally, the capability of printing large-scale scaffolds was highlighted via manufacturing lattices with dimensions of 780mm x 780mm.

Based on in-house printing experience and knowledge from previous studies [38, 222] the following instrument parameters were used for the print quality assessment and characterization of the high-throughput electrospinning capabilities of the HT-MEW printer (P_1, P_2, P_3, Table.7).

System parameter	***Unit***	***P_1***	***P_2***	***P_3***

Applied Pressure (AP)	*[bar]*	1.4	2	2.5
Applied Voltage (AV)	*[kV]*	9	10.5	11.5
Melting Temperature (MT)	*[°C]*	90	90	85
Collection Speed (CS)	*[mm/min]*	2000	1100	750
Working Distance (WD)	*[mm]*	12	12	12
Number of layers	*#*	10	20	30
Pore size	*[µm]*	200	500	1000

Table 7: system parameter settings and their units for the three different printing experiments P_1, P_2 and P_3, which individually have different numbers of layers and pore sizes

Once the MEW scaffolds were printed, images were taken with a digital single-lens camera (D90, NIKON, USA), an inverted bench-top light microscope (Eclipse Ts2R, Nikon, USA) and a Scanning Electron Microscope (TM3000, Hitachi, Japan). Micrographs obtained with the inverted bench-top light microscope were used for the characterization of fiber diameter and fiber spacing using ImageJ (Version 1.51q, National Institutes of Health, USA). Evaluation of the results ($p^* < 0.05$) was conducted using a statistic software (PRISM 7, GraphPad Prism 7 Software, USA).

7.6 RESULTS

7.6.1 Operational functionality of the HT-MEW machine concept

A systematic design approach led to the development of a prototype HT-MEW printer, successfully showing a combination of the fundamental operation principles from conventional AM technologies in regards to deposition accuracy and traditional fiber forming processes in terms of generating high throughput. The functionality of the concept was verified by building a prototype, which comprises eight simultaneously operating print heads to electrospin polymer on both sides of a vertically aligned, moving and grounded collecting platform. The application of suitable parameter settings (Table.7) enabled electrospinning from the side as the influence of gravity on the micron-scaled fiber was observed to be negligible, described elsewhere [32]. The in-house developed parameter-controlling boxes facilitated a stable polymer extrusion behavior and precise control over the fiber placement. The application of the instrument parameters was found to be stable for all instances.

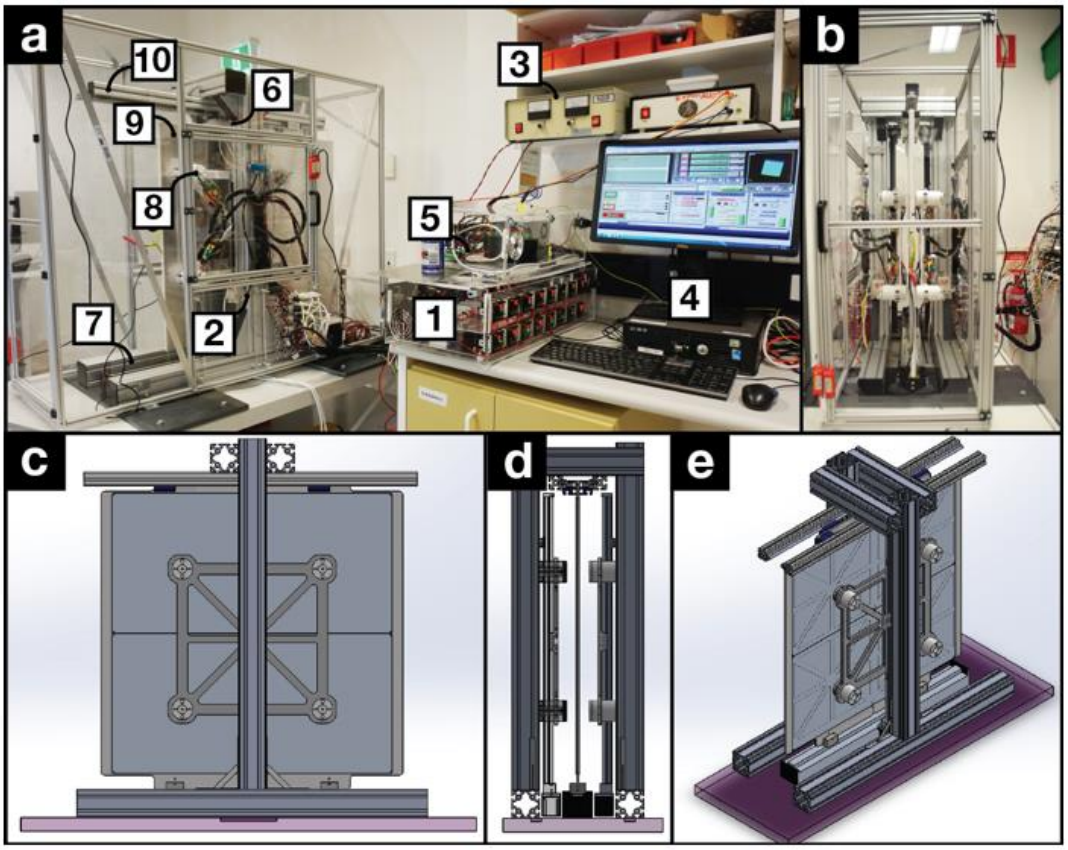

Figure 36: images showing the (a) prototype setup with numbering analogue to Fig. 3, and the (b) printing enclosure from front, (c-d) the CAD models from side, front and isometric view.

7.6.2

Print quality assessment

The performance capacity of the HT-MEW prototype was compared to that of standard "research level" single-head MEW printers with a horizontally-placed collector [38]. The quality of the printing was determined by comparing the diameter and the fiber spacing of the scaffolds using the two configurations. Both fabrication processes were operated under the application of the same parameters, as shown in Table.7. Results shown in Fig. 37, revealed a homogeneous fiber distribution with no significant differences in diameter and fiber spacing between the two printing configurations.

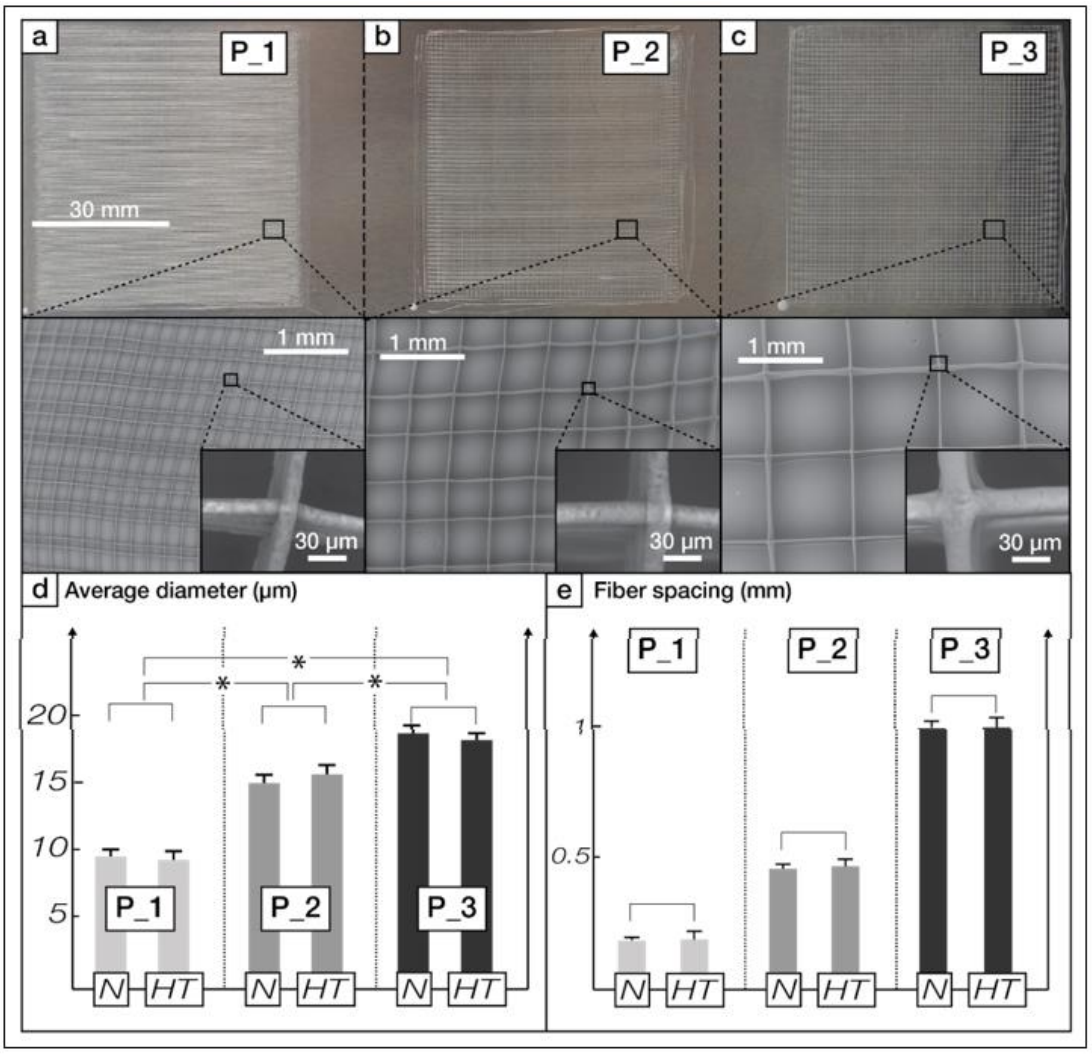

Figure 37: differences between a standard MEW printer and the HT-MEW counterpart was assessed by analysing three lattices (a), (b) and (c) from the settings P_1, P_2 and P_3 respectively. (d) shows the results of the average diameters and (e) fibre spacing for P_1, P_2 and P_3 of lattices printed in a (N) normal horizontal MEW research machine and (HT) with the HT-MEW printer (n=30).

Next, the reproducibility of the HT-MEW printer across all print areas of the eight heads was investigated by programming the device to produce multiple equally-sized melt electrospun lattices across different heights at both sides of the collector. Then the variability of fiber diameter and spacing across the different lattices was analyzed. We applied the parameters settings corresponding to P_2 (Table 7) and coded the relative movement of the heads to repeatable print squares of 2.25 cm2. The resulting 1152 scaffolds were produced in 87 hours applying a transitional collector speed of 1100 mm/min. The results of the analysis of five randomly chosen scaffolds from each print head, shown in Fig. 38, revealed overall good homogeneity of diameters printed by the eight heads. Interestingly, the standard deviations appear to be slightly higher

for the heads located at the top rows (h_1, h_2, h_5, h_6). This smaller accuracy within the upper heads could be attributed to the machining of the prototype HT-MEW printer and could be traced back to slight deviations (from true dimensions and angles) of the aluminum frame.

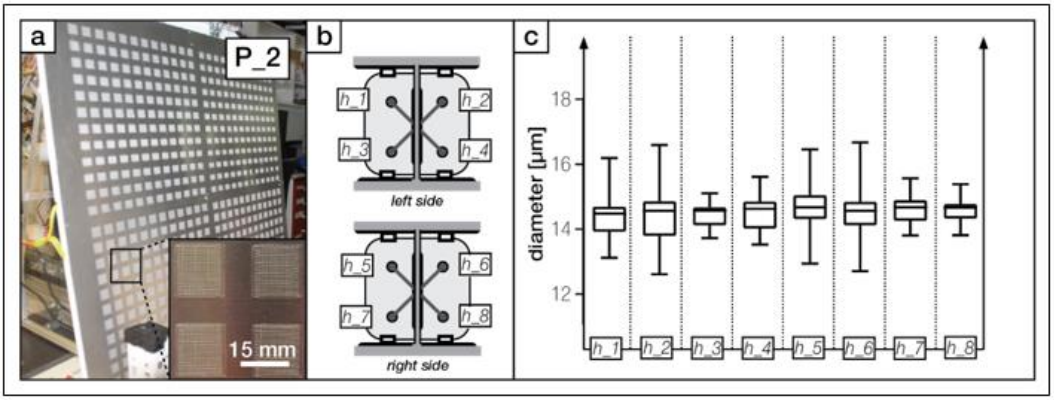

Figure 38: (a) one side of the collector contains 576 lattices, (b) the labelling of the heads and (c) the distribution of fibre diameter and fibre spacing over the eight print heads.

High throughput printability of large-scale lattices

7.6.3 Once the reproducibility of the HT-MEW printer was demonstrated, the capacity of this system to print large-scale scaffolds was investigated by manufacturing lattices with dimensions of 780mm x 780mm and overlapping printing areas between neighboring heads on both collector sides. The large scaffold and its specific areas of overlap are shown in Fig.39. The SEM image demonstrates the fusion of the overlaying areas, which can be minimized in future work by increasing the distances of the head travel. Lattices with dimensions of 780mm x 780mm were successfully, using the parameter settings from P_2 (Table 7).

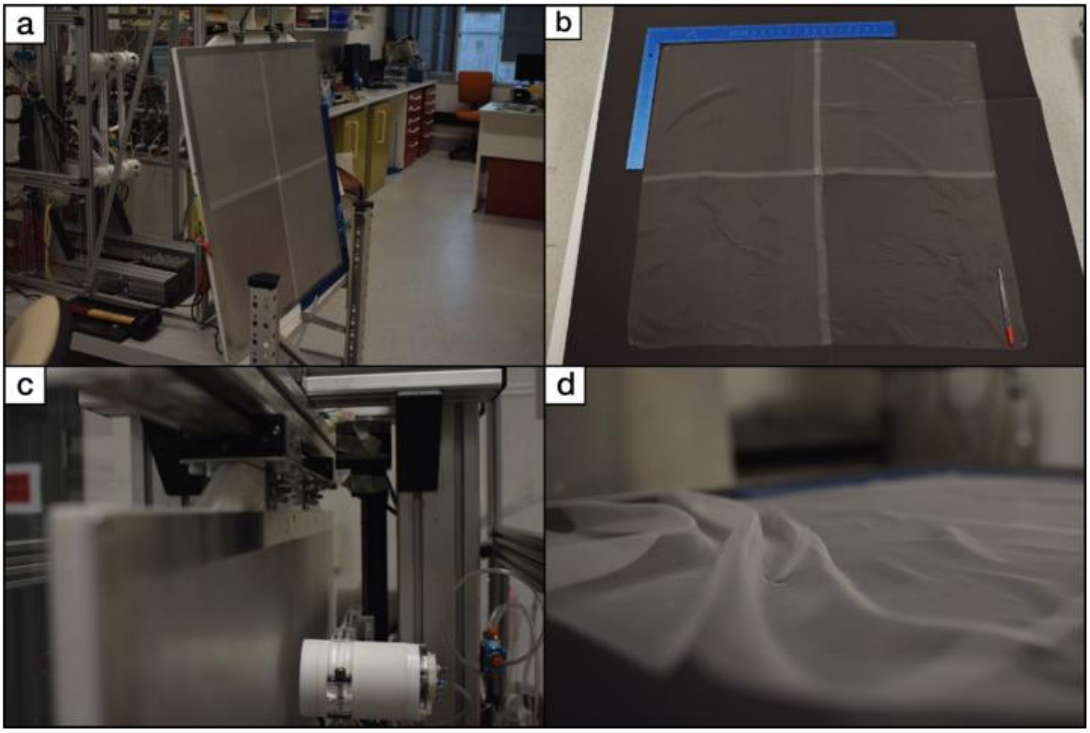

Figure 39: images of the large-scale scaffold with a size of 78 cm x 78 cm (a) on the collector, (b) on a black background with a scale, (c) during production and (d) loosely lying on the background.

7.7 DISCUSSION AND FUTURE WORK

In this study, we present an innovative and systematically engineered concept for scaling-up the process of directly writing molten electrospun polymers to fabricate precise large-scale lattices. The multi-head prototype demonstrated accurate and repeatable direct-writing with multiple extrusion heads, onto a vertically mounted collector.

Since economics are an essential driver for the transfer of new technologies into industrial applications [279], fewer expensive components such as the linear stage essential. The vertical mounting of the collector was designed to double the output of the MEW scaffolds per printer. Additionally, so-called high precision x,y,z stages are significant cost factors in AM machines, yet, a vertically aligned collecting platform requires only one stage, while the platform is guided with a comparably inexpensive slide on top. Furthermore, from an economic perspective, a vertical alignment would minimize design space and hence, additionally would decrease costs in renting laboratory space. Comparable microscale morphologies of all scaffolds were shown with excellent resolution, showing that can be scaled up using a multi-head system and a vertically-mounter collector. The fiber always travelled straight towards the

collector, driven by the high electrostatic forces, and did not visibly deformed due to gravitational forces, in agreement with the results recently reported elsewhere [32] (F.M. Wunner, J. Maartens, O. Bas, K. Gottschalk, E.M. De-Juan-Pardo, D. Hutmacher, W., Electrospinning writing with molten poly (ε-caprolactone) from different directions – discovering the effects of gravity, Materials Letters 213 ((submitted))

Based on the limitations of the processing ability of viscous polymers, this concept successfully shows one path to increase the manufacturing throughput of MEW. For future developments, it can be recommended to alter the number of heads, while aiming at a more economic design, including minimizing the design space of the heads.

The relative movement of an extruding unit in two directions opens up the possibility to fabricate scaffolds with different shapes. Overlapping allows for the production of large-scaled scaffolds, which can be customized to shapes via laser-cutting techniques [173]. As with all AM technologies, the lattice morphology can be readily altered. The HT-MEW printer can also simultaneously produce a range of scaffolds and lattices to improved cell expansion [19].

The fiber spacings and diameters were not statistically different between the heads. At the top position, the error was found to be larger (Fig. 38), suggesting that they were caused by the prototyping nature of the device. Nonetheless, the high degree of accuracy for micron-scaled structures is excellent, and future design will only improve custom-made and highly resolved morphology.

Future optimizations, aiming at improving throughput while maintaining print quality might include the stacking of multiple frames in line. Additionally, it is possible to multiply the number of heads to further increase the throughput, i.e. a combination of scale-out and scale-up.

7.8 CONCLUSION

The presented work describes the first design scale-up concept of an HT-MEW printer which could fulfill the requirements for industrial applications. Since the HT-MEW printer uses the same parameters developed on a single MEW research printer system in a horizontal configuration, this aids in the translation of this 3D printing technology between academia and industry. The HT-MEW printer described here fabricated well-

ordered, high-resolution microstructures that have many applications in ABM. The vertical collector mounting has a low footprint, while printing on both sides of the collector significantly lowers costs, including extra driving stages. Additionally, the concept can have more than eight heads to increase the throughput further.

The individually controlled and respectively moving heads further provide operation flexibility and might motivate general AM applications regarding scaling-up. This systems engineering approach demonstrates how an existing research-level MEW printer in academia can turn into a high throughput manufacturing platform. We propose that such the vertical collector mounting design could deliver the increased demand for controlled, scale-up manufacture of MEW scaffolds, potentially at low cost.

7.9 ACKNOWLEDGMENTS

This research was conducted by the Australian Research Council Industrial Transformation Training Centre in Additive Biomanufacturing (IC160100026) and supported by the Cooperative Research Centre for Cell Therapy Manufacturing (CTMCRC) as well as the Institute for Advanced Study of the Technical University of Munich. Further, the authors acknowledge Pawel Mieszczanek and Ross Kent for their assistance with the building of the prototype.

7.10 DISCLOSURE

There is no financial interest in aspects of this work.

Chapter 8: Discussion and future recommendations

Electrospinning with polymer melts in a direct writing mode gained increasing interest within the TE&RM research community [40]. Melt electrospinning in form of a 3D printing process was first described in 2011 and defines a combination of the traditional fibre forming processes with additive manufacturing operation principles (***Chapter 1)***. This facilitates the fabrication of biocompatible in silico designed polymer architectures in the micron- to submicron scale [116]. From an engineering perspective, yet, less effort was set on optimising the technology and the fabrication process itself, than focusing on the final application of the scaffolds namely biological studies (in vivo or in vitro). Therefore, this Ph.D. project hypothesised that the application of systematic engineering methodologies assists in developing a holistic technology platform, to enhance the understanding of the process, identify stable and reproducible fabrication conditions and lastly, reach scale.

Aim 1: Systematic engineering and verification of integrated and automated MEW devices and qualitative validation of the results

A literature review in ***Chapter 2*** reflects on the existing technological knowledge of electrospinning to define a requirement list for designing optimised MEW devices. Existing hardware was strategically dissected to identify and define the most important process functionalities, such as “generation of heat” or “application of pressure”. This assisted in defining technological and functional requirements serving as a basis to develop the novel MEW devices. A major focus of the Ph.D. project was set on the design of the print head, as this component integrates the majority of the process functionalities, such as heating, electrically charging and applying pressure, all executed around the tip of the needle. Therefore, multiple design iterations were required (the mechanical drawings are given in the appendix). Additionally, we implemented a double heating system, which heats the polymer around the spinneret to the targeted melting temperature, while heating the material stored within the

syringe, which has a much lower temperature to prevent thermal degradation [16]. For the next generation of MEW print heads, it is recommended to implement instruments measuring the remaining amount of polymer within the syringe as the polymer mass has an influence on the pressure at the time the polymer reservoir runs out of material. Further optimisation potential is seen in the implementation of materials, which provide lower manufacturing tolerances, than experienced with the used Perspex plates (collector, head). One recommendation for future design improvement includes the design of high-temperature MEW heads to print polymers with higher melting temperatures, such as Polypropylene (PP). A study on electrospinning PP in a direct writing mode was recently published and underlines the potential in the medical fields [229]. Additionally, future head designs might provide the opportunity to use different spinneret sizes, which is proven to influence the resulting diameter of the fibres [41, 128] and most likely will assist in manufacturing consistent sub-micron structures [116]. The units within the parameter control box revealed high functionality and provided the targeted signals and information to the head, the collector and the interlocks. An experiment on the general influence of the parameters on the fibre diameter and its deviation concluded the chapter and verifies the functionality of the designed hardware.

The use of multiple MEW machines over long production periods (from days to weeks to month) facilitated the collection of a considerable body of printing experience established among various users in the Additive biomanufacturing lab. This work is collated in ***Chapter 3*** and published in form of a video protocol, which provides fundamental information and training for any MEW user to the achieve desired scaffold/lattice architectures. Additionally, this assisted in identifying distinct process characteristics, such as cases of process instability under given system parameters settings. The phenomena of jet pulsing has a major effect on the result in form of deviating fibre diameters [205]. For instance, in case the jet travels in a straight line towards the collector, it coils and leads to unordered scaffold architectures [31]. Moreover, we explored the capability of the MEW devices to print different fibre diameters via adjusting the mass flow and the electrostatic stretching forces on the fibre, respectively. Visually monitoring and capturing via a camera the geometry of the fibre flight path led to derive estimation-based actions, explained in the video tutorial. This way of qualitatively assessing the stability of the process motivated us to

design and develop an in-process control system, with automated monitoring capabilities.

Aim 2: Design of an in-process control system to generate large data for determining process stability and identifying the correlations between the geometry of the jet and the diameter

The experienced based knowledge, generated in the previous chapters on the usability and the process supported the development of the first ever MEW monitoring setup (***Chapter 4)***, which includes a conductive conveyor belt system, two individually triggering microscopic cameras, which monitor the angle and the diameter respectively, and a software environment for controlling the process. Additionally, the system is capable of regulating the parameters to achieve holistic process control. An orthogonal array is applied to permute all possible correlations of the four investigated parameters under three different settings. The automated monitoring setup facilitated the generation of approximately 15.000 entries (diameter and fibre angle), which is new to the fields and overcame the contemporary challenges of manually characterising the outcomes of MEW.

Initially, a linear regression analysis was applied and demonstrated the correlation between the geometry of a falling jet and the resulting morphology of a deposited fibre. In particular, the results reveal that a deviating angle (over time) also produce inhomogeneous fibre diameters. This finding proves the hypothesis and underlines that, from a monitoring perspective, essential information on the process and its stability can be gathered by verifying the geometry of a fibre. In fact, this study confirms that if a stable angle of a fibre flight path is achieved, the resulting diameter does not have any significant deviations. The monitoring can be conducted in real time and significantly minimises the efforts of manually characterising the final diameters. Further, we foresee this method to be a promising candidate to determine the quality of large scale industrial processes, where multiple extrusion units require observation. In this case, the monitoring of a fibre is particularly less cost-intense, than the process of verifying the quality at a final scaffold. The former can be conducted with conventional cameras, while the latter requires cost intense microscopic equipment to analyse the micron scaled diameters.

As a next steps, the application of a Generalised Estimated Equation (GEE) model yielded original findings describing the influence of four simultaneously varying system parameters on the angle as well as the final diameter. For both outcomes, the

results reveal four-way-interactions, which describe that every parameter combination leads to a different result and would require separate consideration. This underlines the high degree of complexity of the process. Based on this, the results were visualised via heat maps considering the variation of all four parameters and assisted in identifying their major influences on the geometry of the fibre flight path. The results show that the mechanical drag forces of the collector in the majority of the cases significantly dominate the influence of the electrostatic forces. Both reactions, however, strongly depend on the amount of the extruded mass, its particular viscosity and hence, the respective charge density within the jet. The findings regards the diameter supports already existing information from literature or in-house printing experience. The chapter concludes with the creation of a library for MEW, which allows users to apply the most stable parameter settings.

The chapter comprises novel findings, however, alludes to the need for assistance of data specialists, as the results of the statistical model are highly complex. Nevertheless, the development of the automation setup for large data collection forms the basis to conduct more holistic studies to faster unravel the complexity of the process. Additionally, it opens up the possibilities to also test different materials and verify their specific printability behaviours in shorter time periods. As mentioned before, the demand for high-temperature print heads exits and testing their respective functionality and behaviour would be facilitated by the novel machine.

The established understanding of the most stable conditions led to the development of a system with a micro-controller discussed in ***Chapter 5***, which is capable of surpassing the contemporary limitations of MEW to print scaffolds, exceeding 2-3 mm in height [144]. The implementation of an original micro-controlled system facilitates the printing of scaffolds, with heights surpassing 7mm via accommodating the distance between spinneret and collector, while gradually increasing the applied voltage. The former was realised via the implementation of a linear stage (z-direction) to lift the print head. This prevents the scaffold to grow too close into the highly charged region, which would lead to significant distortions of the micron scaled layers on top. Based on Coulomb's law [133], this increase subsequently initiates decreasing electrostatic forces and initiates an imbalance, which leads to fibre pulsing, described in Chapter 3 and verified in chapter 4. Therefore, the micro-controlled system strategically increases the applied voltage to keep the electrostatic forces on a constant level, which facilitates the extrusion of homogeneous fibres. The respective increases were derived

from numerical simulations of the printing environment in three-dimensional space. Subsequent studies will be conducted to print different pore sizes and test the scaffolds for mechanical properties. From a design perspective, we foresee the standardisation of implemented z-axis travel of the print heads in future MEW devices. This would, in combination with preprogramed voltage iterations within the firmware add great value to the technology. Initial in vitro and in vivo studies (images in the Appendix) already reveal promising results of the implemented multi-layered scaffolds.

Aim 3: ***Design and development of a high throughput MEW device under consideration of previously established functional requirements and economic influences – verified by a functional prototype***

The last phase of the Ph.D. project consisted in systematically developing a machine setup, which can produce sufficient throughput to meet industrial demands. This approach comprises the transfer of the established knowledge regards the design and stability of the process and further considers essential economic factors to minimise cost drivers, such as the linear stages. A functional analysis revealed that this reduction can be achieved via electrospinning on both sides of the collector, hence, utilising only one stage for moving the collector. This, however implied a preliminary study on investigating the influence of gravity on a MEW process, as this technological requirement prerequisites either the printing from top and bottom on the collector or printing from both sides on the vertically aligned collector. Hence, a statistical study was conducted in ***Chapter 6*** to verify the differences between printing from top, the side, and bottom-up direction. In general, the results show expected trends due to changed settings, such as increasing diameter along higher pressures or smaller diameters when the collection speed is increased. In particular, the study reveals stable cases of printing from all directions, while exploring that gravity specifically influences the formation of a Taylor cone, yet does not affect a travelling fibre [32]. Moreover, we observed that all scaffolds properly adhere to the collector (up to 30 layers). For the first time, MEW was conducted in a side and bottom-up printing direction and further opens the discussion of a dynamic printing mechanism, i.e. the integration a robot arm, to design complex 3D objects in the three-dimensional space. These findings were integrated into the design process of the first high throughput MEW device, demonstrated in ***Chapter 7***. This led to the construction of a proof of concept framework, showing a vertically aligned collecting platform including eight individually operating electrospinning print heads, operating from both sides. At first,

a study was conducted comparing scaffolds printed with the HT-MEW device to scaffolds from the machines, developed in chapter 2. The results reveal no significant differences and successfully evidence that the objected technology transfer is feasible. Secondly, the HT-MEW device was tested to verify its accuracy at repeated experiments, shown via the printing of 1156 scaffolds (each 2,25cm^2) in a time span of 56 hours and thirdly, the fabrication of largely scaled scaffolds (760mm*760mm) was realised. The characterisations of the results showed minor deviations in diameter and fibre spacing, which are negligible, and most potentially occur from the large dimension of the device and the induced potential mechanical tolerances. Therefore, we foresee the next generation of MEW devices to substitute the off the shelf aluminium profiles with highly precise materials to overcome this prototyping status. The system is designed to verify the conceptual idea of operating with multiple single extruding units. This also enhances the production flexibility for unknown future demands from the commercial fields. In fact, next to the capability of printing large scale sheets, the novel HT-MEW design concepts can also fabricate customised shapes, which for instance would fit existing bioreactors. We put a major focus on this, as future requirements on the scaffolds remain unknown to this point of time. From an engineering perspective, the vertical alignment was proven to be inevitable if using the collector from both sides, however, offers additional benefits such as saving space in laboratories, which constitutes another cost driver. Future design concepts, aiming at increasing the throughput might comprise the increase of heads per side and stacking of the structural frames next to each other in laboratory environments. As mentioned previously, the developments of the process-control equipment to verify process stability via monitoring the flight path of the fibre (Chapter 4) might be a viable solution at low costs.

The following figure provides an overview of the aims and the correlations between the achievements of my Ph.D. project.

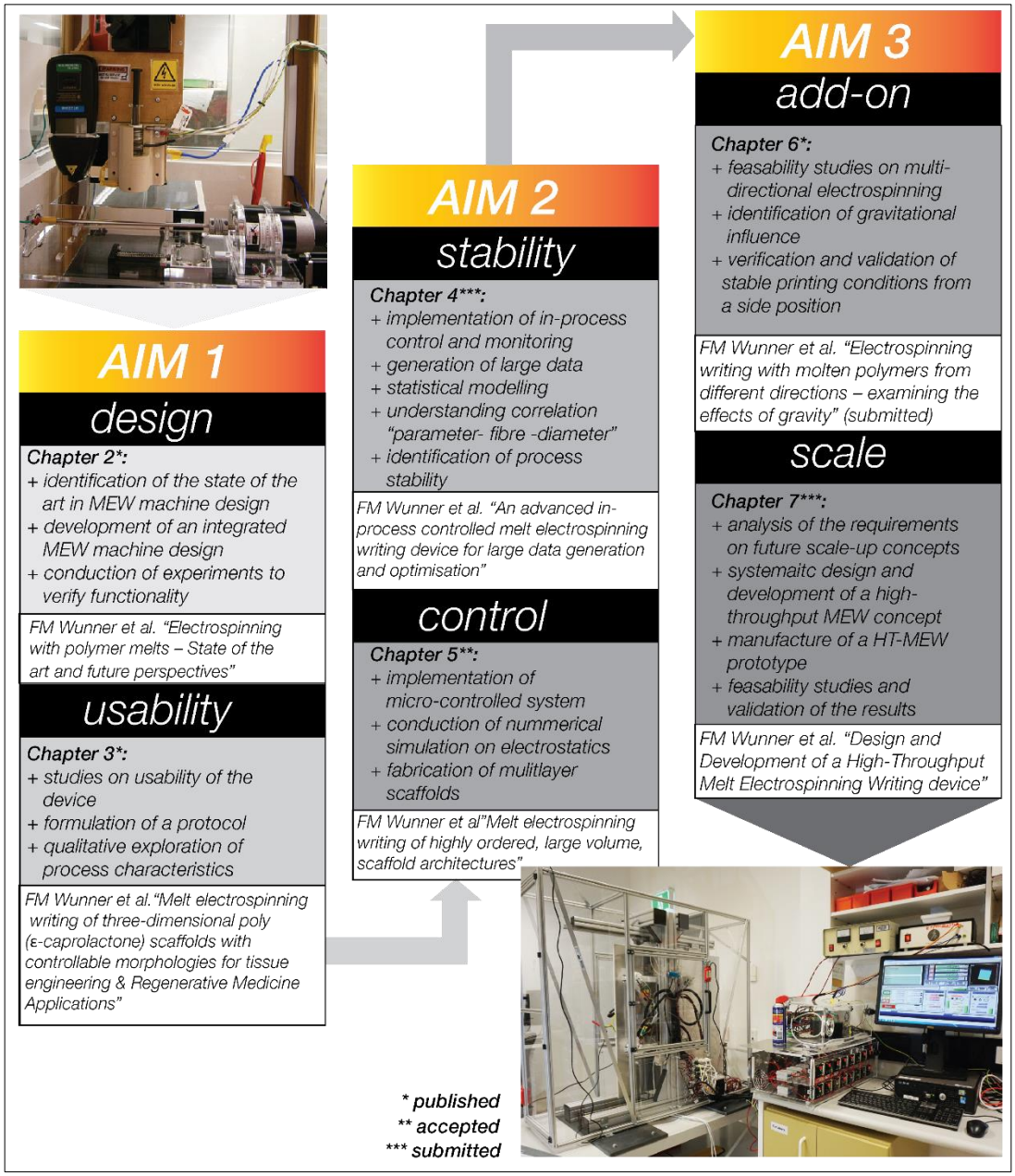

Figure 40: graphical illustration of the Ph.D. project under consideration of the individual aims. The image on top left shows the initial machine design and right bottom the final product, which comprises all elaborated results

Table 9 represents a summary of all achieved results (diameters) and their respective settings from the novel MEW machines. Positively, the results are all comparable with minor negligible deviations along the different studies. In summary, however, all results reveal mutual trends of the diameters when changing the respective system parameters, determined in Chapter 4.

(i) Increasing diameters along higher electrostatic forces

(ii) Significant thinning of the diameters in case of altered collecting speeds

(iii) Small diameter growths in case of higher temperatures

(iv) Substantial increase in diameter along rising pressure

(v) Minor thinning effects due to larger distances between spinneret and collector

Ø [µm]		1	2					3		4				5		6			7						
Chapter_2	CD	30	21	21	30	30	30	30	12	12	21	21	21	21	30				12	12	12	12	12	21	30
	CS	1800	1800	2400	1800	2400	2400	1800	1200	2400	1200	2400	2400	1800	2400				1200	1200	1800	1800	1800	1200	1200
	AP	2	3	2	2	2	2	2	2	3	2	2	2	3	2				2	2	2	2	2	2	3
	MT	95	75	85	95	75	75	95	75	95	95	85	85	75	75				75	75	85	85	85	95	85
	AV	10	7	7	7	7	10	13	7	7	7	10	13	10	13				10	13	7	10	13	10	10
Chapter_3	CD									12															
	CS									1700															
	AP									1															
	MT									82															
	AV									8															
Chapter_4	CD							12		12				12		12			12						
	CS							1000		3000				3000		3000			3000						
	AP							1		1				1		1			1						
	MT							83		70				70		70			70						
	AV							8		8				12		10			10						
Chapter_5	CD																								
	CS																								
	AP																								
	MT																								
	AV																								
Chapter_6	CD									10	10	12		6		8	8	8	6	12					
	CS									2250	3000	3000		720		1470	2250	3000	1470	2250					
	AP									1	1	1		1		1	3	2	1	1					
	MT									83	76	89		76		96	76	83	83	96					
	AV									11	10	9		8		10	9	8	9	8					
Chapter_7	CD																								
	CS																								
	AP																								
	MT																								
	AV																								

Ø [µm]		8				9		10	11	12	13	14	15	16	17		18	20			25
Chapter_2	CD	12	21	30	30	12	21														
	CS	2400	1800	1200	1200	2400	1200														
	AP	3	3	3	3	3	2														
	MT	95	75	85	85	95	95														
	AV	10	13	7	13	13	13														
Chapter_3	CD										12										12
	CS										1200										700
	AP										2										3
	MT										82										82
	AV										11										12
Chapter_4	CD	12				12		12	12	12	12	12	12	12	12			12			
	CS	3000				2000		3000	3000	3000	1000	1000	1000	1000	1000			1000			
	AP	2				1		1	2	2	1	1	2	1	2			2			
	MT	83				83		95	83	95	83	95	83	95	95			95			
	AV	8				12		12	12	10	12	10	10	10	10			12			
Chapter_5	CD																	8	8	8	
	CS																	1500	1750	2000	
	AP																	3	3	3	
	MT																	85	85	85	
	AV																	7	8	9	
Chapter_6	CD	6	12			6		8				10			10	12					
	CS	2250	1470			3000		720				1470			720	720					
	AP	2	2			3		1				3			2	3					
	MT	89	76			96		89				89			96	83					
	AV	10	11			11		11				8			9	10					
Chapter_7	CD							12					12				12				
	CS							2000					1100				750				
	AP							1.4					2				2.5				
	MT							85					85				90				
	AV							10					11				12				

Table 8: summary of all elaborated results, listed along the diameters and the individual chapters (CD = Collector Distance (mm) | CS = Collector Speed (mm\min) | AP = Applied Pressure (bar) | MT = Melting Temperature (°C) | AV = Applied Voltage (kV))

This research project and the development of the devices and the application of scaffolds additionally led to a wider impact in the Centre of Regenerative Medicine and the ARC ITTC in Additive Biomanufacturing and positively influenced multiple studies during the time of my Ph.D. Fig.41 shows the three research directions arising from the study:

(i) Direct application of the electrospun meshes at biological implementations (vivo and in vitro)

(ii) Use of the machines to widen the design space of the scaffolds and create synthetic tissues from different materials with multiple functionalities

(iii) Establishing the technological basis for high throughput MEW processes for the cell manufacturing industry

(i) First was facilitated via the use of in-house designed mandrel systems to fabricate tubular scaffolds, which serve as a structural framework for enhanced cell attachment and proliferation (Fig. 40.b). The original mandrel system is based on design approaches know from literature [124] and extensively explained in Chapter 3. A conductive rod is rotated and moved along its vertical axis to collect the fibres for creating tubular scaffolds. The fibre orientation and number of layers is strongly depending on the linear and rotational speed of the collector. Multiple studies within our group revealed promising results for applications in the biological fields (in vivo and vitro) [280]. In the future, it will become necessary to further investigate the mechanical drag forces on the fibre, as these, compared to printing on two dimensional collectors, lead to additional stretch forces on the fibre. It is conceivable to conduct further investigation of fibres collected by such mandrel system by using the monitoring setup, introduced in Chapter 4.

(ii) Second, the high degree of accuracy in deposition and achievable process stability achievable with the novel MEW devices (chapter 2 and 3) facilitated to widen the contemporary design options of depositing fibres in a linear manner. For the first time, Bas et al. introduced the printing of curved MEW structures (Fig. 39.c), which significantly enhance the functional capabilities of the implanted scaffolds [213, 240]. These designs, for instance, are used for soft tissue applications can reveal distinct mechanical properties, facilitated via curved structures. Additionally, the discovery of implementing hydrogels into MEW structures to create highly functional composite

[173] receives increasing attention for applications at biological studies [195]. This can be supported via the fabrication of scaffolds with multiphasic structures and can be enhanced with the implementation of different printing technologies, such as FDM. The benefits of combining such structures were already highlighted in 2008 [191, 192], where FDM scaffold provided structural support and the electrospun meshes generate high surface to volume ratios for enhanced cell growths [193].

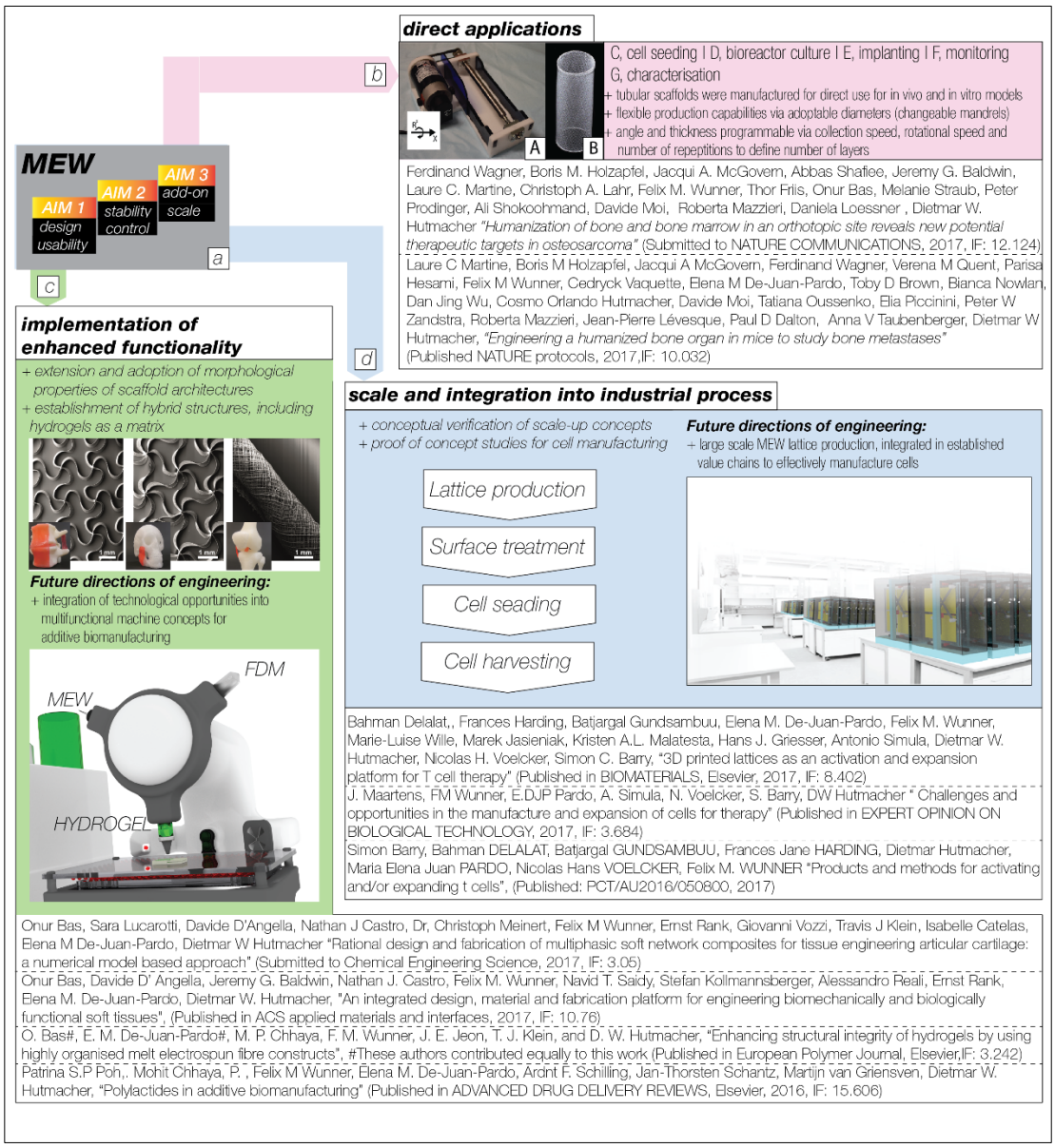

Figure 41: developments of the elaborated technology platform (a). (b) Direct applications in the fields of TE&RM, (c) further potential of machine design for bench top applications and (d) demonstration of future scale concepts for the cell manufacturing industry

To our knowledge, there is no such machine, which can fulfil the listed processing steps on one platform and therefore, researchers need to manually transport the fabricated scaffolds to the hydrogel printers. From an engineering point of view, the

establishment of such highly functional frameworks and most importantly the consideration of all specific requirements to design one integrated machine concept will rise the complexity of the design. Therefore, the consideration of systematic methodological design and development approaches will play a key role in successfully engineering these multifunctional devices.

(iii) Thirdly, the design and development of the HT-MEW device within my Ph.D. allowed to fabricate large scaled scaffolds which is a condition sine qua non for being translated into the T cell manufacturing industry. In strong collaboration with a participating university and supported by industrial and governmental funding, initial proof of concept studies demonstrated the efficiency of MEW lattices in comparison to conventionally implemented polystyrene beads (small polymer particles) to effectively grow Treg cells [19]. The product and method of fabricating MEW lattices, treating the surface and subsequently seeding with Treg cells within a bioreactor [281] was successfully filed in a PCT patent [282], which underlines the validity of the process. From an engineering perspective, future work will include the consideration and fulfilment of regulatory demands, the establishment of good manufacturing practises, the optimisation of process sequences and the introduction of quality control measurements. In conclusion, the introduction and the establishment of MEW lattices in the cell manufacturing industry is seen as a promising candidate for optimising traditional technologies.

Appendix

Appendix A

Supporting Information for Chapter 2: *"Electrospinning with polymer melts – state of the art and future perspectives"*

A.1:

Theoretical compare of 90/0 scaffolds of 100µm, 200µm, 400µm, 500µm and 1000µm fibre distance and 10µm and 17µm fibre diameter. The Area of compare is 1cm2

Fibre size	10µm				
Fibre distance	100µm	200µm	400µm	500µm	1000µm
Theoretical surface area of 10 Layers (app. Scaffold height 105µm)	5.99E+08 µm²	3.18E+08 µm²	1.99E+08 µm²	1.30E+08 µm²	6.86E+07 µm²
Theoretical surface area for 100 µm height	5.70E+08 µm²	3.03E+08 µm²	1.89E+08 µm²	1.24E+08 µm²	6.54E+07 µm²

Table A.1.1: distances, pore sizes and surfaces, Fibre size 10µm

Fibre size	17µm				
Fibre distance	100µm	200µm	400µm	500µm	1000µm
Theoretical surface area of 10 Layers (app. Scaffold height 178.5µm)	9.60E+08 µm²	5.30E+08 µm²	3.35E+08 µm²	2.19E+08 µm²	1.16E+08 µm²
Theoretical surface area for 100 µm height	5.38E+08 µm²	2.97E+08 µm²	1.88E+08 µm²	1.23E+08 µm²	6.50E+07 µm²

Table A.1.2: Fibre size 17µm

Bead	
Bead diameter	4.5 µm
Surface area of one bead	6,62 µm²

Surface area of X beads (1:1 to number of cells)	(63.61725124*X) μm^2
Surface area of beads in cultures seeded at 1.25 x 10^5 cells`	7952156,405 μm^2 = 7.95E+06 μm^2

Table A.1.3: respective bead surfaces * X ;(X=number of cells)

Method of calculation:

The CAD software SolidWorks was used to design the differing scaffold architectures. A generative application of the program provides the theoretical surface area of each construct.

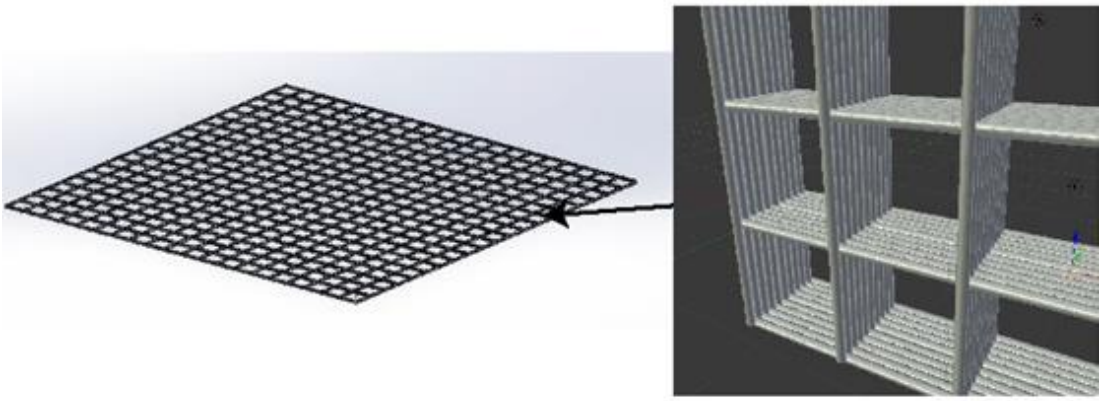

Figure A.1.1 shows the scaffold with 17µm fibre diameter, 500µm fibre distance and 178.5 µm (10 Layers) height. The dimensions are 10mm * 10mm

Result

Table 3: A comparison of surface area between the 48 well plate, dynal bead and scaffold

Details	SA				
Theoretical surface area of 10 Layers, 17 µm fibre size (app. Scaffold height 178.5µm) and X= *poresize* , 5mm*5mm (I UNDESTAND THIS AS 0.25% OF THE VALUES MENTIONED ABOVE OF 1CM^2)	X=100µm	X=200µm	X=400µm	X=500µm	X=1000µm
	2.40E+08 μm^2	1.33E+08 μm^2	8.37E+07μm^2	5.47E+07μm^2	2.90E+07 μm^2
Surface area of beads in cultures seeded at 1.25 x 10^5 cells seeded at 1:1 ratio	7.95E+06 μm^2				
Surface area of epoxy plasma treated well, 48 well plate, functional with 320µL volume antibody solution (includes base area	3.06E+08 μm^2 (use of 48 Wellplate/ Corning, standard diameter bottom 11mm With 320 µL → liquid height of 3.367 mm)				

and sides of well to depth of solution)	

Table A.1.4: results and compares between scaffold and beads

A 2: technical drawings for the novel MEW devices

Technical drawings of the head MEW design

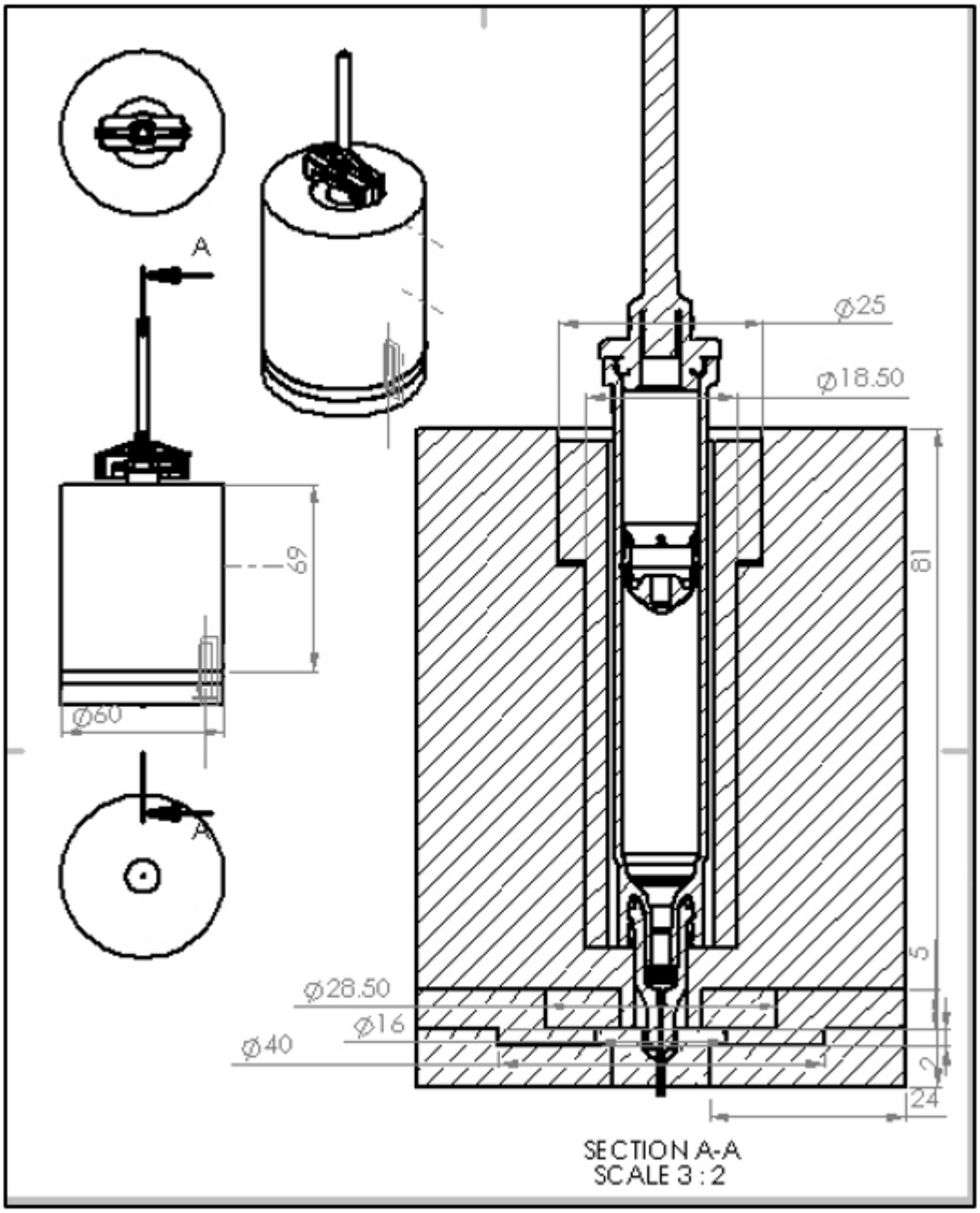

Figure A.2.1: Technical drawing for the MEW head

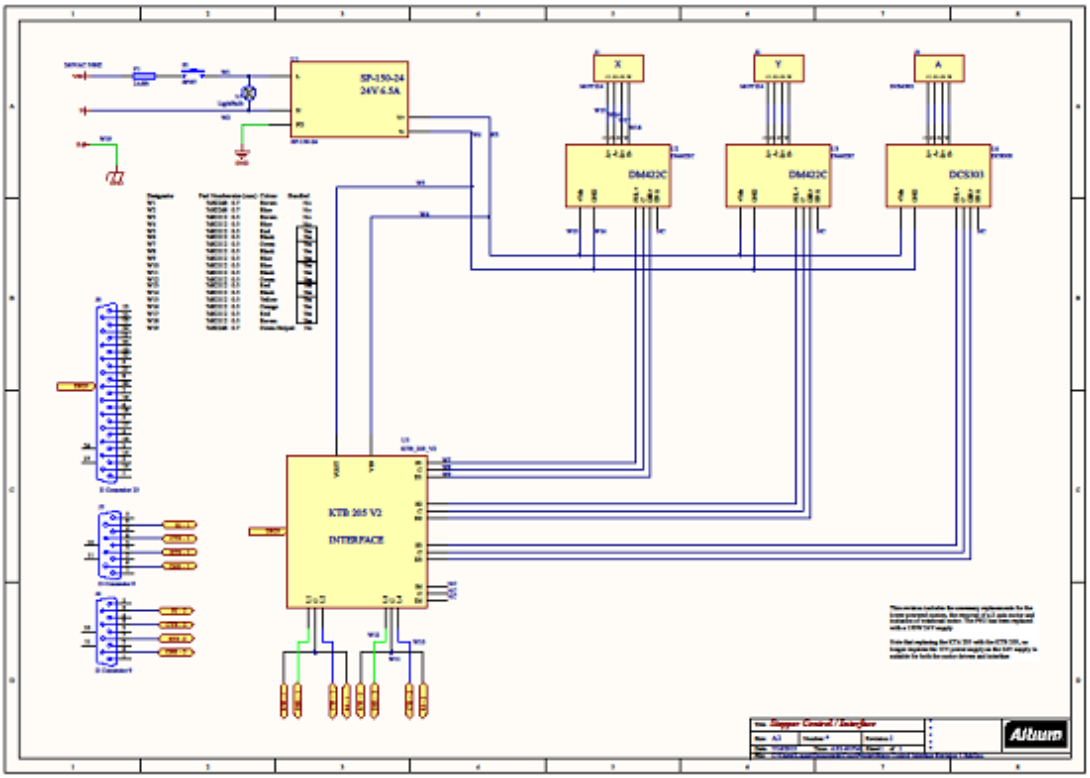

Figure A.2.2: Electrical drawings and circuits for the control boxes

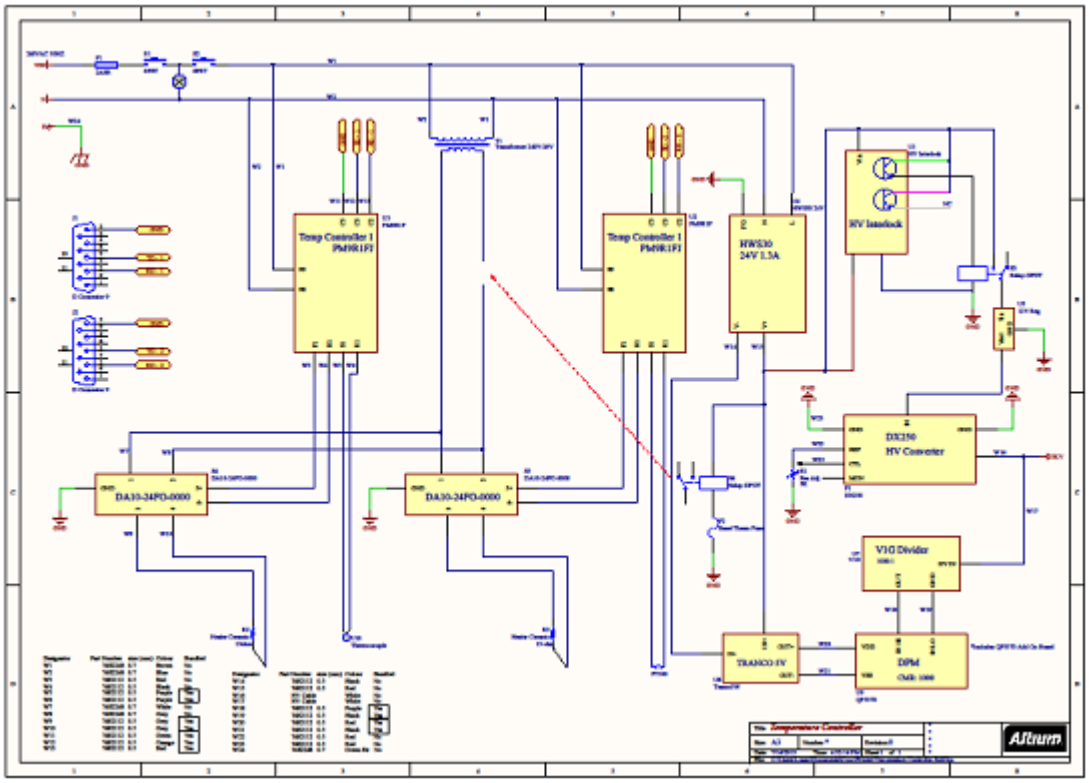

Figure A.2.3: Circuit for the heating, pressure and voltage units

Appendix B

Supporting Information for Chapter 3, *"Melt Electrospinning Writing of Three-*

dimensional Poly(ε-caprolactone) Scaffolds with Controllable Morphologies for Tissue Engineering Applications "

The final video can be found on the data CD

Name	Company	Catalog number	Comments
Plastic syringe	Nordson Australia Pty Ltd	7012072	EFD BARREL O 3mL Clear 50
Medical grade Poly (ε-caprolactone) (mPCL)	Corbion Purac, The Netherlands	PURASORB® PC12,	
23 GA needle	Nordson Australia Pty Ltd	7018302	#23GP .013 X .25 ORANGE 50 PC
Plunger	Nordson Australia Pty Ltd	7012166	PISTON O 3mL WH WIPER 50
Pressure adapter	Nordson Australia Pty Ltd	7012059	ADAPTER ASM O 3mL BL 1.8M
Aluminium collector	Action Aluminium, Australia	SHP2	Sheet 5005 H34
Acrylic glass	Mulford Plastics Pty Ltd	ACC6-13094	
Mach 3 software	Art Soft		Purchased online
Safety switch interlock	RS components Pty Ltd	12621330	
High voltage generator	EMCO High Voltage Co.	DX250R	
Temperature controller	WATLOW	PM9R1FJ	
X and Y positioning slide	VELMEX Inc.	XN-10-0020-M011	

Table B.1: Materials List for the JOVE

Appendix C

Supporting Information for Chapter 4, *"An explorative investigation of the influence of the system parameters on the geometry of a falling jet via an automated MEW device"*

Tests of Model Effects

Source	Type III		
	Wald Chi-Square	df	Sig.
(Intercept)	15146.274	1	0
speed	396.826	2	0
temperature	266.536	2	0
pressure	329.53	2	0
voltage	126.353	2	0
batch_number	46.389	2	0
speed * temperature	6.232	4	0.182
speed * pressure	29.214	4	0
speed * voltage	11.165	4	0.025
temperature * pressure	21.024	4	0
temperature * voltage	28.773	4	0
pressure * voltage	10.022	4	0.04
speed * temperature * pressure	17.149	8	0.029
speed * temperature * voltage	31.309	8	0
speed * pressure * voltage	19.336	8	0.013
temperature * pressure * voltage	20.429	8	0.009
speed * temperature * pressure * voltage	73.765	16	0

Table C.1: results from the GEE model regards the DIAMETER

Tests of Model Effects

Source	Type III		
	Wald Chi-Square	df	Sig.
(Intercept)	18939.029	1	0
speed	1143.625	2	0
temperature	27.964	2	0
pressure	316.296	2	0
voltage	142.731	2	0
batch_number	14.715	2	0.001
speed * temperature	21.598	4	0
speed * pressure	38.006	4	0
speed * voltage	26.528	4	0
temperature * pressure	20.991	4	0
temperature * voltage	9.572	4	0.048
pressure * voltage	12.367	4	0.015
speed * temperature * pressure	6.886	8	0.549
speed * temperature * voltage	25.23	8	0.001
speed * pressure * voltage	12.032	8	0.15
temperature * pressure * voltage	5.982	8	0.649
speed * temperature * pressure *	32.431	16	0.009

Table C.2: results from the GEE model regards the ANGLE

Appendix D

Supporting Information for Chapter 5, "*Melt* electrospinning writing of highly ordered, large volume, scaffold architectures"

A video explaining the systematics can be found in the Data CD (file name: mechanism.mp4)

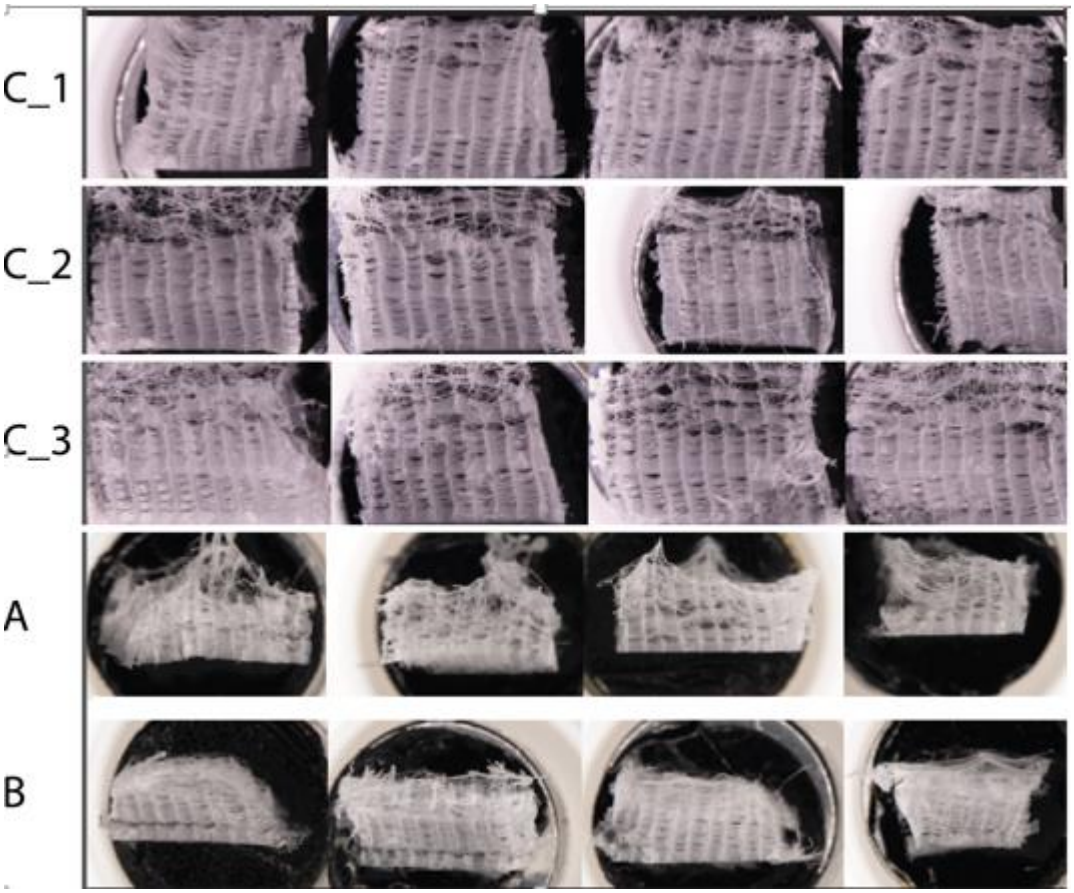

Figure D.1: images of the sections of the scaffold groups

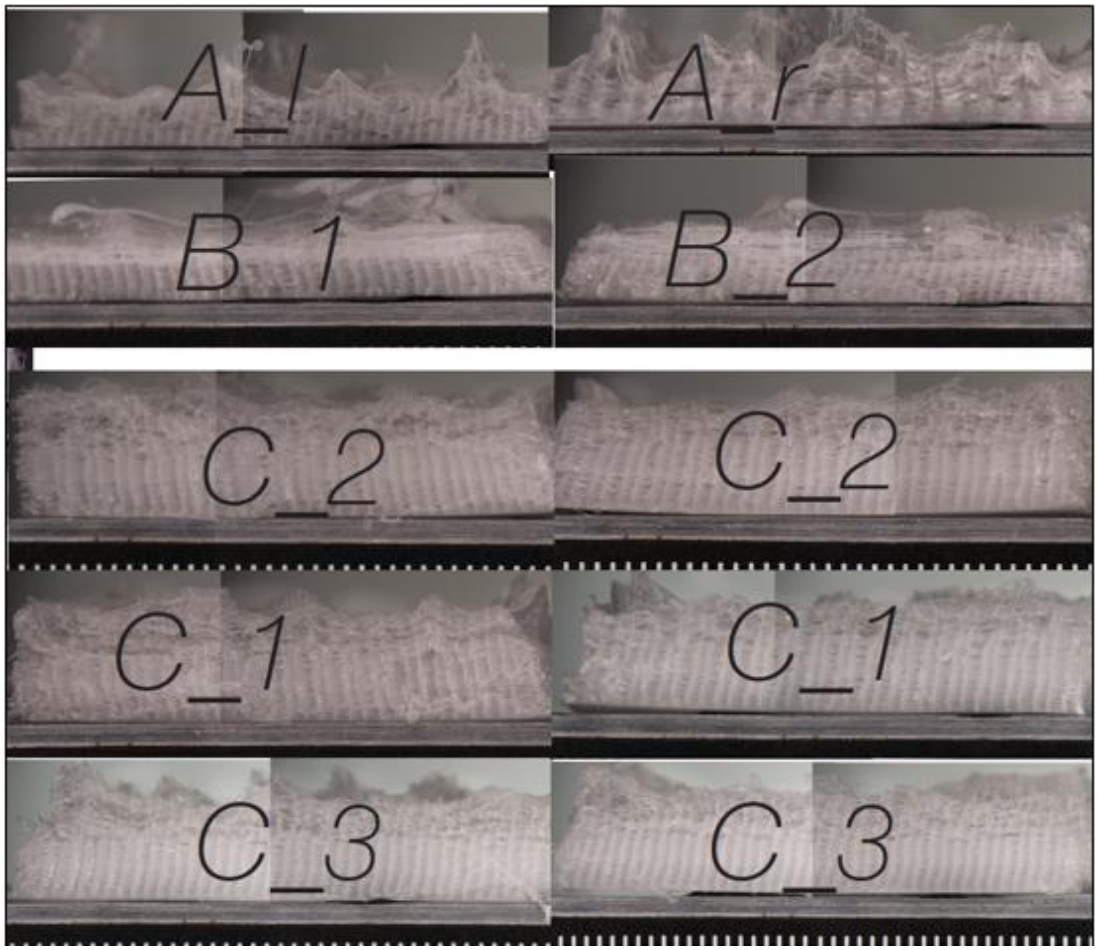

Figure D.2: images of scaffold groups

D.3 in vitro studies

To study the biocompatibility of the constructs 2 x 10^6 of either human marrow stromal cells (hMSCs) or Periodontal Ligament (PDL) cells in 200uL volume of serum free media was seeded on each scaffold in a sterile non-treated 6-well plate and incubated at 37 °C under humidified conditions for 2hr before being topped up with MEM-α (Invitrogen, USA) supplemented with 16.5% FBS (Sigma, USA) and 100IU/mL penicillin-streptomycin (Invitrogen, USA). Samples were fixed at 48hr and 14 day time points in 4% PFA for 20 mins. The constructs were washed with PBS twice and samples were permeabilized with 0.2% Triton-X in 2%BSA/PBS for 1hr. Scaffolds were stained with Alexa-568 phalloidin (Invitrogen, USA; A12380, 1:300) and DAPI (Sigma, Australia; D9542, 1:1,000) for 40 mins. Whole scaffold images were taken using Nikon Stereo Microscope SMZ25 (Nikon, Japan) and high resolution images were taken using Nikon A1R confocal (Nikon, Japan) at 10x objective.

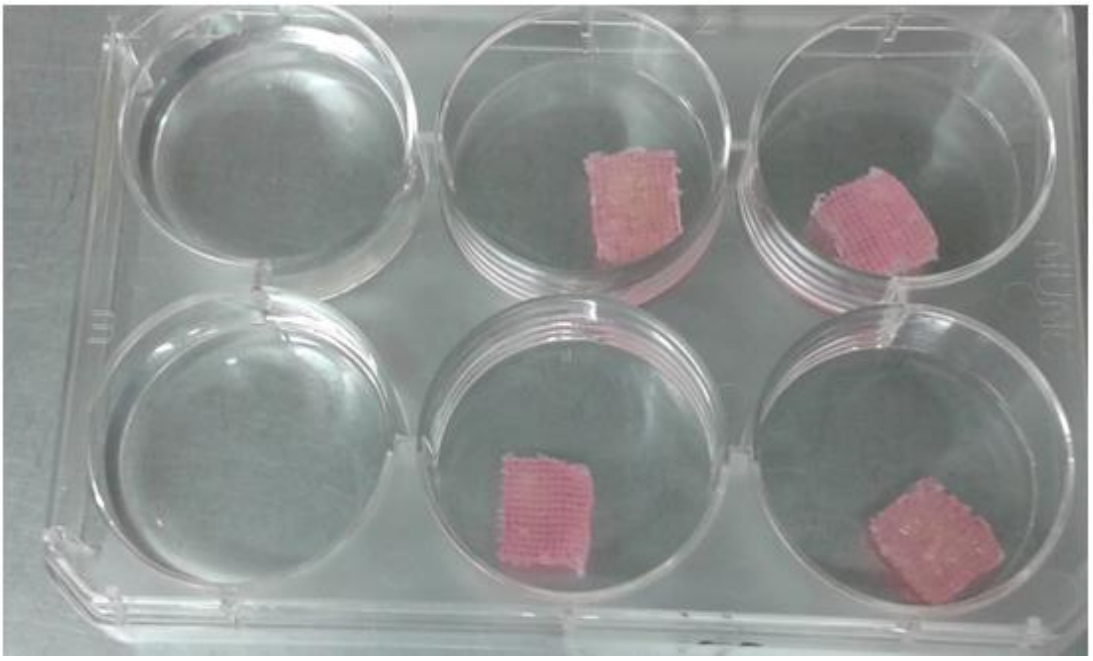

Figure D.3: images of scaffold groups Scaffolds in a 6-well plate. Interestingly, the capillary forces the medium to reside within the scaffold

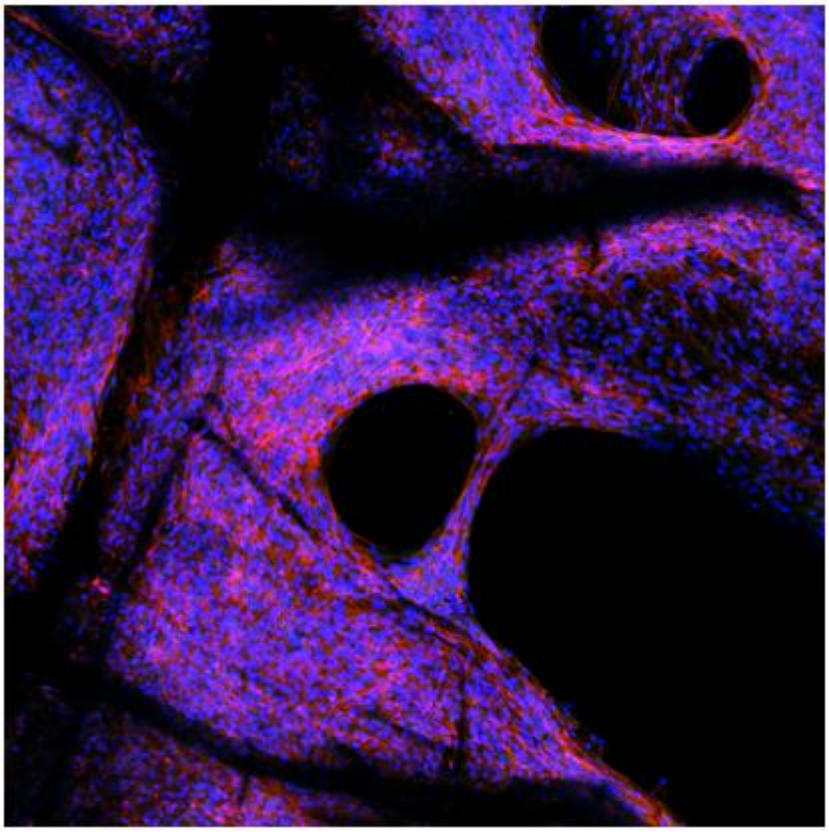

Figure D.4: images of groups PDL cells, 48hr on a multilayer scaffold

A high resolution video can be found here (PDL day 14 whole scaffold imaging) (file name: PPDL.ts)

D.4 In vivo study

Image showing implantation of large scaffold of sheep tibial defect model.

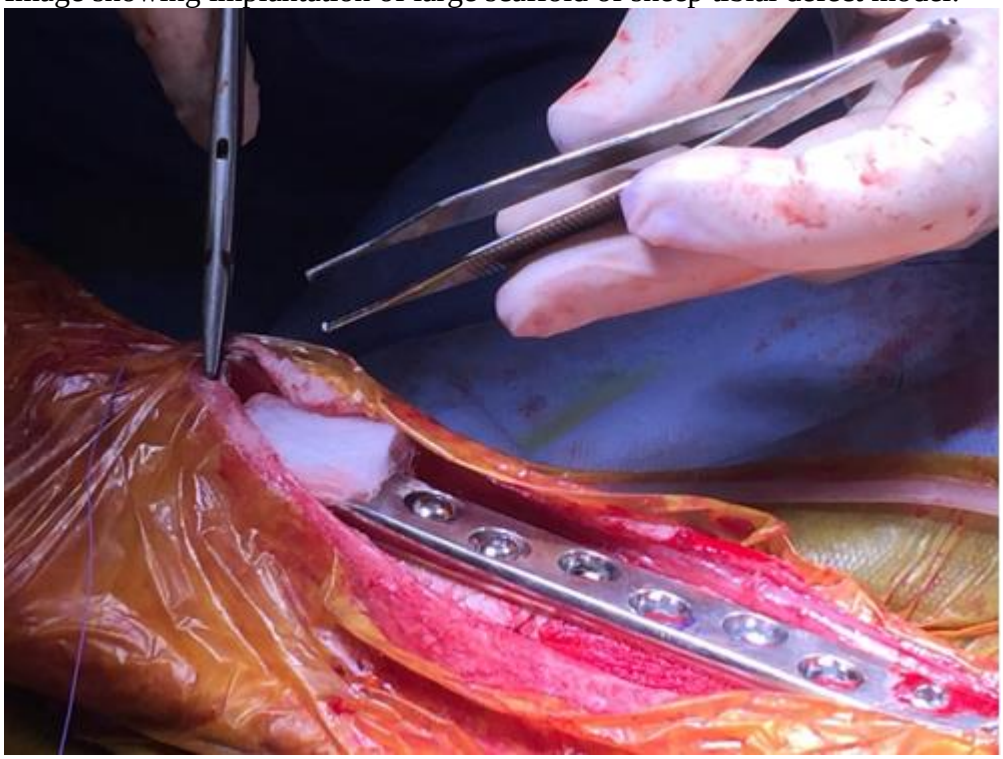

Figure D.5: Image showing implantation of large scaffold of sheep tibial defect model

Appendix E

Supporting Information for Chapter 5, *"Melt* spinning writing with molten poly (ε-caprolactone) from different directions – examining the effects of gravity"

E..1 Videos showing side and bottom can be found in the Data CD

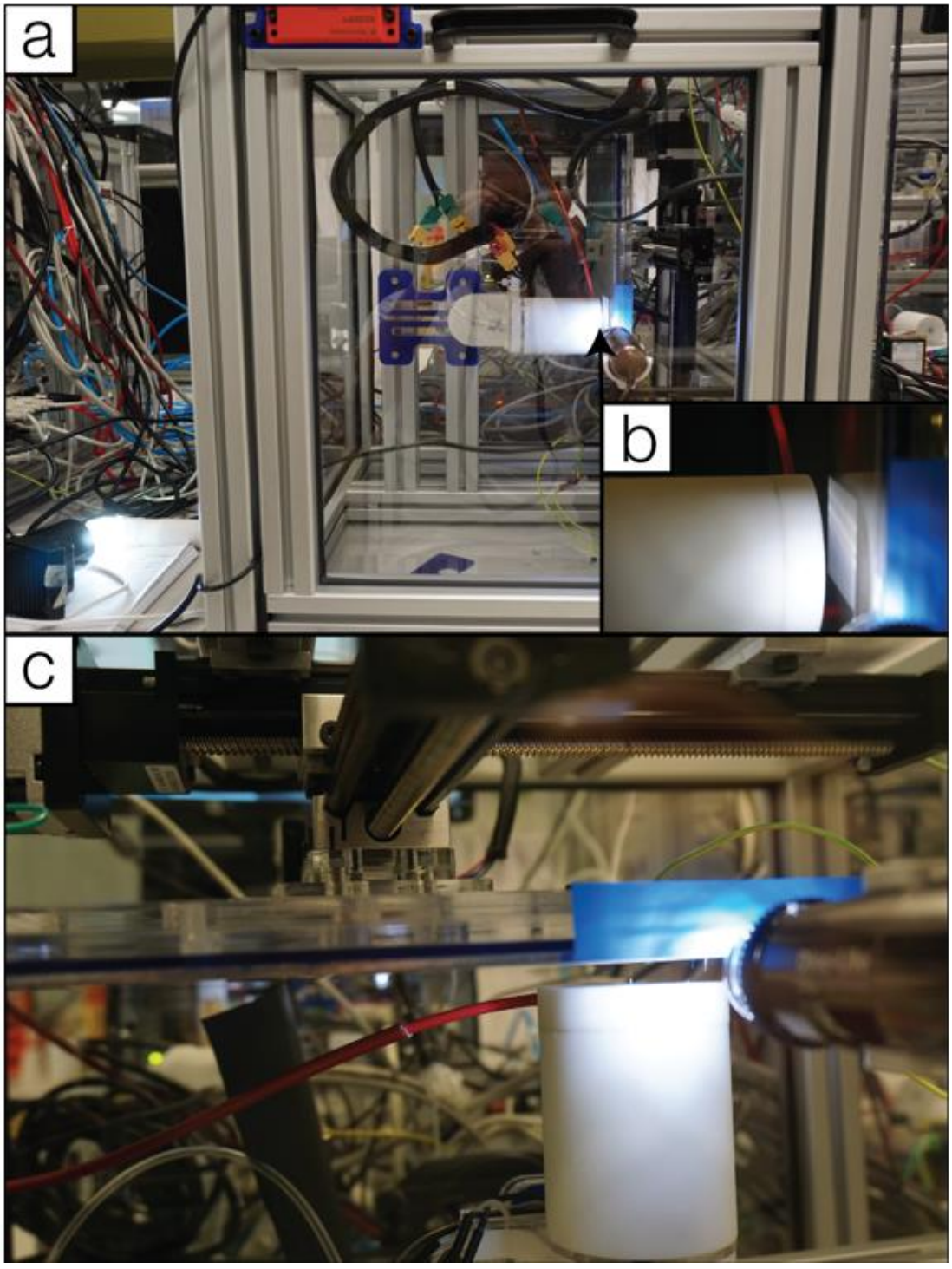

Figure E.1: images from the side and bottom printing setup

Appendix F

Supporting Information for Chapter 5, *"Design* and Development of a 3D Printing High-Throughput Melt Electrospinning Writing Device"

Videos showing different scaled-up Concepts can be found in the Data CD

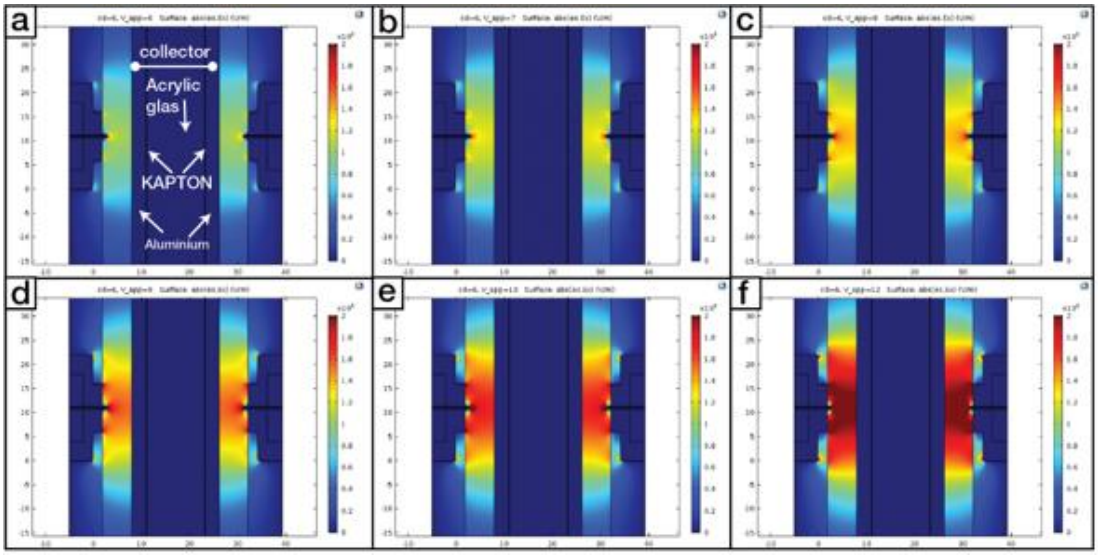

Figure F.1: Study of electrical interference of two electrically-charged heads directed at each other in small distances. The simulation (COMSOL) revealed lack of interference due to the highly conductive and individually earthed aluminium plates in combination with highly insulating KAPTON tape. (f) shows the maximum applied voltage of 12 kV and a respective collector – needle distance of 6 mm. The anticipated lack of interference was also observed in real printing
Demonstration of operation of HT-MEW. The inventors remove the collector from the machine after print has finished. This facilitates easy lattice collection. The collector can subsequently be cleaned and returned and fixed in the printing enclosure.

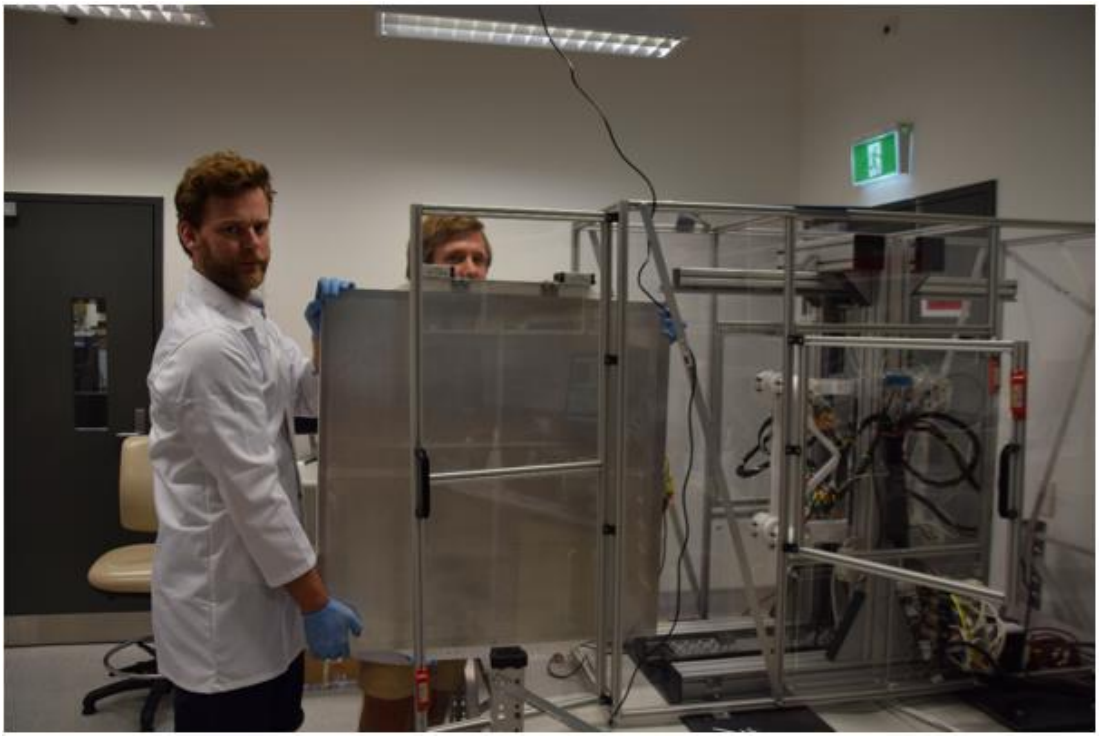

Figure F.2: removing the collector

Figure F.3:A rendering showcasing potential further scale-up via assembling multiple vertically operating HT-MEW devices in line.

Appendix G

Supporting Information: "WO2017035577 A1, Products and methods for activating and/or expanding t cells"

WIPO
WORLD
INTELLECTUAL PROPERTY
ORGANIZATION

DOCUMENT MADE AVAILABLE UNDER THE PATENT COOPERATION TREATY (PCT)

International application number:		**PCT/AU2016/050800**
International filing date:		**26 August 2016 (26.08.2016)**
Document type:		**Certified copy of priority document**
Document details:	Country/Office: Number: Filing date:	**AU** **2015903495** **28 August 2015 (28.08.2015)**
Date of receipt at the International Bureau:		**27 September 2016 (27.09.2016)**

Remark: Priority document submitted or transmitted to the International Bureau in compliance with Rule 17.1(a),(b) or (b-*bis*)

Figure G.1: cover shot from the official PCT application

Inventors: Simon Barry, Bahman Delalat, Batjargal Gundsambuu, Frances Jane Harding, Dietmar W. hutmacher, Maria Elena De-Juan Pardo, Nicolas Hans Voelcker, ***Felix Wunner***

Applicant: Ctm@Crc Ltd.

Publication Date: Mar. 9, 2017

Abstract:

The present disclosure relates to products and methods for activating and/or expanding T cells. Certain embodiments of the present disclosure provide a porous scaffold comprising one or more conjugated T cell stimulatory molecules.

Claims:

1. A porous scaffold comprising one or more conjugated T cell stimulatory molecules.

2. The porous scaffold according to claim 1, wherein the one or more T cell stimulatory molecules comprise a binding molecule for one or more of CD3, CD28, CD5, CD2, CD44, CD137, CD9, CD278, an integrin alpha and or an integrin beta.
3. The porous scaffold according to claims 1 or 2, wherein the one or more T cell stimulatory molecules comprise a binding molecule for CD3 and/or a binding molecule for CD28.
4. The porous scaffold according to any one of claims 1 to 3, wherein the one or more stimulatory molecules comprise an antibody.
5. The porous scaffold according to any one of claims 1 to 4, wherein the one or more T cell stimulatory molecules comprise an anti-CD3 antibody and/or an anti-CD28 antibody.
6. The porous scaffold according to claim 1, wherein the one or more T cell stimulatory molecules comprise fibronectin and/or a fragment or derivative thereof.
7. The porous scaffold according to any one of claims 1 to 6, wherein the porous scaffold comprises an average pore size of greater than 100 μπι.
8. The porous scaffold according to any one of claims 1 to 7, wherein the porous scaffold comprises an average pore size in the range from 100 μπι to 1 mm.
9. The porous scaffold according to any one of claims 1 to 7, wherein the porous scaffold comprises an average pore size of about 200 μπι.
10. The porous scaffold according to any one of claims 1 to 9, wherein the porous scaffold comprises a fibrous scaffold.
11. The porous scaffold according to claim 10, wherein the fibrous scaffold comprises an average fibre spacing of greater than 100 μπι.
12. The porous scaffold according to claims 10 or 11, wherein the fibrous scaffold comprises fibres with an average diameter of 5 to 20 μπι.
13. The porous scaffold according to any one of claims 10 to 12, wherein the fibrous scaffold comprises 5 to 20 layers.
14. The porous scaffold according to any one of claims 10 to 13, wherein the fibrous scaffold comprises an ordered arrangement of fibres.
15. The porous scaffold according to any one of claims 1 to 14, wherein the porous scaffold comprises a mesh, a mat, a woven matrix and/or a sponge.
16. The porous scaffold according to any one of claims 1 to 15, wherein the porous scaffold comprises melt electrospun fibres.
17. The porous scaffold according to any one of claims 1 to 16, wherein the porous scaffold comprises one or more of a polylactide polymer, a polyglycolic acid polymer, a polycaprolactone polymer, a poly (amino acid alkyl ester) phosphazene polymer, a poly(caprolactone co-ethyl ethylene phosphate) polymer, a polycarbonate polymer, a polyethyleneimine polymer, a polyethyleneglycol polymer, a polyurethane polymer, and a poly vinyl alcohol polymer.
18. The porous scaffold according to any one of claims 1 to 17, wherein the one or more T cell stimulatory molecules are directly or indirectly covalently linked to the porous scaffold via a plasma polymerised functional group.
19. The porous scaffold according to claim 18, wherein the plasma polymerised functional group comprises a plasma polymerised epoxy group.
20. A method of activating a T cell, the method comprising exposing a T cell to a porous scaffold according to any one of claims 1 to 16 and thereby activating the T cell.
21. The method according to claim 20, wherein the T cell comprises a $CD4^+$ T cell, a $CD8^+$ T cell (a killer T cell), a CD3+ T cell, a $CD4^+CD25^+$ T cell (a regulatory T cell),

a chimeric antigen receptor expressing T cell, a natural killer cell or a tumour infiltrating lymphocyte
22. A T cell activated by the method according to claims 20 or 21.
23. A method of expanding a T cell, the method comprising exposing a T cell to a porous scaffold comprising one or more conjugated T cell stimulatory molecules and cul turing the T cell so as to expand the T cell.
24. The method according to claim 23, wherein the one or more T cell stimulatory molecules comprise a binding molecule for one or more of CD3, CD28, CD5, CD2, CD44, CD 137 and CD9, CD278, an integrin alpha and or an integrin beta.
25. The method according to claims 23 or 24, wherein the one or more T cell stimulatory molecules comprise a binding molecule for CD3 and/or a binding molecule for CD28.
26. The method according to any one of claims 23 to 25, wherein the one or more T cell stimulatory molecules comprise an antibody.
27. The method according to any one of claims 23 to 26, wherein the one or more T cell stimulatory molecules comprise an anti-CD3 antibody and/or an anti-CD28 antibody.
28. The method according to claim 23, wherein the one or more T cell stimulatory molecules comprise fibronectin and/or a fragment or a derivative thereof.
29. The method according to any one of claims 23 to 28, wherein the porous scaffold comprises an average pore size of greater than 100 μπι.
30. The method according to any one of claims 23 to 29, wherein the porous scaffold comprises an average pore size in the range from 100 μιη to 1 mm.
31. The method according to any one of claims 23 to 30, wherein the porous scaffold comprises an average pore size of about 200 μιη.
32. The method according to any one of claims 23 to 31, wherein the porous scaffold comprises a mesh, a mat, a woven matrix and/or a sponge.
33. The method according to any one of claims 23 to 32, wherein the porous scaffold comprises a fibrous scaffold.
34. The method according to claim 33, wherein the fibrous scaffold comprises an average fibre spacing of greater than 100 μπι.
35. The method according to claims 33 or 34, wherein the fibrous scaffold comprises fibres with an average diameter of 5 to 20 μπι.
36. The method according to any one of claims 33 to 35, wherein the fibrous scaffold comprises 5 to 20 layers.
37. The method according to any one of claims 33 to 36, wherein the fibrous scaffold comprises an ordered arrangement of fibres.
38. The method according to any one of claims 23 to 37, wherein the porous scaffold comprises melt electrospun fibres.
39. The method according to any one of claims 23 to 38, wherein the porous scaffold comprises one or more of a polylactide polymer, a polyglycolic acid polymer, a polycaprolactone polymer, a poly (amino acid alkyl ester) phosphazene polymer, a poly(caprolactone co-ethyl ethylene phosphate) polymer, a polycarbonate polymer, a polyethyleneimine polymer, a polyethyleneglycol polymer, a polyurethane polymer, and a poly vinyl alcohol polymer.
40. The method according to any one of claims 23 to 39, wherein the one or more T cell stimulatory molecules are directly or indirectly covalently linked to the porous scaffold via a plasma polymerised functional group.
41. The method according to claim 40, wherein the plasma polymerised functional group comprises a plasma polymerised epoxy group.

42. The method according to any one of claims 23 to 41, wherein the T cell comprises a $CD4^+$ T cell, a $CD8^+$ T cell (a killer T cell), a $CD3^+$ T cell, a $CD4^+CD25^+$ T cell (a regulatory T cell), a chimeric antigen receptor expressing T cell, a natural killer cell or a tumour infiltrating lymphocyte.
43. The method according to any one of claims 23 to 42, wherein the culturing of the T cell comprises culturing in the presence of the porous scaffold.
44. The method according to any one of claims 23 to 43, wherein the method comprises culturing the T cell, and/or expanded cells therefrom, in the presence of accessory cells and/or an exogenous growth factor.
45. The method according to claim 44, wherein the exogenous growth factor comprises IL-2.
46. The method according to any one of claims 23 to 45, wherein the method further comprises separating expanded T cells from the porous scaffold.
47. T cells expanded by the method according to any one of claims 23 to 46.
48. A composition comprising one or more T cells activated by exposing the one or more T cells to a porous scaffold comprising one or more conjugated T cell stimulatory molecules.
49. A composition comprising one or more T cells and a porous scaffold comprising one or more conjugated T cell stimulatory molecules.
50. A complex comprising a T cell bound to a porous scaffold comprising one or more conjugated T cell stimulatory molecules.
51. A kit for activating and/or expanding T cells, the kit comprising a porous scaffold according to any one of claims 1 to 19.
52. A method of producing a porous scaffold for activating a T cell, the method comprising conjugating one or more T cell stimulatory molecules to a porous scaffold.
53. The method according to claim 47, wherein the porous scaffold comprises melt electrospun fibres.
54. The method porous scaffold according to claims 52 or 53, wherein the fibrous scaffold comprises an ordered arrangement of fibres.
55. A porous scaffold produced by the method according to any one of claims 52 to 54.
56. A cell culture vessel comprising a porous scaffold according to any one of claims 1 to 19.

The full patent description can be found under the following link:

https://encrypted.google.com/patents/WO2017035577A1?cl=en

Appendix H

Supporting Information: information of co-authored studies

O. Bas[#], E. M. De-Juan-Pardo[#], M. P. Chhaya, ***F. M. Wunner***, J. E. Jeon, T. J. Klein, and D. W. Hutmacher, "Enhancing structural integrity of hydrogels by using highly organised melt electrospun fibre constructs," (published in European Polymer Journal, vol. 72, pp. 451–463), Elsevier, 2015. ([#] These authors contributed equally to this work) (IF: 3.242)

ABSTRACT: Applying additive manufacturing technology to the principles of fibre reinforcement of hydrogels, we have fashioned weak hydrogels into mechanically enhanced composites. We combined the extracellular matrix-like structure of gelatin-methacrylamide (GelMA) and GelMA/hyaluronic acid-methacrylamide (HAMA) hydrogels with highly oriented poly(e-caprolactone) (PCL) fibres fabricated by Melt Electrospinning Writing (MEW) to achieve fibre-reinforced GelMA/HAMA composites with improved compressive properties. Stacked fibres with lay-down patterns of 0–90 and 0–60–120, and spacing of 400 and 800 lm were prepared by MEW. These defined fibrous structures were infiltrated with hydrogels, namely GelMA (10%) and GelMA/HAMA (0.125%, 0.25% and 0.5%) in custom-made moulds and crosslinked by a reduction–oxidation initiating system (ammonium persulphate/tetramethylethylenediamine). Mechanical properties and deformation characteristics of the constructs were evaluated under uniaxial compression loading conducted at 37C in culture media with an integrated camera. Reinforced constructs showed more than a 35-fold-increase of the compressive Young's modulus. However, the compressive Young's moduli were highly strain-rate dependent. The fibre reinforcement has a particular impact on the Poisson's ratio of the composite constructs, decreasing from values of approximately 0.4 to 0.01. The high interfacial surface area between the fibre structure and the hydrogel matrix is believed to be one of the main factors responsible for the significant increase in the mechanical properties of the constructs. In summary, we have found that reinforcement of hydrogels with defined MEW fibre architectures achieves an outstanding increase in the mechanical properties at high strain rates.

Onur Bas, Davide D' Angella, Jeremy G. Baldwin, Nathan J. Castro, ***Felix M. Wunner***, Navid T. Saidy, Stefan Kollmannsberger, Alessandro Reali, Ernst Rank, Elena M. De-Juan-Pardo, Dietmar W. Hutmacher, "An integrated design, material and fabrication platform for engineering biomechanically and biologically functional soft tissues" (accepted by), RSC publishing, 2017 (IF: 10.76)

ABSTRACT: We present a design rationale for stretchable soft network composites for engineering tissues that predominantly function under high tensile loads. The convergence of 3D-printed fibres selected from a design library and biodegradable interpenetrating polymer networks (IPNs) result in biomimetic tissue engineered constructs (bTECs) with fully tunable properties that can match specific tissue requirements. We present our technology platform using an exemplary soft network composite model that is characterized to be flexible, yet ~125 times stronger (E = 3.19 MPa) and ~100 times tougher (WExt = ~2000 kJ m-3) than its hydrogel counterpart.

Patrina S.P Poh,. Mohit Chhaya, P. , ***Felix M Wunner***, Elena M. De-Juan-Pardo, Ardnt F. Schilling, Jan-Thorsten Schantz, Martijn van Griensven, Dietmar W. Hutmacher,

"Polylactides in additive biomanufacturing" (published in ADVANCED DRUG DELIVERY REVIEWS), Elsevier, 2016 (IF: 15.606)

ABSTRACT: New advanced manufacturing technologies under the alias of additive biomanufacturing allow the design and fabrication of a range of products from pre-operative models, cutting guides and medical devices to scaffolds. The process of printing in 3 dimensions of cells, extracellular matrix (ECM) and biomaterials (bioinks, powders, etc.) to generate in vitro and/or in vivo tissue analogue structures has been termed bioprinting. To further advance in additive biomanufacturing, there are many aspects that we can learn from the wider additive manufacturing (AM) industry, which have progressed tremendously since its introduction into the manufacturing sector. First, this review gives an overview of additive manufacturing and both industry and academia efforts in addressing specific challenges in the AM technologies to drive toward AM-enabled industrial revolution. After which, considerations of poly(lactides) as a biomaterial in additive biomanufacturing are discussed. Challenges in wider additive biomanufacturing field are discussed in terms of (a) biomaterials; (b) computer-aided design, engineering and manufacturing; (c) AM and additive biomanufacturing printers hardware; and (d) system integration. Finally, the outlook for additive biomanufacturing was discussed.

Bahman Delalat,, Frances Harding, Batjargal Gundsambuu, Elena M. De-Juan-Pardo, ***Felix M. Wunner***, Marie-Luise Wille, Marek Jasieniak, Kristen A.L. Malatesta, Hans J. Griesser, Antonio Simula, Dietmar W. Hutmacher, Nicolas H. Voelcker, Simon C. Barry, "3D printed lattices as an activation and expansion platform for T cell therapy: (published in BIOMATERIALS), Elsevier, 2017 (IF: 8.402)

One of the most significant hurdles to the affordable, accessible delivery of cell therapy is the cost and difficulty of expanding cells to clinically relevant numbers. Immunotherapy to prevent autoimmune disease, tolerate organ transplants or target cancer critically relies on the expansion of specialized T cell populations. We have designed 3D-printed cell culture lattices with highly organized micron-scale architectures, functionalized via plasma polymerization to bind monoclonal antibodies that trigger cell proliferation. This 3D technology platform facilitate the expansion of therapeutic human T cell subsets, including regulatory, effector, and cytotoxic T cells while maintaining the correct phenotype. Lentiviral gene delivery to T cells is enhanced in the presence of the lattices. Incorporation of the lattice format into existing cell culture vessels such as the G-Rex system is feasible. This cell expansion platform is user-friendly and expedites cell recovery and scale-up, making it ideal for translating T cell therapies from bench to bedside.

J. Maartens**,** ***FM Wunner***, E.DJP Pardo, A. Simula, N. Voelcker, S. Barry, DW Hutmacher " Challenges and opportunities in the manufacture and expansion of cells for therapy" (published in EXPERT OPINION ON BIOLOGICAL TECHNOLOGY), Taylor&Francis, 2017, (IF: 3.684)

Laboratory-based ex vivo cell culture methods are largely manual in their manufacturing processes. This makes it extremely difficult to meet regulatory requirements for process validation, quality control and reproducibility. Cell culture concepts with a translational focus need to embrace a more automated approach where cell yields are able to meet the quantitative production demands, the correct cell lineage and phenotype is readily confirmed and reagent usage has been optimized. Areas covered: This article discusses the obstacles inherent in

classical laboratory-based methods, their concomitant impact on cost-of-goods and that a technology step change is required to facilitate translation from bed-to-bedside. Expert opinion: While traditional bioreactors have demonstrated limited success where adherent cells are used in combination with microcarriers, further process optimization will be required to find solutions for commercial-scale therapies. New cell culture technologies based on 3D-printed cell culture lattices with favourable surface to volume ratios have the potential to change the paradigm in industry. An integrated Quality-by-Design /System engineering approach will be essential to facilitate the scaled-up translation from proof-of-principle to clinical validation.

Laure C Martine, Boris M Holzapfel, Jacqui A McGovern, Ferdinand Wagner, Verena M Quent, Parisa Hesami, ***Felix M Wunner***, Cedryck Vaquette, Elena M De-Juan-Pardo, Toby D Brown, Bianca Nowlan, Dan Jing Wu, Cosmo Orlando Hutmacher, Davide Moi, Tatiana Oussenko, Elia Piccinini, Peter W Zandstra, Roberta Mazzieri, Jean-Pierre Lévesque, Paul D Dalton, Anna V Taubenberger, Dietmar W Hutmacher, "Engineering a humanized bone organ in mice to study bone metastases" (published in NATURE protocols), 2017 (IF: 10.032)

Current in vivo models for investigating human primary bone tumors and cancer metastasis to the bone rely on the injection of human cancer cells into the mouse skeleton. This approach does not mimic species-specific mechanisms occurring in human diseases and may preclude successful clinical translation. We have developed a protocol to engineer humanized bone within immunodeficient hosts, which can be adapted to study the interactions between human cancer cells and a humanized bone microenvironment in vivo. A researcher trained in the principles of tissue engineering will be able to execute the protocol and yield study results within 4-6 months. Additive biomanufactured scaffolds seeded and cultured with human bone-forming cells are implanted ectopically in combination with osteogenic factors into mice to generate a physiological bone 'organ', which is partially humanized. The model comprises human bone cells and secreted extracellular matrix (ECM); however, other components of the engineered tissue, such as the vasculature, are of murine origin. The model can be further humanized through the engraftment of human hematopoietic stem cells (HSCs) that can lead to human hematopoiesis within the murine host. The humanized organ bone model has been well characterized and validated and allows dissection of some of the mechanisms of the bone metastatic processes in prostate and breast cancer.

F. Wagner, B. M. Holzapfel, J. Baldwin, L. C. Martine, J. McGovern, C. A. Lahr, ***F. Wunner***, T. Friis, O. Bas, A. Shokoohmand, R. Mazzieri, D. Loessner, D. W. Hutmacher. Humanization of bone and bone marrow at an orthotopic site reveals new potential therapeutic targets in osteosarcoma. In preparation for Science Translational Medicine

Existing preclinical murine models often fail to predict effects of anti-cancer drugs. Here, we describe an orthotopic humanized bone model which comprises human bone matrix, bone marrow and vascular components. Orthotopic humanized tissue engineered bone constructs (ohTEBC) were fabricated by 3D printing of medical-grade polycaprolactone scaffolds, which then were seeded with human osteoblasts and embedded within polyethylene glycol-based

hydrogels containing human umbilical vein endothelial cells (HUVECs). To evaluate the preclinical relevance of this platform, human osteosarcoma (OS) was induced within the ohTEBC. Tumor growth and metastatic progression represented striking similarities to the pathology and physiology seen in human osteosarcoma patients. Interestingly, engineered tumors recruited the co-implanted HUVECs for neo-angiogenesis. Moreover, both our humanized OS model and most common subtypes of OS patients, expressed the recently discovered musculoskeletal gene C12orf29, thus demonstrating that the newly developed preclinical animal model allows controlled and predictive marker studies of bone malignancies

References

1. Melchels, F.P.W., et al., *Additive manufacturing of tissues and organs.* Progress in Polymer Science, 2012. **37**(8): p. 1079-1104.
2. Mota, C., et al., *Additive manufacturing techniques for the production of tissue engineering constructs.* J Tissue Eng Regen Med, 2012.
3. Santos, A.R.C., H.A. Almeida, and P.J. Bártolo, *Additive manufacturing techniques for scaffold-based cartilage tissue engineering.* Virtual and Physical Prototyping, 2013. **8**(3): p. 175-186.
4. Giannitelli, S.M., et al., *Combined additive manufacturing approaches in tissue engineering.* ACTA BIOMATERIALIA, 2015. **24**: p. 1-11.
5. Wong, K.V. and A. Hernandez, *A Review of Additive Manufacturing.* ISRN Mechanical Engineering, 2012. **2012**: p. 10.
6. Kruth, J.P., M.C. Leu, and T. Nakagawa, *Progress in Additive Manufacturing and Rapid Prototyping.* CIRP Annals, 1998. **47**(2): p. 525-540.
7. Bikas, H., P. Stavropoulos, and G. Chryssolouris, *Additive manufacturing methods and modelling approaches: a critical review.* The International Journal of Advanced Manufacturing Technology, 2016. **83**(1): p. 389-405.
8. Gao, W., et al., *The status, challenges, and future of additive manufacturing in engineering.* Computer-Aided Design, 2015. **69**(Supplement C): p. 65-89.
9. Dalton, P.D., et al., *Electrospinning and additive manufacturing: converging technologies.* Biomaterials Science, 2013. **1**(2): p. 171-185.
10. Chhaya, M.P., et al., *Additive manufacturing in biomedical sciences and the need for definitions and norms.* Expert Review of Medical Devices, 2015. **12**(5): p. 537-543.
11. Hutmacher, D.W., *Scaffolds in tissue engineering bone and cartilage.* Biomaterials, 2000. **21**(24): p. 2529-43.
12. Zein, I., et al., *Fused deposition modeling of novel scaffold architectures for tissue engineering applications.* Biomaterials, 2002. **23**(4): p. 1169-1185.
13. Hutmacher, D.W., M. Sittinger, and M.V. Risbud, *Scaffold-based tissue engineering: rationale for computer-aided design and solid free-form fabrication systems.* Trends Biotechnol, 2004. **22**(7): p. 354-62.
14. Langer, R. and J. Vacanti, *Tissue engineering.* Science, 1993. **260**(5110): p. 920-926.
15. Poh, P.S.P., et al., *Evaluation of polycaprolactone − poly-D,L-lactide copolymer as biomaterial for breast tissue engineering.* Polymer International, 2017. **66**(1): p. 77-84.
16. Woodruff, M.A. and D.W. Hutmacher, *The return of a forgotten polymer—Polycaprolactone in the 21st century.* Progress in Polymer Science, 2010. **35**(10): p. 1217-1256.
17. Bock, N., et al., *Composites for Delivery of Therapeutics: Combining Melt Electrospun Scaffolds with Loaded Electrosprayed Microparticles.* Macromolecular Bioscience, 2014. **14**(2): p. 202-214.
18. Pham, Q.P., U. Sharma, and A.G. Mikos, *Electrospun Poly(ε-caprolactone) Microfiber and Multilayer Nanofiber/Microfiber Scaffolds: Characterization*

of Scaffolds and Measurement of Cellular Infiltration. Biomacromolecules, 2006. **7**(10): p. 2796-2805.
19. Delalat, B., et al., *3D printed lattices as an activation and expansion platform for T cell therapy.* Biomaterials, 2017. **140**: p. 58-68.
20. Vasita, *Nanofibers and their applications in tissue engineering.* 2006.
21. Kim, B.-S. and I.-S. Kim, *Recent Nanofiber Technologies.* Polymer Reviews, 2011. **51**(3): p. 235-238.
22. Ellison, C.J., et al., *Melt blown nanofibers: Fiber diameter distributions and onset of fiber breakup.* Polymer, 2007. **48**(11): p. 3306-3316.
23. Cicero, J.A., et al., *Effects of molecular architecture on two‐step, melt‐spun poly (lactic acid) fibers.* Journal of Applied Polymer Science, 2002. **86**(11): p. 2839-2846.
24. Zander, N.E., *Formation of melt and solution spun polycaprolactone fibers by centrifugal spinning.* Journal of Applied Polymer Science, 2015. **132**(2).
25. Vaquette, C. and J.J. Cooper-White, *Increasing electrospun scaffold pore size with tailored collectors for improved cell penetration.* Acta Biomaterialia, 2011. **7**(6): p. 2544-2557.
26. Brown, T.D., P.D. Dalton, and D.W. Hutmacher, *Melt electrospinning today: An opportune time for an emerging polymer process.* Progress in Polymer Science, 2015.
27. Dalton, P.D., D. Klee, and M. Möller, *Electrospinning with dual collection rings.* Polymer, 2005. **46**(3): p. 611-614.
28. Larrondo, L. and R. St. John Manley, *Electrostatic fiber spinning from polymer melts. I. Experimental observations on fiber formation and properties.* Journal of Polymer Science: Polymer Physics Edition, 1981. **19**(6): p. 909-920.
29. Zeltinger, J., et al., *Effect of Pore Size and Void Fraction on Cellular Adhesion, Proliferation, and Matrix Deposition.* Tissue Engineering, 2001. **7**(5): p. 557-72.
30. Hutmacher, D.W. and P.D. Dalton, *Melt electrospinning.* Chem Asian J, 2011. **6**(1): p. 44-56.
31. Brown, T.D., P.D. Dalton, and D.W. Hutmacher, *Direct writing by way of melt electrospinning.* Adv Mater, 2011. **23**(47): p. 5651-7.
32. Wunner, F.M., et al., *Electrospinning writing with molten poly (ε-caprolactone) from different directions – discovering the effects of gravity.* Materials Letters, (submitted). **213**.
33. Collins, G., et al., *Charge generation, charge transport, and residual charge in the electrospinning of polymers: A review of issues and complications.* Journal of Applied Physics, 2012. **111**(4): p. 044701.
34. Yarin, A.L., S. Koombhongse, and D.H. Reneker, *Taylor cone and jetting from liquid droplets in electrospinning of nanofibers.* Journal of Applied Physics, 2001. **90**(9): p. 4836-4846.
35. Catalani, L., et al., *Charge generation, charge transport, and residual charge in the electrospinning of polymers: A review of issues and complications.* Journal of Applied Physics, 2012. **111**(4): p. 044701-044701-18.
36. Yarin, A.L., S. Koombhongse, and D.H. Reneker, *Taylor cone and jetting from liquid droplets in electrospinning of nanofibers.* Journal of Applied Physics, 2001. **104**(9): p. 4836-4846.
37. Li, X., et al., *Preparation and characterization of poly(ε-caprolactone) nonwoven mats via melt electrospinning.* Polymer, 2012. **53**(1): p. 248-253.

38. Wunner, F.M., et al., *Electrospinning with polymer melts – state of the art and future perspectives*, in *Comprehensive Biomaterials II*. 2017, Elsevier. p. 217-235.
39. Dalton, P.D., et al., *Direct in Vitro Electrospinning with Polymer Melts.* Biomacromolecules, 2006. **7**(3): p. 686-690.
40. Dalton, P.D., *Melt electrowriting with additive manufacturing principles.* Current Opinion in Biomedical Engineering, 2017. **2**(Supplement C): p. 49-57.
41. Zhmayev, E., H. Zhou, and Y.L. Joo, *Modeling of non-isothermal polymer jets in melt electrospinning.* Journal of Non-Newtonian Fluid Mechanics, 2008. **153**(2-3): p. 95-108.
42. Muerza-Cascante, M.L., et al., *Melt Electrospinning and Its Technologization in Tissue Engineering.* Tissue Engineering Part B: Reviews, 2015. **21**(2): p. 187-202.
43. Dalton, P.D., et al., *Patterned melt electrospun substrates for tissue engineering.* Biomedical Materials, 2008. **3**(3): p. 034109.
44. Brown, T.D., et al., *Melt electrospinning of poly(ε-caprolactone) scaffolds: Phenomenological observations associated with collection and direct writing.* Materials Science and Engineering: C, 2014. **45**(0): p. 698-708.
45. Bu, N., et al., *Tunable bead-on-string microstructures fabricated by mechano- electrospinning.* Journal of Physics D: Applied Physics, 2012. **45**(40).
46. Wei, C. and J. Dong, *Direct fabrication of high-resolution three-dimensional polymeric scaffolds using electrohydrodynamic hot jet plotting.* Journal of Micromechanics and Microengineering, 2013. **23**(2).
47. Zhou, H., T.B. Green, and Y.L. Joo, *The thermal effects on electrospinning of polylactic acid melts.* Polymer, 2006. **47**(21): p. 7497-7505.
48. Hu, D. and R. Kovacevic, *Sensing, modeling and control for laser-based additive manufacturing.* International Journal of Machine Tools and Manufacture, 2003. **43**(1): p. 51-60.
49. *Automation Unlimited 'closes the loop' in automated robotic soldering process control.* Soldering & Surface Mount Technology, 2000. **12**(2): p. null.
50. Hacker, C., et al. *Electrospinning of polymer melt: steps toward an upscaled multi-jet process*. in *Proceedings of the International Conference on Latest Advances in High Tech Textiles and Textile-Based Materials*. 2009.
51. Li, H., et al., *Interjet distance in needleless melt differential electrospinning with umbellate nozzles.* Journal of Applied Polymer Science, 2014. **131**(15): p. n/a-n/a.
52. Eisner, H., *Systems Engineering: Building Successful Systems.* Synthesis Lectures on Engineering, 2011. **6**(2): p. 1-139.
53. Hitchins, D.K., *Systems Engineering : A 21st Century Systems Methodology*. 2008, Wiley.
54. Crisp, H., *Systems engineering vision 2020.* Seattle, Washington, 2007.
55. Sakairi, T., et al., *Model Based Control System Design Using SysML, Simulink, and Computer Algebra System.* Journal of Control Science and Engineering, 2013. **2013**: p. 1-14.
56. Defense, D.o., *Systems Engineering Fundamentals.* http://www.dau.mil/pubs/pdf/SEFGuide%2001-01.pdf, 2001.
57. Gilbert, W., *De magnete, magneticisque corporibus, et de magno magnete*

tellure: physiologia noua plurimis et argumentis, et experimentis demonstrata. 1600: excudebet Petrus Short.
58. Rayleigh, L., *XX. On the equilibrium of liquid conducting masses charged with electricity.* Philosophical Magazine Series 5, 1882. **14**(87): p. 184-186.
59. Zeleny, J., *The Electrical Discharge from Liquid Points, and a Hydrostatic Method of Measuring the Electric Intensity at Their Surfaces.* Physical Review, 1914. **3**(2): p. 69-91.
60. Cooley, J.F., *Electrical method of dispersing fluids*. 1903, Google Patents.
61. Cooley, J.F., *Apparatus for electrically dispersing fluids*. 1902, Google Patents.
62. *On the 100th anniversary of the birth of I.V. Petryanov-Sokolov.* Izvestiya, Atmospheric and Oceanic Physics. **43**(3): p. 395-395.
63. Doshi, J. and D.H. Reneker, *Electrospinning process and applications of electrospun fibers.* Journal of Electrostatics, 1995. **35**(2–3): p. 151-160.
64. Persano, L., et al., *Industrial Upscaling of Electrospinning and Applications of Polymer Nanofibers: A Review.* Macromolecular Materials and Engineering, 2013. **298**(5): p. 504-520.
65. Norton, C.L., *Method of and apparatus for producing fibrous or filamentary material*. 1936, Google Patents,.
66. Kim, J.-S. and D.S. Lee, *Thermal Properties of Electrospun Polyesters.* Polym J, 2000. **32**(7): p. 616-618.
67. Lyons, J., C. Li, and F. Ko, *Melt-electrospinning part I: processing parameters and geometric properties.* Polymer, 2004. **45**(22): p. 7597-7603.
68. Rangkupan, R. and D.H. Reneker, *Electrospinning Process of Molten Polypropylene in Vacuum.* Journal of Metals, Materials and Minerals, 2003. **12**(2): p. 81-87.
69. Ogata, N., et al., *Poly(lactide) nanofibers produced by a melt‐electrospinning system with a laser melting device.* Journal of Applied Polymer Science, 2007. **104**(3): p. 1640-1645.
70. Ogata, N., et al., *Melt‐electrospinning of poly(ethylene terephthalate) and polyalirate.* Journal of Applied Polymer Science, 2007. **105**(3): p. 1127-1132.
71. Ogata, N., et al., *Effects of ethylene content of poly(ethylene‐co‐vinyl alcohol) on diameter of fibers produced by melt‐electrospinning.* Journal of Applied Polymer Science, 2007. **104**(2): p. 1368-1375.
72. Zhmayev, E., D. Cho, and Y.L. Joo, *Modeling of melt electrospinning for semi-crystalline polymers.* Polymer, 2010. **51**(1): p. 274-290.
73. Li, X., et al., *Effect of oriented fiber membrane fabricated via needleless melt electrospinning on water filtration efficiency.* Desalination, 2014. **344**(0): p. 266-273.
74. Thibaudeau, L., et al., *A tissue-engineered humanized xenograft model of human breast cancer metastasis to bone.* Disease models & mechanisms, 2014. **7**(2): p. 299-309.
75. Farrugia, B.L., et al., *Dermal fibroblast infiltration of poly(ε-caprolactone) scaffolds fabricated by melt electrospinning in a direct writing mode.* Biofabrication, 2013. **5**(2): p. 025001.
76. Brown, T.D., et al., *Design and Fabrication of Tubular Scaffolds via Direct Writing in a Melt Electrospinning Mode.* Biointerphases, 2012. **7**(1): p. 1-16.
77. Ahn, Y.C., et al., *Development of high efficiency nanofilters made of nanofibers.* Current Applied Physics, 2006. **6**(6): p. 1030-1035.
78. Li, X., et al., *Water filtration properties of novel composite membranes*

combining solution electrospinning and needleless melt electrospinning methods. Journal of Applied Polymer Science, 2015. **132**(10): p. n/a-n/a.
79. Dong, Y., et al., *Materials design towards sport textiles with low-friction and moisture-wicking dual functions.* Materials & Design, 2015. **88**: p. 82-87.
80. Wu, D.Z., et al., *Electrospun Nanofibers for Sandwiched Polyimide/Poly (vinylidene fluoride)/Polyimide Separators with the Thermal Shutdown Function.* ELECTROCHIMICA ACTA, 2015. **176**: p. 727-734.
81. Peng, Y.-T. and C.-T. Lo, *Electrospun porous carbon nanofibers as lithium ion battery anodes.* Journal of Solid State Electrochemistry, 2015. **19**(11): p. 3401-3410.
82. Singer, J.C., R. Giesa, and H.-W. Schmidt, *Shaping self-assembling small molecules into fibres by melt electrospinning.* Soft Matter, 2012. **8**(39): p. 9972.
83. Zou, L., et al., *A Blind Source Separation Framework for Monitoring Heart Beat Rate Using Nanofiber-Based Strain Sensors.* IEEE Sensors Journal, 2016. **16**(3): p. 762-772.
84. Zhang, L., et al., *Femtoliter-scale optical nanofiber sensors.* Optics express, 2015. **23**(22): p. 28408.
85. Brown, T.D., P.D. Dalton, and D.W. Hutmacher, *Melt Electrospinning Today: An Opportune Time for an Emerging Polymer Process.* Progress in Polymer Science, 2016.
86. Agarwal, S., A. Greiner, and J.H. Wendorff, *Functional materials by electrospinning of polymers.* Progress in Polymer Science, 2013. **38**(6): p. 963-991.
87. Melchels, F.P.W., J. Feijen, and D.W. Grijpma, *A review on stereolithography and its applications in biomedical engineering.* Biomaterials, 2010. **31**(24): p. 6121-6130.
88. Duan, B., et al., *Three-dimensional nanocomposite scaffolds fabricated via selective laser sintering for bone tissue engineering.* Acta Biomaterialia, 2010. **6**(12): p. 4495-4505.
89. Butscher, A., et al., *Structural and material approaches to bone tissue engineering in powder-based three-dimensional printing.* Acta Biomaterialia, 2011. **7**(3): p. 907-920.
90. Lee, H., et al., *Fabrication, characterization, and in vitro biological activities of melt-electrospun PLA micro/nanofibers for bone tissue regeneration.* Journal of Materials Chemistry B, 2013. **1**(30): p. 3670-3677.
91. Agarwal, S. and A. Greiner, *On the way to clean and safe electrospinning—green electrospinning: emulsion and suspension electrospinning.* Polymers for Advanced Technologies, 2011. **22**(3): p. 372-378.
92. Góra, A., et al., *Melt-Electrospun Fibers for Advances in Biomedical Engineering, Clean Energy, Filtration, and Separation.* Polymer Reviews, 2011. **51**(3): p. 265-287.
93. Eian, G. and P.G. Cheney, *Durable melt-blown fibrous sheet material*. 1987, Google Patents.
94. Dalton, P.D., et al., *Electrospinning of polymer melts: Phenomenological observations.* Polymer, 2007. **48**(23): p. 6823-6833.
95. Detta, N., et al., *Melt electrospinning of polycaprolactone and its blends with poly(ethylene glycol).* Polymer International, 2010. **59**(11): p. 1558-1562.
96. Kress, R., *The Heat Equation*, in *Linear Integral Equations*. 1989, Springer Berlin Heidelberg: Berlin, Heidelberg. p. 132-141.

97. Crank, J. and P. Nicolson, *A practical method for numerical evaluation of solutions of partial differential equations of the heat-conduction type.* Advances in Computational Mathematics, 1996. **6**(1): p. 207-226.
98. Kwok, D.Y., et al., *Study on the surface tensions of polymer melts using axisymmetric drop shape analysis.* Polymer Engineering and Science, 1998. **38**(5): p. 757-764.
99. Wei, C., et al., *Critical condition for the transformation from Taylor cone to cone-jet.* Chinese Physics B, 2014. **23**(6): p. 064702.
100. Mora, J.F.d.l., *The Fluid Dynamics of Taylor Cones.* Annual Review of Fluid Mechanics, 2007. **39**(1): p. 217-243.
101. Bear, J., *Dynamics of fluids in porous media*. 2013: Courier Corporation.
102. Bellan, L.M., H.G. Craighead, and J.P. Hinestroza, *Direct measurement of fluid velocity in an electrospinning jet using particle image velocimetry.* Journal of Applied Physics, 2007. **102**(9): p. 094308.
103. Filippini, J. and C. Meyer, *Water treeing using the water needle method: the influence of the magnitude of the electric field at the needle tip.* IEEE transactions on electrical insulation, 1988. **23**(2): p. 275-278.
104. Alj, A., et al., *Creation of charge carriers in nonpolar liquids.* IEEE Transactions on Electrical Insulation, 1985(2): p. 221-231.
105. Shrimpton, J., *Charge injection systems: physical principles, experimental and theoretical work*. 2009: Springer Science & Business Media.
106. Heeger, A.J., I. Parker, and Y. Yang, *Carrier injection into semiconducting polymers: Fowler-Nordheim field-emission tunneling.* Synthetic Metals, 1994. **67**(1): p. 23-29.
107. Marginean, I., et al., *Flexing the electrified meniscus: the birth of a jet in electrosprays.* Analytical chemistry, 2004. **76**(14): p. 4202-4207.
108. Fridrikh, S.V., et al., *Controlling the fiber diameter during electrospinning.* Physical Review Letters, 2003. **90**(14): p. 144502/4.
109. Spivak, A. and Y.A. Dzenis, *Asymptotic decay of radius of a weakly conductive viscous jet in an external electric field.* Applied Physics Letters, 1998. **73**(21): p. 3067-3069.
110. Zhmayev, E., D. Cho, and Y. Lak Joo, *Electrohydrodynamic quenching in polymer melt electrospinning.* Physics of Fluids (1994-present), 2011. **23**(7): p. -.
111. Han, T., A.L. Yarin, and D.H. Reneker, *Viscoelastic electrospun jets: Initial stresses and elongational rheometry.* Polymer, 2008. **49**(6): p. 1651-1658.
112. Hagedorn, J.G., N.S. Martys, and J.F. Douglas, *Breakup of a fluid thread in a confined geometry: droplet-plug transition, perturbation sensitivity, and kinetic stabilization with confinement.* Physical Review E, 2004. **69**(5): p. 056312.
113. Toimil Molares, M.E., et al., *Fragmentation of nanowires driven by Rayleigh instability.* Applied Physics Letters, 2004. **85**(22): p. 5337-5339.
114. Jian, H.Y., S.V. Fridrikh, and G.C. Rutledge, *The role of elasticity in the formation of electrospun fibers.* Polymer, 2006. **47**(13): p. 4789-4797.
115. Marr-Lyon, M.J., et al., *Stabilization of electrically conducting capillary bridges using feedback control of radial electrostatic stresses and the shapes of extended bridges.* Physics of Fluids, 2000. **12**(5): p. 986-995.
116. Hochleitner, G., et al., *Additive manufacturing of scaffolds with sub-micron filaments via melt electrospinning writing.* Biofabrication, 2015. **7**(3): p. 035002.

117. Lowell, J., *Absorption and conduction currents in polymers: a unified model.* Journal of Physics D: Applied Physics, 1990. **23**(2): p. 205.
118. Mishra, A., *Studies of polymer electrets. II. Factors governing the stabilities of homoelectrets obtained from polystyrene and its derivatives.* Journal of Applied Polymer Science, 1982. **27**(4): p. 1107-1118.
119. Filatov, Y., A. Budyka, and V. Kirichenko, *Electrospinning of micro-and nanofibers: fundamentals in separation and filtration processes.* J. Eng. Fibers Fabrics, 2007. **3**: p. 488.
120. De Vrieze, S., et al., *The effect of temperature and humidity on electrospinning.* Journal of materials science, 2009. **44**(5): p. 1357-1362.
121. Kalayci, V.E., et al., *Charge consequences in electrospun polyacrylonitrile (PAN) nanofibers.* Polymer, 2005. **46**(18): p. 7191-7200.
122. Griffiths, D.J., *Introduction to Electrodynamics*. 2013: Pearson.
123. Wan, Y.-Q., Q. Guo, and N. Pan, *Thermo-electro-hydrodynamic model for electrospinning process.* International Journal of Nonlinear Sciences and Numerical Simulation, 2004. **5**(1): p. 5-8.
124. Jungst, T., et al., *Melt electrospinning onto cylinders: effects of rotational velocity and collector diameter on morphology of tubular structures.* Polymer International, 2015. **64**(9): p. 1086-1095.
125. Fang, J., et al., *Needleless Melt-Electrospinning of Polypropylene Nanofibres.* Journal of Nanomaterials, 2012. **2012**: p. 1-9.
126. Komarek, M. and L. Martinova. *Design and evaluation of melt-electrospinning electrodes*. in *Proceedings of 2nd NANOCON International Conference, Olomouc*. 2010.
127. Singer, J.C., et al., *Melt Electrospinning of Small Molecules.* Macromolecular Materials and Engineering, 2015. **300**(3): p. 259-276.
128. Deng, R., et al., *Melt electrospinning of low-density polyethylene having a low-melt flow index.* Journal of Applied Polymer Science, 2009. **114**(1): p. 166-175.
129. Zhao, F., et al., *Orthogonal design study on factors affecting the degradation of polylactic acid fibers of melt electrospinning.* Journal of Applied Polymer Science, 2012. **125**(4): p. 2652-2658.
130. Liu, Y., et al., *Solvent-free preparation of polylactic acid fibers by melt electrospinning using umbrella-like spray head and alleviation of problematic thermal degradation.* Journal of the Serbian Chemical Society, 2012. **77**(8): p. 1071-1082.
131. Nayak, R., et al., *Melt-electrospinning of polypropylene with conductive additives.* Journal of Materials Science, 2012. **47**(17): p. 6387-6396.
132. Nayak, R., et al., *Effect of viscosity and electrical conductivity on the morphology and fiber diameter in melt electrospinning of polypropylene.* Textile Research Journal, 2013. **83**(6): p. 606-617.
133. Ko, J., et al., *Fabrication of poly (ϵ-caprolactone) microfiber scaffolds with varying topography and mechanical properties for stem cell-based tissue engineering applications.* Journal of Biomaterials Science, Polymer Edition, 2014. **25**(1): p. 1-17.
134. Kadomae, Y., et al., *Relation between tacticity and fiber diameter in melt-electrospinning of polypropylene.* Fibers and Polymers, 2009. **10**(3): p. 275-279.
135. Hunley, M.T., et al., *Taking Advantage of Tailored Electrostatics and Complementary Hydrogen Bonding in the Design of Nanostructures for*

Biomedical Applications. Macromolecular Symposia, 2008. **270**(1): p. 1-7.
136. Mitchell, S.B. and J.E. Sanders, *A unique device for controlled electrospinning.* Journal of Biomedical Materials Research Part A, 2006. **78A**(1): p. 110-120.
137. Xiao-fei Wang Zheng-ming, H., *Melt-Electrospinning of PMMA.* 高分子科学：英文版, 2010. **28**(1): p. 45-53.
138. McCann, J.T., M. Marquez, and Y. Xia, *Melt coaxial electrospinning: a versatile method for the encapsulation of solid materials and fabrication of phase change nanofibers.* Nano letters, 2006. **6**(12): p. 2868-2872.
139. Bhullar, S.K., et al., *Fabrication and Characterization of Nonwoven Auxetic Polymer Stent.* Polymer-Plastics Technology and Engineering, 2015. **54**(15): p. 1553-1559.
140. Bhullar, S.K., B. Kaya, and M.B.-G. Jun, *Development of Bioactive Packaging Structure Using Melt Electrospinning.* Journal of Polymers and the Environment, 2015. **23**(3): p. 416-423.
141. Praeger, M., et al., *Fabrication of nanoscale glass fibers by electrospinning.* Applied Physics Letters, 2012. **100**(6): p. 063114-063114-3.
142. Shimada, N., et al., *Spot laser melt electrospinning of a fiber bundle composed of poly(lactide)/poly(ethylene‐co‐vinyl alcohol) pie wedge fibers.* Journal of Applied Polymer Science, 2012. **125**(S2): p. E384-E389.
143. Takasaki, M., et al., *Ultra-fine fibers produced by laser-electrospinning.* 繊維学会誌, 2008. **64**(1): p. 29-31.
144. Blackwood, K.A., et al. *Improving electrospun fibre stacking with direct writing for developing scaffolds for tissue engineering for non-load bearing bone*. in *IFMBE Proceedings*. 2015.
145. Rajabinejad, H., et al., *Recycling of Used Bottle Grade Poly Ethyleneterephthalate to Nanofibers by Melt-electrospinning Method.* International Journal of Environmental Research, 2010. **3**(4).
146. Kim, S.J., et al., *Fabrication and characterization of 3-dimensional PLGA nanofiber/microfiber composite scaffolds.* Polymer, 2010. **51**(6): p. 1320-1327.
147. Kim, B.S., et al., *Effect of nanofiber content on bone regeneration of silk fibroin/poly(epsilon-caprolactone) nano/microfibrous composite scaffolds.* INTERNATIONAL JOURNAL OF NANOMEDICINE, 2015. **10**: p. 485-502.
148. Lee, S. and S. Kay Obendorf, *Developing protective textile materials as barriers to liquid penetration using melt-electrospinning.* Journal of Applied Polymer Science, 2006. **102**(4): p. 3430-3437.
149. Dalton, P.D., et al., *Melt electrospinning of poly-(ethylene glycol-block-ϵ-caprolactone).* Biotechnology Journal, 2006. **1**(9): p. 998-1006.
150. Hacker, C., et al., *Functionally modified, melt-electrospun thermoplastic polyurethane mats for wound-dressing applications.* Journal of Applied Polymer Science, 2014. **131**(8).
151. Ko, J., et al., *Design and fabrication of auxetic stretchable force sensor for hand rehabilitation.* SMART MATERIALS AND STRUCTURES, 2015. **24**(7).
152. Tourlomousis, F., et al. *A Novel Melt Electrospinning System for Studying Cell Substrate Interactions*. in *ASME 2015 International Manufacturing Science and Engineering Conference*. 2015. American Society of Mechanical Engineers.

153. Wang, X., et al., *A patterned ZnO nanorod array/gas sensor fabricated by mechanoelectrospinning-assisted selective growth.* Chemical Communications, 2015. **51**(15): p. 3117-3120.
154. Mazalevska, O., M.H. Struszczyk, and I. Krucinska, *Design of vascular prostheses by melt electrospinning—structural characterizations.* Journal of Applied Polymer Science, 2013. **129**(2): p. 779-792.
155. Chrzanowska, O., et al., *Elaboration of small‐diameter vascular prostheses—Selection of appropriate sterilisation method.* Journal of Applied Polymer Science, 2014. **131**(18): p. 9611-9620.
156. Chrzanowska, O., M.H. Struszczyk, and I. Krucinska, *Small diameter tubular structure design using solvent-free textile techniques.* Journal of Applied Polymer Science, 2014. **131**(8).
157. Mota, C., et al., *Melt electrospinning writing of three-dimensional star poly(ϵ-caprolactone) scaffolds.* Polymer International, 2013. **62**(6): p. 893-900.
158. Gazzarri, M., et al., *Fibrous star poly(ε-caprolactone) melt-electrospun scaffolds for wound healing applications.* Journal of Bioactive and Compatible Polymers, 2013. **28**(5): p. 492-507.
159. Cao, L., et al., *Morphologies and crystal structures of styrene–acrylonitrile/isotactic polypropylene ultrafine fibers fabricated by melt electrospinning.* Polymer Engineering & Science, 2013. **53**(12): p. 2674-2682.
160. Mota, C., et al., *Melt electrospinning writing of three‐dimensional star poly(ϵ‐caprolactone) scaffolds.* Polymer International, 2013. **62**(6): p. 893-900.
161. Wang, H., Y. Xu, and Q.F. Wei, *Preparation of bamboo-hat-shaped deposition of a poly(ethylene terephthalate) fiber web by melt-electrospinning.* TEXTILE RESEARCH JOURNAL, 2015. **85**(17): p. 1838-1848.
162. Hochleitner, G., et al., *High definition fibrous poly(2-ethyl-2-oxazoline) scaffolds through melt electrospinning writing.* Polymer, 2014. **55**(20): p. 5017-5023.
163. Shimada, N., et al., *Poly(ethylene-co-vinyl alcohol) and nylon 6/12 nanofibers produced by melt electrospinning system equipped with a line-like laser beam melting device.* Journal of Applied Polymer Science, 2010. **116**(5): p. 2998-3004.
164. Tian, S., et al., *Melt electrospinning from poly(L-lactide) rods coated with poly(ethylene-co-vinyl alcohol).* Journal of Applied Polymer Science, 2009. **113**(2): p. 1282-1288.
165. Yamamoto, M., et al., *Effect of the take-up velocity on the higher-order structure of the melt-electrospun PLLA/PDLA blend fibers.* Sen'i Gakkaishi, 2015. **71**(3): p. 127-133.
166. Kong, C.S., et al., *Effects of the Spin Line Temperature Profile and Melt Index of Poly(propylene) on Melt-Electrospinning.* Polymer Engineering and Science, 2009. **49**(2): p. 391-396.
167. Li Cao Dun-fan Su Zhi-qiang Su Xiao-nong, C., *Morphology, Crystallization Behavior and Tensile Properties of β-Nucleated Isotactic Polypropylene Fibrous Membranes Prepared by Melt Electrospinning.* 高分子科学：英文版, 2014. **32**(9): p. 1167-1175.

168. Mohtaram, N.K., et al., *Electrospun biomaterial scaffolds with varied topographies for neuronal differentiation of human ‐induced pluripotent stem cells.* Journal of Biomedical Materials Research Part A, 2015. **103**(8): p. 2591-2601.
169. Malakhov, S.N., et al., *Method of manufacturing nonwovens by electrospinning from polymer melts.* Fibre Chemistry, 2009. **41**(6): p. 355-359.
170. Liu, Y., et al., *Orthogonal design study on factors effecting on fibers diameter of melt electrospinning.* Polymer Engineering & Science, 2010. **50**(10): p. 2074-2078.
171. Cho, D., E. Zhmayev, and Y.L. Joo, *Structural studies of electrospun nylon 6 fibers from solution and melt.* Polymer, 2011. **52**(20): p. 4600-4609.
172. Malakhov, S.N., et al., *Electrospinning of Non-Woven Materials from the Melt of Polyamide-6 with Added Magnesium, Calcium, and Zinc Stearates.* Fibre Chemistry, 2015. **47**(1): p. 14-19.
173. Bas, O., et al., *Enhancing structural integrity of hydrogels by using highly organised melt electrospun fibre constructs.* EUROPEAN POLYMER JOURNAL, 2015. **72**: p. 451-463.
174. Karchin, A., et al., *Melt electrospinning of biodegradable polyurethane scaffolds.* Acta Biomaterialia, 2011. **7**(9): p. 3277-3284.
175. Park, S.J., et al., *Melt-spun shaped fibers with enhanced surface effects: Fiber fabrication, characterization and application to woven scaffolds.* Acta Biomaterialia, 2013. **9**(8): p. 7719-7726.
176. Zhmayev, E., D. Cho, and Y.L. Joo, *Nanofibers from gas-assisted polymer melt electrospinning.* Polymer, 2010. **51**(18): p. 4140-4144.
177. Casper, C.L., et al., *Controlling surface morphology of electrospun polystyrene fibers: effect of humidity and molecular weight in the electrospinning process.* Macromolecules, 2004. **37**(2): p. 573-578.
178. Medeiros, E.S., et al., *Effect of relative humidity on the morphology of electrospun polymer fibers.* Canadian Journal of Chemistry, 2008. **86**(6): p. 590-599.
179. Cho, D., et al., *Structural properties and superhydrophobicity of electrospun polypropylene fibers from solution and melt.* Polymer, 2010. **51**(25): p. 6005-6012.
180. Dasdemir, M., M. Topalbekiroglu, and A. Demir, *Electrospinning of thermoplastic polyurethane microfibers and nanofibers from polymer solution and melt.* Journal of Applied Polymer Science, 2013. **127**(3): p. 1901-1908.
181. Reneker, D.H. and A.L. Yarin, *Electrospinning jets and polymer nanofibers.* Polymer, 2008. **49**(10): p. 2387-2425.
182. Nakamoto, H. and H. Tsutsumi, *Electrospun sulfur fibers as a template for micrometer-sized copper sulfide tubes.* Materials Letters, 2014. **136**: p. 26-29.
183. Liu, Y., et al., *Effect of polar additives on melt electrospinning of non-polar polypropylene.* Journal of the Serbian Chemical Society, 2014. **79**(5): p. 587-596.
184. Costa, P.F., et al., *Advanced tissue engineering scaffold design for regeneration of the complex hierarchical periodontal structure.* Journal of Clinical Periodontology, 2014. **41**(3): p. 283-294.
185. Ko, J., D. Kan, and M.B. Jun, *Combining melt electrospinning and particulate leaching for fabrication of porous microfibers.* Manufacturing

Letters, 2015. **3**: p. 5-8.
186. Kim, D. and K. Yoshino, *Morphological characteristics and electrical conduction in syndiotactic polypropylene.* Journal of Physics D: Applied Physics, 2000. **33**(4): p. 464.
187. Lyons, J. and F. Ko, *Feature Article: Melt Electrospinning of Polymers: A Review.* Polymer News, 2005. **30**(6): p. 170-178.
188. Xie, G., et al., *Orthogonal design preparation of phenolic fiber by melt electrospinning.* Journal of Applied Polymer Science, 2015. **132**(38): p. n/a-n/a.
189. Ivanovski, S., et al., *Multiphasic Scaffolds for Periodontal Tissue Engineering.* Journal of Dental Research, 2014. **93**(12): p. 1212-1221.
190. Jeon, J.E., et al., *Perspectives in Multiphasic Osteochondral Tissue Engineering.* The Anatomical Record, 2014. **297**(1): p. 26-35.
191. Kim, G., et al., *Hybrid Process for Fabricating 3D Hierarchical Scaffolds Combining Rapid Prototyping and Electrospinning.* Macromolecular Rapid Communications, 2008. **29**(19): p. 1577-1581.
192. Moroni, L., J. De Wijn, and C. Van Blitterswijk, *Integrating novel technologies to fabricate smart scaffolds.* Journal of Biomaterials Science, Polymer Edition, 2008. **19**(5): p. 543-572.
193. Yang, G.H., M. Kim, and G. Kim, *A hybrid PCL/collagen scaffold consisting of solid freeform-fabricated struts and EHD-direct-jet-processed fibrous threads for tissue regeneration.* JOURNAL OF COLLOID AND INTERFACE SCIENCE, 2015. **450**: p. 159-167.
194. Kang, Y.O., J.N. Im, and W.H. Park, *Morphological and permeable properties of antibacterial double-layered composite nonwovens consisting of microfibers and nanofibers.* COMPOSITES PART B-ENGINEERING, 2015. **75**: p. 256-263.
195. Visser, J., et al., *Reinforcement of hydrogels using three-dimensionally printed microfibres.* NATURE COMMUNICATIONS, 2015. **6**: p. 6933.
196. Ren, J., et al., *Melt‐electrospun polycaprolactone strontium‐substituted bioactive glass scaffolds for bone regeneration.* Journal of Biomedical Materials Research Part A, 2014. **102**(9): p. 3140-3153.
197. Malda, J., et al., *Cartilage tissue engineering: controversy in the effect of oxygen.* Critical reviews in biotechnology, 2003. **23**(3): p. 175-194.
198. Nayak, R., et al., *Recent advances in nanofibre fabrication techniques.* Textile Research Journal, 2012. **82**(2): p. 129-147.
199. Zhou, F.-L., R.-H. Gong, and I. Porat, *Mass production of nanofibre assemblies by electrostatic spinning.* Polymer International, 2009. **58**(4): p. 331-342.
200. Zheng, Y. and Y. Zeng, *Electric field analysis of spinneret design for multihole electrospinning system.* Journal of Materials Science, 2014. **49**(5): p. 1964-1972.
201. Ying, Y., et al., *A shield ring enhanced equilateral hexagon distributed multi-needle electrospinning spinneret.* Dielectrics and Electrical Insulation, IEEE Transactions on, 2010. **17**(5): p. 1592-1601.
202. Liu, Y., X. Li, and S. Ramakrishna, *Melt electrospinning in a parallel electric field.* Journal of Polymer Science Part B: Polymer Physics, 2014. **52**(14): p. 946-952.
203. Brown, T.D., et al., *Melt electrospinning of poly (ε-caprolactone) scaffolds: Phenomenological observations associated with collection and direct writing.*

Materials Science and Engineering: C, 2014. **45**: p. 698-708Materials & Design.
204. Mikl, et al., *Discrete viscous threads.* ACM Trans. Graph., 2010. **29**(4): p. 1-10.
205. Hochleitner, G., et al., *Fibre pulsing during melt electrospinning writing.* BioNanoMaterials, 2016. **17**(3-4): p. 159.
206. Poh, P.S.P., et al., *Polylactides in additive biomanufacturing.* Advanced Drug Delivery Reviews, 2016. **107**: p. 228-246.
207. Holzapfel, B.M., et al., *Species-specific homing mechanisms of human prostate cancer metastasis in tissue engineered bone.* Biomaterials, 2014. **35**(13): p. 4108-4115.
208. Haigh, J.N., et al., *Hierarchically Structured Porous Poly(2-oxazoline) Hydrogels.* Macromolecular Rapid Communications, 2016. **37**(1): p. 93-99.
209. Wagner, F., et al., *A validated preclinical animal model for primary bone tumor research.* JBJS, 2016. **98**(11): p. 916-925.
210. Baldwin, J., et al., *Periosteum tissue engineering in an orthotopic in vivo platform.* Biomaterials, 2017. **121**: p. 193-204.
211. Tourlomousis, F. and R.C. Chang, *Dimensional Metrology of Cell-matrix Interactions in 3D Microscale Fibrous Substrates.* Procedia CIRP, 2017. **65**: p. 32-37.
212. Muerza-Cascante, M.L., et al., *Endosteal-like extracellular matrix expression on melt electrospun written scaffolds.* Acta biomaterialia, 2017. **52**: p. 145-158.
213. Bas, O., et al., *Biofabricated soft network composites for cartilage tissue engineering.* Biofabrication, 2017. **9**(2): p. 025014.
214. Hansske, F., et al., *Via precise interface engineering towards bioinspired composites with improved 3D printing processability and mechanical properties.* Journal of Materials Chemistry B, 2017.
215. Hochleitner, G., et al., *Fibre pulsing during melt electrospinning writing*, in *BioNanoMaterials*. 2016. p. 159.
216. Loh, Q.L. and C. Choong, *Three-Dimensional Scaffolds for Tissue Engineering Applications: Role of Porosity and Pore Size.* Tissue Engineering Part B: Reviews, 2013. **19**(6): p. 485-502.
217. Ristovski, N., et al., *Improved fabrication of melt electrospun tissue engineering scaffolds using direct writing and advanced electric field control.* Biointerphases, 2015. **10**(1): p. 011006.
218. Wei, C. and J. Dong, *Direct fabrication of high-resolution three-dimensional polymeric scaffolds using electrohydrodynamic hot jet plotting.* Journal of Micromechanics and Microengineering, 2013. **23**(2): p. 025017.
219. Liao, S., et al., *Effect of humidity on melt electrospun polycaprolactone scaffolds*, in *BioNanoMaterials*. 2016. p. 173.
220. Chen, F., et al., *Additive manufacturing of a photo-cross-linkable polymer via direct melt electrospinning writing for producing high strength structures.* Biomacromolecules, 2016. **17**(1): p. 208-214.
221. Schubert, C., M.C. van Langeveld, and L.A. Donoso, *Innovations in 3D printing: a 3D overview from optics to organs.* British Journal of Ophthalmology, 2014. **98**(2): p. 159-161.
222. Wunner, F.M., Bas, O., Saidy, N. T., Dalton, P. D., Pardo, E. M., Hutmacher, D. W. , *Melt Electrospinning Writing of Three-dimensional Poly(ε-caprolactone) Scaffolds with Controllable Morphologies for Tissue*

Engineering Applications. J. Vis. Exp. , 2017.
223. Delalat, B., et al., *3D printed lattices as an activation and expansion platform for T cell therapy.* Biomaterials, 2017.
224. Feng, J.J., *Stretching of a straight electrically charged viscoelastic jet.* Journal of Non-Newtonian Fluid Mechanics, 2003. **116**(1): p. 55-70.
225. Taylor, G., *Electrically Driven Jets.* Proceedings of the Royal Society of London. A. Mathematical and Physical Sciences, 1969. **313**(1515): p. 453-475.
226. Blount, M.J. and J.R. Lister, *The asymptotic structure of a slender dragged viscous thread.* Journal of Fluid Mechanics, 2011. **674**: p. 489-521.
227. Strategy, M.E.a.O.C.-B.P.a.O. *Generate all Permutations*. 2012 [cited 2015 0306]; Available from: http://www.tushar-mehta.com/publish_train/xl_vba_cases/generate_all_permutations.htm.
228. Hiskes, J.R., *Dissociation of molecular ions by electric and magnetic fields.* Physical Review, 1961. **122**(4): p. 1207.
229. Haigh, J.N., T.R. Dargaville, and P.D. Dalton, *Additive manufacturing with polypropylene microfibers.* Materials Science and Engineering: C, 2017. **77**(Supplement C): p. 883-887.
230. Grosvenor, M.P. and J.N. Staniforth, *The effect of molecular weight on the rheological and tensile properties of poly(ϵ-caprolactone).* International journal of pharmaceutics, 1996. **135**(1): p. 103-109.
231. Han, T., D.H. Reneker, and A.L. Yarin, *Pendulum-like motion of straight electrified jets.* Polymer, 2008. **49**(8): p. 2160-2169.
232. Catalani, L.H., G. Collins, and M. Jaffe, *Evidence for Molecular Orientation and Residual Charge in the Electrospinning of Poly(butylene terephthalate) Nanofibers.* Macromolecules, 2007. **40**(5): p. 1693-1697.
233. Shin, Y.M., et al., *Electrospinning: A whipping fluid jet generates submicron polymer fibers.* Applied Physics Letters, 2001. **78**(8): p. 1149-1151.
234. Bright, A.W. and B. Makin, *Polar liquids: A survey of purification, conduction mechanisms, and interfacial effects.* Journal of Materials Science, 1967. **2**(2): p. 184-193.
235. Hümmelgen, I.A., et al., *Polymer and polymer/metal interface characterization via Fowler–Nordheim tunneling measurements.* Applied Physics Letters, 1996. **68**(22): p. 3194-3196.
236. Coe, G., J.F. Hughes, and P.E. Secker, *High-current injection into liquid hexane using field emitters.* British Journal of Applied Physics, 1966. **17**(7): p. 885.
237. Zhmayev, E., D. Cho, and Y.L. Joo, *Electrohydrodynamic quenching in polymer melt electrospinning.* Physics of Fluids, 2011. **23**(7).
238. Brown, T.D., P.D. Dalton, and D.W. Hutmacher, *Direct writing by way of melt electrospinning.* Advanced Materials, 2011. **23**(47): p. 5651-5657.
239. Hutmacher, D.W. and P.D. Dalton, *Melt electrospinning.* Chemistry–An Asian Journal, 2011. **6**(1): p. 44-56.
240. Bas, O., et al., *An Integrated Design, Material, and Fabrication Platform for Engineering Biomechanically and Biologically Functional Soft Tissues.* ACS Applied Materials & Interfaces, 2017. **9**(35): p. 29430-29437.
241. Reneker, D.H., et al., *Bending instability of electrically charged liquid jets of polymer solutions in electrospinning.* Journal of Applied physics, 2000. **87**(9): p. 4531-4547.
242. Han, T., D.H. Reneker, and A.L. Yarin, *Buckling of jets in electrospinning.*

Polymer, 2007. **48**(20): p. 6064-6076.
243. Melchels, F.P.W., et al., *Additive manufacturing of tissues and organs.* Prog Polym Sci, 2012. **37**(8): p. 1079-1104.
244. Kang, H.W., et al., *A 3D bioprinting system to produce human-scale tissue constructs with structural integrity.* Nat Biotechnol, 2016. **34**(3): p. 312-9.
245. Kaushik, G., J. Leijten, and A. Khademhosseini, *Concise Review: Organ Engineering: Design, Technology, and Integration.* Stem Cells, 2017. **35**(1): p. 51-60.
246. Youssef, A.B., S.J. Hollister, and P.D. Dalton, *Additive manufacturing of polymer melts for implantable medical devices and scaffolds.* Biofabrication, 2017. **9**(1): p. 012002.
247. Probst, F.A., et al., *Calvarial reconstruction by customized bioactive implant.* Handchir Mikrochir Plastische Chir, 2010. **42**(6): p. 369-373.
248. Bhise, N.S., et al., *A liver-on-a-chip platform with bioprinted hepatic spheroids.* Biofabrication, 2016. **8**(1): p. 014101.
249. Homan, K.A., et al., *Bioprinting of 3D Convoluted Renal Proximal Tubules on Perfusable Chips.* Sci Rep, 2016. **6**: p. 34845.
250. Zadpoor, A.A. and J. Malda, *Additive Manufacturing of Biomaterials, Tissues, and Organs.* Annals of Biomedical Engineering, 2017. **45**(1): p. 1-11.
251. Li, X., et al., *Additive Manufacturing of Biomedical Constructs with Biomimetic Structural Organizations.* Materials, 2016. **9**(11): p. 909.
252. Hunsberger, J., et al., *Manufacturing Road Map for Tissue Engineering and Regenerative Medicine Technologies.* Stem Cells Translational Medicine, 2015. **4**(2): p. 130-135.
253. Giannitelli, S.M., et al., *Current trends in the design of scaffolds for computer-aided tissue engineering.* Acta Biomaterialia, 2014. **10**(2): p. 580-594.
254. Hutmacher, D.W., *Scaffolds in tissue engineering bone and cartilage.* Biomaterials, 2000. **21**(24): p. 2529-2543.
255. Holzapfel, B.M., et al., *How smart do biomaterials need to be? A translational science and clinical point of view.* Advanced Drug Delivery Reviews, 2013. **65**(4): p. 581-603.
256. Hutmacher, D.W., T.B.F. Woodfield, and P.D. Dalton, *Scaffold design and fabrication*, in *Tissue Engineering*, C. van Blitterswijk and J. De Boer, Editors. 2014, Elsevier: Amsterdam. p. 311-346.
257. Albrecht, L.D., S.W. Sawyer, and P. Soman, *Developing 3D Scaffolds in the Field of Tissue Engineering to Treat Complex Bone Defects.* 3D Printing and Additive Manufacturing, 2016. **3**(2): p. 106-112.
258. Therriault, D., S.R. White, and J.A. Lewis, *Chaotic mixing in three-dimensional microvascular networks fabricated by direct-write assembly.* Nature Materials, 2003. **2**(4): p. 265-271.
259. Kolesky, D.B., et al., *Three-dimensional bioprinting of thick vascularized tissues.* Proc Natl Acad Sci U S A, 2016. **113**(12): p. 3179-84.
260. Miller, J.S., et al., *Rapid casting of patterned vascular networks for perfusable engineered three-dimensional tissues.* Nature Materials, 2012. **11**(9): p. 768-774.
261. Brown, T.D., et al., *Electrospinning for Regenerative Medicine*, in *Polzmeric Materials> Structure and Function*, S. Dumitriu and V. Popa, Editors. 2013. p. 539–592.

262. Greiner, A. and J.H. Wendorff, *Electrospinning: A Fascinating Method for the Preparation of Ultrathin Fibers.* Angewandte Chemie International Edition, 2007. **46**(30): p. 5670-5703.
263. Huang, Z.-M., et al., *A review on polymer nanofibers by electrospinning and their applications in nanocomposites.* Composites Science and Technology, 2003. **63**(15): p. 2223-2253.
264. Fridrikh, S.V., et al., *Controlling the fiber diameter during electrospinning.* Physical Review Letters, 2003. **90**(14).
265. Doshi, J. and D.H. Reneker, *Electrospinning process and applications of electrospun fibers.* Journal of Electrostatics, 1995. **35**(2): p. 151-160.
266. Varesano, A., et al., *Multi-jet nozzle electrospinning on textile substrates: observations on process and nanofibre mat deposition.* Polymer International, 2010. **59**(12): p. 1606-1615.
267. Muerza-Cascante, M.L., et al., *Melt electrospinning and its technologization in tissue engineering.* Tissue Engineering Part B-Reviews, 2015. **21**(2): p. 187-202.
268. Brown, T.D., P.D. Dalton, and D.W. Hutmacher, *Melt electrospinning today: An opportune time for an emerging polymer process.* Prog Polym Sci, 2016. **56**: p. 116-166.
269. Brown, T.D., et al., *Melt electrospinning of poly(epsilon-caprolactone) scaffolds: Phenomenological observations associated with collection and direct writing.* Materials Science & Engineering C-Materials for Biological Applications, 2014. **45**: p. 698-708.
270. Baldwin, J.G., et al., *Periosteum tissue engineering in an orthotopic in vivo platform.* Biomaterials, 2017. **121**: p. 193-204.
271. Muerza-Cascante, M.L., et al., *Endosteal-like extracellular matrix expression on melt electrospun written scaffolds.* Acta Biomater, 2017. **52**: p. 145-158.
272. Bas, O., et al., *An Integrated Design, Material, and Fabrication Platform for Engineering Biomechanically and Biologically Functional Soft Tissues.* ACS Appl Mater Interfaces, 2017. **9**(35): p. 29430-29437.
273. Martine, L.C., et al., *Engineering a humanized bone organ model in mice to study bone metastases.* Nat Protoc, 2017. **12**(4): p. 639-663.
274. Dalton, P.D., *Melt electrowriting with additive manufacturing principles.* Current Opinion in Biomedical Engineering, 2017. **2**: p. 49-57.
275. Gao, W., et al., *The status, challenges, and future of additive manufacturing in engineering.* Computer-Aided Design, 2015. **69**: p. 65-89.
276. Malda, J., et al., *Engineering hydrogels for biofabrication.* Adv Mater, 2013. **25**(36): p. 5011-5028.
277. Adamiak, K. and P. Atten, *Simulation of corona discharge in point–plane configuration.* Journal of Electrostatics, 2004. **61**(2): p. 85-98.
278. Hansen, C.J., et al., *High-Throughput Printing via Microvascular Multinozzle Arrays.* Advanced Materials, 2013. **25**(1): p. 96-102.
279. Esmaeilian, B., S. Behdad, and B. Wang, *The evolution and future of manufacturing: A review.* Journal of Manufacturing Systems, 2016. **39**(Supplement C): p. 79-100.
280. Martine, L.C., et al., *Engineering a humanized bone organ model in mice to study bone metastases.* Nature Protocols, 2017. **12**: p. 639.
281. Maartens, J.H., et al., *Challenges and opportunities in the manufacture and expansion of cells for therapy.* Expert Opinion on Biological Therapy, 2017. **17**(10): p. 1221-1233.

282. Barry, S., et al., *Products and methods for activating and/or expanding t cells*. 2017, Google Patents.